Holocene Variations in the North Atlantic Marine Radiocarbon Reservoir Effect

Philippa Ascough B.sc. (Hons.)

Thesis for the degree of Doctor of Philosophy

2005

School of GeoSciences
The University of Edinburgh

Abstract

This thesis aims to examine the spatial and temporal characteristics of the ^{14}C marine reservoir effect (MRE) in the North Atlantic over the Holocene. The MRE is a time dependant offset in ^{14}C age between the atmospheric and ocean carbon reservoirs and accurate quantification of MRE correction values is crucial for radiocarbon chronologies. In a specific ocean area the MRE may show a deviation (known as ΔR) from the average value for the global average surface oceans given by the marine calibration curve (currently MARINE04). This occurs as a function of local oceanographic and climatic variables and current research has identified the potential for both spatial and temporal variations in ΔR values. A new and rigorous sample selection protocol was developed for this study to produce a large number of ΔR determinations that have a high degree of accuracy and precision. This involved selection of multiple single entity samples of both marine and terrestrial material from 30 clearly-defined deposits at 20 archaeological sites in Western Ireland, the island belts of Northern and Western Scotland, the western and northern Scottish mainland coast and the Faroe Isles. A total of 301 radiocarbon (^{14}C) measurements were made of sample material and the overall results demonstrate observable spatial and temporal variability in ΔR within the study area over the past c.8000 years. These can be related to climate and oceanographic changes previously identified as potential mechanisms for producing variation in ΔR. The interpretations drawn from this study were as follows:

1. At sites selected according to the study protocol a range of marine mollusc species can be used to accurately determine ΔR.
2. In the Early Holocene (c.6480-1940 BC) ΔR values were greater relative to that of later periods.
3. During the periods c.400 BC – 60 AD and c.1000-1200 AD, ΔR values were reduced relative to those of the present day
4. During the period c.1200-1400 AD, ΔR values were higher compared to the present.
5. In addition, there is evidence for spatial variation in ΔR within the study area over the Holocene. This is illustrated at c.1000-1200 AD when a large number of measurements indicate an increase in ΔR value northwards from the west coast of Ireland to the Faroe Isles.

The results of this study have important implications for our understanding of the MRE and the effective application of correction values to marine samples for ^{14}C measurement within both paleoenvironmental and archaeological research.

I declare that all the work within this thesis is original and my own, unless indicated otherwise, and none of the contents have been presented for examination elsewhere.

Signed:

Philippa Ascough. Date:.....5/5/06.....

Acknowledgements

This research has been supported by many people and organisations, including Historic Scotland, AOC Scotland Ltd, the Leverhulme Trust, the National Science Foundation of America Polar Programmes, the Carnegie Trust for the Universities of Scotland, the Moray Fund, and the University of Edinburgh small projects grants. In addition, this thesis would not have been possible without the input of a large number of people, whom I would like to thank. I have been very fortunate in having two excellent PhD supervisors, Andrew Dugmore and Gordon Cook, to whom I am deeply indebted for their unfailing support and assistance throughout all stages of the past four years. The advice and help of Marian Scott with statistical concerns and Paula Reimer with ΔR and marine reservoir calculations has been invaluable. Philip Naysmith, Robert Anderson and Elaine Dunbar at SUERC have taught me a vast amount regarding the technical and theoretical aspects of the ^{14}C method, their patience and time is very much appreciated. Patrick Ashmore at Historic Scotland has played a major role within the project from its initiation and has always been available to offer both academic and practical support. The archaeological samples from which over 300 ^{14}C measurements were produced were kindly provided by archaeologists from many institutions and organisations, all of whom devoted time to assisting me in my quest for samples that met a highly specific set of criteria. Both sample materials and input regarding archaeological questions were provided by Símun Arge, Beverley Ballin-Smith, John Barber, James Barrett, Cathy Batt, Julie Bond, Anne Brundle, Mike Church, Steve Dockrill, Alan Duffy, Simon Gilmour, Richard Gregory, Karen Hardy, Ailene Maule, Tom McGovern, Emily Murray, Tim Neighbour, Rebecca Nicholson Rachel Parks, Jennifer Rose, Peter Rowley-Conway, Alison Sheridan, Alexandra Shepherd, and Caroline Wickham-Jones. The carbonate $\delta^{18}O$ work was made possible by Mary Elliott from the School of GeoSciences, University of Edinburgh and Terry Donally and Andrew Tait at SUERC. Along with thanking people for professional support I am very glad to have so many good friends who have been there for me, listened and made me laugh. Finally I want to thank my family, without them I would not be who I am. I have been incredibly lucky to have my sister Stephanie and my Mum and Dad who always make me feel their love and support, wherever I am. Thank you.

Nomenclature

The following conventions are observed throughout this thesis:

- BC/AD: Calendar years. Used to refer to calibrated ^{14}C years.
- BP: Uncalibrated ^{14}C years
- cal. yr BP: Calibrated ^{14}C years.
- yr: year
- kyr: 1000 years

Abbreviations used throughout this thesis are outlined below

Subscripts in Equations

"s" is used to indicate a measured sample

"surf" is used to refer to a quantity of the surface ocean carbon reservoir

"atm" is used to refer to a quantity of the atmospheric carbon reservoir

"bio" is used to refer to a quantity of the biospheric carbon reservoir

"VPDB" refers to the Vienna Peedee Belemite standard for ^{13}C analysis

"R" is used to refer to a carbon reservoir other than the atmosphere

^{14}C production and measurement

- ^{14}C: Radiocarbon
- t: Time, with respect to radiocarbon years
- AMS: Accelerator mass spectrometry
- MRE: Marine radiocarbon reservoir effect
- σ: Sigma error term
- $\delta^{13}C$: Per mille deviation from the VPDB international standard
- CRA: Conventional radiocarbon age
- $^{14}A_0$: The ^{14}A of a sample at $t = 0$
- Q: Rate at which ^{14}C is produced in the atmosphere
- pCO_2: Partial pressure of CO_2
- GCR: Galactic cosmic ray
- SCR: Solar cosmic ray
- OXII: The current reference material provided by the National Institute of Standards and Technology for ^{14}C age calculation (SRM-4990C = Oxalic acid II)

- $\Delta^{14}C$: Per mille deviation of $^{14}A_{atm}$ from the international standard value of $^{14}A_0$
- C_{terr}: Carbon contained within the coeval atmosphere and terrestrial biosphere
- R: Reservoir effect. A ^{14}C age offset between carbon in a reservoir and the coeval atmosphere.
- C_{mar}: Carbon contained within the marine (ocean) reservoir

Ocean currents:

- EGC: East Greenland Current
- NADW: North Atlantic deep water
- NAC: North Atlantic current
- NC: Norwegian current
- NCC: Norwegian Coastal current
- IC: Irminger current
- WGC: West Greenland Current

Contents

Tables

Chapter 1

Chapter 2

Chapter 3

Chapter 4

Chapter 5

Chapter 6

Appendix A

Appendix B

Appendix C

Figures

Chapter 2

Chapter 5

Chapter 6

Figure 6.14: Comparison of ΔR values from Shetland, Ireland and Iceland for c.650-1000 AD, showing modern regional mean ΔR values for the British Isles and Iceland.

Figure 6.15: ΔR values for the later Holocene, within the study area, showing geographic location of individual contexts.

Appendix A

Figure A.1: The study area: Red circles show the location of sites sampled for modern coastal water and *Patella vulgata*. Atlantic Ocean waters are shown as red arrows and coastal water currents as grey arrows. The identifier codes for sites are given in Table A.2. Green circles show the location of four FRS water-monitoring stations (1: Scalloway, 2: Fair Isle, 3: Skapa Flow, 4: Lochmaddy).

Figure A.2: Red diamonds show measured average $\delta^{18}O_w$ values for sampled sites versus salinities calculated using the Austin and Inall, (2002) regional salinity: $\delta^{18}O_w$ mixing line for Scottish west coast waters. The green diamonds indicate measured average annual salinity versus the average $\delta^{18}O_w$ values measured in this study at FRS monitoring sites **LM** and **SF**. The Austin and Inall, (2002) mixing line is indicated on the graph.

Figure A.3: variation in $\delta^{18}O_w$ at sampled sites showing average variation in values at a single site. Shaded areas indicate different geographic areas (see Figure A.1), A: mainland Scotland; B: Outer Hebrides; C: Orkney Isles; D: Faroe Isles.

Figure A.4: variation in $\delta^{18}O_c$ of modern samples at sites showing average difference in values at a single site.

Figure A.5: Predicted equilibrium values of $\delta^{18}O_c$ for the sample sites showing the average measured value of $\delta^{18}O_c$ at each site. The dashed line indicates low temperature $\delta^{18}O_c$ based upon salinity measurements from three FRS monitoring stations and the Austin and Inall, (2002) salinity: $\delta^{18}O_w$ mixing line.

Figure A.6: Comparison of mean $\delta^{18}O_c$ measured at six sites from archaeological and modern *Patella vulgata* specimens. Modern values are shown in red and archaeological values in blue. The larger of the average variability on the archaeological and modern shell samples is shown.

Appendix B

Figure B.1: Location of Hrísheimar relative to the sites from which material for measurement was obtained during this thesis, showing modern surface circulation patterns of Atlantic (grey arrows) and Arctic (black arrows) derived currents.

Figure B.2: Location of Hrísheimar within the Mývatn area (northeast Iceland).

Chapter 1: Introduction

The overall aim of this thesis is to examine spatial and temporal characteristics of the ^{14}C marine reservoir effect (MRE) in the North Atlantic over the Holocene using paired terrestrial and marine samples from terrestrial archaeological deposits. To achieve this several specific study objectives have been identified (Table 1.1).

Specific objective:	**Achieved by:**
To produce relevant ΔR determinations of a high degree of precision and accuracy.	The development of a rigorous protocol for selection of samples for ^{14}C measurement and measurement of multiple individual samples at each site.
To examine spatial variability in ΔR	The selection of samples for measurement from a geographic range covering Western Ireland, Northern and Western Scotland and the Faroe Isles
To examine temporal variability in ΔR	The measurement of samples from archaeological deposits covering the past c.8000 years
To identify potential paleoenvironmental mechanisms for any observed variability in ΔR	Relating results to climate and oceanographic changes in paleoenvironmental records

Table 1.1: Specific study objectives.

Rationale for this study

Chronological information obtained *via* ^{14}C measurements has become invaluable in both paleoclimatic and archaeological research. However, where ^{14}C measurements are made on sample material that contains marine-derived carbon, the marine reservoir effect (MRE) is a crucial consideration. The MRE is a ^{14}C offset that exists at any point in time between the atmosphere and contemporaneous oceans and is the product of atmospheric and oceanic circulation and exchange mechanisms, for example the rate and nature of atmosphere-ocean gas exchange and ocean circulation, that are described in detail in Chapter 2. The net effect is that the specific ^{14}C activity of marine carbon is depleted relative to that of terrestrial carbon;

therefore, ^{14}C ages of marine carbon-containing samples appear greater than those of terrestrial samples, even though the two were formed at the same point in time. In order to obtain accurate ^{14}C ages when using samples containing marine carbon, the MRE must consequently be accounted for.

A MRE correction is available *via* a separate calibration curve, MARINE04 (Hughen *et al.*, 2004) for use with ^{14}C measurements on marine samples. The marine calibration curve is produced by modelling the oceanic response to solar-derived atmospheric ^{14}C variations and gives a time-series of the atmosphere-ocean ^{14}C offset for the global average surface and deep oceans. However, in any specific area of the ocean the MRE may deviate from the global average provided by MARINE04 and this deviation (known as ΔR), must be quantified by empirical measurement of local samples (Stuiver and Braziunas, 1993). At present, ΔR values are available for the modern (pre-bomb), global surface ocean from a large number of studies. These have been collated in the on-line Marine Reservoir Correction Database (Stuiver and Reimer, 1993; Reimer and Reimer, 2001; Reimer and Reimer, 2005) to provide regional corrections for specific modern ocean areas. As a first assessment, the ΔR for an area of surface ocean was assumed to be time-independent (Stuiver and Braziunas, 1993). However, there is a growing body of evidence that this is not necessarily the case (e. g. Monge Soares, 1993), particularly in areas of sensitive climatic and oceanographic boundaries. In these areas significant shifts in the climatic and oceanographic mechanisms that are thought to determine the size of ΔR values can occur over relatively short timescales. One such region is the North Atlantic, which is of key importance to our understanding of present and past climatic systems.

At present the distribution of regional mean ΔR values in the North Atlantic (see Figure 2.6 Chapter 2) appears to broadly reflect that of known climatic and oceanographic variables, such as the relative extent of Arctic and Atlantic-derived water masses. However, there is a lack of comprehensive or standardised studies of spatial variability to address this phenomenon. In addition, there is a lack of information concerning characteristics of the MRE through time in this climatically important region. The modern MRE in the North Atlantic is c.400 y, corresponding to a ΔR of c. 0 y. However, several studies have identified large variations in MRE, eg. increases of c. 400 yr at times of large climatic transitions in this region, such as the Younger Dryas cold interval (Bard *et al.*, 1994; Austin *et al.*, 1995; Haflidason *et al.*, 1995; 2000). Although there is evidence for MRE variability on a range of spatial and temporal scales,

there is an absence of a quantitative relationship between potential forcing mechanisms and the corresponding size of a MRE offset. One reason for this may be the level of temporal resolution to which the variables (including the MRE) can be studied. This thesis therefore uses a standardised methodology to investigate characteristics of the MRE in order to provide data on spatial and temporal scales that is currently lacking. The North Atlantic is a particularly suitable region for this type of study as it is a zone where variations in climatic and oceanographic variables could produce variation in the MRE on a variety of spatial and temporal scales. The aims of this study are particularly relevant due to the potential impact of MRE corrections upon correlations and comparisons of paleoclimatic and archaeological records. Here, interpretations of event chronologies and synchronicity often rest upon ^{14}C measurements that may be made using marine-derived samples. In addition to the importance of accurate and precise MRE assessments to construct chronologies, variability in the MRE within an area may integrate with both paleoclimatic and archaeological research in other ways. The nature of climatic and oceanographic mechanisms linked to observed MRE variations implies that changes in the MRE during a particular time period are likely to coincide with environmental changes within the wider North Atlantic. These paleoclimatic changes would also have impacted upon human communities and therefore could be reflected within the archaeological record.

Study structure

Past MRE determinations are made using ^{14}C measurements of paired samples of terrestrial and marine material from archaeological sites in the island belts of Northern and Western Scotland, the western and northern Scottish mainland coast, Western Ireland and the Faroe Isles. These are coastal regions exposed to the open currents of the North Atlantic that are sensitive to changes in patterning and intensity of North Atlantic oceanography. The samples are selected according to a strict protocol, developed within this study (see Chapters 3 and 4, and also Ascough *et al.*, in press) that has maximized the available precision and accuracy of MRE determinations, based on the paired sample approach.

Samples of carbonized cereal grain, hazelnut shell or terrestrial mammal bone were taken, along with marine mollusc shells from 30 archaeological deposits at 20 sites. These were prepared for ^{14}C measurement and the data analysed using the methodology outlined in Chapter 4. The mollusc shells were predominantly of the species *Patella vulgata* (common limpet), although

different species were used in 5 instances. To account for this potential source of variation, a sub-study was undertaken that examined the potential for species-dependant variations in mollusc shell ^{14}C content. The results are presented in Chapter 5 and ΔR determinations made within this study cover a calibrated interval of c. BC 6500 to c. AD 1400 (c. 7900 y), lying within the Holocene paleoenvironmental period of the last c.10, 000 y. These data show that it is possible to identify characteristics of the MRE using this methodology. The observed features of the data are considered in Chapter 6 and placed within the context of multi-proxy oceanographic and environmental change records. A range of climatic and oceanographic mechanisms is identified in current paleoenvironmental data that may be responsible for the variations in surface ocean ^{14}C content observed in this thesis. These include cooler climatic phases, such as the "8.2 kyr event", when the surface salinity of the North Atlantic appears to have been reduced by release of meltwater from the Laurentide ice-sheet (Alley *et al.*, 1997), and the Little Ice Age, a period of climatic cooling, identified in a range of global records, and within the North Atlantic. Warmer phases that may be linked with periods represented by data from this thesis include a period of minima in ice-rafted debris (Bond *et al.*, 1997), and faster rate of overflow of deep water across the Iceland-Scotland ridge (Bianchi and McCave, 1999) at c.2000 BP, and the "Medieval Warm Period" when there is evidence for increased influx of the North Atlantic Current to the study area.

Wider study implications

This research is designed to produce data that will allow refinement of the MRE correction accuracy available for paleoenvironmental and archaeological investigations within the study area. In addition, it is recognised that it will also result in the production of a suite of ^{14}C measurements on constrained terrestrial material at a range of important archaeological sites. It is anticipated that the outcomes of this study will benefit several disciplines including the fields of ^{14}C, paleoenvironmental and archaeological research, due to the integrated nature of the results. The anticipated higher resolution MRE data that should be available through this study ought to lead to a better understanding of the nature and mechanisms of the effect itself, and in Chapter 7, future research directions on the basis of this study are suggested. The correction values produced through this work can be used with the available calibration programs, such as OxCal (Bronk-Ramsey, 1995; 2001) and CALIB (Stuiver and Reimer, 1993) to correct marine samples from specific time periods within the study area.

Chapter 2: Scientific context

2.1 ^{14}C: production and global distribution

The primary cosmic radiation that enters the Earth's atmosphere consists of charged particles arriving from outside the solar system (galactic cosmic rays) and a less energetic component generated by the sun (solar cosmic rays). The particles lose energy in the atmosphere by ionization and nuclear interactions with gaseous molecules and atomic nuclei to generate a cascade of secondary particles, including neutrons with an energy range c.10 MeV to 100keV, known as fast neutrons. Fast neutrons lose energy in elastic and inelastic nuclear collisions, eventually becoming "thermal" neutrons that are in vibrational equilibrium with atmospheric gases (Gosse and Phillips, 2001). Absorption of thermal neutrons by nuclei produces atomic isotopes, and when this reaction occurs with nitrogen atoms (^{14}N) in the upper troposphere/ lower stratosphere the result is radiocarbon (^{14}C), an unstable isotope of carbon that decays by beta emission with a half-life ($t_{1/2}$) of 5730 ± 40 years (Godwin, 1962):

$$^{14}N + n \rightarrow {}^{14}C + p$$

(Equation 2.1)

Following production of atmospheric ^{14}C, the isotope is quickly oxidised to ^{14}CO and further with the hydroxyl radical to $^{14}CO_2$:

$$^{14}CO + OH \rightarrow {}^{14}CO_2 + H$$

(Equation 2.2)

The global average production rate of ^{14}C is c.6 x 10^7 atoms cm^2 yr^{-1} (Finkel and Suter, 1993) which with the ^{14}C atomic mean life of 8270 years ($t_{1/2}$/ln2), means that the ratio of $^{14}C/^{12}C$ in global carbon reservoirs is c.10^{-12} (Stuiver and Braziunas, 1993). Of the total global carbon budget, approximately 1.1% is composed of the ^{13}C stable carbon isotope, while the vast majority of carbon in current circulation is the stable isotope ^{12}C.

The cosmogenic production rate of ^{14}C is dependant upon altitude as this determines the density of ^{14}N target nuclei, and upon latitude due to the variable intensity of the Earths magnetic field. At lower latitudes the magnetic field lines are perpendicular to the velocity of incoming particles and increase deflection of the low-energy GCR component that is

responsible for the majority of ^{14}C production (Rose *et al.*, 1956, Muzikar *et al.*, 2003). Production rates are therefore greatest in the polar regions of the stratosphere, although the rapidity of atmospheric circulation, and the fact that ^{14}C remains within atmospheric CO_2 for several years after production, ensures that relatively homogenous global atmospheric distribution of newly produced ^{14}C is achieved within a few years (Levin *et. al.*, 1980). The mean residence time of CO_2 in the atmospheric reservoir is on the order of 5 yr (Levin and Hesshaimer, 2000) following which, biological and chemical transport mechanisms of the short-term carbon cycle (operating on $<10^5$ years) rapidly distribute ^{14}C throughout the atmospheric, terrestrial and oceanic carbon reservoirs.

The present atmospheric CO_2 inventory is c.750 GtC (1 GtC = 10^9 metric tons C or 10^{15} g C), of which c.20% is annually exchanged with the biosphere, atmosphere, and ocean surface (Schimel *et al.*, 1995).The uptake of CO_2 by these reservoirs is determined by exchange rates and factors of internal mixing, which produce variations in the spatial and temporal distribution of C within each reservoir. These variations are lowest in the atmosphere, which is well-mixed with respect to C (and ^{14}C) relative to the biosphere and oceans. The oceanic reservoir presently exchanges c.90 GtC annually with the atmosphere and contains the largest amount of C that is in circulation over timescales relevant to the ^{14}C mean life (see Figure 2.1).

The constant cosmogenic production of ^{14}C in the atmosphere, coupled with a well-defined radioactive decay rate and rapid, universal global distribution make the isotope highly suitable for use in a range of scientific applications. The time (t) since a sample ceased to exchange ^{14}C with the global carbon reservoir can be determined by relating the remaining (measured) ^{14}C content of a sample to its original level of ^{14}C (i.e. before exchange ceased). Using the known half-life and radioactive decay equation, the amount by which the sample ^{14}C content has decreased is translated to a ^{14}C "age". In principle this makes possible the absolute age measurement of any organic carbonaceous sample material that has been formed within the past c.50 ky. This time range is dictated by both the ^{14}C half-life and the sensitivity of measurement equipment to detect the very low levels of ^{14}C remaining in ancient samples. ^{14}C age measurement is currently used in applications including hydrology, oceanography, geochemistry and archaeology and has over the past 50 years revolutionized our understanding of processes and events within these fields.

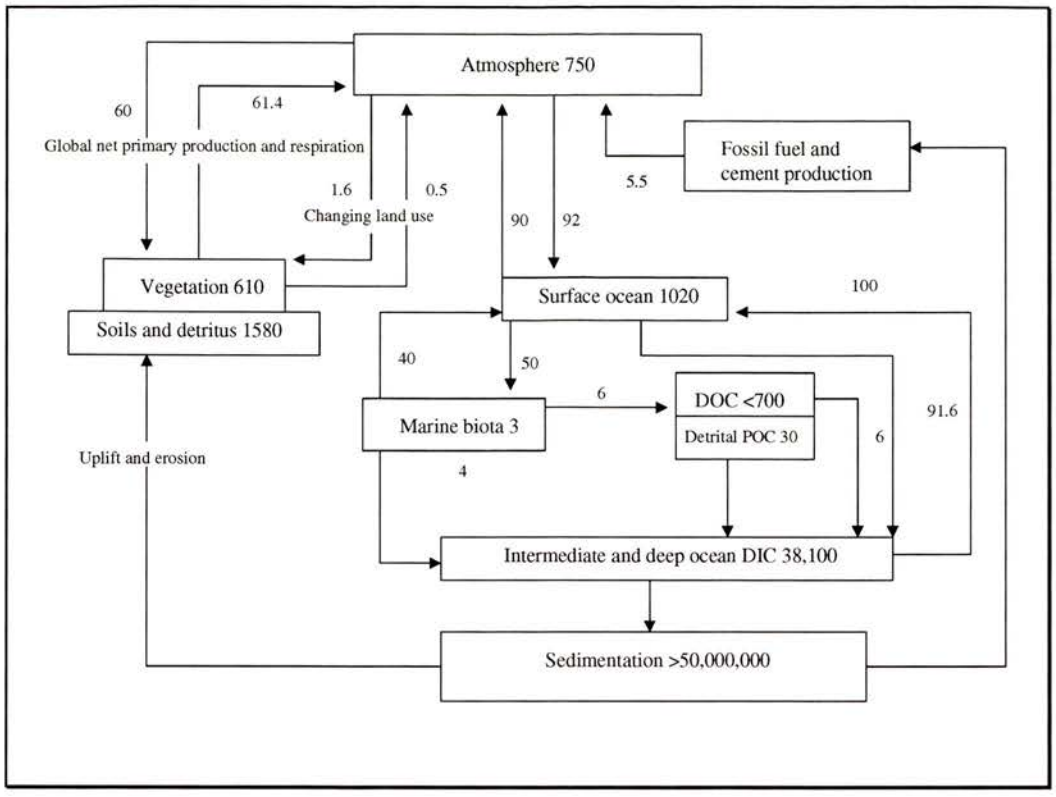

Figure 2.1: Estimates of reservoir volumes (in GtC), and fluxes (GtC yr^{-1}) of the global biogeochemical cycle of carbon. Adapted from Schimel *et al.*, (1995).

2.2 Measuring the ^{14}C content of a sample

Measurement of the amount of ^{14}C in a sample is achieved either indirectly, by counting the number of β emissions per unit time from a known sample weight (radiometric counting method), or directly by measuring the number of ^{14}C atoms in a sample relative to the number of ^{12}C or ^{13}C atoms using accelerator mass spectrometry (AMS). The sample ^{14}C content is commonly reported as an absolute (specific) ^{14}C activity level (^{14}A) in disintegrations per minute (dpm) per gram of carbon (Mook and Van der Plicht, 1999). The low $^{14}C/^{12}C$ ratio of modern carbon (10^{-12}) means that a high level of instrument sensitivity is required in both radiometric and AMS measurement techniques, and that prior to measurement the carbonaceous material within the sample is converted to a compound with a high stoichiometric carbon content (e.g. benzene (C_6H_6) for liquid scintillation counting or pure carbon (graphite) for AMS).

2.2.1 Radiometric measurement

Radiometric measurement involves detection of the product of radioactive decay (β particles) either through ionisation of a gas to produce an electrical pulse, known as gas proportional counting (GPC) or through interaction with a liquid scintillator to produce a light flash in liquid scintillation counting (LSC). In GPC the sample is usually converted to CO_2, CH_4 or C_2H_2 which then also constitutes the inert counting gas. In LSC, the sample is converted to benzene (C_6H_6), which acts as both the sample and the solvent for the scintillator (fluor particles), that are stimulated by the transmission of energy from β-decay events to emit light, which is converted to an electrical pulse for measurement. In radiometric and AMS measurement the level of precision (described by the error term σ) associated with a measurement of sample ^{14}C content is related to the number of observed events (N) over the period of measurement time using Poisson statistics, where $\sigma = \sqrt{N}$ (McNichol *et al.*, 2001). Therefore if N = 100, σ = 10 (10% of N), and the value of σ is reduced by increasing the number of observed events. In this way, the length of time required to achieve a given level of measurement precision for a sample is a function of sample size and ^{14}C content.

Although 1g of modern carbon contains c.6 x 10^{10} ^{14}C atoms, the half life of the isotope means that the activity (^{14}A) of this sample is on the order of c.15 dpm (Ehmann and Vance, 1991). To achieve 1% precision with a radiometric measurement of ^{14}C activity using c.3g modern carbon would therefore require c.4 hours to perform the necessary c.10,000 counts (Trumbore, 2000). As c.1% of the sample ^{14}C atoms decay over 80 years (Aitken, 1990), the counting times required for specific precision levels increase with sample age, meaning that an age limit exists on the measurement of ancient samples with very low ^{14}C activity levels. When the sample ^{14}C activity is indistinguishable from the detector background it is then no longer possible to accurately assess sample ages. This places an upper age limit for sample measurement of c.50 kyr for both radiometric and AMS systems (Muzikar *et al.*, 2003) although samples up to 70 kyr may be analysed through isotopic enrichment and high sensitivity measurement (Grootes *et al.*, 1975; Long and Kalin 1992). Another limitation with very old samples or samples that consist of a very low mass of material is the large proportional impact upon the measured sample ^{14}C activity of contamination with extraneous carbon.

2.2.2 Accelerator Mass Spectrometry (AMS)

Because of the extended counting times and the sufficient (gram) weights of carbon required to achieve acceptable levels of measurement precision using the radiometric technique, the range of samples that can be analysed is limited. This prohibits the measurement of samples which have a low inherent mass, or where the available material for dating is limited, as in the case of rare or valuable objects. An alternative method of sample measurement is to use accelerator mass spectrometry (AMS), which detects individual ^{14}C atoms in a sample by atomic weight (A). Using mainly tandem electrostatic accelerators, AMS systems are able to measure both low isotopic abundances (c.10^4 atoms), and ratios of radioactive to stable isotopes of the order 10^{-15} (Elmore and Phillips, 1987; Fifield, 1999). The main advantages of AMS are the reductions in both count times and required sample size relative to radiometric analysis. Equivalent measurement precision levels of 0.2-0.5% can be achieved using milligram quantities of carbon compared to grams and count times of the order of minutes as opposed to days (Tuniz et al., 1998). The lower sample masses required mean that more rigorous pre-treatment processes, which result in greater loss of sample structure, are possible and also that samples of inherently low weight material, such as pollen grains or foraminifera can be measured (Brown *et al.*, 1989). This has had a revolutionary impact in archaeological and palaeoenvironmental studies, enabling analysis of individual organisms (e.g. mollusc shells, cereal grains), and of µg quantities of rare artefacts.

AMS differs from standard mass spectrometry (MS) in the energies to which ions are accelerated. In MS these are on the order of 10^3 electron volts (KeV), whereas AMS can achieve energies of 10^6 electron volts (MeV). The higher energies allow the measurement of isotopic ratios to a factor of 5 lower than using conventional MS, which is essential to separate isotopes such as ^{14}N which have a very low mass difference from ^{14}C and would not be isolated using MS (Tuniz *et al.*, 1998). The use of AMS allows unwanted nuclides to be rejected without reducing the ^{14}C count rate to unacceptable levels, using multiple mass selection stages to select particles with unique mass-to-charge and energy-to-charge ratios (Muzikar *et al.*, 2003). The importance of separating particles with a low mass difference to ^{14}C means that a central feature of AMS is the formation of negative ions by sputtering with Cs^+ ions as the sample is introduced to the system, displacing sample atoms and ions (C^-) by collision (Middleton *et al.,* 1983, Finkel and Suter, 1993). The instability of the main negative isobaric ions of ^{14}C (including $^{14}N^-$) ensures that high measurement precision can be achieved in a limited time, and means that the isotope can be measured using relatively low energies (c.2-3 MV) (Purser *et al,* 1981; Tuniz *et al.,* 1998).

The negative ion beam is mass analysed before acceleration, discriminating against higher and lower mass values to select ions of masses 12, 13 and 14 (McNichol *et al.*, 2001). The beam is then pre-accelerated to focus at the central terminal and stripper canal, before being accelerated to a positive high voltage terminal where multiple electrons are stripped as the beam passes through a carbon foil or a gas. Stripping coverts negative atomic ions to positive ions and the process dissociates molecular ions to positively-charged atoms. During stripping, ionic molecules with a mass close to that of ^{14}C (e.g. $^{12}CH_2^-$) are dissociated and the fragments are then removed in later analysis (Muzikar *et al.*, 2003). These particles are then repelled by the negative terminal to the other end of the accelerator, where scattered particles, molecular fragments and unwanted charge states are removed with magnetic and electrostatic analysers (a velocity or wein filter may also be used), the number and arrangement of which depends upon the individual accelerator (Elmore and Phillips, 1987). The electrostatic analysers are necessary to remove particles that have a different mass, but the correct mass-energy product to pass the magnetic analyser. Using the principle that the rate of energy loss by matter is determined by atomic number (Z), ions are selected by charge state (q) and energy (E), and subsequently diverted to a detector (^{14}C) or Faraday cups (^{12}C and ^{13}C). Each of these receives a different C isotope, determined by the differing radii of curvature in path of travel of ^{12}C, ^{13}C and ^{14}C. The ^{14}C ions are individually counted in either a solid surface barrier detector or a gas ionization chamber. Because only a fraction of sample carbon atoms are sputtered to negative ions and ions may be lost in the journey between the ion source and detector, it is necessary to measure the ratio of unstable to stable isotopes in the measured sample, and it is the measured ratio which is used to calculate a ^{14}C age (McNichol *et al.*, 2001; Muzikar *et al.*, 2003). The $^{12}C/^{13}C$ beam is measured as an electrical current in the Faraday cups (Fifield, 1999) and the charge is converted to pulses using Coulombs law and the charge of an electron to calculate the sample $^{14}C/^{12}C$ or $^{14}C/^{13}C$ ratio (McNichol *et al.*, 2001).

The efficiency of AMS systems to measure sample ^{14}C content is limited by the ratio of total ^{14}C detected by a measurement to the actual amount of ^{14}C that the sample contains. Several factors that determine the size of this ratio occur outside the measurement system and include contamination of the sample during laboratory processing, as $^{14}CO_2$ may be adsorbed onto any surface, including water, and dissolves readily in basic solutions used in pre-treatment processes (Tuniz *et al.*, 1998). The lower sample volumes used in AMS analysis mean that a relatively small amount of contamination is required to produce a significant shift in measured sample isotopic ratio, therefore the procedures used to limit contamination,

both in the field and laboratory, must be rigorous. To account for measurement variability induced by these factors, a "process blank" is often measured at the same time as the sample. This is a sample of material containing no detectable ^{14}C that has undergone identical chemical processing techniques as the sample prior to measurement (McNichol *et al.,* 2001).

Factors affecting measurement efficiency that occur within the AMS system include the efficiency of negative ion production at the sputter source, the yield of selected charge state and the transmission of ions through the accelerator and analysers (Elmore and Phillips, 1987). In addition, linear and non-linear fractionation may occur within the system during the stripping process or from the action of stray magnetic fields. The efficiency of sample measurement at the detector is affected by the detection of events not derived from sample ^{14}C that are indistinguishable from sample ^{14}C content, (the background). These events can arise from cross contamination of samples, contamination with modern ^{14}C at the ion source, or from detection of molecular ions, isotopes and isobars that have remained unresolved by the system. It is possible for ions with different masses, energies or charges than the ^{14}C ion to reach the detector due to the alteration of their energy/charge ratios by collisions (e.g. with residual gases) in the system, meaning that a good vacuum within the apparatus is essential to measurement efficiency. The formation of stable hydride molecules (e.g. ^{13}CH, $^{12}CH_2$) is a major source of isotopic background (Tuniz *et al.,* 1998; Fifield, 1999).

Each AMS measurement is produced by alternate or simultaneous measurement of the detector count (^{14}C) and the electrical current (^{12}C and / or ^{13}C) of the sample and similar measurements on a standard of known isotopic ratio, which allows normalisation and correction for internal system fractionation (Elmore, 1982). The background of the system is measured by analysis of samples that contain no ^{14}C (blanks). These are usually geological-age carbon, and together with the level of sample contamination and efficiency of ion beam production, determines the detection limit of AMS, which is currently similar to radiometric counting.

The error on a reported AMS measurement (1σ) is an accumulation of statistical and systematic errors. The latter determine measurement accuracy and include the degree of sample contamination, fractionation during processing and variability in measurement accuracy of standards and unknown samples (Tuniz *et al.,* 1998). Accuracy is improved by repeated measurement of each sample to determine variations in efficiency factor ratios (Seguin *et al.,* 1994). The statistical error, together with the degree of measurement reproducibility, determines the precision achieved. The statistical error is a combination of

errors on measurement of the sample, standard and blanks, and is derived from random variation in sample sputtering, transmission and detection of ions (Tuniz *et al.*, 1998).

2.3 Calculation of ^{14}C ages from sample measurements

2.3.1 Correcting for isotopic fractionation

The natural physical and biochemical processes that transfer C between compounds in global reservoirs often preferentially use one of the C isotopes, resulting in a fractionation effect that is a function of atomic mass. In plants that use the Calvin-Benson photosynthetic pathway (C3 plants), photosynthesis favours the uptake of ^{12}C, producing a depletion in ^{14}C relative to coeval atmospheric isotopic ratios. In contrast, gaseous exchange of CO_2 at the atmosphere-surface ocean interface results in an enrichment of ^{14}C within ocean bicarbonate (Aitken, 1990). Artificial fractionation of a sample is also possible in a laboratory prior to ^{14}C measurement through incomplete conversion of sample material during a preparation stage.

The process of isotopic fractionation means that measurements of specific ^{14}C activity (^{14}A) in a sample require a correction, as two samples formed at the same point in time but which have been fractionated to different extents will exhibit different values of ^{14}A, and therefore will have different calculated ^{14}C ages. For this reason, the ^{14}C activity values of all measured samples are normalised relative to an international standard value of $\delta^{13}C = -25‰$, with respect to VPDB (Vienna Peedee Belamite) (Gonfiantini, 1984; Coplen, 1994). The sample ^{13}C content with respect to the international standard is generally expressed in parts per mille (‰) due to the small quantities involved and is quantified by measuring the sample $^{13}C/^{12}C$ ratio, a procedure which can be performed during measurement of a sample with AMS ("online" values) or separately using a standard isotope ratio mass spectrometer ("offline" values). The sample isotopic composition ($\delta^{13}C_s$) is then expressed as the difference in ^{13}C content between the measured sample and the VPDB standard:

$$\delta^{13}C_s = \left(\left(\frac{^{13}R_s}{^{13}R_{VPDB}} \right) - 1 \right) \times 1000$$

(Equation 2.3)

$\delta^{13}C_s = \delta^{13}C‰$ of the measured sample

$^{13}R_s = ^{13}C/^{12}C$ ratio of the measured sample

$^{13}R_{VPDB} = ^{13}C/^{12}C$ ratio of the VPDB standard

The measured sample ^{14}C activity is then normalised to -25‰ by using the value of $\delta^{13}C_s$ to calculate a fractionation factor for the measured sample (FF_s):

$$FF_s = \left(\frac{1 + \left(-25/10^3\right)}{1 + \left(\delta^{13}C_s/10^3\right)} \right)^2$$

(Equation 2.4)

In the above equation, the factor of 2 is required as according to international convention, the $^{14}C/^{12}C$ fractionation in the sample is estimated as double that of the $^{13}C/^{12}C$ fractionation because of the greater atomic mass of ^{14}C. In AMS analysis, the sample $^{14}C/^{13}C$ ratio may be measured instead of the $^{14}C/^{12}C$ ratio. When the $^{14}C/^{13}C$ ratio is used, the equation above becomes:

$$FF_s = \left(\frac{1 + \left(-25/10^3\right)}{1 + \left(\delta^{13}C_s/10^3\right)} \right)$$

(Equation 2.5)

The range of $\delta^{13}C_s$ values varies widely depending upon the sample material, as shown by the general values in Table 2.1 below.

Material	**$\delta^{13}C$ value (‰)**
Wood, peat, C3 plants	-25 ± 3
Bone collagen	-20 ± 2
Freshwater plants	-16 ± 2
Arid zone plants	-13 ± 2
Marine plants	-12 ± 2
Maize	-10 ± 2
Atmospheric CO_2	-9 ± 2
Marine carbonates	0 ± 3

Table 2.1: Estimated $\delta^{13}C$ values for a range of typical sample materials (from Aitken, 1990).

2.3.2 Calculating ^{14}C age from measured sample ^{14}A

The ^{14}C age of a sample (t), is based on the measured specific ^{14}C activity of the sample ($^{14}A_s$) and is calculated by:

$$t = \frac{1}{\lambda} \ln \left(\frac{^{14}A_0}{^{14}A_s} \right)$$

(Equation 2.6)

λ = the ^{14}C decay constant (derived from the ^{14}C half life ($t_{1/2}$))
$^{14}A_0$ = the ^{14}C specific activity of the sample at t = 0 (i.e.: the sample ^{14}C activity at point of death/formation).
$^{14}A_s$ = the present measured ^{14}C specific activity of the sample

The ^{14}C decay constant λ is calculated according to:

$$\lambda = \frac{\ln 2}{t_{1/2}}$$

(Equation 2.7)

In ^{14}C age calculation, the value of 5568 years is used for $t_{1/2}$. This value corresponds to an early assessment for $t_{1/2}$ of 5568 ± 30 years calculated by Libby *et al.* (1949), which was later corrected to 5730 ± 40 years (Godwin, 1962). Because ^{14}C ages were calculated for a large number of samples before the correction, the Libby half-life continues to be used in age calculations to enable comparison and consistency with the large number of early ^{14}C measurements. The 3 % greater value of 5730 ± 40 years is used for specific circumstances, such as the calculation of geochemical mass balances (Stuiver and Polach, 1977).

As shown in Equation 2.6, to calculate a ^{14}C age (t), it is necessary to know or estimate a value for $^{14}A_0$. This quantity is the initial ^{14}C activity that the sample would have had when it last exchanged ^{14}C with the atmospheric reservoir (i.e. at the time of death or formation). Because it is not possible to directly measure the initial ^{14}C activity of a sample, an international standard value, originally based on the ^{14}C activity of tree rings grown in equilibrium with atmospheric CO_2 in 1890 AD is used instead. The year 1890 AD was chosen as the wood was judged not to be significantly affected by the fossil-fuel emissions that subsequently altered atmospheric ^{14}C content. The tree ring ^{14}C activity was then age

corrected to 1950 AD to provide a value for atmospheric ^{14}C activity in 1950 AD. ^{14}C ages are commonly reported in years "before present" (BP), and the use of this standard value means that "present" is taken to be 1950 AD (Stuiver and Polach, 1977). Despite the fact that ^{14}C measurements are now performed after 1950 AD, there is no need to decay correct ages, provided both the sample and standards are reported relative to 1950 AD. This is because the ^{14}C activity of both the sample and standards have been decaying at the same rate since this time.

The value of $^{14}A_0$ is obtained from a modern standard material with a ^{14}C activity that equates to that of wood samples from 1890 AD, judged to be the last year when concentrations of atmospheric ^{14}C represented a "natural" level. The current reference material provided by the National Institute of Standards and Technology for ^{14}C age calculation is Oxalic acid II (OXII), obtained from a 1977 sugar beet molasses harvest, and the accepted standard reference activity is 0.7459 times the specific activity of OXII ($^{14}A_{OXII}$), after normalisation to $\delta^{13}C$ = -25‰ (Donahue *et al.*, 1990).

2.3.3 Using radiometric/AMS assessments of sample fraction modern carbon

The value normally used in age calculation using either radiometric or AMS measurements is the fraction modern (F) of a sample, where ^{14}C age (t) is:

$$t = \frac{1}{\lambda} \ln\left(\frac{1}{F}\right) = 8033 \ln\left(\frac{1}{F}\right)$$

(Equation 2.8)

The value of F for a sample is the ratio of the measured ^{14}C activities for the sample ($^{14}A_s$) and the OXII standard ($^{14}A_{OX}$), where both have been normalised to $\delta^{13}C$ = -25‰ ($^{14}A_{sN}$ and $^{14}A_{OXN}$ respectively):

$$F = \frac{^{14}A_s}{^{14}A_{OXN}}$$

(Equation 2.9)

Where the sample ^{14}C activity has been measured as a ratio (i.e. with AMS), this may be converted to a sample fraction of modern carbon by comparison with the measured ratio for the standard, corrected to modern carbon (McNichol *et al.*, 2001).

2.3.4 Conventional ^{14}C age (CRA) of a sample

The ^{14}C age of a sample produced using the above methodology is known as a conventional radiocarbon age (CRA), meaning that certain criteria are fulfilled, namely:

1. An appropriate standard reference material (currently OXII) has been used during measurement
2. All measured sample and standard ^{14}C activities (radiometric) or ratios (AMS) have been normalised to $\delta^{13}C = -25‰$
3. The Libby half life (5568 years) has been used in calculation
4. The age is reported in years before present (BP) where present is 1950 AD

The CRA has an associated error term reported at ± one sigma (σ) which is a cumulative error of internal laboratory errors, systematic offsets and errors on measurement of the reference standard, background blanks and unknown ^{14}C activities or ratios, and the sample $\delta^{13}C$ measurement. The error is derived by the square root of the sum of all squared individual errors. Together, the CRA and error describe a Gaussian curve representing a distribution that has a specified probability of containing the actual sample age. The CRA of a sample can be compared with other sample CRA's, but in order to place the sample on a calendar timescale, the CRA must be calibrated to convert to calendar years.

2.4 Calibrating sample ^{14}C ages: Determining a calendar age range

In using the OXII standard to provide a known value for the $^{14}A_0$ of all samples an assumption is made that the $^{14}A_0$ of all samples was originally equivalent. As the value of $^{14}A_0$ is taken to represent the global atmospheric reservoir ^{14}C activity ($^{14}A_{atm}$), it follows that this activity is also assumed to have remained constant throughout time. However, it is now known that over time the specific ^{14}C activity of the atmosphere has varied by significant amounts in a non-systematic way, meaning that ^{14}C "years" do not correspond to actual calendar years (Pilcher, 1991). The level of $^{14}A_{atm}$ at a point in time is described by the term

$\Delta^{14}C_{atm}$, which represents the per mille deviation of $^{14}A_{atm}$ from the value of $^{14}A_0$ (i.e. OXII standard activity corrected for age and fractionation effects) (Stuiver and Polach, 1977). The past value of $\Delta^{14}C_{atm}$ can be quantified with measurements of samples for which the calendar age is known, including sequences of tree-rings, where the calendar age of a sample (established with dendrochronology) can be compared with its ^{14}C age.

If $\Delta^{14}C_{atm}$ had remained at a constant level over time, the ^{14}C activity of a tree-ring sequence would decrease linearly with increasing calendar age as ^{14}C decay occurred, and a direct conversion of measured ^{14}C age versus calendar age would be possible. However, the record of $\Delta^{14}C_{atm}$ present in tree rings shows that atmospheric levels of ^{14}C activity have fluctuated, with regular long and short term deviations that have both sporadic and cyclical frequencies (Neftel *et al.,* 1981). The trend of ^{14}C versus calendar ages is consequently non-linear, and a single value of ^{14}C activity measured in a sample can correspond to more than one calibrated (cal) calendar age range. The rate at which $\Delta^{14}C_{atm}$ fluctuations have occurred is not constant, and where levels have risen or fallen rapidly, two samples actually separated by decades in calendar years can have ^{14}C ages that differ on a century scale due to their significantly different values of $^{14}A_0$. Another feature of the atmospheric calibration curve is the presence of "plateaus", where a period of steadily rising $\Delta^{14}C_{atm}$ offsets the reduction in the ^{14}C activity of samples that is due to radioactive decay through time. In this instance a range of samples formed at different points over a long calendar time period will have had increasing values of $^{14}A_0$ through time and their ^{14}C ages are indistinguishable (Figure 2.4).

The changes in $\Delta^{14}C_{atm}$ over time are attributed to both variation in atmospheric ^{14}C production rates and the global redistribution of ^{14}C throughout various reservoirs, resulting from natural and anthropogenically-driven processes (McCormac *et al.,* 1998). As the ^{14}C age of a sample is often interpreted as part of research that compares and correlates processes within a chronological framework, it is necessary to account for the $\Delta^{14}C$ fluctuations that produce varying values of $^{14}A_0$, and any ^{14}C age must be calibrated if its calendar age is to be known. The following section discusses first the various mechanisms responsible for changes in $\Delta^{14}C‰$ and then the construction and application of the atmospheric calibration curves currently used to convert ^{14}C ages to a calendar scale.

2.4.1 Mechanisms for variation-Natural ^{14}C production rate change

The rate at which ^{14}C is produced in the atmosphere depends upon variations in the strength of the primary cosmic radiation flux (PCR) that reaches the Earth. The PCR is derived from various sources including those external to the solar system, known as galactic cosmic rays (GCRs) and from the sun, known as solar cosmic rays (SCRs). SCRs incorporate a high energy component with a flux of c.3 x 10^8 protons cm^{-2} sec^{-1}, and a lower energy component with a flux of c.100 protons cm^{-2} sec^{-1}, where the lower energy rays comprise an ionized plasma, known as the solar wind, that displays a high degree of short-term variation in particle velocity and density (Korff and Mendell, 1980; Tuniz *et al.,* 1998). Variations in the overall SCR flux are proportional to rates of solar activity, (increasing at solar maximum) and are positively correlated with sunspot incidence. The SCR flux is responsible for a more minor component of total annual ^{14}C production than that generated by the action of galactic cosmic rays (GCRs originating from beyond the solar system (Lal, 1991). Although the average GCR flux is c.3 protons $cm^{-2}s^{-1}$, the rays have energies far in excess of the SCR flux, typically up to c.100 GeV (Reedy, 1987).

Because the PCR's consist of charged particles, the rays are deflected from the Earth's atmosphere by magnetic fields generated by the Sun and from the Earth itself. The degree of deflection occurs in proportion to the strength of the magnetic fields, so that when field strength is high the intensity of the PCR flux reaching the Earth is reduced and global atmospheric ^{14}C production rates fall. As PCRs travel towards the Earth they are first modulated by the solar magnetic field, which extends at least 10^{10} km from the sun and is modulated by variations in solar plasma output that result from solar events such as geomagnetic storms (Lal and Peters, 1967).

Variations in solar activity rates also alter the SCR flux generated from the sun, which itself carries a magnetic field and therefore further modulates the GCR flux. This occurs at a distance of 60-100 astronomical units (AU, where 1 AU = c.1.5 x 10^8 km) from the Earth as GCRs enter the heliosphere and undergo electrostatic and electromagnetic interactions with the solar magnetic field and SCRs. Although the GCR flux has remained constant on average (to within c.10%) over the past several million years (Vogt *et al.,* 1990), the portion of GCRs entering the Earths atmosphere is highly modulated by the solar cycle. As it is the lower energy portion of the GCR spectrum that is most strongly attenuated by solar activity, the reduction in global atmospheric ^{14}C production rates is greatest at the high latitudes, which receive the largest proportion of low energy GCR rays. Because these regions are also those

where the highest global production rates of ^{14}C are located, the overall effect is to enhance solar modulated changes in $\Delta^{14}C‰$ (Cerling and Craig, 1994).

Atmospheric ^{14}C production rates therefore vary inversely with solar activity rates which are historically quantified by observation of the frequency of solar features such as sunspot number, and beyond this timeframe by records of cosmogenic isotope production (Pomerantz and Duggel, 1974; Lal, 1988; Masarik and Beer, 1999). Solar activity is strongly linked to the high frequency wiggles (with amplitudes reaching 2-2.5‰) that occur in the tree-ring record of $\Delta^{14}C_{atm}$ on the order of calendar decades to centuries (Castagnoli and Lal, 1980, Stuiver and Quay, 1980; Damon and Linick, 1986). Sporadic solar events overlie a series of cycles in solar activity which have both short (e.g. 11-yr) and long-term (e.g. 200 yr) periodicity (Cerling and Craig, 1994) and appear to have induced regular ^{14}C age fluctuations over significant timescales. The 200-yr solar cycle is correlated with $\Delta^{14}C_{atm}$ variations that produce ^{14}C age changes on the order of c.100 years over the majority of the Holocene period (Suess, 1986; Neftel *et al.,* 1981; Damon and Linick, 1986). In contrast, a maximum variability of c.20 ^{14}C yr between single ^{14}C years has been calculated to result from the 11-yr solar cycle, translating to an overall modulation of c.8 ^{14}C yr around the long-term average $\Delta^{14}C_{atm}$ trend (Stuiver *et al.,* 1998a).

Upon reaching the Earth's atmosphere the PCR flux is further modulated by the strength of the Earth's magnetic field, which shields against the charged particles according to their individual momentum-to-charge ratio (rigidity) and angle of incidence. For each angle of travel with respect to the Earth, there is a critical rigidity value below which the particles cannot penetrate into the atmosphere. Because the Earth's magnetic field strength varies with latitude the value of this critical rigidity decreases as geomagnetic latitude increases which is why the present location of highest atmospheric ^{14}C production rates is at the poles (Desilets and Zreda, 2001). Changes in the magnitude and direction of the geomagnetic field over time (e.g. Wagner, 1988; Guyodo and Valet, 1999; Frank, 2000) have modulated the PCR flux entering the Earth's atmosphere, and produced production rate variations that are inversely proportional to the geomagnetic field strength (Damon *et al.,* 1978, Suess, 1986). Varying dipole field strength appears to be the dominant cause of a long-term sinusoidal pattern in the tree-ring record of $\Delta^{14}C_{atm}$, (upon which the shorter term solar-induced cycles are superimposed), which has a period of c.9 ^{14}C ka and peak-to-peak magnitude of c.10% (Castagnoli and Lal, 1980; Stuiver and Quay, 1980). The geomagnetic influence upon production rates is primarily observed in long term $\Delta^{14}C_{atm}$ change because of the extended timescale over which variation of geomagnetic dipole moment occurs, coupled with the

lagged response of the global carbon cycle system to $\Delta^{14}C_{atm}$ variation. An extended time period of long-term field strength change (c.1000 years) is therefore required to effect significant changes in atmospheric $\Delta^{14}C_{atm}$ and the production of a new global equilibrium state (Aitken, 1990; Tuniz *et al.*, 1998).

2.4.2 Human-induced changes in $\Delta^{14}C_{atm}$

Large changes in $\Delta^{14}C_{atm}$ have also been produced as a result of human action that introduces difficulties in age calculation for samples of recent material. These include alteration of $\Delta^{14}C_{atm}$ through the input of CO_2 with a significantly different ^{14}C activity to the coeval atmosphere, and by alteration of atmospheric ^{14}C production rates through the input of large amounts of ^{14}C-forming neutrons. The former is the result of industrial and domestic combustion of fossil fuels that release large amounts of ancient carbon (CO_2) that contains a negligible ^{14}C content and has resulted in a dramatic fall in $\Delta^{14}C_{atm}$ over the past c.100 calendar y, known as the "Suess effect" (Suess, 1955). The precise magnitude of the effect is unknown and therefore difficult to accurately account for in affected samples, as quantification has been complicated by simultaneous helio and geomagnetic variations (Stuiver, 1978; McCormac *et al.*, 1998).

An opposite effect to the Suess effect has occurred as a result of the atmospheric detonation of nuclear weapons in the 1950s and 1960s, prior to the Nuclear Test Ban Treaty in 1962 (Figure 2.2). The detonations produced large numbers of neutrons that subsequently generated an estimated 630 x 10^{26} atoms of atmospheric ^{14}C, leading to a sharply elevated levels of $\Delta^{14}C_{atm}$ (Hesshaimer *et al.*, 1994; Levin and Kromer, 1997; Levin and Hesshaimer, 2000). The large bomb-induced disequilibrium of ^{14}C between atmospheric, oceanic and biospheric reservoirs has proved very useful as a transient tracer in studies of global carbon transfer processes.

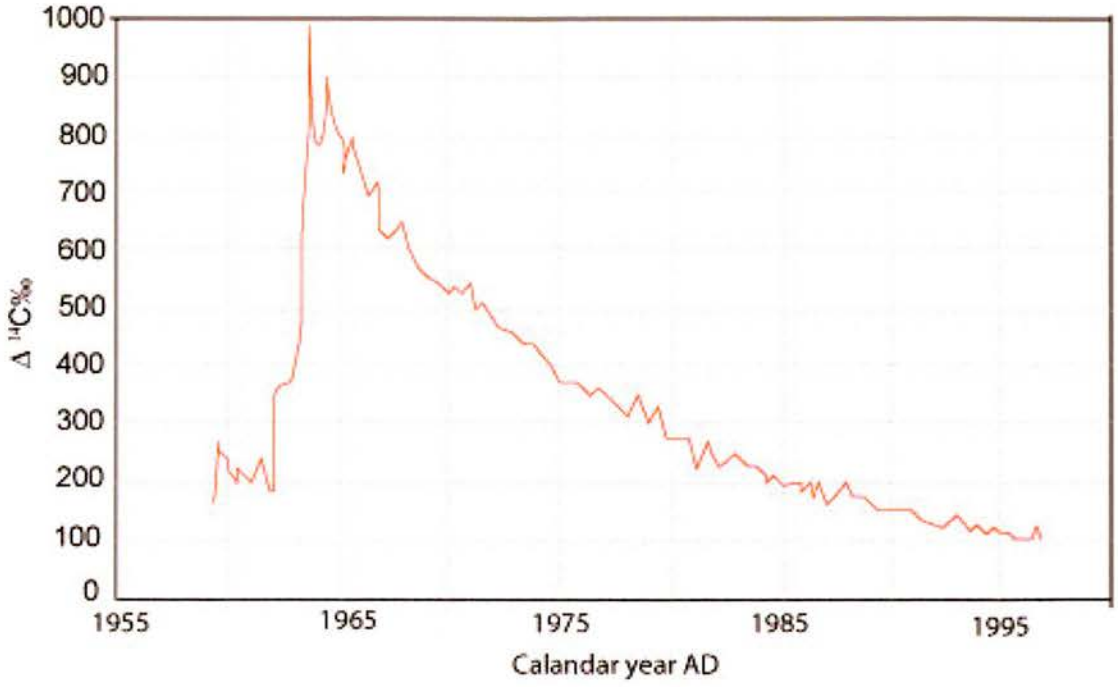

Figure 2.2: The bomb peak recorded in time-series atmospheric $\Delta^{14}C$ data. Adapted from Broecker *et al.*, (1995).

2.4.3 Mechanisms for variation- Climatically-driven redistribution of global ^{14}C

It is important to note that it is not only the strength of the processes outlined above that determine their influence upon $\Delta^{14}C_{atm}$, but the length of time over which they operate. To produce an observable change in $\Delta^{14}C_{atm}$, factors such as an individual change in production rate (Q) must be sustained over a sufficiently long time period (Korff and Mendell, 1980). This is because changes in ^{14}C production are strongly attenuated in the atmosphere, by mixing and dilution with the c.100 years of ^{14}C production present in this reservoir. The level of $\Delta^{14}C_{atm}$ is also determined by constant phase-lagged exchange with the biosphere and surface ocean, each of which itself contains a specific level of $\Delta^{14}C$ ($\Delta^{14}C_{bio}$ and $\Delta^{14}C_{surf}$). The effect of exchange with these other reservoirs acts to modulate and buffer $\Delta^{14}C_{atm}$, meaning that for a solar-induced Q change of c.25%, the estimated result is only a c.0.25% net variation in $\Delta^{14}C_{atm}$ (Stuiver and Braziunas, 1993).

If the rates at which ^{14}C is partitioned between the global atmosphere, ocean and biosphere (AOB) carbon reservoirs were constant, then natural fluctuations in $\Delta^{14}C$ in any of the AOB reservoirs would only result from changes in Q. However, the climatic factors that determine

AOB transfer rate have not remained constant throughout time, and neither has the cycling of carbon within each reservoir, also climatically influenced. Because of the effect of exchange with $\Delta^{14}C_{bio}$ and $\Delta^{14}C_{surf}$ upon $\Delta^{14}C_{atm}$ these large-scale and often rapid changes have resulted in $\Delta^{14}C_{atm}$ variations, both through modulating Q-induced changes, and as a driving mechanism for change in themselves. Determining the mechanisms responsible for $\Delta^{14}C_{atm}$ change is therefore complex, as climatic and Q-derived influences on $\Delta^{14}C_{atm}$ therefore do not necessarily act in an independent way. A fluctuation in solar activity, for example, not only produces a variation in Q, but also changes in solar irradiance that may impact upon the global climate, affecting AOB characteristics and ultimately modulating the Q-induced change in $\Delta^{14}C_{atm}$. This effect is apparent in the $\Delta^{14}C_{atm}$ tree-ring record, where climatically-derived changes in ring thickness are correlated with solar cycles of $\Delta^{14}C_{atm}$ (Suess, 1986). As global climatic changes are driven and influenced by cyclic processes such as variation in the Earths orbit (Milankovich cycles) and levels of solar irradiance, periodicity is also produced in climate states, which is particularly apparent in the periods of extreme global cold (glacial) and warm (interglacial) conditions that extend over millions of years of geological records. The most recent such large-scale climatic shift occurred between the last glacial maximum (LGM) at c.18 kyr BP, when large areas of continental landmass were covered by ice sheets, and the warm conditions of the present Holocene epoch, commencing c. 10 kyr BP.

The atmospheric CO_2 content varies in a stepwise fashion, corresponding to glacial-interglacial transitions, with an atmospheric partial pressure of 180-200 parts per million by volume (ppmv) at the LGM in comparison with a pre-industrial Holocene value of c.280 ppmv (Neftel *et al.*, 1985; Sigman and Boyle, 2000). These changes are strongly linked to changes in reservoir parameters, such as the density of terrestrial biomass and sea surface temperatures (Indermühle *et al.*, 1999), and further to significant fluctuations in the $\Delta^{14}C_{atm}$ record of this period.

The controlling influence of ocean-atmosphere exchange upon $\Delta^{14}C_{atm}$

The greatest exchange of ^{14}C from and to the atmosphere is with the global ocean reservoir, which also contains the greatest volume of ^{14}C in circulation (Stuiver and Braziunas, 1993). Variations in the relative transport rates between these reservoirs therefore affect $\Delta^{14}C_{atm}$. ^{14}C exchange occurs at the atmosphere-surface ocean interface as gaseous CO_2 undergoes dissolution:

$$CO_2\,(g) + H_2O\,(l) \Leftrightarrow H_2CO_3\,(aq)$$

(Equation 2.10)

Within the surface ocean a variety of oceanic inorganic carbon species are then formed, collectively known as dissolved inorganic carbon (DIC):

$$H_2CO_3\,(aq) \Leftrightarrow H^+\,(aq) + HCO_3^-\,(aq) \Leftrightarrow 2H^+\,(aq) + CO_3^{2-}\,(aq)$$

(Equation 2.11)

The rate of exchange at the reservoir interface is dominantly controlled by the partial pressure of CO_2 (pCO_2), with a net transfer from the reservoir with higher pCO_2 to that with lower pCO_2 (Levin and Hesshaimer, 2000; Sigman and Boyle, 2000). The specific value of pCO_2 is the product of several physical and chemical variables which are themselves climatically determined. The solubility of CO_2 increases with decreasing temperature (raising surface ocean pCO_2) and falls in warmer conditions, making relative rates of oceanic uptake and release of ^{14}C a temperature dependent process. The physical characteristics of the ocean surface also influence transfer of CO_2 as variations in wind speed and the presence of breaking waves determine the ocean surface resistance to gas exchange (Merlivat and Memery, 1983). The distribution of CO_2 within the global surface ocean is therefore influenced by the prevailing speed and direction of air currents, where at wind speeds above c. 5m s^{-1} the rate of CO_2 transfer from the atmosphere is increased, a characteristic of the high and mid southern latitudes where high wind speeds induce a large gross atmosphere-ocean gas exchange rate (Broecker *et al.,* 1985; Liss and Merlivat, 1986; Bard *et al.,* 1994; Levin and Hesshaimer, 2000). The pCO_2 of the ocean surface is also chemically determined by the distribution of inorganic carbon species within total DIC, specifically of aqueous CO_2. An increase in total DIC at constant alkalinity also increases the proportion of CO_2 (aq), and therefore of ocean pCO_2. An increase in surface alkalinity on the other hand, results in decreasing CO_2 (aq) within the DIC acid-base equilibrium, and falling oceanic pCO_2 can increase net gaseous transfer from the atmosphere.

Increasing ocean surface pCO_2	**Decreasing ocean surface pCO_2**
Increasing water DIC (constant alkalinity)	Increasing water alkalinity
Decreasing temperature	Increasing temperature
High wind speeds, breaking waves	Reduced wind speeds

Table 2.2: A summary of factors that increase versus those that decrease ocean surface pCO_2 (i.e. determine net uptake or release of ocean CO_2)

Along with characteristics of exchange rates at the atmosphere-ocean surface, features of oceanic circulation contribute to fluctuating $\Delta^{14}C_{atm}$ as the distribution of water masses at the ocean surface varies. Surface ocean water is continually removed from atmospheric contact by vertical descent in the ocean water column (downwelling) in high latitude regions to form water masses circulating in the intermediate and deep waters of the oceans. Once removed from the atmosphere-ocean interface, the $^{14}C/\ ^{12}C$ ratio of the water declines due to radioactive decay, and when water is re-circulated to the surface (upwelling), the ^{14}C content of surface waters is reduced. This is a key mechanism in development of the marine radiocarbon reservoir effect (MRE). During peak glacial periods, a lower rate of exchange between surface and deep ocean waters (known as "ventilation") has been linked to increased atmospheric $^{14}C/^{12}C$ ratios, for example a 1.5-fold increase in $^{14}C/^{12}C$ during the last glacial (Broecker *et al*, 1990). Varying rates of lateral and vertical circulation produce changes in $\Delta^{14}C_{surf}$ which translate to the ^{14}C activity of CO_2 that is transferred to the atmosphere. When an increase in ventilation raises both atmospheric gas absorption and the deep (^{14}C depleted) water flux to the surface, overall $^{14}C_{atm}$ falls because of the increase in ocean to atmosphere transport of carbon with a low ^{14}A. In the LGM to Holocene transition, climatic changes appear to have influenced the levels of $^{14}C_{atm}$ recorded in calibration curve datasets. The climatic warming over this period was not continuous, but was punctuated by a series of cold phases, the last of these (before the onset of the Holocene) known as the Younger Dryas (YD). The variation in $^{14}C_{atm}$ at the YD is larger than that which results solely from production rate change, and does not correlate with records of cosmogenic nuclide production in ^{10}Be records (Clark *et. al.*, 2002). During the early YD $^{14}C_{atm}$ rose rapidly, and then fell steadily until the end of the period when a rapid reduction in $^{14}C_{atm}$ is recorded (Goslar *et. al.*, 1995; Stocker and Wright, 1996). These changes have been attributed to changes in the production rate of North Atlantic deep water (NADW) at high northern latitudes. The removal of surface water masses as they are downwelled to form NADW makes the North Atlantic a "sink" of $^{14}C_{atm}$. The lower rate of overturning circulation at the onset of the YD would have reduced the efficacy of this North Atlantic

sink. The gradual reduction in $^{14}C_{atm}$ may then be the result of increasing ocean-atmosphere CO_2 gas exchange rates, while a rapid reduction in $^{14}C_{atm}$ may have been produced from an increase in NADW production rates (Stocker and Wright, 1996; Broecker *et al*, 1990, Hughen *et al.*, 1998b).

The oceanic contribution to varying $\Delta^{14}C_{atm}$ during the transition period from the LGM to the Holocene would have incorporated a variety of climatic mechanisms, which could both reinforce and counteract each other. For example a net release of CO_2 as sea surface temperatures (SSTs) rose could be accompanied by a decrease in salinity (e.g. from melting ice sheets) that would work to raise CO_2 solubility (Taylor, 1987; Sigman and Boyle, 2000). This effect could also be further complicated by changes in ocean circulation, such as a phase of increased ventilation that speeded the return rate of ^{14}C-depleted deep waters to the surface ocean.

Global spatial variability in $\Delta^{14}C_{atm}$

Along with changes in $\Delta^{14}C_{atm}$ on a temporal scale, there exist a range of spatially-dependant global variations, the most prominent of which is an offset (with an average of 41 ± 14 ^{14}C yr (McCormac *et al.*, 2002)) between the Northern and Southern hemispheres, which shows significant time-dependant variations (McCormac *et al.*, 2002; 2004). This is produced as the greater ocean area (c.40%) in the Southern hemisphere increases exchange between the atmosphere and ^{14}C-depleted ocean bicarbonate (Aitken, 1990; Geyh and Schleicher, 1990), and interhemispheric mixing of $^{14}C_{atm}$ is limited by the opposing directions of the equatorial trade winds. The hemispheric offset operates in conjunction with more intense seasonal $^{14}C_{atm}$ variations in the northern hemisphere due to the high density of seasonal forests. Other local effects have the potential to produce spatial variability in $^{14}C_{atm}$ including altitude and variations in land mass area of sample location (the "island effect"; Olsson, 1983). These factors are generally deemed not to significantly influence ^{14}C measurement as no significant differences in data have been observed between high precision measurements from a range of topographic settings in datasets produced in the Belfast and Seattle laboratories (Stuiver *et al.*, 1998a). Although the influence of volcanic $^{14}CO_2$ on global ^{14}C distribution is negligible, the ^{14}C content of plants near to active geologic CO_2 emissions is significantly reduced, an effect that declines rapidly with distance from the source (Bruns *et al.*, 1980).

2.4.4 Correction for variation: Calibration: how the atmospheric calibration curve is constructed

As discussed above, to convert measured ^{14}C ages to calendar years, it is necessary to quantify the changes in $\Delta^{14}C_{atm}$ over a calendar timescale. The offset between ^{14}C and calendar years varies non-systematically through time, and so cannot be mathematically predicted. To convert ^{14}C ages to calendar years therefore requires direct measurements of a time-series of samples for which the exact calendar date is known or can be calculated (e.g. Pearson and Stuiver, 1993; Stuiver and Braziunas, 1993; Stuiver *et. al.*, 1998a, 1998b; Reimer *et al.*, 2004). These data can then be used to construct a calibration curve of ^{14}C ages BP versus calendar years either BP or BC/AD. Suitable material for curve construction includes extended tree-ring series from long-lived species (e.g. bristlecone pines) or preserved specimens, such as the waterlogged oaks located in Ireland and Germany (Pearson *et al.*, 1993). A continuous tree-ring sequence spanning several thousand years has been established by matching overlaps in ring sequences between individual trees of increasing age. The calibration curve itself incorporates the errors associated with the individual ^{14}C measurements used in its construction.

Since production of the first calibration curve (Suess, 1979) successive curves have since been developed, culminating in the INTCAL04 dataset (Reimer *et* al., 2004). The INTCAL04 curve is produced using data from ^{14}C measurements of dendrochronologically dated tree rings between 0-12.4 cal. kyr BP. Between 12.4-26.0 cal. kyr BP the data was obtained from marine records (measurements of corals and foraminifera) that were converted to an atmospheric age equivalent using a site specific marine reservoir correction. The INTCAL04 calibration curve was produced by combining the data using a random walk model (Buck *et al.*, 2004). The model generates the calibration curve at 5 yr intervals for the period 0-12.4 cal. kyr BP, at 10 yr intervals for 12.4-15.0 cal. kyr BP and 20 yr intervals for 15.0-26.0 cal. kyr BP. Although calibration beyond 24.0 cal. kyr BP is not recommended (Reimer *et al.*, 2004), calibration curves are available for extended calendar ranges produced from a variety of data sources. These include varved sediments (Hajdas *et. al.*, 1993) and U/Th dated corals (Bard *et. al.*, 1990); however the uncertainties within these calibrations are increased as there is not complete agreement between the various datasets used (Reimer *et al.*, 2004).

2.4.5 Using the calibration curve

The standard curves used in ^{14}C calibration plot ^{14}C years on the vertical axis versus calendar years BP and BC/AD on the horizontal axes. To calibrate a sample ^{14}C age, the point at which the measured ^{14}C age intercepts the curve is translated to a corresponding calibrated age on the x-axis. The upper and lower σ limits associated with the ^{14}C age (σ_s) are also translated to calibrated ages, after the σ error of the curve itself (σ_c) is accounted for by combining σ_c and σ_s to produce overall upper and lower ^{14}C σ values:

$$\sigma = \sqrt{(\sigma_s^2 + \sigma_c^2)}$$

(Equation 2.12)

The conversion of upper and lower σ values for a ^{14}C age to calibrated ages gives the upper and lower bounds of a range of calendar ages on the calibration curve x-axis. All ages that lie within these limits are considered valid possible calendar ages for the ^{14}C age at 1σ confidence (i.e. 68% probability). The calibrated (cal.) age of a sample is therefore not a central point with associated error term, but is an age range that depends upon the σ of both the sample measurement and of the section of curve used for calibration (Stuiver and Pearson, 1993), and also on the shape of the calibration curve. Because the curve is non-linear, once a ^{14}C measurement and its σ limits are converted to a calendar age range, the calendar age distribution produced is no longer Gaussian in form (Taylor, 1987). The shape of the relevant section of calibration curve determines the width of the possible calibrated age ranges for a specific ^{14}C measurement and σ_s, as it determines the separation between upper and lower intercepts with the curve on the calendar axis. If the curve declines steeply, the gap between upper and lower calendar ages will be reduced, however there are many sections where calibration curves display a shallow slope and appear relatively flatter, known as a "plateau" where a wide range of calendar ages are possible for a single ^{14}C age (Figure 2.4). The nature of $\Delta^{14}C_{atm}$ changes through time means that an individual ^{14}C age and associated σ may intercept with the curve at not one, but several points, as an identical level of $\Delta^{14}C_{atm}$ occurred at several points in time. In this case all calendar ranges corresponding to the intercepts are considered equally valid (Pearson, 1987).

This method of calibration is known as the "intercept" method, and can be performed using graphs of calibration curve sections or more commonly with computer programs such as CALIB (Stuiver and Reimer, 1993; Stuiver *et* al., 2005) or OXCAL (Bronk Ramsey 1994;

1995; 2005). As the probability of ages within a calendar range may vary, these calibration programs can also calculate a probability distribution for the age range produced from the intercept method. This is achieved by calibrating not only the upper and lower σ limits of the ^{14}C distribution, but also other points (ages) within the distribution. Each age calibrated therefore has a Gaussian probability, which is attached to the resulting cal. age, and the calibrated dates can then be grouped into sections (e.g. every 10 years) and the probabilities for each group summed to produce a histogram. The most probable age range for the calibration may then be determined by summing the groups to the required probability level (Taylor, 1987).

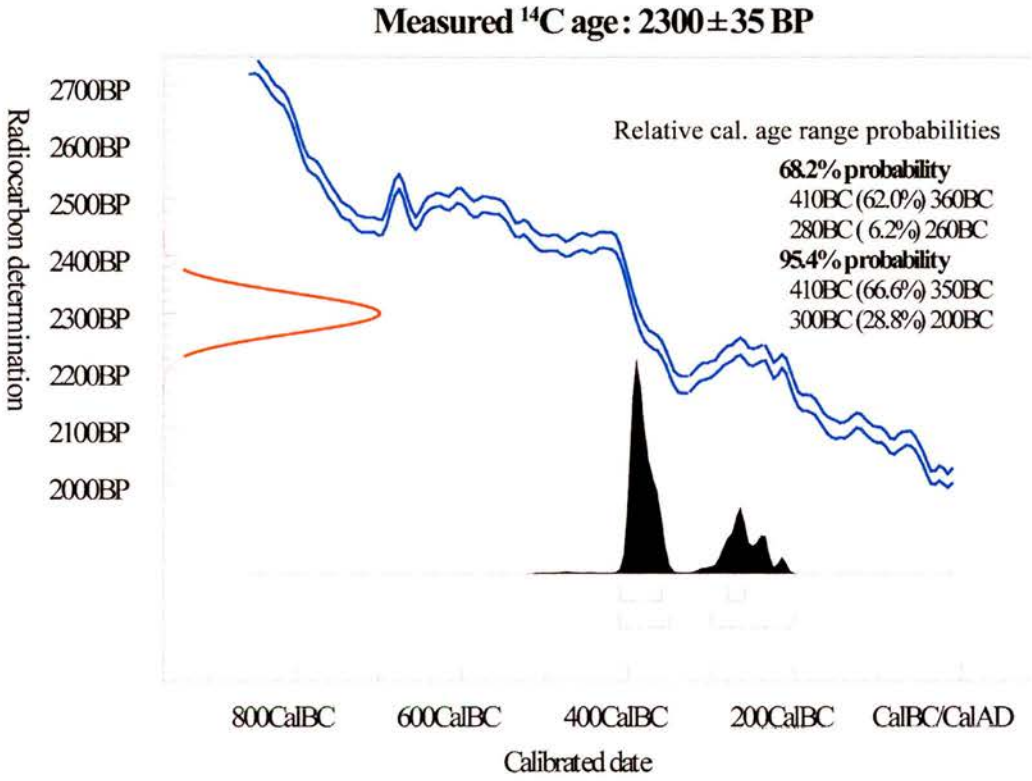

Figure 2.3: Calibration curve section showing probability distribution of calibrated age ranges. Here a relatively rapid $\Delta^{14}C_{atm}$ decrease results in a more constrained calibrated age range obtained from a particular measured sample age (Calibration performed using Oxcal v.3.01 (Bronk-Ramsey, 2005) and atmospheric data from Reimer *et al.*, (2004)).

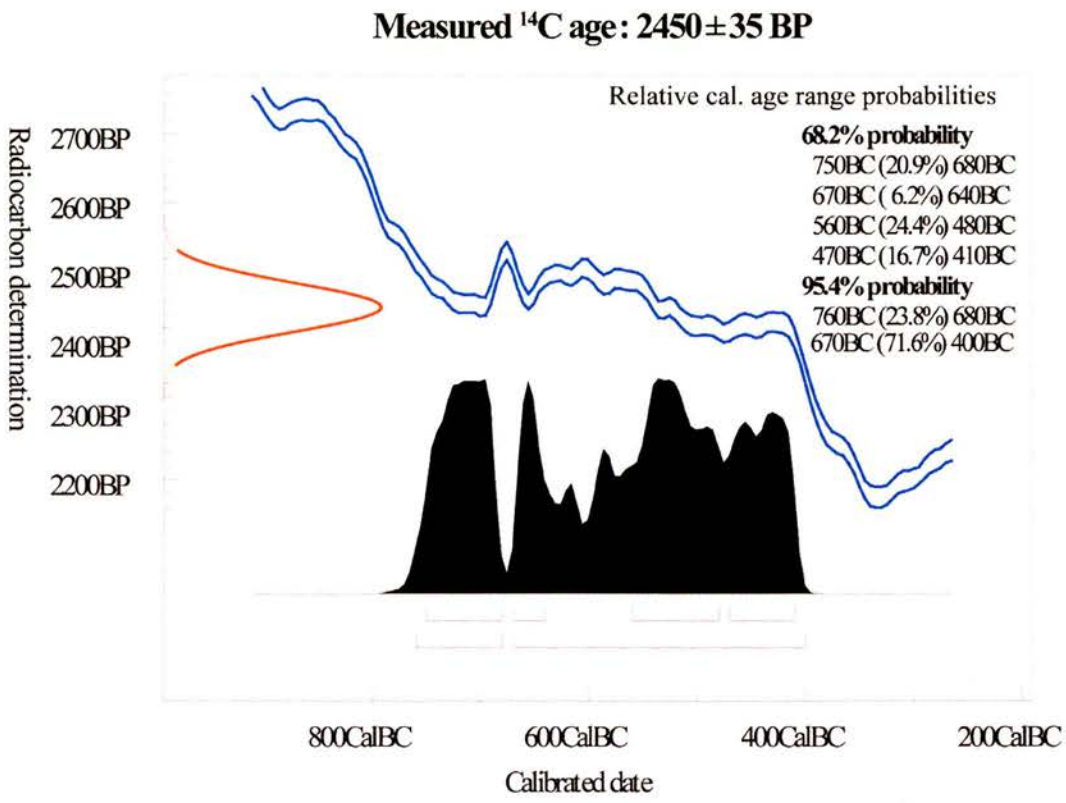

Figure 2.4: Calibration curve section showing probability distribution of calibrated age ranges. Here a ^{14}C plateau results in a larger calibrated age range obtained from a particular measured sample age (Calibration performed using Oxcal v.3.01 (Bronk-Ramsey, 2005) and atmospheric data from Reimer *et al.*, (2004)).

2.5 Sample effects: Contamination and transformation

As discussed above, a key assumption made by the ^{14}C dating method is that the remaining measured ^{14}C activity of a sample represents the decayed remains of an initial sample ($^{14}A_0$). The unit "0" indicates the time (t) at which the sample ceased to exchange carbon (and therefore ^{14}C) with the environment, when the sample would have displayed a ^{14}C age of 0 years, corresponding to the time of death for organic samples and time of final formation for inorganic samples.

The ^{14}C method therefore assumes that the remaining sample ^{14}C activity is a function only of radioactive decay since t = 0, and therefore if the sample ^{14}C content has been modified between t = 0 and the time of measurement, the final calculated ^{14}C age will not represent the actual age of the sample. Modification of sample ^{14}C activity in the time between final formation and measurement results from contamination of the sample with a quantity of ^{14}C

from an external source which has a different ^{14}C activity to that of the sample. This process can occur though the physical introduction of material that adheres to the sample structure or by chemical alteration of the sample structure itself to incorporate external ^{14}C at a point after t = 0 (diagenesis). The effect of contamination or diagenesis upon measured sample age (A_m) depends upon the amount of contamination (f), the age of the contaminant (A_x) and the "true" (A_s) sample age:

$$A_m = f(A_x) + (1 - f) A_s$$

(Equation 2.13 [Taylor, 1987])

The extent to which a measured sample ^{14}C activity represents the effects of external ^{14}C sources is difficult to assess accurately as compounds containing the external ^{14}C may be indistinguishable from original sample structure. It is possible for the primary carbonates of mollusc shells (originally deposited by the organism) to undergo dissolution and re-precipitation after the organisms death. Typically this process occurs though exchange of shell carbonates with those contained in soils or percolating groundwater (Bezerra *et al.*, 2000). In this instance there are usually physical indications that diagenesis has occurred that can be identified through visual inspection. In order to maximize the accuracy of a ^{14}C age an essential part of sample preparation is the physical and chemical pre-treatment of samples, aimed at removal of ^{14}C that did not form part of the original sample structure at t = 0, either by physical removal or extraction of a sample component not subject to diagenetic processes. In addition, care must be taken within the laboratory to minimize further introduction of any contamination during sample preparation, and to accurately measure the characteristics of the contamination itself so that it can be accounted for in age measurement (Mueller and Muzikar, 2002). The specific techniques adopted within this work for sample pre-treatment and the rationale behind their selection is discussed in detail in Chapter 4 as part of the discussion of laboratory methodology.

2.6 ^{14}C in the marine environment: Effects of the oceanic carbon reservoir

2.6.1 Reservoir effects: Implications for ^{14}C age measurement

When the OXII international standard is used to calculate a ^{14}C age, and when the INTCAL04 atmospheric curve is used to calibrate this age, the implicit assumption is that the sample $^{14}A_0$ was equal to that of the coeval atmosphere. This assumption is correct for the

terrestrial biosphere, once samples are corrected for fractionation, as this reservoir undergoes rapid cycling and exchange with the atmosphere (Trumbore, 2000). The carbon of the coeval atmosphere and terrestrial biosphere is therefore assumed to have equal values of ^{14}C activity and is hereafter referred to as C_{terr}. In other reservoirs however, specific processes mean that the reservoir ^{14}C activity is different to that of the coeval atmosphere, an effect that is translated to the $^{14}A_0$ of sample material formed within the reservoir. This offset between atmosphere ^{14}C activity ($^{14}A_{atm}$) and reservoir ^{14}C activity ($^{14}A_R$) is produced when the average residence time of a ^{14}C atom within the reservoir is significantly longer than in the atmosphere. This means that there is a larger degree of radioactive decay during residence of a ^{14}C atom in the reservoir than in the atmosphere and consequently that $^{14}A_R$ is lowered relative to $^{14}A_{atm}$. An offset can also be produced where there is a large input to a reservoir of material that has a different ^{14}C activity to that of the atmosphere.

The average ^{14}C activity of a specific reservoir is a function of the rate of exchange with atmospheric CO_2 relative to reservoir size (Geyh and Schleicher, 1990), internal reservoir processes (e.g. carbon cycling and mixing), and of the quantity and ^{14}C activity of inputs to the reservoir from other carbon sources. The $^{14}A_0$ of samples formed within a reservoir results from these factors, and at any point in time these samples have a $^{14}A_0$ that is not equal to the atmosphere, and is different to that of samples formed from C_{terr} at the same calendar date. When the ^{14}C age of coeval samples formed in the reservoir and from C_{terr} are calculated using the international standard value of $^{14}A_0$ there is an offset between the two, even though the samples are of the same "actual" calendar age (Stuiver *et. al.*, 1986). This offset in ^{14}C ages is known as a "reservoir effect" (R), the size of which is not necessarily constant either temporally or geographically (Stuiver and Polach, 1977). The largest reservoir that exhibits an R value is also the largest reservoir to undergo transfer and exchange on timescales relevant to global ^{14}C circulation, namely the global ocean reservoir.

Atmospheric ^{14}C enters the surface ocean via gaseous exchange of CO_2, a process that favours the uptake of the heavier ^{14}C isotope and hence relative enrichment of ^{14}C. This fractionation effect is however offset by a global ocean reservoir size c.60 times greater than that of the atmosphere, and an oceanic mean residence time for ^{14}C atoms of c.1000 years (Mangerud, 1972). The net effect is that the global ocean reservoir ^{14}C activity is lowered relative to the contemporary atmosphere, producing an offset in atmospheric and marine ^{14}C ages known as the marine reservoir effect (MRE). The value of the MRE is a function of the rate at which atmospheric CO_2 is absorbed by the surface ocean, and of the subsequent length of time that ocean water masses are separated from the ocean-atmosphere interface

after downwelling, during which the water ^{14}C content is depleted by radioactive decay. The value of the MRE in the global surface ocean (0-75 m depth), is less than in the thermocline (75-1000 m) and deep (1000-3800 m) ocean regions where there is no direct exchange with atmospheric CO_2 and the degree of possible equilibrium that can be achieved with coeval atmospheric ^{14}C activity is reduced (Kovanen and Easterbrook, 2002). Because atmosphere-ocean gas exchange rates, and characteristics of water masses (i.e. ^{14}C activity and flow rates) operating in an area of ocean are not constant either geographically or temporally, the value of the MRE at any specific location is strongly dependant on local factors of climate and oceanography.

2.6.2 Calibration for the global ocean reservoir: quantifying the MRE

The existence of the MRE means that the ^{14}C age of any sample containing carbon from the ocean reservoir (C_{mar}) will be inaccurate as the initial sample value of $^{14}A_0$ was less than that of the coeval atmosphere. Because the remaining ^{14}C activity of a sample formed from C_{mar} is therefore less than that of a sample formed at the same time from C_{terr}, samples of marine material appear older when dated using the ^{14}C technique, and must be corrected for the MRE. This procedure would be relatively easy if the MRE correction had remained a constant value throughout time and for all ocean areas. In this case variations in MRE through time would only be the result of $\Delta^{14}C_{atm}$ changes and the ocean ^{14}C activity would parallel atmospheric ^{14}C activity at all times. Once corrected for a constant MRE value therefore, the ^{14}C age of a marine sample could be calibrated with the atmospheric curve (Stuiver *et al.*, 1986).

A constant value of MRE is not applicable however (Stuiver *et al.*, 1986), and the offset has changed through time because the ocean response to specific fluctuations in $\Delta^{14}C_{atm}$ is non-linear. The $\Delta^{14}C_{atm}$ variations induced by changes in production rate and climate are not reflected directly in ocean ^{14}A, but are attenuated in the ocean record as a function of oceanic reservoir parameters, including atmosphere-ocean gas exchange rates and the ^{14}C activity of water mass input to the surface ocean. In the surface ocean, high frequency $\Delta^{14}C_{atm}$ signals are smoothed or absent, while in the deeper ocean layers the atmospheric signal is more severely modified and only long term trends in $\Delta^{14}C_{atm}$ remain apparent (Stuiver *et al.*, 1986). These characteristics mean that the relevant correction value (in ^{14}C years) for a specific sample depends on the size of the MRE at the time of formation, and in order to produce useful ^{14}C ages using marine material, it is vital to accurately quantify the time dependant correction value.

To establish the offset between ^{14}C ages in the atmosphere and ocean requires known values of both atmospheric and marine ^{14}C ages at points on a calendar timescale, where the MRE is the difference between the two for each single calendar age. Values of atmospheric ^{14}C age versus calendar age are available from the atmospheric calibration curve dataset. Establishing marine ^{14}C ages for the same calendar scale however is problematic. This is because there is a lack of suitable material with similar high resolution, continuous annual deposition characteristic to tree rings for the ocean reservoir. Annually-deposited samples of coral can be calibrated using $^{234}U/^{230}Th$ measurements (e.g. Bard *et al.,* 1993), however the cumulative effect of measurement errors on both U/Th and ^{14}C ages prevents the level of required chronological precision. A time series of marine ^{14}C ages as a function of calendar age has instead been produced using a global box diffusion model (Oeschger *et al*, 1975) of oceanic response to $\Delta^{14}C_{atm}$ change (Stuiver *et al.,* 1986; Stuiver and Braziunas, 1993; Stuiver *et al.,* 1998b).

The modelled marine ^{14}C ages versus calendar age make it possible to construct a calibration curve for the conversion of a marine ^{14}C age to a calendar age range. Calibration of marine samples follows the same technique using the marine curve as for calibration of atmospheric ^{14}C ages with the atmospheric curve. The marine calibration curve reflects the variable response of the ocean to $\Delta^{14}C_{atm}$ change, particularly the smoothing of high-frequency $\Delta^{14}C_{atm}$ fluctuations, which reduces the width of calibrated age ranges and the number of intercepts for a specific marine sample ^{14}C measurement when calibrated with the marine curve (Stuiver and Braziunas, 1993). The most recent curve presently available for calibration of marine samples is MARINE04 (Hughen *et al.*, 2004), which produces a series of ^{14}C ages versus cal. years for the averaged entire global surface oceans.

Between 0-10.5 cal. kyr BP the MARINE04 data is produced by converting the measured tree ring ^{14}C ages used in INTCAL04 with the box diffusion model to give ^{14}C ages for the mixed layer of the oceans. The data are combined using the random walk model that is employed to derive the INTCAL04 calibration curve in order to estimate the underlying MARINE04 curve. Between 10.5-26.0 cal. kyr BP a single calibration for the global mixed ocean layer is produced from ^{14}C measurements of corals and foraminifera, which have been corrected with a site-specific marine reservoir age. The site-specific correction is calculated from the weighted mean difference of marine and tree ring ^{14}C ages of overlapping data from 0.5-12.5 cal. kyr BP. Therefore the offset between atmospheric and marine ^{14}C ages (known as R) from the INTCAL04 and MARINE04 curves varies between 0-10.5 cal. kyr BP. After

10.5 cal. kyr BP the global value of R is calculated from the box diffusion model simulations for AD 1350-1850, and is a constant value of 405 ± 22 ^{14}C yr (Hughen *et al.*, 2004).

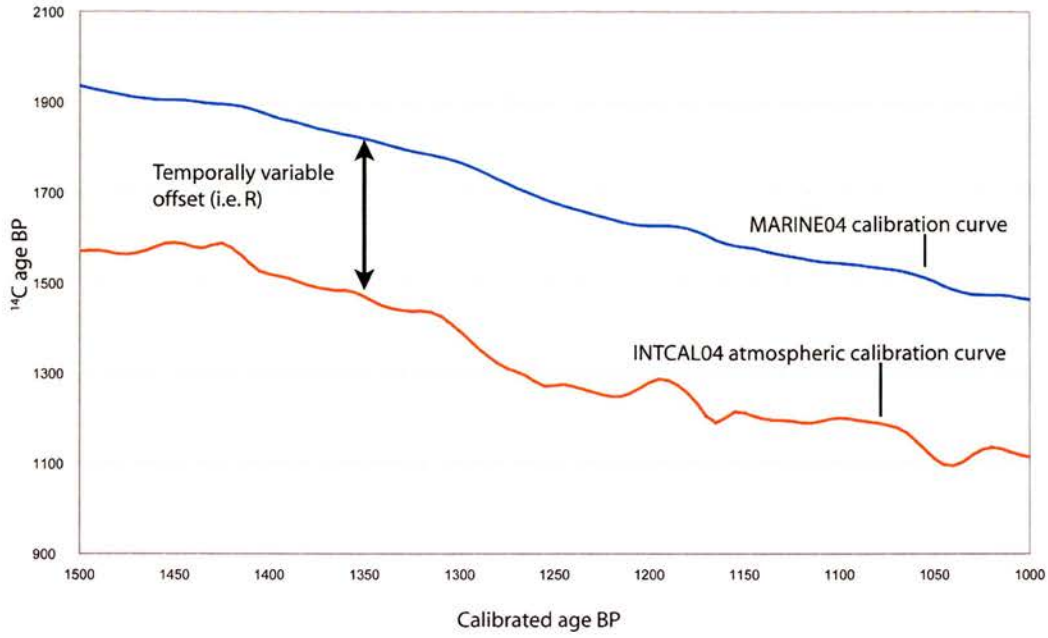

Figure 2.5: INTCAL04 and MARINE04 equivalent calibration curve sections showing variable R through time

All variation in $\Delta^{14}C_{atm}$ within the model is attributed to geo- and helio-magnetic induced production rate changes, and the climatically influenced atmosphere-ocean CO_2 exchange (F), vertical diffusion within the ocean (K) and atmosphere-terrestrial biosphere carbon flux (B) are treated as constant parameters through time. This is due to a lack of definite century scale data concerning fluctuations in these factors, and as a consequence the characteristics of global ocean circulation used by the model to calculate marine ^{14}C ages exist in a fixed mode. An important consideration is therefore that the marine ^{14}C ages calculated from model output are a result of the values chosen for the climatically-influenced parameters, and that MRE change resulting from variations in these parameters is not accounted for. Changes in MRE that are observed in empirical data measurements may be absent from the modelled data if these observed variations are the result of oceanographic change. For example MRE shifts from c.400 to c.500 ^{14}C years between 12 and 10 ka cal BP that are based upon empirical sample measurements and linked to ocean circulation variations are not simulated by the model (Stuiver *et al.*, 1998b). It is difficult however to quantitatively examine the level to which the model accurately represents reality because of the lack of empirical measurements of MRE through time with which the model output could be compared (Stuiver *et al.*, 1986).

The fluctuating MRE values for the modelled period are obtained by comparing the atmospheric ^{14}C age for each cal. decade with the equivalent modelled marine ^{14}C age. These values produced by the model for the global ocean vary on average by 200-400 ^{14}C years for the modelled period. Tests of the model sensitivity over the Holocene indicate that general surface ocean MRE fluctuations are on the order of ±100 ^{14}C yr (Bard, 1998), increasing to up to 200 ^{14}C yr as a result of particularly sharp production-rate driven $\Delta^{14}C_{atm}$ changes. Even with a fixed mode of ocean circulation the ^{14}C age offset between the modelled surface and deep oceans can vary by up to 200 ^{14}C years. This is supported by observational data from Atlantic deep water corals, where significant century scale variations in MRE between 16000 -12000 cal BP are attributed to changes in the depth and strength of individual deepwater masses with specific ^{14}C contents, rather than production rate driven $\Delta^{14}C_{atm}$ changes (Adkins *et al.*, 1998).

Variation in the oceans from the (modelled) global average MRE

The marine ^{14}C ages used to construct the marine calibration curve are average values for the global ocean reservoir as a whole, and therefore the MRE values obtained from this data (from the difference at a single cal. point between model marine ^{14}C age and atmospheric ^{14}C age) are also only valid as a global average value. Because the parameters used in the model (e.g. CO_2 exchange and ocean mixing rates) may be different from those that operate in a specific area of ocean, the ^{14}C age (and therefore MRE) in any geographic area may itself be offset from the model-calculated value. This geographic variation in marine ^{14}C ages means that to produce an accurate ^{14}C age and calibrated age range for a marine sample the specific MRE of the ocean area in which it was formed must be accounted for.

The MRE value that is valid for a specific geographic ocean area is established using empirical ^{14}C measurements of local samples, for example a comparison of the ^{14}C age of terrestrial and marine samples known to be of the same calendar age. It is also possible to calculate the positive or negative deviation (defined by the term ΔR) of local marine sample ^{14}C ages from the modelled global average values (Stuiver *et al.*, 1986). This is achieved using ^{14}C age measurements of marine samples for which the equivalent atmospheric ^{14}C age is known or can be calculated. The measured marine ^{14}C age (P) is equated to a ^{14}C age (Q) from the modelled curve where both P and Q correspond to the same atmospheric ^{14}C age. ΔR is then the difference between measured and model marine ^{14}C ages, i.e.:

$$\Delta R = P - Q$$

(Equation 2.14 [Stuiver *et al.*, 1986])

For samples with a known value of ΔR, a calibrated age range is obtained by subtracting the relevant value of ΔR from the sample CRA before calibrating with the marine curve. If no information is available for the local offset, Stuiver *et al.* (1986), recommend an assumption of ΔR = 0 for calibration of marine samples. Currently, a large number of ΔR values are available from studies performed in a range of global locations, and these data demonstrate the wide variation in surface ocean ^{14}A, with differences in ΔR on the order of several hundred ^{14}C years apparent in 19th century samples from contrasting ocean regions (Stuiver *et al.*, 1998b).

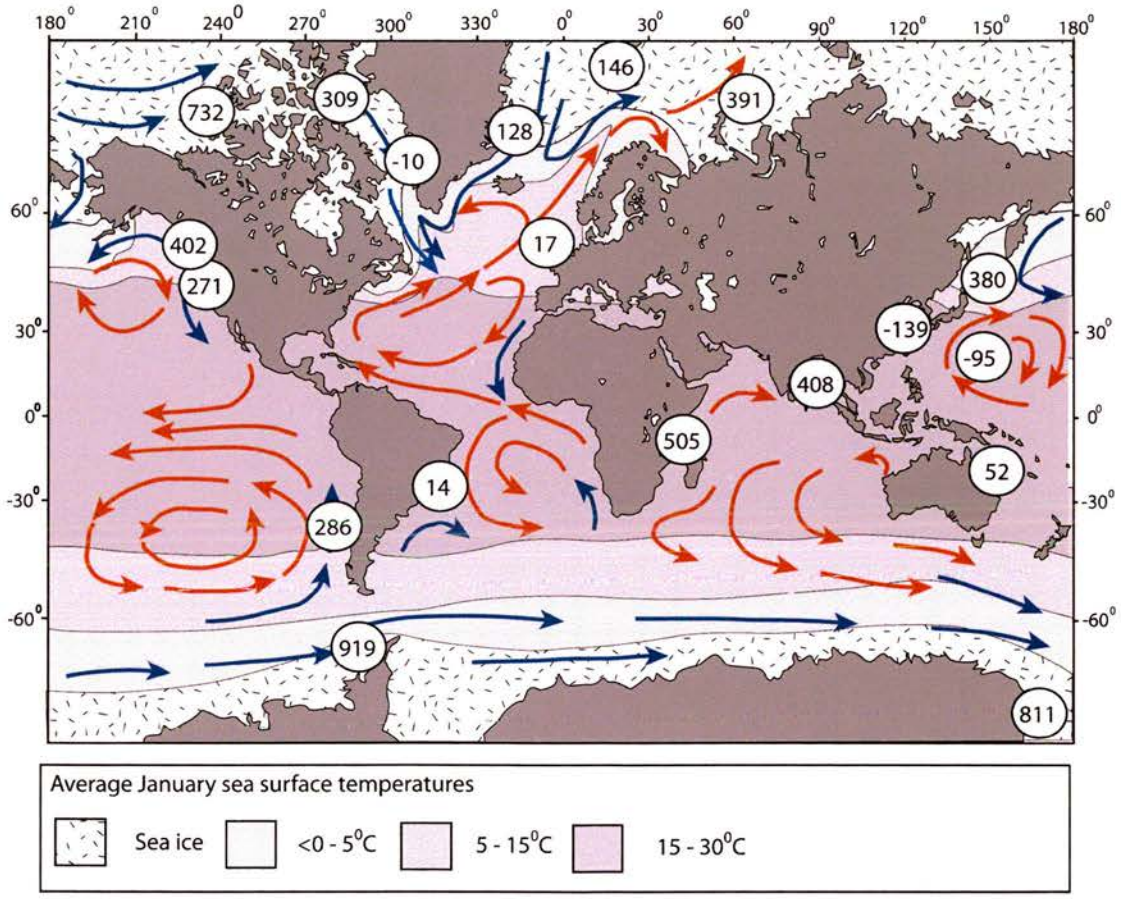

Figure 2.6: Modern global ΔR values showing major ocean circulation (weighted mean regional ΔR values from Reimer and Reimer, 2005)

2.6.3 Variations in MRE values: the need for accurate quantification

What determines geographic variations?

The range of geographic variations in surface ocean ΔR shown in Figure 2.6 reflect geographic variations in the ^{14}C age of the surface ocean, and therefore in the MRE. The variety of mechanisms that determine the ^{14}C activity of a specific ocean area can be assessed by correlation of environmental factors with the size of MRE or ΔR. The key mechanisms that underlie geographic variability in MRE are the rate and nature of atmosphere-ocean gas exchange and ocean circulation. Gas exchange rates influence both $\Delta^{14}C_{atm}$ and the $\Delta^{14}C$ of the surface ocean ($\Delta^{14}C_{surf}$) by determining the net oceanic uptake or release of CO_2, while specific ocean circulation conditions determine the flux of water masses with varying ^{14}C activity values to a surface ocean area.

Significantly different gas exchange rates exist in different ocean areas as a result of environmental variables such as temperature. The net effect of latitudinally-dependant global insolation levels is an overall release of CO_2 from the ocean surface in equatorial regions and higher absorption rates of atmospheric CO_2 at high latitudes where cooling of surface waters results in under-saturation with respect to the gas (Kratz *et al*, 1983). The physical effects of temperature are also important in high latitudes through the distribution and annual duration period of sea-ice, which raises ΔR values by inhibiting atmosphere-ocean gas exchange (Stocker and Wright 1996). Results of modelling suggest that an increase in ΔR of 150-200 ^{14}C yr would result from 7-8 months of annual sea ice cover in a local ocean area (Barber *et. al.* 1999).

As well as influencing global CO_2 distribution, the prevailing strength and direction of wind currents drive motion in the surface oceans through energy transfer. The northern and Southern hemisphere wind belts drive major ocean currents that are modified by the Coriolis force to produce clockwise gyres in North Hemisphere ocean basins, and counter clockwise gyres in the Southern Hemisphere (see Figure 2.6). Wind-driven circulation influences surface ocean water flow to a depth of c.100 m as energy is transferred vertically by movement of successive water layers of decreasing velocity and increasing deflection from the initial wind direction (Ekman transport [Thurman, 1990]).

Along with lateral movement of water, wind action also influences vertical ocean circulation as currents direct water into or out of an area. Where the wind driven flow results in net movement of water away from a point, volume conservation means that replacement water is drawn upwards from depth (upwelling). Trade winds on either side of the equator are deflected in opposite directions by the Coriolis force, resulting in the equatorial upwelling zone. Upwelling also occurs at continental margins where prevailing wind direction results in movement of water to the open ocean, which is replaced through the upward movement of deep water with low temperatures and high nutrient content. Where wind driven surface water masses converge (e.g. at the Antarctic convergence), or are moved towards a coastal margin, surface water is forced downwards (downwelling).

The pattern of vertical ocean water circulation is central to the range of geographic variations in MRE, as surface ocean areas where there is increased transfer between surface and deep water are consequently more depleted in ^{14}C than the global ocean average. The majority of vertical circulation is not wind-driven, but powered by surface temperature and density changes in a system known as thermohaline circulation (THC). At high latitudes, lower temperatures and raised salinity increase the density of surface water masses to a level at which sinking occurs, producing the major deepwater masses present in the ocean basins (Boyle and Kegwin, 1987). The main regions of deepwater formation are the Weddle Sea in the Antarctic, where Antarctic bottom water is formed as rapid winter freezing and brine rejection increase surface salinity, and in the Norwegian, Greenland and Iceland Seas in the North Atlantic, where North Atlantic deep water (NADW) is produced. The deep and intermediate water masses formed by downwelling are circulated throughout global ocean basins, separated from atmospheric contact by vertical density stratification for varying lengths of time before eventually being returned to the surface via upwelling. During circulation at depth, the ^{14}C activity of a downwelled water mass is reduced by radioactive decay as a function of the time since it was last at the surface. There is a global trend towards high positive ΔR values at high latitudes. Specific geographical variations in MRE value are dependant upon the ^{14}C activity characteristics of upwelled water, which as well as the time elapsed since downwelling are influenced by factors such as the amount of ^{14}C input from carbonate dissolution and the oxidation rate of sinking organic material over this period.

The effects of lateral and vertical ocean circulation upon a local MRE value operate in conjunction with other specific oceanographic, topographic and climatic effects including sea-ice extent, the release of "fossil" CO_2 from iceberg melting (Voelker *et al*, 2000) and evaporation versus precipitation rates. The latter can significantly influence surface ocean

^{14}C content through the introduction in coastal regions of varying quantities of continental runoff to the surface ocean, further complicating the signal in these locations.

Temporal variations

As a first approximation, the MRE and ΔR value for a specific ocean area are assumed to vary through time in direct proportion to the changing model global average MRE, and therefore to have remained constant (Stuiver and Braziunas, 1993; Stuiver *et. al.,* 1986, 1998b). This assumption implies that changes in local ocean reservoir parameters have not been sufficient to produce significant variation in water ^{14}C content. It is now apparent however that such temporal variations may occur that are significant with respect to the precision of the ^{14}C method (Monges Soares, 1993; Ingram and Southon, 1996). The geographically-dependent variations in atmosphere-ocean ^{14}C age offset (MRE) discussed above depend upon localised climate and ocean characteristics. These are not necessarily constant, and if a climatic or oceanographic shift were of a sufficient magnitude it may induce a change in the local ocean water ^{14}C activity relative to the global atmosphere. In this case, the MRE value would not be constant in an ocean area and ΔR would fluctuate independently from the pattern of modelled global average values. Palaeoclimatic data from a range of sources indicate that ocean and climate changes over the past 30 kyr BP include fluctuations in the distribution of water masses and ocean-atmosphere exchange rates that have impacted variously in different ocean areas (e.g. Koç *et al.*, 1993). Because of the complex nature of interaction between ocean and climatic variables, any specific climate/ocean fluctuation will not necessarily induce a MRE change. For a MRE change to be observed in the record, fluctuations must be firstly of sufficient magnitude, and secondly of sufficient duration, to produce a corresponding shift in ocean water ^{14}A.

Throughout the last c.2 million years (the Quaternary), global reorganisation of the Earth's climate system is characterised by a cycle of fluctuations in the extent of continental ice sheets. Periods of climatic cooling and major ice expansion (glacial) were followed by ice retreat, culminating in warmer (interglacial) conditions. These glacial/interglacial changes were accompanied by large-scale physical and chemical changes in the atmosphere, ocean and biosphere carbon reservoirs. The most recent of these cycles occurred between the end of the last northern hemisphere glacial stage (c.13 ^{14}C kyr BP) and the onset of the present (Holocene) interglacial period at c.10 ^{14}C kyr BP, and consists of an overall warming trend upon which climatic fluctuations are superimposed. Marine samples from this period have been used to demonstrate the potential for large changes in MRE offsets in surface and

deepwater masses (Austin *et al.*, 1995; Haflidason *et al.*, 2000). Increasing improvement in the precision of AMS measurements, e.g. errors of c.35 years on samples aged >11 ^{14}C kyr BP, means that with increased counting times, samples from beyond c.18 ^{14}C kyr BP could be measured with similarly low associated errors (G. Cook pers. com.). This would make it possible to investigate patterns of MRE variations over a greatly extended time period, for which there already exists a wide range of palaeoenvironmental data.

2.6.4 Determining MRE/ΔR: Methodological approaches

As discussed above, a local ocean MRE and ΔR value is established using ^{14}C measurement of appropriate marine samples, and three main methodological approaches have been adopted for this purpose. These are the use of analogue samples, onshore/offshore tephras and paired samples, all of which are designed to accurately assess the appropriate atmospheric ^{14}C age that equates on a calendar scale to a measured sample marine age. This is achieved by measurement of marine samples for which a calendar age range is known and therefore an equivalent atmospheric ^{14}C age can be established from the atmospheric calibration dataset, or by comparing measured ^{14}C ages of marine and terrestrial samples demonstrably of the same calendar age. Where samples are taken for which a record of calendar age is not extant (e.g. prehistoric material) only an equivalent atmospheric ^{14}C age will be available for MRE/ ΔR determination. This has implications when using the atmospheric ^{14}C age to obtain a calendar age for the sample from the atmospheric curve dataset. Beyond the end of the tree-ring data at 11,857 cal BP the atmospheric curve ^{14}C ages are derived from marine corals and varve data that are corrected for an approximated MRE by 400 ^{14}C yr to 10 cal BP and 500 ^{14}C years beyond this cal age. This means that the calculation of ΔR for samples beyond 8800 cal BP will reveal little information as the atmospheric dataset used to obtain the ΔR value has already been corrected by an approximated MRE value (P. Reimer pers. comm.).

Analogue samples

Analogue samples are marine samples (e.g.: molluscs) collected live before 1950 AD (ideally pre-1890) from the location for which the MRE or ΔR is to be determined. The atmospheric ^{14}C age of the marine sample is obtained using the known calendar age from the atmospheric calibration curve dataset, which can then be directly compared with the

measured marine age to provide a MRE value. To obtain ΔR, the measured sample age is compared with the model marine age for the known sample cal. age, using the marine calibration dataset. The ^{14}C age offset between the two then gives the ΔR for the location (Stuiver and Braziunas, 1993; Dutta *et. al.* 2001). Museum archives often prove a useful source of suitable material for this approach (Mangerud and Gulliksen, 1975), although some material may have historical significance which precludes its availability for destructive analysis. Analogue samples are a useful resource, but the spatial and temporal range of any study that is undertaken is limited to material already collected, and few suitable collections exist from prior to c.1700 AD, preventing study of temporal variations in ΔR over extended time periods. Other limitations associated with analogue materials are the lack of opportunities for analysis of multiple or repeat samples, and problems surrounding the accuracy of sample provenance, both with timing and location of sample collection (Yoneda *et al.,* 2001). Where these factors apply, the accuracy of MRE and ΔR values calculated on the basis of such samples is limited.

Onshore/offshore tephras

This method uses the rapid and simultaneous deposition of a single volcanic ash (tephra) layer in both marine and terrestrial deposits to obtain coeval marine and terrestrial ^{14}C ages. It is assumed that marine and terrestrial organisms in close association with the same tephra layer share a calendar date of death, and therefore that the offset in measured ^{14}C ages between the two sample types can be used to establish the local MRE at the time of tephra deposition (Haflidason *et al.*, 2000; Bondevik *et al.*, 2001). Although the method is inherently limited to certain spatial and temporal ranges that are determined by both the distribution of individual identifiable tephra layers and the frequency of tephra deposition events, tephra marker horizons are often deposited over a wide geographic area which potentially allows spatial variations in MRE / ΔR at a single calendar age to be tracked. In some areas, the presence of several different tephra horizons at a single location has enabled temporal changes in regional MRE to be estimated for the North Atlantic Younger Dryas/ Holocene transition, and during the Holocene period (Haflidason *et al.*, 2000; Sikes *et al.*, 2000).

The central limitation to the tephra isochron approach concerns uncertainty over the assumption that the measured marine and terrestrial ^{14}C ages measured for a single deposition event represent a single calendar age. The accuracy of this assumption is

proportional to the accumulation rates of marine and terrestrial sediments, degree of sediment mixing after deposition of the sample material and the extent to which an equivalent point in marine and terrestrial sediments can be identified using a tephra horizon. Material selected for determination of a marine ^{14}C age is often marine microfauna (e.g. foraminifera) which necessitates the combination of many individual organisms, thus yielding a ^{14}C measurement that is an average of the activity of the organisms which may not all be of the same age. This approach may compromise the accuracy of the "marine" ^{14}C age obtained, and it is preferable to select dissolution resistant or larger species that are less mobile following deposition (Austin, 1995).

If sediment accumulation rates in the sample locations vary significantly, or there has been differential sediment mixing during and after incorporation into terrestrial or marine deposits, the equivalence of measured marine and terrestrial ^{14}C ages will be compromised. Post-deposition movement of material may occur through mixing and bioturbation of sediments, and can affect both the measured sample material and the distribution of tephra shards. The problems are exacerbated by the variability of localised sedimentation rates and uncertainties are increased in areas with low sediment accumulation rates, particularly in conjunction with significant surface sediment mixing zones (Jones *et al.*, 1989; Paull *et al.*, 1991). The processes involved in mixing and bioturbation are difficult to identify and quantify (Broecker *et al.*, 1991), and are generally indirectly calculated by modelling or estimation. Rate of incorporation, residence time and degree of mixing in the surface mixed layer (SML) of a deposit are a function of the sedimentation rate, to which inherent dating uncertainties increase with inverse proportion.

Tephras may be incorporated into sediments by time-lagged processes rather than direct fallout from the atmosphere, for example by the incorporation in marine sediments of particles entrained in glacial ice that have been stored for decades or centuries following atmospheric deposition. Often, difficulties surround identification of an equivalent point of tephra deposition in marine and terrestrial sediments, as the shards may be diffused vertically within the cores by mixing. Although the modal point of highest shard concentration is usually used, concentration peaks may be poorly defined, or several peaks may exist, and the mean or median tephra distribution points may fall substantially higher or lower than the modal concentration in the core. To address these problems, it is recommended that ^{14}C ages above and below the tephra deposit are compared, and that tephra layers are used where there are sharp basal contacts and characteristics of atmospheric deposition (Sikes *et al.*, 2000). In studies of more ancient sediments, larger dating uncertainties associated with the

methodology may be acceptable. Within later Holocene studies the variety and extent of mixing effects may lessen the suitability of the tephra isochron approach to a restricted range of areas and times.

Paired samples

A comparison of equivalent marine and terrestrial ^{14}C ages from a single location is also possible where marine and terrestrial material of the same calendar age was deposited simultaneously. This approach has been used in a number of studies with both samples from natural deposits including isolation basins (e. g. Bondevik *et al.*, 1999), and coastal archaeological sites (e. g. Reimer *et al.*, 2002), where it is often possible to identify individual deposits that represent very restricted and rapid deposition events (e.g. on the order of days or seasons). Using this material, the MRE can be determined from comparison of marine and terrestrial ^{14}C ages, and ΔR calculated by using the atmospheric ^{14}C age to establish the equivalent model marine ^{14}C age for the sample (Stuiver and Braziunas, 1993; Reimer *et. al.* 2002).

When MRE / ΔR values are obtained using a comparison of marine and terrestrial material, the accuracy of calculated values depends upon the degree to which the ^{14}C ages of the samples are equivalent. This factor is not directly quantifiable and must be inferred, meaning that rigorous protocols must be used when selecting material for the paired sample approach that consider the likelihood of post-depositional bioturbation and other mixing processes. The degree of sediment disturbance should be quantified for the deposit both *in situ,* by factors including the presence of articulated remains, absence of root penetration and where possible with laboratory analysis including soil micromorphology, mineral magnetism, and other provenancing techniques. The reliability of MRE / ΔR determinations using the paired sample methodology is improved by multiple sampling and sample replication to confirm that marine and terrestrial materials within a single layer are representative of a short deposition period. Statistical analyses (*e.g.* chi squared tests [c.f. Ward and Wilson, 1978]) of measurement groups can further demonstrate the degree to which samples are contemporaneous, where an anomalous result in an otherwise coherent set of ages from a single deposit may represent intrusive or reworked material

Because of these considerations, the nature of sample material selected for this methodology can also affect measurement accuracy. Samples should ideally represent as short a time

interval as possible, where materials such as plant caryopses (representing one growth season), and identifiable twigs or leaves, are preferable to longer-lived tree sections or other material which may be subject to anthropogenic effects of extended re-use periods prior to incorporation in the final deposit (Albero *et al.*, 1986; Reimer *et al.*, 2002). There must be a high likelihood that the samples share an equivalent age of death, and were grown in the same location. For this reason the use of migratory or commonly transported material should be avoided.

The limitations of the paired sample methodology outlined above may constrain the number of suitable sampling sites, and suitable sites may be absent in the region of research interest. Despite the high density of coastal archaeology on the Atlantic seaboard of Europe, anthropogenic deposits with appropriate integrity for this methodology are rare beyond c.6000 BP and investigation of a wider temporal range necessitates the use of naturally deposited material. The paired sample approach using archaeological material in the North Atlantic region is presently under-utilised.

2.7 The North Atlantic: Modern environments and MRE values

A crucial aspect of the MRE is the nature of modern spatial variations and the extent to which these are reflected in changes through time. At present, variations in the MRE exist over both large spatial scales, (i.e. between ocean basins) and on a smaller, regional level. As described above, these are the result of present climatic and oceanic regimes, which have not been constant over time, but have varied on both larger (e.g. glacial to interglacial transitions) and smaller scales within various spatial zones. The key question is therefore at what point do these spatial and temporal differences in environmental variables become significant with respect to the MRE? The nature of the MRE as a ^{14}C age offset means that the precision to which a value can be determined is limited by inherent errors. These are a culmination of errors associated with ^{14}C measurements and the method by which the MRE value is calculated from the measurements. In order for an environmentally-induced variation in the MRE to be observable, it must therefore be significant with respect to the error terms associated with the values. The climatic and oceanographic changes that produce variations in ocean surface ^{14}C activity and drive MRE variation must be on a sufficient scale to induce observable fluctuations in values. The North Atlantic region is one in which climatic and oceanographic factors show a high level of variability, over both large and small spatial and temporal scales. This makes the area highly suitable for investigation of the nature of MRE values, particularly the nature of spatial and temporal variations. These

dynamic environmental changes through time have coincided with extensive human settlement and exploitation of natural resources. Because of the long archaeological record there exists a range of suitable materials in the region for the paired sample approach to determining the MRE. Added value for this research comes from the global significance of environmental changes in the North Atlantic. In addition to providing the scales of change and type of sample material ideal for this type of study, the data that is produced can feed into investigations of changes that have very wide significance. For example changes in the global thermohaline circulation may be driven by variations in the North Atlantic, and human-environment interactions here have implications of global relevance. This means that in addition to environmental research, the region also has great importance through the Holocene for the study of interactions between human communities and the environment.

The following sections place the MRE within a North Atlantic context. Firstly, the present climate and oceanography of the region is outlined, followed by the current assessments of MRE values that are influenced by these variables. Secondly the palaeoenvironmental changes in climate and ocean that are recorded from the end of the last glaciation to the late Holocene are outlined. These are followed by a summary of the evidence for variations in the MRE that may have accompanied the temporal environmental changes.

2.7.1 North Atlantic modern climate and oceanography

The North Atlantic is a key region for regulation of the global climate, due to its role within the global thermohaline circulation system. The surface water mass that flows north to the North Atlantic is dominated by the northeast drift of the Gulf Stream, which originates from Equatorial surface currents. At c. 40^0N and 45^0 W the Gulf Stream becomes the North Atlantic Current (NAC). To the west of Norway and north of Iceland the NAC surface waters are cooled and the surface salinity (already elevated by evaporation during northward transport), is increased. These effects mean the density of surface waters is increased, and surface NAC waters sink to form North Atlantic deep water (NADW), which then flows southwards at depth. The formation of NADW releases a large amount of latent heat and plays a major role in regulation of both North Atlantic and global climates (Broecker *et al.*, 1985; Lehman and Keigwin, 1992).

Modern surface circulation within the North Atlantic is characterised by the distribution of northward-flowing warm, saline NAC waters, and the southward flow of cold, fresher Arctic-derived waters. Because the surface waters of the NAC spend an extended period in

contact with the atmosphere during northward transport in the Gulf Stream, gaseous exchange with contemporary atmospheric CO_2 means that NAC waters have relatively high ^{14}C content (Campin *et al.*, 1999). A branch of the NAC flows north-west to travel in a clockwise direction around Iceland as the Irminger Current (IC). The remainder of the NAC continues northward and branches around both the western coast of the British Isles and the Faroe Isles. These branches subsequently move through the Shetland-Faroe and Iceland-Faroe channels. NAC water flowing around the British Isles moves in coastal currents into the North Sea, and the flow through the Iceland-Faroe-Shetland gap moves northwards up the Norwegian coast as the Norwegian Current (NC). At c.62^0N the NC meets the Norwegian Coastal Current (NCC), a northwards flow of water from the Baltic that is influenced by terrestrial run-off from Norwegian fjords. At the North Cape of Norway the NC then branches into the North Cape Current and the Spitsbergen Current.

Southward flowing surface waters in the North Atlantic are dominated by the East Greenland Current (EGC) flowing down from the Arctic along the east Greenland coast, where it is confined to the shelf region, subsequently forming the West Greenland Current (WGC) and thereafter entering the Labrador Sea. Along the east Greenland coast the East Iceland Current (EIC) is formed from components of EGC and IC water, flowing eastwards along the north Icelandic coast. Upon leaving the coast the boundary between Atlantic and EIC water forms the Iceland-Faroe Front as the EIC flows eastward along the Iceland-Faroe Ridge (Pistek and Johnson 1992) to enter the Norwegian Sea.

The interface between northward-flowing warm and saline Atlantic water currents and southward-flowing cold, low-salinity Arctic water is known as the Polar Front, presently located to the North of Iceland. The interaction between these zones means that the North Atlantic is a climatically sensitive region, and the relative position of the Polar Front over time is strongly correlated with records of climatic and oceanographic changes (Ruddiman and McIntyre, 1981; Dansgaard *et al.*, 1993; Haflidason *et al.*, 1995). Hydrographic changes in the vicinity of frontal systems in the North Atlantic have been observed on a decadal and inter-annual scale, for example the "Great Salinity Anomaly" during the 1960s in Icelandic waters (Dickson *et al.*, 1984). The modern position of the Polar Front however appears to be relatively well constrained, although as mentioned above, there is a considerable amount of evidence to demonstrate that the oceanographic regimes in the modern North Atlantic are not static but respond dynamically to climatic forcing.

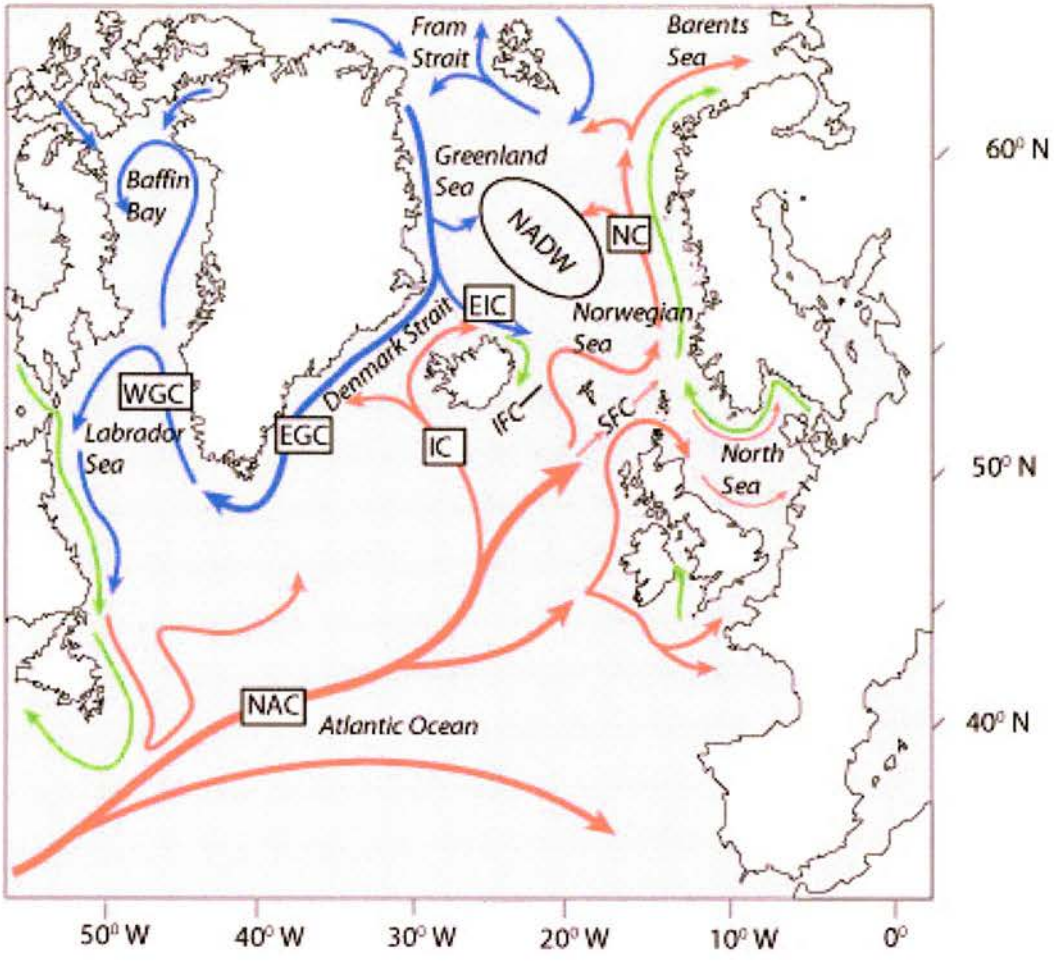

Figure 2.7: Present surface ocean circulation in the North Atlantic showing the zone of NADW formation, and circulation of warm (red arrows), cold (blue arrows) and coastal (green arrows) currents. Currents mentioned in the text are marked in boxes, the positions of the Shetland-Faroe Channel (SFC) and Iceland-Faroe Channel (IFC) are shown (after Levitus, 1982; OSPAR, 2000).

2.7.2 The MRE and ΔR in the North Atlantic: current values

The ^{14}C content of the NAC is high relative to that of surface waters in regions of strong upwelling, (e.g. the Antarctic coast) and equates to apparent ages between c.320-520 ^{14}C yr in modern Atlantic surface water between c.40^{0}N and 40^{0}S, (Broecker and Olsson, 1961). Present assessments of the MRE and ΔR values show considerable variation across the North Atlantic, generally increasing to the north and west and this variation is often associated with oceanographic variables, such as temperature and salinity, that are reflected in the distribution of Atlantic and Arctic water masses (e.g. Mangerud, 1972; Mangerud and

Guliksen, 1975; Eiríksson *et al.*, 2004). In surface ocean areas more strongly influenced by the NAC, the offset between atmospheric and marine ^{14}C ages is lower, due to the higher ^{14}C content of surface waters. This contrasts with areas where higher MRE values are associated with the Arctic-dominated waters, such as the EGC (Hjort *et al.*, 1973). On the east Greenland coast, modern pre-bomb MRE values include 530 ^{14}C yr (Tauber and Funder, 1975) and 515 ± 25 ^{14}C yr (Hjort, 1973, Håkansson, 1983), with a modern (pre-bomb) regional average ΔR of 128 ± 23 ^{14}C yr (Reimer and Reimer, 2005). Around the northern Canadian coast MRE values of c.540 ^{14}C yr increase to c.610 ^{14}C yr in the north shore and estuary of the Gulf of St. Lawrence (Dyke *et al.*, 2003). The largest suggested reservoir corrections in this region (of c.740 ^{14}C y) are located in the Arctic Ocean (Mangerud and Gulliksen, 1975; Dyke *et al.*, 2003), where greater stratification of the water column due to high salinities, is allied with the effect of extensive sea ice cover to prevent CO_2 exchange between the atmosphere and deep ocean. The East Greenland and Arctic values are higher than those for Iceland, where MRE values include 365 ± 20 ^{14}C yr (Håkansson, 1983) and the regional average ΔR is 52 ± 19 ^{14}C yr (Reimer and Reimer, 2005). This results in a modern (pre-bomb) apparent age difference of c.100-150 yr in surface waters across the Polar Front (Eiríksson *et al.*, 2004).

To the east, in the path of inflowing NAC water, values of MRE and ΔR for the British Isles are based upon known-age marine shells from the English and Scottish coasts. These provide a modern regional MRE of 405 ^{14}C yr (Harkness, 1983), and ΔR of 17 ± 14 ^{14}C yr (Reimer and Reimer, 2005). MRE and ΔR values increase northwards along the Norwegian coast with a regional mean ΔR of -3 ± 27 ^{14}C yr for South Norway and the North Sea that increases to ΔR = 65 ± 35 ^{14}C yr for northern Norwegian waters (Mangerud and Gulliksen, 1975; Olsson, 1980; Reimer and Reimer, 2005). The value for the south of Norway may be influenced by the admixture of Baltic Sea water (ΔR = -107 ± 24 yr (Reimer and Reimer, 2005)) to the North Sea and Southern Norwegian coast water. Further north, the increasing influence of Arctic water is also apparent in the West Spitsbergen coastal water (a mix of Arctic and Atlantic water) that displays a MRE of 510 ± 30 ^{14}C yr (Mangerud and Gulliksen, 1975) and ΔR of 93 ± 23 ^{14}C yr (Reimer and Reimer, 2005).

Along with the relative inflow of various surface ocean currents, North Atlantic MRE values are further modified by geographical constraints such as the relative influence of coastal features (e. g. fjords, bays and estuaries) on ^{14}C of surface water. Large fjords, located on many western North Atlantic coasts, may form a spatially-distinct, non-uniform local carbon

reservoir. In these environments the influence of marine currents upon water ^{14}C is attenuated by the influx of variable amounts of freshwater, from terrestrial runoff. Where a large amount of terrestrial water with a significantly different ^{14}C activity to that of marine water enters a fjord, large variations in MRE values can be produced. The large variation in MRE values in Scandinavian fjords for example, has been attributed to this factor (Heier-Neilsen *et al.*, 1995).

The pattern in MRE across the modern North Atlantic indicates that the size of the offset increases in areas more heavily influenced by Arctic water masses. This is particularly apparent in a comparison of values from the far eastern zone (e.g. the North Sea and Southern Norway), and the far western zone (e.g. Labrador and Baffin Bay). However variability in the available data exists for many areas, including the transitional zones between Arctic and Atlantic water at the location of modern North Atlantic frontal systems. This introduces uncertainties when attempting to examine spatial patterns in present MRE values at higher resolution. The implication of spatial patterns in MRE allied with climatic and oceanographic variables is that an understanding is also required of how fluctuations in these variables through time may also be allied with variability in MRE values.

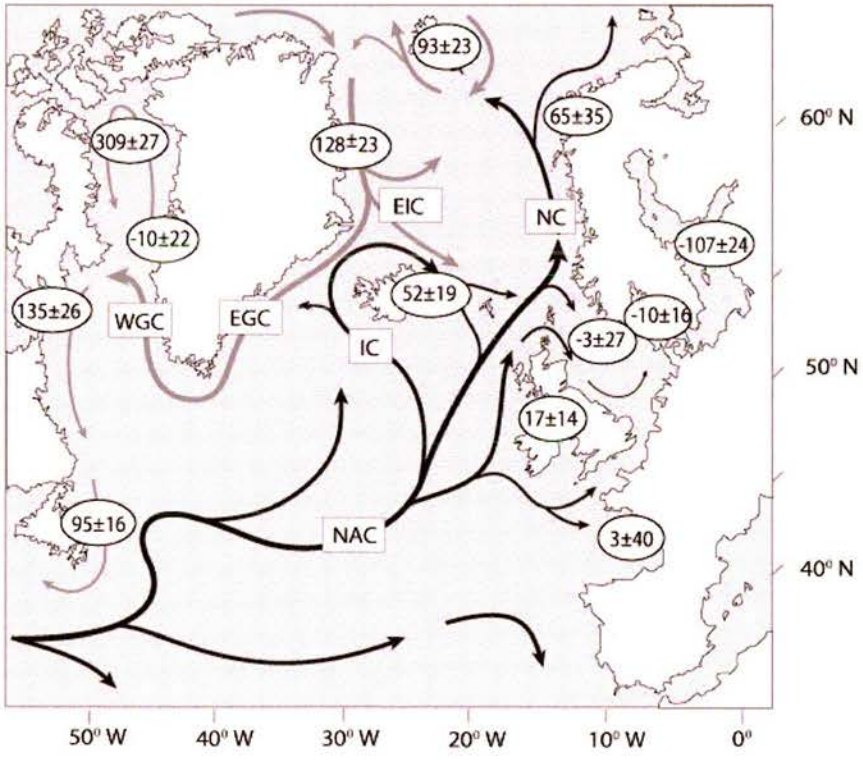

Figure 2.8: Simplified present surface ocean circulation in the North Atlantic showing modern regional mean ΔR values (from Reimer and Reimer, 2005)

2.8 The North Atlantic over the past c.13 kyr BP: evidence for changes in palaeoenvironments and MRE

2.8.1 Changes in palaeoclimate and environment

The ^{14}C method is used for dating samples from the past c.30 kyr within the North Atlantic. Over this time, large environmental changes have been identified in a range of proxy data sources, obtained from both terrestrial and marine sediments, and within cores taken from the Greenland ice sheet. The ice sheet cores (GRIP and GISP2), provide a proxy record of climatic changes over >200, 000 yr (Mayewski and White, 2002) that can be correlated with data obtained from other sources, such as marine sediments. The ratio of $^{18}O/^{16}O$ within the annual ice layers provides a high-resolution proxy record of temperature fluctuations that details both the scale and rate of the inferred climatic changes. From this, palaeoclimatic transitions such as the progression between glacial and interglacial conditions can be identified on a calendar timescale. The most recent transition from full glacial conditions to the present warmer climate (the Holocene) occurred c.15,000 years ago (13,000 ^{14}C BP) and does not appear to have occurred as a constant warming. Instead, climatic conditions fluctuated and included two periods of temporary climatic cooling, known as the Older and Younger Dryas. The Younger Dryas (YD) appears to have been an abrupt return to glacial-type conditions between c.13,000 -11,500 years ago before the final onset of the current Holocene period. These climatic changes were rapidly propagated throughout the North Atlantic atmospheric and oceanic systems, with shifts between warm interglacial conditions and cooling phases on decadal scales (Alley *et al.*,1993; Haflidason *et al.* 1995).

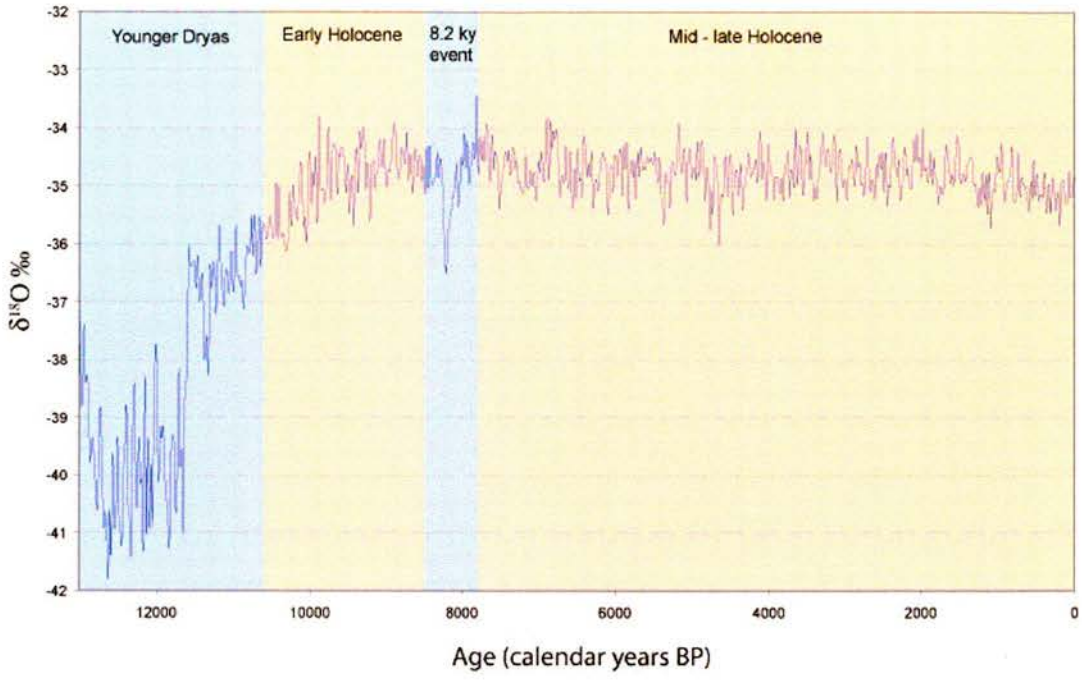

Figure 2.9: GISP2 bidecadal ice core record showing the fluctuations in $\delta^{18}O‰$ through time that are correlated to climatic changes. Lower $\delta^{18}O$ values correspond to colder conditions, including the Younger Dryas interval and 8.2 kyr event, which are themselves linked to shifts in the position of the Polar Front (c.f. Figure 2.10). Data from Stuiver *et al.*, 1997; Stuiver *et al.*, 1995; Meese *et al.*, 1994; Steig *et al.*, 1994.

Key features of these palaeoenvironmental changes include the distribution of Atlantic and Arctic surface waters (Koç *et al.*, 1993), and therefore the position of the Polar Front (Ruddiman and McIntyre, 1981; Dansgaard *et al.*, 1993; Haflidason *et al.*, 1995). Ocean core evidence (e.g. proxy records based on analysis of foraminifera), provides a record of spatial variations in environmental conditions at times of climatic change. These resources show that during colder phases the Polar Front (PF) was shifted south, reflecting a reduction in the strength of the NAC inflow and increase in the extent of continental ice sheets and sea ice cover (Ruddiman and McIntyre, 1981). During periods of climatic warming the PF moved rapidly northwards, reflecting the rate at which warming occurred. Variation in surface water characteristics could have affected the rate at which warm NAC waters were drawn northwards and the rate at which NADW formation occurred at high latitudes. These factors would have altered the amount of latent heat released in the North Atlantic during NADW formation and may have been an important causal mechanism for climatic change. As the Polar Front moved north during early deglacial warming a high influx of warm, saline NAC water may have enhanced NADW production rates and contributed to the climatic warming

(Kroon *et al.,* 1997). As warming continued however, the input of meltwater from continental ice sheets to the surface of the North Atlantic increased, lowering the sea surface salinity (SSS). This process reached a maximum at c.14 cal. kyr BP (Fairbanks, 1989) and the decreased density of high latitude surface water may have inhibited the sinking of NAC waters. As a result NADW production would have been reduced or even halted, lowering both the amount of latent heat released by sinking NAC waters, and the rate at which warm NAC water was drawn northwards (Haflidason *et al.,* 1995).

The YD cold period appears to also be characterised by rapid Polar Front movement and variation in NADW production rates. This climatic phase is linked to extreme temperature decrease, glacial re-advances and increased aridity recorded in both sedimentary and ice core records (Taylor *et al.,* 1997, Björck *et al.,* 1996). The onset of the YD is associated with a sudden southwards PF movement, and very dramatic fall in sea surface temperature (SST) and salinity on a decadal scale (Lehman and Keigwin, 1992; Karpuz and Jansen, 1992; Haflidason *et al.,* 1995; Kroon *et al.,* 1997). The changes in SSS and SST appear to have had the net effect of reducing NADW production, allied to overall reduced northward advection of the NAC (Bondevik *et al,* 2001). The salinity variations at the YD are attributed to meltwater from the Laurentide and Fennoscandian ice sheets (Broecker *et al.*, 1985), and may have been influenced at the onset of the YD by increased precipitation over the North Atlantic due to falling insolation rates (Stuiver and Braziunas, 1993).

The transition from the YD to the Early Holocene appears to have occurred very rapidly, with a 90% complete Polar Front retreat to the far Northwest Atlantic at c.9300 BP (Ruddiman *et al*, 1977). SSTs rose sharply, with an increase of c.9^{0}C over 50 years recorded in the Greenland-Iceland-Norwegian Seas (Koç *et al.*, 1993). Within the early Holocene period a cooling event, (known as the 8.2 kyr event) occurred between 8400-8000 cal yr BP (7650-7200 ^{14}C yr BP (Barber *et al.*, 1999). This is linked to the final meltwater pulses from the Laurentide ice sheet (Barber *et al.,* 1999; Alley *et al.,* 1997; Klitgaard-Kristensen *et al.,* 1998; Birks and Koç, 2002) and is correlated with temperature decreases of 4-8^{0}C in central Greenland (Alley *et al.,* 1997) and a concurrent fall in SST at marine sites in the north eastern North Atlantic (Bond *et al.,* 1997).

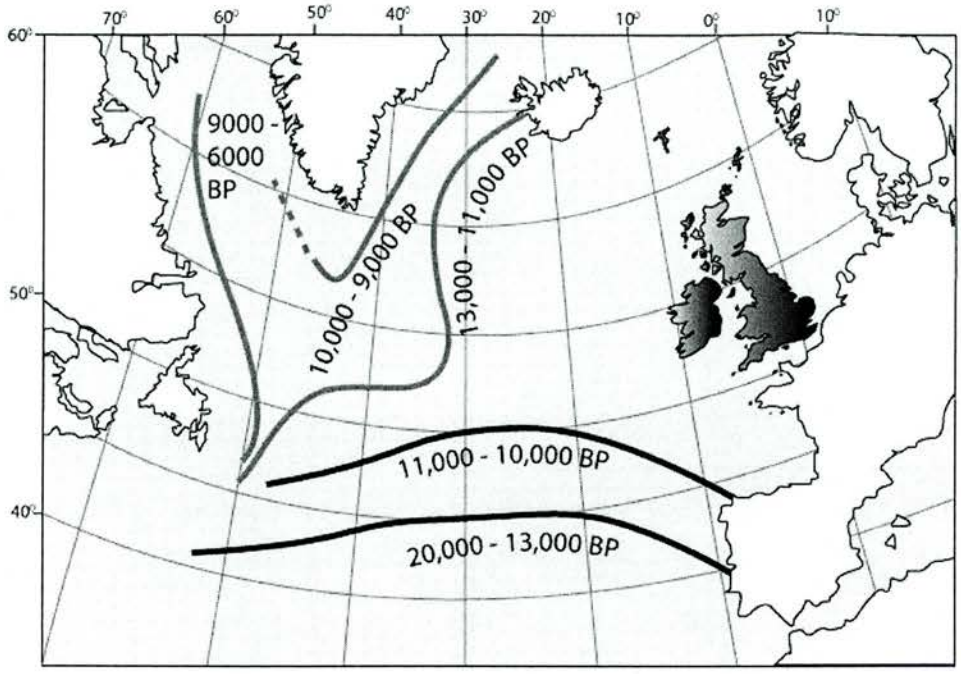

Figure 2.10: Movement of the Polar Front within the North Atlantic from the period 13,000 BP to 6000 BP (redrawn from Ruddiman and McIntyre, 1981). Positions in black mark cold intervals and positions in grey indicate Polar Front location during warmer intervals. The area within which sites investigated in this study are located is shaded. A chronological scale of change is given in ^{14}C yr BP.

SSTs stabilised with the final melting of the Laurentide and Scandinavian ice sheets (Birks and Koç, 2002) and the subsequent Holocene period appears to have been one of stable environmental conditions relative to changes during glaciation (Sarnthein *et al.,* 1995). Holocene proxy records do show however that fluctuations in climatic and oceanographic conditions have been a feature of the past 10 ky. These include periodic peaks in the concentration of ice-rafted debris (IRD) located in marine sediment cores. The seven IRD events appear to have each occurred rapidly over 100-200 yr and to be spaced at intervals of c.1500 yr periodicity (Bond *et al.*, 1997). Two different oceanic regimes are implied; with minimum IRD concentrations linked to elevated SST's and an ocean circulation system that resembles modern conditions. Maxima in IRD concentrations are associated with south eastward advection of ice-bearing surface waters from the Greenland-Iceland Seas into the core of the NAC (Bond *et al.*, 1997; Bond *et al.,* 2001, Giraudeau *et al.* 2000). The long-term Holocene environmental trend appears to have been an early warm phase that culminated in a climatic optimum c.5000 ^{14}C yr BP. This was followed by an overall cooling trend that persisted up to the present time (Eiríksson *et al*, 2000a,b; Marchal *et al.*, 2002; Calvo *et al.*,

2002), and occurred along with falling summer insolation levels. Fluctuations throughout this period include marked cooling events, for example a drop in SSTs at c.3000 cal yr BP (Eriksson *et al*, 2000a,b), which coincides with deposition of the Hekla 3 tephra, and increased terrestrial glacial expansion between 3700-3000 cal yr BP (Stötter *et al*, 1999). This event is followed by a peak in IRD concentration in marine cores at 2800 cal yr BP (Bond *et al*, 1997). Over the past c.2000 years evidence for pronounced climatic fluctuations continues, with two periods in particular identified in the North Atlantic region, termed the Medieval warm period (MWP) and subsequent Little Ice Age (LIA). These terms are a convenient shorthand for apparent warmer conditions in the north Atlantic region between 900 to 1250 AD (c.1050 - 700 cal. yr BP) (Lamb, 1985; Grove and Switsur, 1994), followed by pronounced climatic cooling from c.1300-1400 AD (c.650-550 cal. yr BP) that lasted c.500 yr (Lamb, 1985). The evidence for these phases is derived from a range of data sources within which regional environmental changes are correlated with those apparent in the archaeological record.

North Atlantic ^{14}C yr BP	**Cal yr BP**	**Zone**	**Major features**
To c.13000	25000-15000	Last Glacial	Glacial conditions. Ice cover
c.13000	c.15000	Heinrich event 1 (H1)	Massive ice discharge event to surface ocean
12750-12350	14600-14300	Bølling	Warmer conditions
12350-12150	14300-14000	Older Dryas	Cooling episode.
12150-11350	14000-13000	Allerød	Warmer conditions
11350-10000	13000-11500	Younger Dryas	Short, abrupt and significant climatic cooling. Ice re-advance in many areas
10000-7650	11500-8200	Boreal	Warming temperatures, moister climate
7650-7200	8200-8000	8.2 kyr event	Sudden cool and dry phase in many areas
7500-5000	8200-5700	Atlantic	Holocene climatic optimum. Summer temperature maxima, mild winters, wetter climate
5000-2500	5700-2600	Sub-boreal	Similar to boreal
2500-0	2600-0	Sub-Atlantic	Significant summer temperature decrease, mild winters, precipitation increase

Table 2.3: Table of the major climatic sub-divisions in the North Atlantic from c.13, 000 ^{14}C yr BP. Based on classic European Holocene-Late glacial sequence (Blytt, 1876; Sernander, 1908).

2.8.2 Changes in North Atlantic MRE: links to Palaeoclimatic variations

Palaeoclimatic variations over the period from the last glacial to the Holocene are correlated with changes in the ^{14}C concentration of both the atmosphere and oceans. Climatic changes therefore provide a potential forcing mechanism for fluctuations in North Atlantic MRE values over this time period. As well as being correlated with climatically-driven variability in $\Delta^{14}C_{atm}$ (see section 2.4.3 above), the timing of changes in the ^{14}C activity of the surface and deep oceans coincides with palaeoclimatic changes in proxy records. The factors commonly suggested as forcing mechanisms for observed MRE variations are changes in ocean circulation and sea ice distribution, due to their impact upon the distribution of water masses with varying ^{14}C contents and rates of exchange with atmospheric CO_2. Because these climatic changes are deemed the most probable causal mechanisms to underlie MRE variation, observed ^{14}C variation in North Atlantic water masses has often been used to infer evidence that palaeoclimatic changes (such as differences in the ventilation rates of deep waters) have occurred.

In the North Atlantic, changes in the source and distribution of various water masses since the last glacial have been identified in proxy palaeoclimatic data. These oceanographic changes are cited as a probable cause of MRE variation, and a key mechanism appears to have been variation in NADW production rates. For example, model simulations (Stocker and Wright., 1996) of successive changes in the ventilation times (i.e. rates of overturning circulation) suggest that as NADW production slowed, surface MREs would at first be reduced. This would occur because removal of atmospheric $^{14}CO_2$ to the deep ocean in sinking surface water masses would be reduced. The water masses would instead spend longer periods at the surface where their ^{14}C content would be increased by exchange with atmospheric CO_2, at a time when gaseous exchange rates would also be enhanced by rising levels of $^{14}C_{atm}$ (Stocker and Wright, 1996). During this time, the ^{14}C activity of deep waters would be depleted through radioactive decay while exchange with the surface reservoir was reduced. Increasing sea ice cover leads to a larger increase in $^{14}C_{atm}$, and would further inhibit carbon exchange between the atmosphere and deep ocean, in turn leading to further depletion of deep water ^{14}A. As NADW production rates rose once more models indicate that a rapid rise in surface MRE would result as exchange with ^{14}C-depleted deep waters resumed. These MRE values would subsequently be reduced as increased rates of NADW production persisted, because of increasing rates of NAC inflow and lowered sea ice cover in response to warmer conditions (Bard *et al.,* 1994).

As discussed above, uncertainties associated with the available data limit the level of precision and accuracy to which patterns in modern MRE values can be confidently ascribed. These uncertainties also extend to pre-modern MRE values and are often an inherent product of the methodological approach used to assess values. Uncertainties may be increased for pre-Holocene samples, due to the limitations of sample availability and the methods used to obtain an equivalent terrestrial ^{14}C age for marine measurements. For example, these could include uncertainties over the exact correlation between palaeotemperature variations in ice-core records and terrestrial sediments. The net effect is that there is a lack of high-resolution data for MRE variations from the end of the last glacial to the Holocene.

When examining pre-modern MRE values, the known-age sample methodological approach cannot generally be applied, and suitable pre-Holocene material for determination of the MRE is limited to deposits produced by natural processes. This is due to a lack of North Atlantic coastal archaeological deposits for the pre- and early Holocene because of both the low density of pre-Holocene human populations and removal of previous material by ice action. Marine material for pre-Holocene MRE assessments is therefore obtained from either marine sediment cores or terrestrial deposits containing both marine and terrestrial material. The latter are generally produced by gradual isolation from a fully marine setting, for example by progressively falling sea levels (Bondevik *et al.*, 1999). An equivalent terrestrial age is provided for ^{14}C measurements of marine carbonates from ocean cores by various means in these studies. The tephra isochron approach (see section 2.6.4 above) is often used, where terrestrial ^{14}C measurements are made when a tephra can be located in onshore deposits (e.g. Bard *et al.*, 1994; Haflidason *et al.*, 2000). A terrestrial age for a tephra located in a marine core may already be available from previous assessments.

Allied with, or instead of the tephra isochron method, an equivalent terrestrial ^{14}C or calibrated age is also estimated by authors for marine sediments using palaeoclimatic records. Fluctuations in sea surface temperature (SST) can be reconstructed from marine core sediments using records of foraminiferal abundance and isotopic values (i.e. $\delta^{18}O$). These are then correlated with records of atmospheric conditions in dated terrestrial deposits and the Greenland ice cores (e. g. Waelbroeck *et al.*, 2001; Björck *et al.*, 2003).

It is important to note that ΔR values are not generally calculated from pre-Holocene marine ^{14}C values as the atmospheric calibration dataset for this period that would be used in calculation is itself derived from measurements of marine samples corrected for a site-specific MRE (see section 2.4.5 above). Instead, assessments focus on deviations of the

apparent surface age of Atlantic water from present MRE values of c.400 yr at a range of sites across the North Atlantic.

The impetus behind the majority of studies that seek to quantify MRE values from the last glacial onwards is the need for a better understanding of the MRE in order to facilitate palaeoclimatic investigation. There is a desire to correlate between ice-core, marine and terrestrial records from the period of the last deglaciation so that the timing of palaeoclimatic changes such as temperature variations and the way in which these changes were propagated through terrestrial and marine systems can be determined. To achieve this aim there is a requirement for a reliable chronological method that can place the different types of data on an equivalent timescale. The ice-core chronology is given in calendar years before present, achieved by layer counting for this period, with associated uncertainties of <550 yr over the past 15ky (Alley *et al.*, 1993). The terrestrial and marine records generally lack annual layers, therefore sediments must be dated by other means, and ^{14}C measurements are generally used. Precise correlations between ice-core, terrestrial and marine records have often been proposed and used to draw interpretations of palaeoclimatic variation (e. g. Bond *et al.*, 1993). However, the precise nature of the North Atlantic MRE from the last deglaciation is at present imperfectly understood. This is due to several factors, including a limited range of available data that often exhibits relatively large associated uncertainties.

Assessments of the ^{14}C age of both surface and deep North Atlantic water masses during the last glacial indicate that increased offsets between atmosphere and ocean existed during this time. Broecker *et al.* (1990) found the ^{14}C age of NADW in the tropical Atlantic appears to be 675 ± 80 yr during the peak glacial, which they compared to an estimated modern value of c.350 y. Surface MRE assessments in the West Iceland Sea include c.950 yr at c.25,000 cal yr BP, increasing to c.2240 yr at the glacial maximum (c.18,000 cal yr BP (Voelker *et al.*,1998). These were inferred from the difference in planktonic and benthic foraminiferal ages in a marine core where contrary to expected, the ^{14}C age of the benthic specimens were considerably younger than the planktonic. This effect was not observed in a core of similar age taken off the west coast of Norway, and the authors attribute the effect to a phase of younger deepwaters and older surface waters in the area. The higher surface MRE calculated from the planktonic specimens was attributed to increased sea ice cover (that inhibited atmosphere-ocean gas exchange) west of Iceland during this phase. The younger benthic ages were attributed to the influx of newly-produced glacial deepwater which had formed in a largely ice-free Norwegian Sea. In contrast, elevated glacial MRE values relative to present are not observed further south in the Mediterranean Sea, where Siani *et al.* (2001) record an

MRE of 350 ± 150 y, close to the present value for this area of 390 ± 80 yr (Siani *et al.*, 2000).

The onset of the deglacial period is marked by proxy records in North Atlantic marine cores of a massive iceberg discharge, known as Heinrich Event 1 (H1). During this event Mediterranean MRE values apparently increase to 820 ± 120 yr at c.17,000 cal. yr BP and 810 ± 130 yr at c.15,700 cal yr BP (Siani *et al.*, 2001). A concurrent rapid increase in western North Atlantic intermediate water of c.670 ^{14}C yr is recorded at 15,410 cal. yr BP in corals situated at 40^{0}N (Adkins *et al.*, 1998). This apparent ageing of intermediate waters is postulated as a mechanism for surface MRE increases south of the Polar Front by Siani *et al.*(2001), and both authors suggest that a reduction in thermohaline circulation (due to H1) and increasing input of ^{14}C-depleted Southern Ocean source waters may be responsible for the observed MRE increases. North of the Polar Front at c.15,000 cal. yr BP, surface MRE values of 1630 ± 600 and 2340 ± 750 yr are derived from marine cores between 37-55^{0} N (Waelbroeck *et al.*, 2001). Raised MRE values for H1 are also recorded by Voelker *et al.* (1998) in the West Iceland Sea, who observe MRE values of between c.630 and c.1160 yr at 14,600-18,100 cal yr BP.

MRE values for the Bølling/Allerød along the west coast of Norway at 12,300-11,000 ^{14}C yr BP are 380 ± 32 y, almost identical to present values for Southern Norway of 379 ± 20 yr (Bondevik *et al.*, 1999). These authors hypothesised that it was possible for lower values to be observed in this area due to the persistence of an ice-free zone along the Norwegian coast from the deglacial to the Younger Dryas (Sarnthein *et al.*, 1995). Other authors also infer a MRE similar to present values during the Bølling/Allerød (Waelbroeck *et al.*, 2001), and values close to modern (with an upper limit of 700 y) are inferred at 13,000 cal. yr BP in North Atlantic intermediate waters (Adkins *et al.*, 1998). In contrast, Younger Dryas MRE values appear significantly greater relative to present-day data in several studies. At the Vedde Ash layer, dated to 10310 ± 50 BP (Birks *et al.*, 1996), corresponding to c.12,000 cal yr BP (11830-12387 cal yr BP at 2σ), elevated MRE values are observed across the North Atlantic. Here, values at on the West Norwegian coast are 610 ± 55 yr (Bondevik *et al.*, 2001), and an increase is apparent in determinations made from the coast of Norway to the open North Atlantic and Nordic Seas (Bondevik *et al.*, 2001). This effect has been linked to a change in North Atlantic oceanic circulation rates and distribution of sea ice cover in the region during the Younger Dryas (Bard *et al.*, 1994).

MRE values at the Vedde Ash layer are 700-800 yr in four cores across the North Atlantic (Bard *et al.*, 1994), 700-800 yr on the Hebridean Shelf off the northwest coast of Scotland (Austin *et al.*, 1995), between 700 and 1100 yr off the Norwegian coast (Bard *et al.*, 1994; Haflidason *et al.*, 1995) and 750-800 yr on the North Icelandic Shelf (Haflidason *et al.*, 2000). At the end of the Younger Dryas period, Waelbroeck *et al.*, (2001) observed MRE values of 1220 ± 430 and 1410 ± 340 y. Raised MRE values relative to present during the Younger Dryas north of the Polar Front position (see Figure 2.10) contrast with values for the Mediterranean at 10,450 ± 40 ^{14}C yr BP (12,634-12,315 cal yr BP), which at 380 ± 100 yr are similar to present (Siani *et al.*, 2001). This suggests that these differences may reflect a surface ocean latitudinal ^{14}C gradient across the Polar Front at the Younger Dryas that is similar to present. In the Norwegian Sea, MRE values appear to be c.1000 ^{14}C years between c.15,000-11,000 cal. yr BP. Over this time the values fluctuate, reaching maxima at 12,300 and 13,600 cal yr BP and minima at 11,500, 13,000, and 14,500 cal yr BP (Björck *et al.*, 2003). However there does not appear to be any consistent increasing or decreasing trend in values over c.4000 y, which is inconsistent with the pattern observed by other authors of decreasing MRE values from H1 to the Bølling/Allerød (Björck *et al.*, 2003).

Fluctuations in MRE values for the Holocene in the North Atlantic are recorded from sites over the past 10 ^{14}C kyr BP, and have been linked to oscillations in the position of the Polar Front and periodic eastward incursions of polar waters. During the Early Holocene at c.9000 ^{14}C yr BP MRE values larger than present have been observed, e.g. 690 yr off the west coast of Norway, and 730 years off the North Icelandic coast (Haflidason *et al.*, 2000). Over the past 4600 cal y, Eiriksson, *et al.* (2000a) associate lower MRE values (c.400 ^{14}C y) on the North Icelandic shelf with dominance of the Irminger Current and an increase in MRE to 530 ^{14}C yr with increasing influence of the East Icelandic Current in the area. Overall, ΔR values on the North Icelandic shelf obtained using correlation of tephra markers found in marine cores show values higher by up to 450 y, than those predicted by the marine model curve for the last 4500 yr (Eiríksson *et al.*, 2004). In this dataset, lower ΔR values occur around c.4000 cal yr BP, generally increasing to 2650 cal BP, with lower values observed at 3700 cal yr BP. ΔR values are also lower at 2000 cal yr BP and 800 cal BP, and also possibly within the last 150 y.

must be taken into account, and an assessment of sedimentation rates made. While some sites display very high sediment accumulation rates, for example c.1cm y^{-1} for the Younger Dryas interval on the Hebridean Shelf (Austin *et al.*, 1995), rates at other sites may be lower than this (eg. c.8-20 cm ky^{-1}, (Voelker *et al.*, 1998)) and a correction for bioturbation bias may be required (eg. Bard *et al.*, 1994). The uncertainties associated with pre-Holocene MRE determinations are often relatively large, and inhibit the production of a precise value. This not only limits determination of the timing of specific palaeoclimatic events, but also the study of temporal fluctuations in MRE itself. This is because of the requirement that data be of a high enough resolution to observe events that may often be rapid. For example, Stocker and Wright (1998) note that an increase in MRE values during Younger Dryas-type climatic cooling events in the North Atlantic, and subsequent fall in MREs following climatic warming occur within a relatively short time interval and ^{14}C dating at resolutions of <100 ^{14}C yr would be required to adequately resolve the signal.

It is also important that caution is exercised when interpreting observed or estimated MRE variations in terms of palaeoclimatic forcing mechanisms. In the modern oceans there is a lack of information concerning a quantified relationship between the intensity of climatic variables and the size of the MRE in a location. This is due to limitations on the level of resolution to which both the MRE and the potential climatic and oceanographic forcing mechanisms have been determined. Model simulations of oceanographic change can provide such quantifiable data (Stocker and Wright, 1996; 1998), however, there is a lack of an extensive empirical dataset with which model simulations can be compared. This means that specific links between MRE values and climatic and oceanographic change remain theoretical, and an identified MRE variation in a dataset is not in itself definitive evidence of a specific climatic or oceanographic change and vice versa. It is important to avoid summoning of palaeoclimatic explanations that best fit the observed variations in MRE but which have no definite demonstrable link to the data as a causal mechanism. In this way unexpected data can be explained in terms of pre-existing palaeoclimatic variations. The data should rather be assessed critically and factors such as the range of inherent uncertainties in the sample and data itself should be taken into account. Therefore, a more rigorous approach is required to provide a higher resolution dataset by reducing uncertainties associated with examining temporal change in the MRE. It is also important to determine the level to which it is possible to identify variation in the MRE throughout specific periods of palaeoclimatic change recorded in proxy data such as the ice-cores.

At present these difficulties remain unresolved. Ambiguity in the available data means the absence of an agreed consensus value for MRE correction in many areas and many time periods. Approaches to the problem include working with marine ^{14}C ages in their uncalibrated form, adoption of the modern c.400 yr North Atlantic MRE value for all time periods, or use of a correction value that is either selected from an available dataset or independently determined. The various applications of these approaches could reduce the level to which various datasets are easily inter-comparable, and would therefore be detrimental to the aim of resolving ice, terrestrial and marine records of palaeoclimatic data.

2.8.3 The importance of accurately defining North Atlantic MRE values

The existence of a relevant MRE correction value is crucial to the production of accurate, useful ^{14}C ages using marine material, as it is through this quantity that marine ages from a specific ocean area can be compared with other ^{14}C ages of marine and terrestrial material within a chronological framework. The applicability of a MRE or ΔR correction value based upon empirical measurement is directly proportional to the accuracy and precision of the ^{14}C measurements, and the degree to which methodological assumptions are correct. The currently available dataset of MRE and ΔR values has been obtained using a wide variety of methodologies, measurement techniques, and sample materials over more than 30 years. Previous determinations made using radiometric measurements were limited by considerations of sample size, which may have led to selection of less than optimum samples for measurement. Although understanding of the MRE has been improved by increased numbers of studies in recent years, the present range of data on temporal variations in ΔR and MRE is somewhat variable and limited in extent. Such studies have been limited by the availability of material and have tended to focus upon a small number of measurements from a single geographic location.

The palaeoenvironmental changes in the North Atlantic from the end of the last glacial period have great importance for our understanding of global environmental systems. A common theme raised by studies of MRE variation since the last glacial is the need for a common temporal framework for terrestrial, ice-core and marine records of palaeoenvironmental change.

Records of North Atlantic palaeoclimate and palaeoceanography are the subject of intensive study, and a key aspect of this is the ability to correlate changes between sources of data such as ice cores and marine sediments. To achieve this there is a requirement to obtain the

best chronological information possible, to place data on an absolute chronological timescale. The status of ^{14}C measurements as an invaluable tool in North Atlantic environmental reconstructions, coupled with the use of marine sediments and marine organisms for ^{14}C measurements has made the MRE a crucial consideration. As discussed above, as well as being a climatically important region, the North Atlantic has great archaeological significance for our understanding of past human cultures. The region is very rich in the remains of human settlement, which includes an abundance of coastal archaeological sites, where the inhabitants made extensive use of marine resources. This means that marine carbon is often present in sample material for ^{14}C measurement, both in the remains of marine organisms such as fish and shellfish, and in terrestrial organisms, including humans, that fed upon marine resources. The implication is that accurate assessments of MRE values are essential in order to produce relevant palaeoenvironmental and archaeological chronologies within the North Atlantic. This includes an understanding of spatial and temporal variations in the MRE in the region.

Chapter 3: Methodology A: Materials, sites and contexts

As discussed in the previous chapter, certain methodological factors can result in uncertainties associated with MRE assessments that limit the level of accuracy and precision available. The methodology developed in this study was specifically designed to reduce such uncertainties that may result in variability in MRE values. To achieve this aim the paired sample approach was used and ^{14}C measurements were made of terrestrial and marine material from coastal archaeological deposits. An essential requirement of the approach is that the measured terrestrial and marine samples that are used to produce a value of MRE and ΔR were formed at the same point in time. To meet this requirement a strict protocol was adopted for selection of samples to measure (see section 3.2 below and Ascough *et al.*, in press). Another key consideration was to choose sample material that would maximise the spatial and temporal range of the data. This chapter describes the rationale behind the type of terrestrial and marine material chosen for measurement, and the choice of specific sites and specific deposits from which to obtain samples. The result was the selection of multiple samples of terrestrial cereal grains, hazelnut shells or mammal bones and marine mollusc shells from 30 sealed archaeological deposits (known as contexts). These were located at 20 archaeological sites on the west coast of Ireland, western and northern Scotland and the Faroe Isles, covering the period from the Mesolithic (c.6000 BC) to the Medieval (c. 1500 AD).

3.1 Sample material chosen for measurement

3.1.1 Selection criteria

Each terrestrial or marine sample chosen for ^{14}C measurement met four criteria:

- A short (<20 yr) time of formation
- Part of a single organism (single entity)
- Likely to have entered the deposit a short (<5 yr) time after death
- A low likelihood of carbon exchange after death

The importance of a short (<20yr) formation time

The ^{14}C content of a sample reflects that of the environment in which it grew. If the sample was formed over a long period its ^{14}C content will be an average of changes in atmospheric or marine ^{14}C over this time. This can affect the level of precision and accuracy to which MRE values can be calculated. Firstly, it is easier to establish that a terrestrial and a marine sample represent the same calendar time span when using material with a short formation period. This is because any difference in the time taken for the samples to form will not be significant with respect to the precision of the ^{14}C method. If a sample formed over 5 yr is compared with one formed over 100 yr the ^{14}C content of the samples will represent an average of different time periods, even if the samples share the same calendar age of death. In some samples with a long formation period, a second problem is that the mass of material associated with different ^{14}C ages varies within a sample. This may apply to wood or charcoal samples, as the inner, older tree rings comprise less mass than outer rings. In this case, the overall sample ^{14}C age is biased towards the ^{14}C age of the sample part that has the greatest mass. When a fragment of wood or charcoal is measured it may not be possible to determine whether the sample represents an inner or outer portion of the tree. The measured age of these samples may not be an accurate representation of the ^{14}C age of terrestrial carbon at the time the tree died.

The importance of a single entity

The improved accuracy gained by measuring short-lived organisms can be reduced if many individual organisms are combined for a ^{14}C measurement. This is often necessary with radiometric analysis due to the small mass of individual short-lived (i.e.<5 yr) species (e.g. cereal grains) and means that the final measurement is derived from an average of many potentially different ^{14}C ages. This may not be a problem where enough material is available from an archaeological context that meets selection requirements (i.e. it is likely all material within a deposit is of the same calendar age range). However the range of such deposits is small and therefore a severe limitation is placed upon the number of suitable contexts. It is impossible to determine how accurately an age produced from measuring many individual organisms represents the range of ^{14}C ages that are combined. If a number of measured organisms have an age that is very different to that of others in the sample this will reduce the accuracy of the final ^{14}C age. If multiple single entities are measured from a context using AMS it is possible to more

accurately assess the range in ^{14}C age of samples within that context. This improves the confidence level to which interpretations can be drawn from the measured ages.

The importance of a short interval (<5 yr) between death and deposition

The likelihood that marine and terrestrial samples represent the same calendar age range is greatly increased if there was a short (e.g. <5 yr) time between death of the organisms and deposition of the samples in a context. If the time between death and deposition is extended, it is more likely that the terrestrial and marine samples were grown at significantly different points in time with respect to the typical measurement precision (c. ± 35 ^{14}C yr). The various natural and human processes that determine how, when and where a sample entered an archaeological deposit and its location when excavated are known collectively as the "taphonomy" of an object (Evans and O'Connor, 1999). It is important therefore that material used for the paired sample approach to determine MRE is likely to have experienced a minimum of taphonomic processes. Certain types of sample are likely to have undergone more taphonomic processes, such as reuse or transport between sites. These include objects that are of specific cultural significance or can be recycled for several purposes, such as building timbers. In addition, certain materials are likely to have survived an extended period in the environment, such as driftwood that has been burnt as fuel. Samples for the paired sample approach should therefore be material that is often deposited as the direct result of short-lived (sub-annual) intensive human economic activities such as cereal processing or dumping of food waste.

The importance that post-death carbon exchange has not occurred

It is possible for certain materials to take part in exchange with environmental carbon after death or final formation. Sources of carbon exchanged with the sample include groundwater or soil porewater, and this will change the ^{14}C age of the sample. It is not possible therefore to derive an accurate MRE value from samples that have undergone carbon exchange after death or formation. The sample materials used in this study were chosen because they were not likely to have taken part in such exchange. In addition the possible mechanisms of exchange for the types of sample material used are well characterised and for each sample type an effective laboratory method exists to remove this type of contamination.

3.1.2 The sample materials selected

Terrestrial samples

The majority of terrestrial samples were carbonised cereal grains, and burnt hazelnut shells were used in two instances. This material is not subject to reuse, represents a seasonal growth period and once carbonised is relatively inert and is therefore resistant to carbon exchange. For these reasons the use of carbonised plant remains for MRE determination is advocated by a number of authors (Facorellis, 1998; Albero *et al.*, 1986; Reimer *et al.*, 2002). At sites where cereals had not been cultivated or consumed in large quantities terrestrial mammal bones (red deer and cattle) were used. The time for complete replacement of bone collagen (turnover time) within a mammal is estimated as 10-30 years (Libby *et al.*, 1964; Stenhouse and Baxter, 1979). It is possible for terrestrial mammals to incorporate marine carbon into bone collagen if marine material forms a significant component of the diet (Arneborg *et al.*, 1999). This effect would reduce the accuracy of MRE values calculated using such samples and the $\delta^{13}C$ of all bone samples was examined for any evidence of a marine dietary component. Signs that bone material has undergone exchange with environmental carbon include a lack of structural integrity and low standard of preservation. This can be identified by examination of the sample to determine whether the bone has retained its original structure and is not "crumbly" in texture or has been strongly discoloured (e. g. yellow or brown colouration). Bone that has been used at a site to produce artefacts such as tools can have survived an extended time between death and deposition in a context. For this reason the selected bone samples had not been modified by any means other than butchery.

Marine samples

The marine samples were all marine mollusc shells of species with lifecycles of c. 5-15 y. Molluscs precipitate their shell carbonate in isotopic equilibrium with the ambient water (Keith *et al.*, 1964; Grossman and Ku, 1986; Forman and Polyack, 1997) and have limited mobility. These samples are therefore a good record of surface water ^{14}C at a location, compared to migratory marine species such as whales, whose ^{14}C content reflects an average of water over a wide area (Schell *et al*, 1988). Marine molluscs in archaeological contexts are often the result of economic practices, including use as fishing bait or collected as food, and experience a short time period between collection and being discarded (Barber, 2003). It is possible for marine

mollusc shells to undergo exchange with environmental carbon while within a deposit by recrystalisation of the shell surface (Bezerra *et al.*, 2000). This contamination can usually be identified by inspection of the shell to ensure that the surface morphology resembles that of living specimens, where structures such as ridges and growth lines are preserved across the entire specimen. Standard pre-treatment processes for marine shell involve removal of surfaces that can undergo carbon exchange.

Terrestrial		**Marine**	
Material /species	***No. of contexts***	***Material /species***	***No. of contexts***
Barley grain (*Hordeum sp.*)	24	Limpet (*Patella sp.*)	25
Oat grain (*Avena sp.*)	1	Periwinkle (*Littorina littorea*)	3
Hazelnut shell (*Corylus avellana*)	2	Cockle (*Cerastoderma edule*)	3
Cattle bone (*Bos sp.*)	1	Mussel (*Mytilus edulis*)	2
Red deer bone(*Cervus elaphus*)	2	Razor shell (*Ensis sp.*)	1

Table 3.1: Summary of all selected sample materials and species

3.2 The archaeological sites

Samples of marine and terrestrial material were taken from contexts at 20 archaeological sites in northern and western Scotland, western Ireland and the Faroe Isles. This covered a total latitudinal range between 53^0- 61^0 N and a longitudinal range of 10^0-1^0 W. This region has an abundance of suitable sites from which to obtain material for the paired sample methodology. This is due to a large amount of extant archaeological remains in coastal settings at which the inhabitants made extensive use of both terrestrial and marine resources. In addition, samples from these sites are easily accessible because of a large number of completed and ongoing archaeological excavations from which detailed records and sample materials are available. It was possible using the selection protocol described below to obtain samples from sites that covered a total calendar age range of c.8000 years of human activity.

3.2.1 Selection criteria

Three main factors were examined to select each site that was included in the study:

- The geographic location and relation to offshore conditions
- The type of prehistoric activity that had taken place
- The programme of archaeological excavation that had been applied.

The importance of site location

The influence of local geographic features was avoided by selecting sites from exposed coastal locations away from estuarine settings that could potentially introduce significant amounts of terrestrial organic detritus and carboniferous geological material (Spiker, 1980, Reimer *et al.*, 2002).

Certain geographic features such as sheltered topography (e.g. fjords) and carbonate geology can modify the ^{14}C content of surface ocean water in a specific location. Because this also alters the ^{14}C content of marine samples, these geographic features can determine the size of calculated MRE values. In this case it can be difficult to make meaningful comparisons between MRE values at sites where the size of the offset between terrestrial and marine ^{14}C ages is the result of different controlling mechanisms. In areas of enclosed coastal topography the extent of mixing with open ocean currents may be limited and there is an intensified contribution of terrestrial runoff to the surface water (Spiker, 1980; Heier-Neilsen *et al.*, 1995). The ^{14}C content of terrestrial freshwater contains variable amounts of terrestrial organic material, and of bicarbonate from dissolution of carboniferous rocks. This means that the ^{14}C activity of freshwater may be significantly different to that of open ocean surface water (Tanaka *et al.*, 1986; Heier-Nielsen, 1995; Goodfriend and Flessa, 1997).

The importance of the type of prehistoric activity

Sample sites were chosen by examination of detailed excavation reports and close consultation with the excavators of each site. The factors that were considered for each site were:

- The time period during which activity took place
- The duration of activities
- The use of resources
- The presence of deposit types relating to specific cultural and economic practices (e.g.: stratified middens produced by dumping of economic refuse)

An effort was made to include sites from a wide range of time periods, using the chronological information (including ^{14}C measurements) available from site excavation records. Other information obtained from site records concerned the site deposits that had been formed by prehistoric activity. To achieve precise and accurate MRE values meant that certain types of deposit that were the result of specific human processes had to be present. Therefore, the activity at a site had to be of sufficient duration to produce a sequence of individually identifiable, stratified deposits. In addition, both local marine and terrestrial resources had to be present in these deposits in significant amounts. Furthermore, it should be likely that the activities that had produced the deposits occurred over a short time interval, such as dumps of refuse in a midden resulting from cereal processing and fishing using marine molluscs as bait.

The importance of the programme of archaeological excavation

Where an archaeological site was in a suitable geographic location and contained suitable deposits from which to obtain samples, the final consideration was how the site had been excavated, specifically:

- The extent of excavated deposits
- The site sampling programme
- The range of investigative techniques applied at the site
- The availability of site records and environmental samples

In order to obtain useful samples, the excavation programme must have resulted in the excavation, recording and collection of environmental samples from suitable deposits. The excavation records had to contain a large amount of contextual information, including data on the matrix within which samples were located, its position within the soil or sediment profile and its association with both other environmental remains and human activities.

3.2.2 The selected sites

According to the criteria identified above, 20 archaeological sites were selected. The site locations are given in Figure 3.1 and the sites are briefly described in Table 3.3. The references for each site given in Table 3.4 provide full details of the archaeological excavation, including the extent and nature of excavated deposits, and the interpretations drawn concerning prehistoric activity at the site.

There are similarities in the location of all selected sites within the study region:

- Located on or next to the coastal zone
- In an area of exposed coastal topography (e.g. non-estuarine)
- In an area of non-calcareous geology
- In an area with a prevalence of archaeological remains and favourable conditions for preservation

The sites are located in coastal zones of Atlantic islands and the waters offshore lie upon the continental shelf, which influences circulation patterns and exchange with the North Atlantic Current. In deeper waters (>150m) beyond the continental shelf break the water is of Atlantic origin with salinities >35‰. Closer to the coast the continental shelf modifies exchange between the deep ocean and coastal seas and water masses consist of a mixture of source waters. For example water on the Scottish western continental shelf has three sources. The main source is Atlantic water (salinity >35‰), with a portion of northward flowing water from the Irish Sea (salinity 34.0-34.5‰) and of lower salinity coastal water derived from terrestrial runoff from the Scottish mainland (OSPAR, 2000; Gillibrand *et al.*, 2003). The area is geologically diverse, with underlying rock types that range from sedimentary (e.g. Old Red Sandstone) to metamorphic (e.g. Lewisian gneiss). However, no site is located on or near to calcareous geological sources,

and these tend not to be a feature of the area within which any site is situated. The climate of all areas is characteristic of the western coastline of North Atlantic islands, with cool, fresh summers and mild winters, also high prevailing wind speeds and rainfall that strongly influences vegetation coverage. Climatic similarities are also visible across the study region in terrestrial palaeoenvironmental records which share the large-scale features within the North Atlantic from the last deglaciation that are described in Chapter 2. The changes in topography and vegetation that were produced by these climatic changes do however show variation between areas, being influenced and modified by local factors.

There is evidence for a human presence across the region from various initial dates over the Holocene, and once established, human occupation of the region has produced a wealth of archaeological remains. These cover a variety of time periods that are commonly subdivided into units based upon cultural attributes and chronological information (see Table 3.2). In this thesis, subdivisions used to describe these chronological periods are based upon the general schemes of several authors (Parker Pearson and Sharples, 1999; Edwards and Ralston, 1997). These subdivisions are used to relate sites to one another and later within the interpretation of ^{14}C measurement results. Stratigraphic preservation of archaeological remains in areas close to the sites is excellent due to an absence of intensive post-industrial agriculture or large urban areas, and in several locations to the deposition of dune sands over prehistoric settlements, which sealed structures and deposits.

Period	**Approx. calendar age range**	**Approx. ^{14}C age range BP**
Mesolithic	8000 BC – 4000 BC	8800 - 5200
Neolithic	4000 BC – 2500 BC	5200 – 4000
Bronze Age	2500 BC – 700 BC	4000 – 2500
Early Iron Age	700 BC – 100 BC	2500 – 2100
Mid Iron Age	200 BC – AD 200	2100 – 1800
Late Iron Age	AD 200 – AD 900	1800 – 1200
Norse	AD 900 – AD 1100	1200 – 900
Historic/Medieval	AD1100 – AD 1400	900 – 600

Table 3.2: Archaeological subdivisions of cultural periods apparent within the wider study area.

For convenience, the wider study region is divided into six areas, within each of which several selected archaeological sites are located. In the following section the sites are placed in context of their specific geographic area, considering each area in turn. This includes oceanographic characteristics as well as features of geology and topography. These features should not be considered in isolation, because it is the interactions between them that have dictated both

palaeoenvironmental histories and present landscapes. For example, the underlying geologies in all areas have influenced topographic features by determining patterns of differential erosion by glacial ice, fluvial and marine action, and these features have in turn influenced human settlement patterns.

A system of notation has been adopted throughout this thesis by which the various selected sites and contexts will be referred. This consists of an abbreviation of the site name, followed by the specific context number that was assigned by the site excavators to the sampled context. The abbreviations assigned to each site are in bold in Table 3.3, and the context identification codes are in Table 3.5. When a site is referred to in the text hereafter it is by the site code (e.g. **SA**), and when a context is referred to it is by the site code and context code (e.g. **SA-13**).

Area	Location	Site (site code)	Time period	Site type
1	West Ireland	Omey Island **(OI)**	Bronze Age - post-medieval	Settlement and associated deposits, Christian burial site
		Doonloughan 3 **(DL-3)**	Norse/Early Christian	Structure and associated deposits
		Doonloughan 11 **(DL-11)**	Norse/Early Christian	Settlement and associated deposits
2	Mainland Scotland	Sand **(SA)**	Mesolithic	Large shell midden sequence
		Carding Mill Bay **(CMB)**	Neolithic - Bronze Age	Shell middens and cist burial
		Freswick Links **(FL)**	Pictish - Norse	Settlement and associated deposits
		Roberts Haven **(RH)**	Norse - Medieval	Settlement and associated deposits
3	Outer Hebrides	Northton **(NO)**	Neolithic - Mediaeval	Small scale structure and associated midden
		Baleshare **(BA)**	Bronze Age - late Iron Age	Settlement and associated deposits
		Hornish Point **(HP)**	Iron Age	Settlement and associated deposits
		Berie **(BE)**	Iron Age - later Pictish	Settlement and associated deposits
		Bostadh **(BO)**	Iron Age - Norse	Settlement and associated deposits
		Galson **(GA)**	Iron Age - Norse	Cist cemetery, settlement and associated deposits
4	Orkney Islands	Skara Brae **(SkB)**	Neolithic	Settlement and associated deposits
		Lopness **(LO)**	Bronze Age	Burial cist containing possible ritual deposits
		Birsay Bay **(BB)**	Bronze Age	Small scale structure and associated midden
		St. Boniface **(StB)**	Bronze Age - Norse	Settlement and associated deposits
		Quoygrew **(QG)**	Norse - Medieval occupation	Settlement and associated deposits
5	Shetland Islands	Scatness **(SC)**	Bronze Age - post-medieval	Settlement and associated deposits
6	Faroe Islands	Undir Junkarinsfløtti **(UJ)**	Norse – Medieval	Sequence of midden deposits

Table 3.3: Selected archaeological sites showing geographical area within the wider study region, period of prehistoric occupation and excavated deposits. References for each site are summarised in Table 3.4.

Site	References
OI	O'Keeffe, 1994
DL-3	Murray, 1999
DL-11	Murray, 1999
SA	Finlayson *et al.*, 1999; Hardy and Wickham-Jones, 2003; 2004; in press
CMB	Connock, 1988; 1990; Connock *et al.*, 1992
FL	Morris *et al.*, 1995
RH	Barrett, 1992; 1993
NO	Gregory *et al.*, in press
BA	Barber, 2003
HP	Barber, 2003
BE	Harding and Gilmour, 2000
BO	Neighbour and Burgess, 1996
GA	Neighbour and Church, 2001
SkB	Clarke, 1976
LO	GUARD, 2004
BB	Morris, 1979; 1989
StB	Lowe, 1998
QG	Barrett and Moore, 2001; Barrett and Gerrard, 2002
SC	Dockril *et al.*, 1995; 1997; 1998; 1999; 2000; 2001; 2002; 2003; Turner *et al*, 1996,
UJ	Church *et al.*, in press

Table 3.4: References for each selected archaeological site (c.f. Table 3.3).

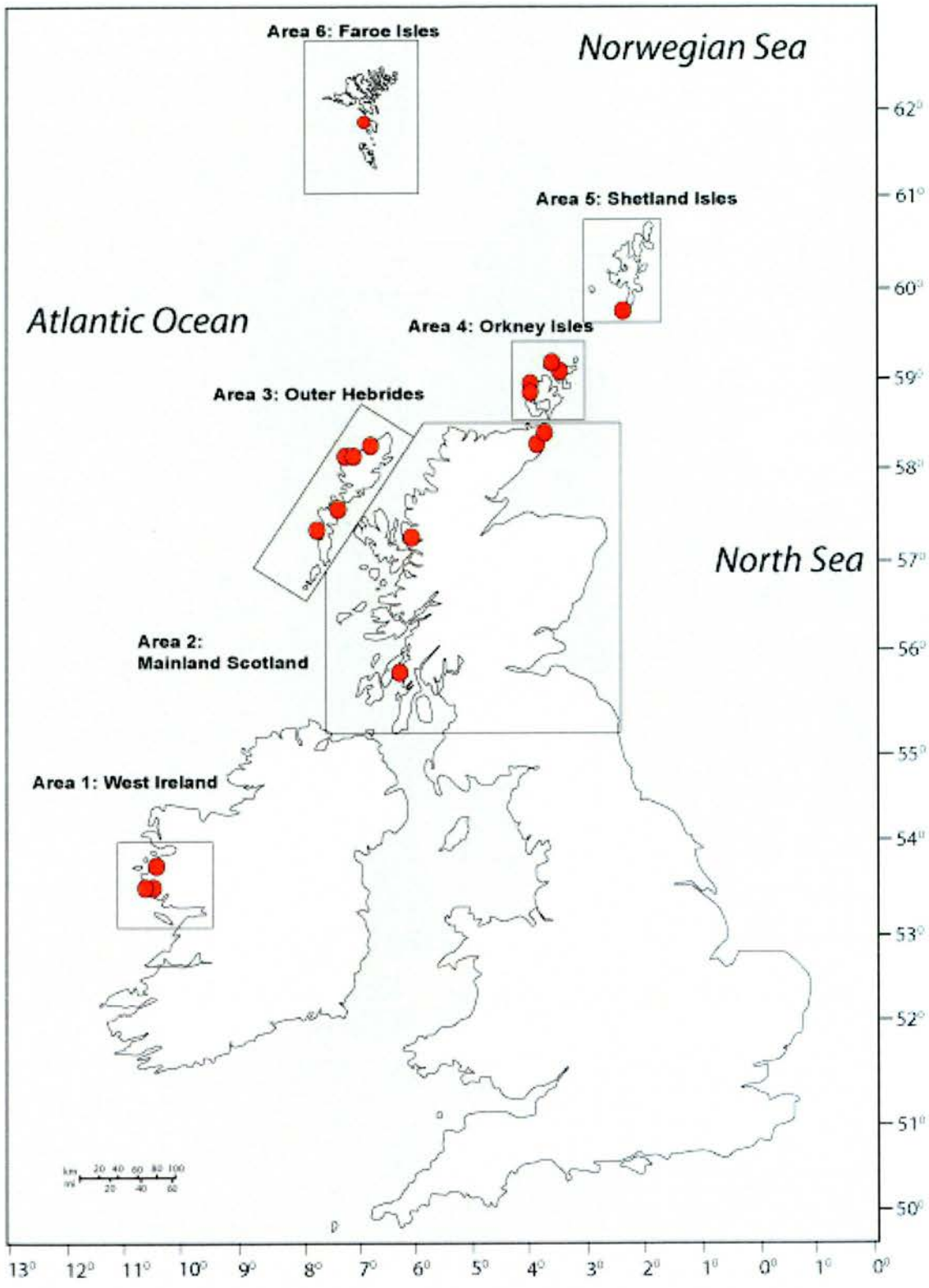

Figure 3.1: Location of sites within overall study area, showing location of areas 1 to 6.

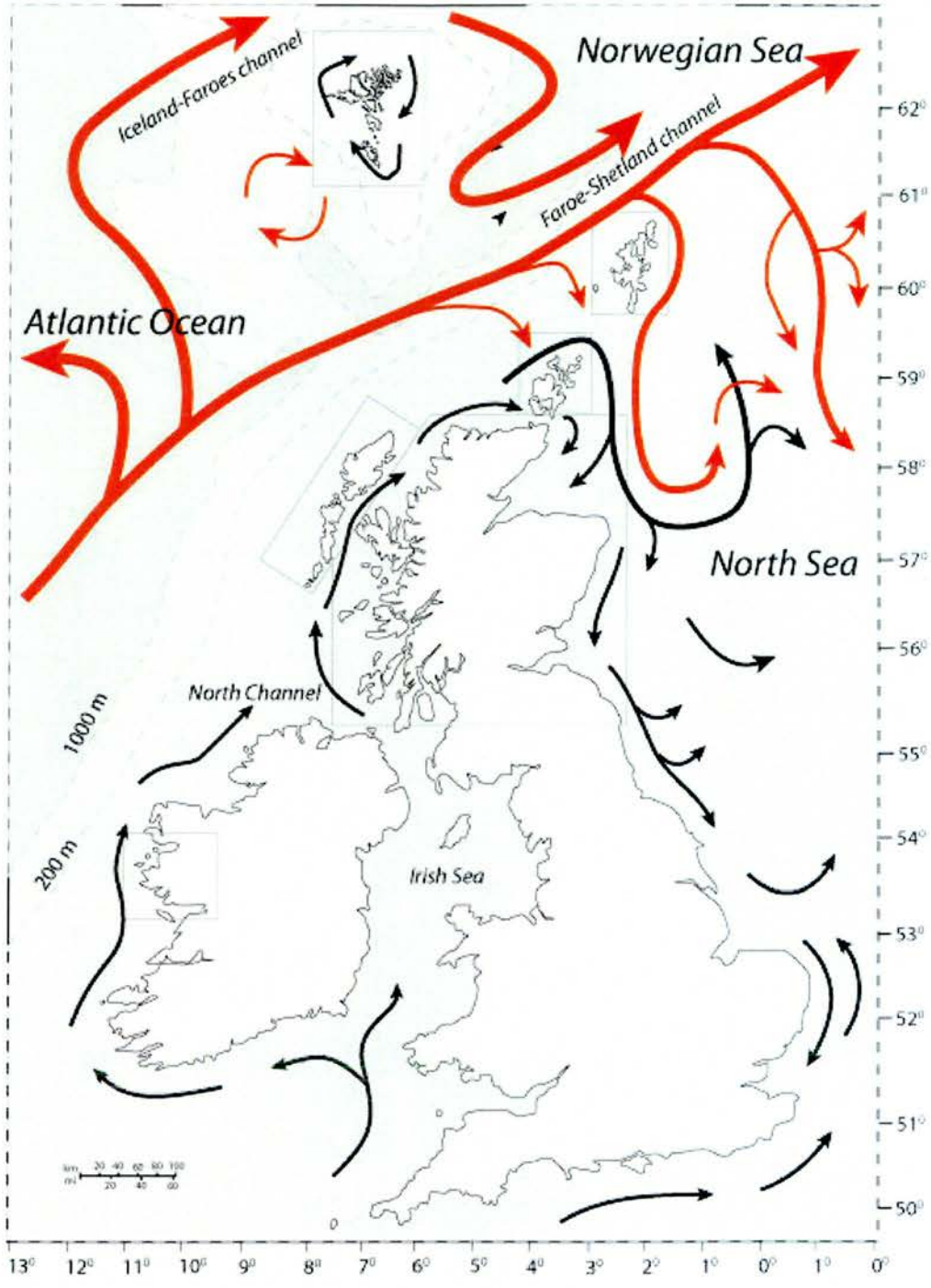

Figure 3.2: Surface circulation in the overall study area showing Atlantic water (red arrows) and coastal currents including the Scottish Coastal Current (black arrows) (after OSPAR, 2000). Bathymetry is given with the 200m and 1000 m contours (from Burrows and Thorpe, 1999).

Area 1: Western Ireland

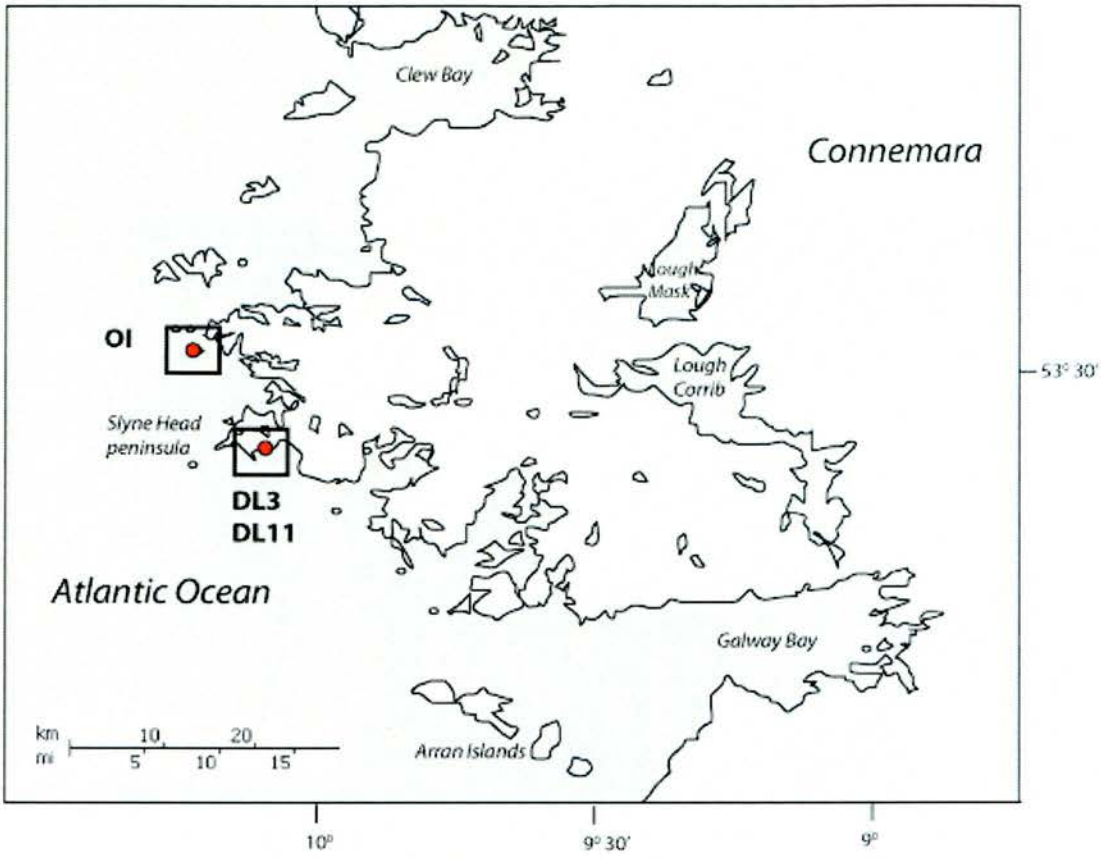

Figure 3.3: Site locations within Area 1

The three sites are located on the west coast of Ireland around Mannin Bay, Connemara. **DL-3** and **DL-11** lie on the mainland coast, while **OI** is on the north side of Omey Island, a tidal island <1 km from the mainland coast. **DL-3** and **DL-11** are the location of small- scale early Christian activity (Murray, 1999). The earliest human activity at **OI** took place in the Bronze Age, followed by early Christian burials and ecclesiastical use and final abandonment c.1840 AD (O'Keefe, 1994). Winter near shore (<c.50km) salinities off the west coast of Ireland average >35‰, and summer salinities 35.4-35‰, indicating the water is mainly of Atlantic origin (OSPAR, 2000). The temperature range of surface waters in the region of the sites averages c.6-16^{0}C (Donohoe *et al.*, 2000). The coastal water flows in a clockwise direction from the south of Ireland northwards parallel to the coast. These waters then pass into the Minch (between mainland Scotland and the Outer Hebrides) and flow up the western coast of Scotland. The local geology consists of igneous basement rocks, and vegetation cover in the hinterland is dominated by peat accumulations.

Area 2: Mainland Scotland

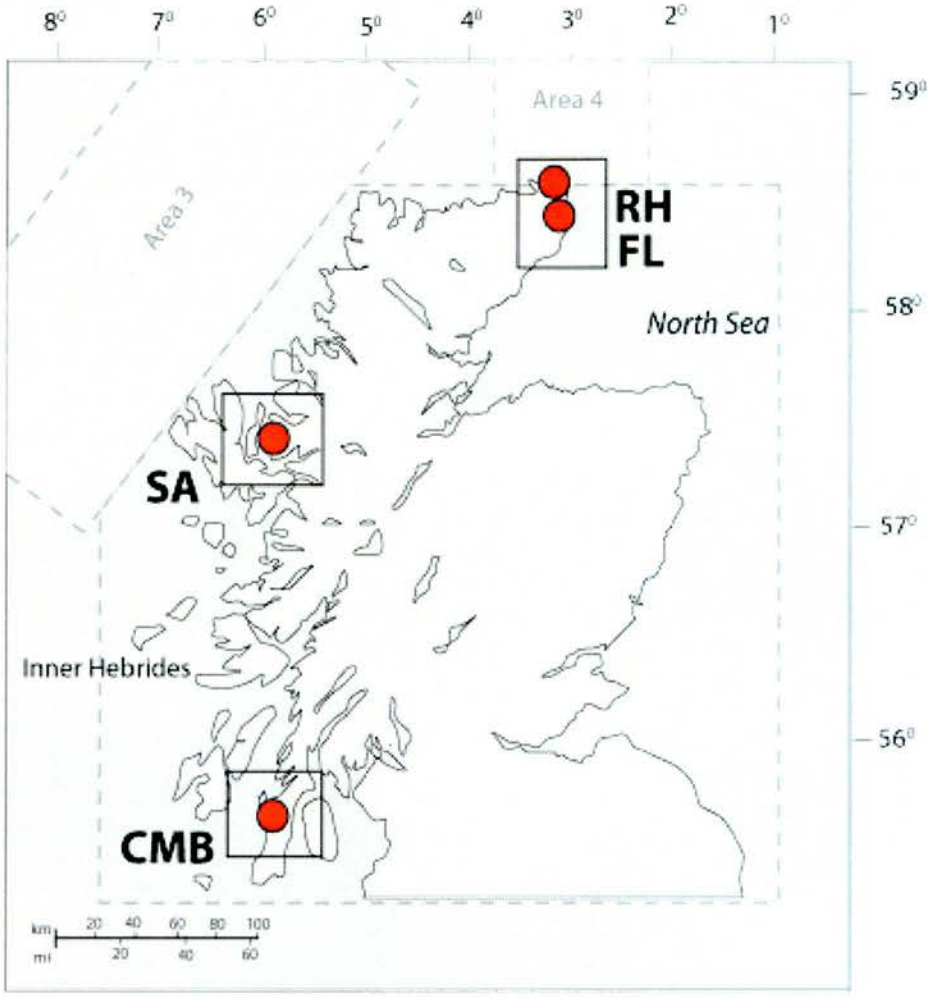

Figure 3.4: Site locations within area 2

Occupation deposits at **CMB** on the west mainland coast date from the Bronze Age, and the site lies in a region that includes andesitic and basaltic lavas and tuffs, schists, and Old Red Sandstone rocks (Gillen, 2003). **SA** is a Mesolithic shell midden further north on the Applecross peninsula in Wester Ross, an area of Torridonian rocks backed by the Torridonian highlands. The coastal topography at both sites reflects the fall in relative sea level from the main postglacial maximum (c.6 kyr BP (Lambeck, 1995)) due to postglacial isostatic uplift in response to removal of ice loading. This is apparent in a series of raised beaches in Argyll and Wester Ross with prehistoric sea cliffs now located several metres above the present shoreline

(Whittow, 1992). **CMB** and **SA** are in more moderately exposed coastal zones than other selected sites, due to the Inner Hebridean islands directly to the west. These constrain the flow of offshore waters that are part of the Scottish Coastal Current (SCC), originating from Atlantic and Irish Sea waters (Knight and Howarth, 1999), and reinforced by lower-salinity water from the major west coast Firths (McKay *et al.*, 1996). **RH** and **FL** are located on the north and far north east mainland coast, respectively, and are a sequence of late Norse and post-medieval middens and structural remains (**RH**) and a settlement dating from the Pictish and Norse period (**FL**). **RH** and **FL** lie in Caithness, an area dominated by rocks of the Old Red Sandstone series, which form part of the Orcadian basin (Whittow, 1992). The surface waters around **RH** and **FL** are also derived from the SCC as general circulation around Scotland continues in a clockwise direction, and flows into the North Sea.

Area 3: Outer Hebrides

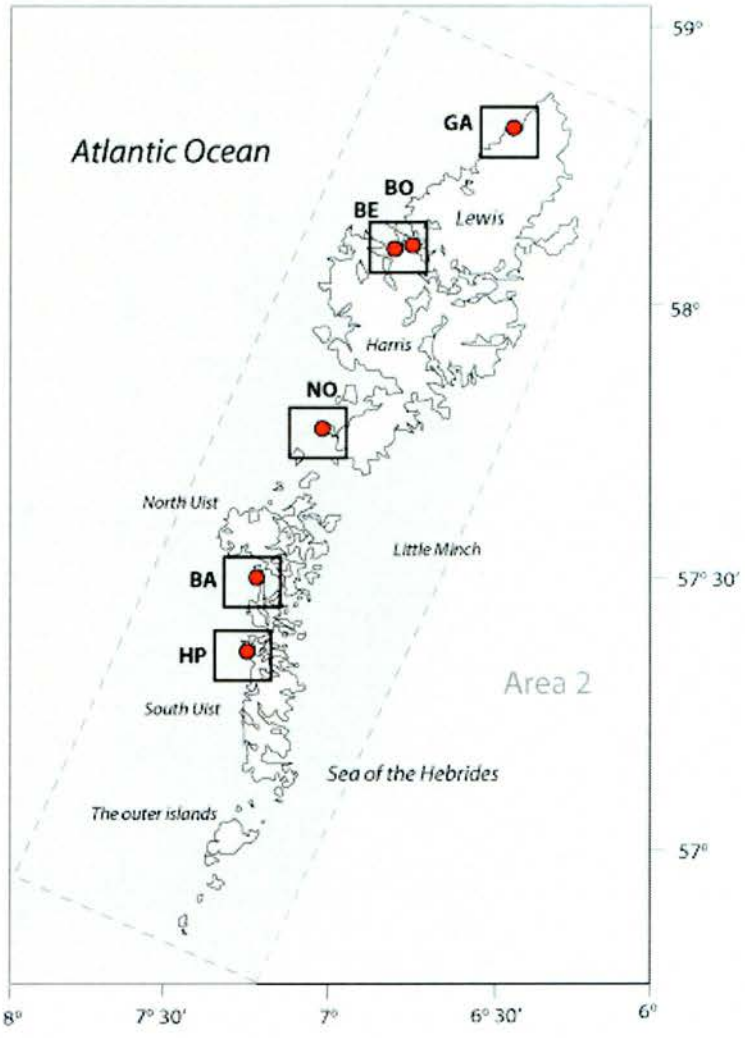

Figure 3.5: Site locations within area 3

Occupation phases at the six sites range from the Neolithic to the Medieval period, and all are located on the exposed west coast of the Outer Hebrides. Surface waters in this area consist of the SCC flowing northwards through the Minch and to the west of the Outer Hebrides and are not modified by further land masses to the west. The Outer Hebridean geology is dominated by Lewisian gneiss, apart from some igneous intrusions (Myers, 1971) and limited exposures of schist on the Isle of Harris (Whittow, 1992), and the landscape is heavily influenced by the impact of glaciation with many erosive landforms (Whittow, 1992). The Outer Hebrides, like the Orkney, Shetland and Faroe Islands was at the periphery of major ice influence during the last glacial, and has been gradually submerged by eustatic sea level rise since this time (Ritchie, 1985). Glacial processes also resulted in extensive deposits of calcareous shell sand or *machair*

along the western coasts as post-glacial debris on the continental shelf has been reworked and deposited by onshore winds and currents (Gillen, 2003). The major *machair* formation phase occurred by the 4th millennium BC (Gilbertson *et al.*, 1996, Ritchie, 1979), and encouraged prehistoric settlement in coastal areas due to fertile calcareous soils. *Machair* deposits are located in the vicinity of all sites within area 3.

Area 4: Orkney Isles

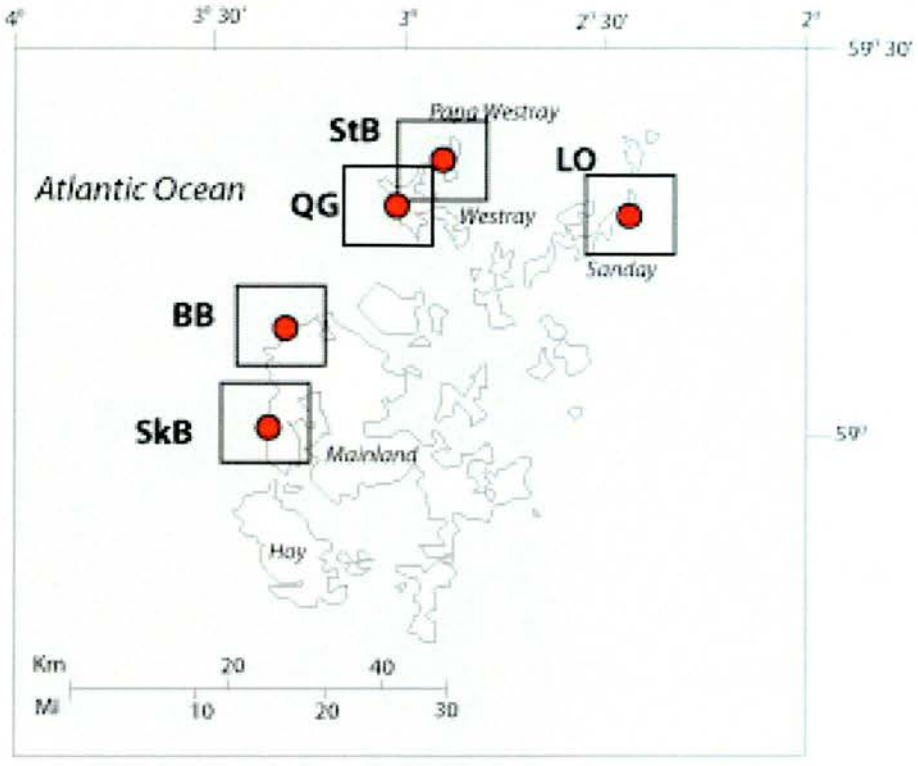

Figure 3.6: Site locations within area 4

StB, **QG**, **BB** and **SkB** are all located on west island coasts, while **LO** is located on the east coast of Sanday, one of the Northern Isles. **LO** is a Bronze Age burial cist, while the other sites are the location of settlements and associated deposits. **SkB** was an extensive settlement occupied between the Neolithic and Bronze Age, whereas **BB** consisted of less extensive middens and structural remains from the Bronze Age. **StB** comprises Bronze Age and Iron Age settlements, and Norse farm midden deposits, while **QG** was inhabited between the 9th century AD and the post-medieval period. The area is exposed to the west to the open North Atlantic, although there is a relatively wider continental shelf area west of Orkney than to the west of the Hebrides. To the south and north, water is derived from the SCC flowing eastwards into the North Sea. The Orkney Island geology is dominated by rocks of the Old Red Sandstone series and with Caithness forms part of the Orcadian basin. *Machair* deposits are also located on the western coasts of the Orkney Islands, and shell sand inclusions are found at points within the stratigraphy at the majority of selected sites.

Area 5: Shetland Isles

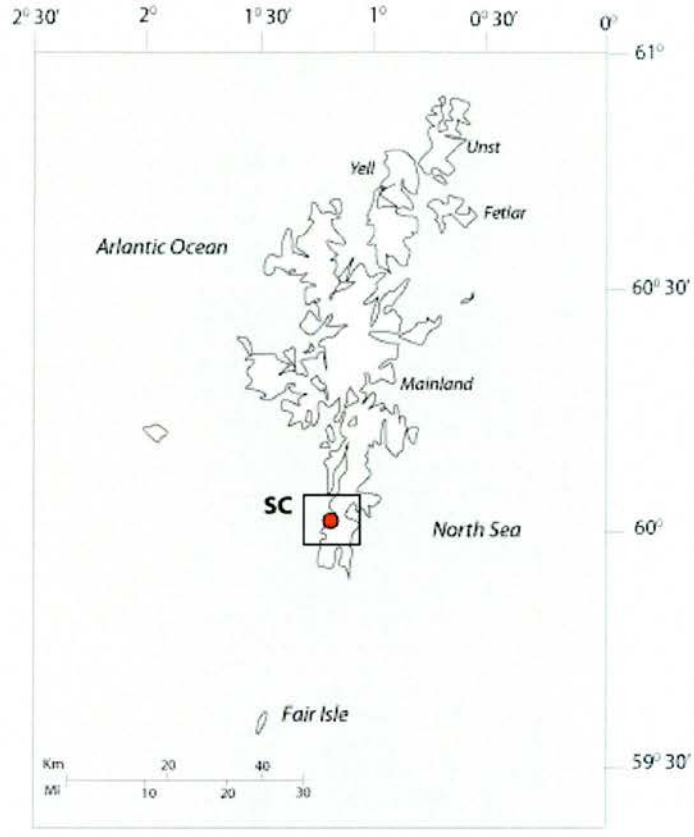

Figure 3.7: Site locations within area 5

SC is a multi-period settlement site representing a sequence of activities from the Bronze Age to the post-Medieval. The Shetland Islands are located south of the Shetland-Faroes Channel, part of the Iceland-Scotland gap which forms the main route for inflow of Atlantic water to the Nordic Seas and Arctic Ocean. Atlantic waters are transferred onto the continental shelf west of Shetland (Dooley *et al.*, 1976) and water from the North Atlantic enters the North Sea mainly from the north and west of Shetland (Rhode, 1998). The Shetland geology is more complex than that of Orkney or the Outer Hebrides, consisting of Lewisian, Moine and Dalradian metamorphic rocks, Devonian lavas and Old Red Sandstone with several large granite intrusions (Gillen, 2003). *Machair* deposits are also a feature of the western island coasts. Shetland comprises a greater land area than Orkney but has only about a quarter of the arable and grassland coverage as two thirds of the land is covered by peat bog and moorland (Whittow, 1992).

Area 6: Faroe Isles

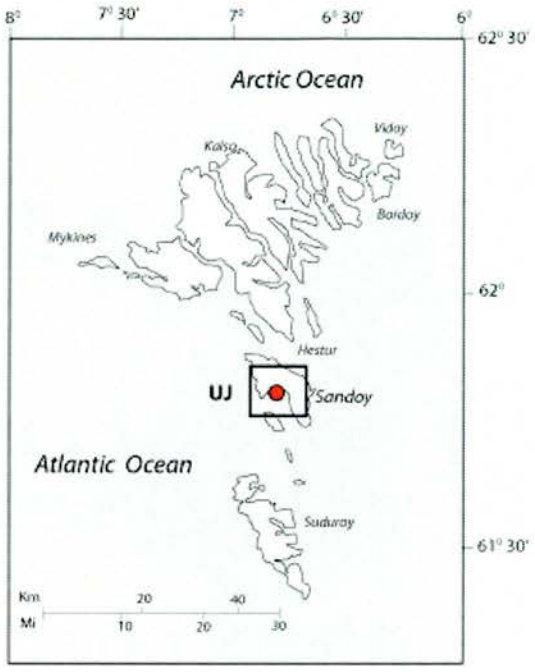

Figure 3.8: Site locations within area 6

The Faroe Islands are the most northerly study area and **UJ** is a series of Norse period middens on the west coast of Sandoy. Permanent human settlements were only established on the islands from c. AD 500-700 (Jóhansen, 1985, Hannon and Bradshaw, 2000, Hannon *et al.*, 2001), and therefore the archaeological record covers a much shorter time period than in other study areas. The geology of the Faroe Islands is mainly composed of igneous basement rocks and the action of glaciation has produced a large series of fjords around the island coastlines. The Islands are situated on the Faroe Plateau c.300 km north west of Shetland in the path of eastward flowing North Atlantic Current water which moves through the Shetland-Faroes and Iceland-Faroes channels. The NAC water forms the Faroes current north of the Islands which flows into the Norwegian Sea, and also flows eastwards to the south of the islands through the Faroe-Shetland channel. Overall surface water flow around the Faroe Plateau is cyclonic and strongly influenced by topography. Surface waters around the islands are dominantly modified North Atlantic water that is produced by the admixing of lower salinity terrestrial freshwater input (Hansen and Østerhus, 2000). This water has annual average temperatures of around 8°C and salinities of around 35.25 and produces a relatively well defined water mass of intermediate salinity that forms the coastal water around the islands (Hansen, and Østerhus, 2000; OSPAR , 2000).

3.3 The sampled contexts

30 contexts were chosen from the 20 archaeological sites to take paired terrestrial and marine samples. At the majority of sites a single context was selected, however, at six sites, more than one context was selected (**BA**, **SC**, **QG**, **RH**, **StB**, and **SkB**). From each context ^{14}C measurements were made of multiple samples of terrestrial and marine material. At each site the selection criteria described below were applied, which allowed optimum samples for the paired sample method to be obtained. The central aim of these criteria was to maximize the likelihood that samples of marine and terrestrial material represented a comparable calendar age range.

3.3.1 Selection criteria

Contexts from which to take terrestrial and marine material for ^{14}C measurement were chosen on the basis of several requirements.

- Clear, well defined boundaries
- Spatially confined
- A high content of terrestrial and marine material relative to context size
- The absence of signs that disturbance had occurred after deposition

The importance of well defined boundaries and confined spatial extent

There is a greater likelihood that the material within a context is of the same calendar age if the context is the product of a short, defined process. Such a process that deposited both terrestrial and marine material is likely to be the result of human actions, eg. the dumping of refuse material. This type of deposit can be identified by well-defined boundaries and a limited spatial extent. Context formation processes that can occur over extended time periods include natural sediment accumulations and cultivation phases, and these often mean that material from a wide range of sources is incorporated into the context. This material can have a wide range of calendar (and therefore ^{14}C) ages on the order well over 100 yr, as material such as carbonised cereal grains can potentially survive repeated cycles of erosion and redeposition at a site, and this would reduce the accuracy of calculated MRE values. Contexts that had highly diffuse

boundaries or were likely to have accumulated slowly were therefore avoided in favour of defined, discreet sedimentary units.

The importance of a high content of terrestrial and marine sample material

Terrestrial and marine material within a context is also more likely to be of the same calendar age if it is present in larger amounts, as this increases the chance the samples were deposited as the result of deliberate human activity. Where such material is present in low volumes there is a higher possibility that its presence in a context is the result of chance events or natural processes. These are more likely to incorporate material that has a range of calendar ages into a context, and contexts that contained larger amounts of both terrestrial and marine samples were preferentially selected. A central feature of the methodology was to measure multiple terrestrial and marine samples from each context, with at least four samples of each type of material measured wherever possible. This allowed uncertainties derived from context formation processes and depositional histories to be assessed that are not accounted for when single marine and terrestrial samples are compared.

The importance that signs of post-deposition disturbance were absent

Once deposition of a context has ended, it is possible for material to be introduced at a later date by natural or human disturbance. Natural processes include burrowing by animals and root growth through the sediments, while human processes usually involve exhumation of sediments, for example during building construction. The material that enters a context in this way can either date to the time of disturbance, or be of an earlier date than the initial context formation. In either instance there is a greatly increased chance that any individual terrestrial and marine material samples from this context will not be of the same calendar age. To increase the probability that selected samples were of the same age, contexts with obvious signs of disturbance were avoided. These are often apparent on examination of the sedimentary profile, such as rabbit burrows, worm casts or cultivation marks. Contexts with good stratigraphic definition (see above) are also less likely to have suffered disturbance, and contexts that contained articulated remains such as fish, and/or mammal bones were also used as an indication that a context had not been significantly disturbed since initial deposition.

3.3.2 The selected contexts

Table 3.5 shows the 30 contexts that were selected from the sample sites. The majority of contexts were midden deposits that were associated with a period of prehistoric occupation. Middens are generally the result of a sequence of material dumps (often domestic refuse) or are the result of specialised subsistence strategies (e.g. fishing). It may be possible to identify specific individual formation events within the sequence (Uerpmann, 1990) that occurred over a short time interval. From several contexts it was possible to take samples from defined individual dumps of material that represented human activity over a sub-annual scale. The composition of an individual sequence of midden deposits reflects different types and intensities of activity, and the composition of individual deposits is the result of cultural preferences and environmental conditions. As can be seen from Table 3.6, the majority of terrestrial samples obtained from contexts were carbonised barley (*Hordeum sp.*) grains, and the majority of marine mollusc samples were limpet species (*Patella sp.*).

Site	Context	Description
SA	013	Shell midden deposit
CMB	XIII	Shell midden deposit
FL	JM, sample 76	Midden deposit
RH	3004	Upper midden deposit
RH	3019	Lower midden deposit
BA	39	Midden deposit
BA	146	Midden deposit
BA	139	Midden deposit
HP	201	Midden deposit
NO	5	Occupation surface containing midden material
BO	64	Midden deposit
BE	503	Hearth deposit
GA	165	Midden deposit
SkB	68	Midden deposit
SkB	26	Midden deposit
BB	XF	Midden deposit
LO	006	Possible ritual deposit
St B	2136	Fill of grain-drying flue or hearth
St B	2044	Primary fill of enclosure ditch containing midden material
St B	1063B	Midden deposit
QG	A004	Upper midden deposit
QG	A023	Lower midden deposit
SC	543	Discreet, thin limpet midden layer within structure
SC	1269	Surface directly overlying stone flagging in a structure entrance
SC	3083	Shell midden deposit within structure
SC	206	Midden deposit within a test pit (Pit 2 C2)
OI	6	Midden deposit
DL-3	19	Ash layer within a charcoal lined pit
DL-11	2	Enclosure surface containing domestic refuse
UJ	23	Midden deposit

Table 3.5: Contexts chosen according to selection protocol, showing the site at which each context was located.

Each context is referred to in the following text by a combination of the site identifier code and context number.

Context	Terrestrial sample material	Marine sample material
SA-013	*Cervus elaphus* bone	*Patella sp.*
CMB-XIII	*Corylus avellana* nutshell	*Patella sp.*
FL-JM76	*Hordeum sp.*	*Patella sp.*
RH-3004	*Hordeum sp.*	*Patella sp.*
RH-3019	*Hordeum sp.*	*Patella sp.*
BA-39	*Hordeum sp.*	*Cerastoderma edule*
BA-146	*Hordeum sp.*	*Cerastoderma edule*
BA-139	*Hordeum sp.*	*Patella sp.*
HP-201	*Hordeum sp.*	*Patella sp., Littorina littorea, Mytilus edulis, Ensis sp, Cerastoderma edule*
NO-5	*Corylus avellana* nutshell	*Littorina littorea*
BO-64	*Hordeum sp.*	*Patella sp.*
BE-503	*Hordeum sp.*	*Mytilus edulis*
GA-165	*Hordeum sp.*	*Patella sp.*
SkB-68	*Hordeum sp.*	*Patella sp.*
SkB-26	*Bos sp.*	*Patella sp.*
BB-XF	*Cervus elaphus* bone	*Patella sp.*
LO-6	*Hordeum sp.*	*Patella sp.*
StB-2136	*Hordeum sp.*	*Patella sp.*
StB-2044	*Hordeum sp.*	*Patella sp.*
StB-1063	*Hordeum sp.*	*Patella sp.*
QG-A004	*Hordeum sp.*	*Patella sp.*
QG-A023	*Hordeum sp.*	*Patella sp.*
SC-543	*Hordeum sp.*	*Patella sp.*
SC-1269	*Hordeum sp.*	*Patella sp.*
SC-3083	*Hordeum sp.*	*Patella sp.*
SC-206	*Avena sp.*	*Littorina littorea*
OI-6	*Hordeum sp.*	*Patella sp.*
DL3-19	*Hordeum sp.*	*Patella sp.*
DL11-2	*Hordeum sp.*	*Patella sp.*
UJ-23	*Hordeum sp.*	*Patella sp.*

Table 3.6: Sample material obtained for ^{14}C measurement from selected archaeological contexts.

Chapter 4: Methodology B: Laboratory techniques and data analysis

The following chapter first describes the laboratory methodology that was applied to the samples for isotopic measurements. This includes removal of contaminants (pre-treatment), physical and chemical preparation of samples for measurement and the specific measurement technique applied. This is followed by a discussion of the techniques used to analyse the measurement data.

A total of 275 samples were selected from the 30 archaeological contexts described in the previous chapter for ^{14}C measurement. In the majority of instances this involved four samples of terrestrial carbonised plant material or mammal bone, and four samples of marine mollusc shells. The total number of ^{14}C measurements made was 301 as multiple measurements were made of certain individual samples, and a $\delta^{13}C$ value was obtained for each ^{14}C measurement using conventional mass spectrometry. The number of measured samples and total number of measurements are summarised in Table 4.1.

	Terrestrial samples		Marine samples	
Context	**No. measured samples**	**No. individual ^{14}C measurements**	**No. measured samples**	**No. individual ^{14}C measurements**
SA-013	4	6	4	4
CMB-XIII	4	6	4	4
FL-JM76	6	6	4	9
RH-3004	4	4	4	4
RH-3019	4	4	4	4
BA-39	4	4	4	4
BA-146	4	4	4	4
BA-139	4	4	4	4
HP-201	4	4	20	24
NO-5	3	3	2	2
BO-64	6	6	4	6
BE-503	6	6	4	5
GA-165	4	4	4	8
SkB-68	6	6	4	5
SkB-26	4	4	4	4
BB-XF	4	4	4	4
LO-6	4	4	4	4
StB-2136	4	4	4	4
StB-2044	4	4	4	4
StB-1063	4	4	4	4
QG-A004	6	6	4	4
QG-A023	8	8	4	6
SC-543	6	4	4	10
SC-1269	6	4	4	4
SC-3083	4	2	4	6
SC-206	8	4	4	6
OI-6	4	4	4	4
DL3-19	4	4	4	7
DL11-2	4	4	4	4
UJ-23	4	4	4	4
Total	**141**	**135**	**134**	**166**

Table 4.1: A summary of the number of individual samples measured and total number of ^{14}C measurements made from all archaeological contexts.

4.1 ^{14}C Measurement: Pre-treatment, CO_2 extraction and conversion to graphite

4.1.1 Sample pre-treatment: Removing contaminants

Carbonised plant material

Carbonised plant material typically has a high carbon content (>50%) and is relatively chemically inert. Contaminants from environmental sources are carbonates and organic (humic or fulvic) acids that are derived from inorganic and organic soil components, respectively. These adhere to the physical structure of the sample rather than combine with the sample chemically. The standard pre-treatment methods for carbonised grain are the removal of carbonates by acid hydrolysis with HCl and of organic acids with alkali solution (NaOH) in a series of successive washes (acid-alkali-acid or AAA method). This method provides a rapid and effective, although non-selective removal of contaminants (Santos *et al.*, 2001).

Samples of plant material were inspected to select intact, clean samples with a good surface structure and minimal surface damage or adhering soil. Sample weight was recorded and the sample heated for one hour at 80^0C in 50 ml 0.25M HCl after which the solution was filtered using a vacuum pump, and neutralised by washing with distilled water. After neutralisation the sample was heated for one hour at 80^0C in 50 ml 0.25% NaOH solution before filtration and neutralisation, followed by a final acid wash to remove any carbonate contamination through absorption of atmospheric CO_2 by the alkaline solution. Following final filtration and neutralisation the sample was oven dried and the sample weight recorded.

Bone

The two main bone fractions are a protein (collagen), and a phosphate (calcium hydroxyapatite). The open lattice of the bone phosphate structure can combine chemically with carbonates precipitated from infiltrating groundwater, and can also incorporate soil humic acids (Yoneda *et al.*, 2002). Bone collagen is however resistant to post-depositional carbon exchange and standard bone pre-treatment involves extraction and purification of collagen. A minimum of c. 5% collagen yield is recommended for reliable dating. (Hedges and Van Klinken, 1992).

Bone samples were pre-treated with a modified Longin (1971) method. The sample surface was cleaned with a Dremmel® drill using a buffing attachment, weighed and roughly crushed into 1-2 cm pieces. The sample was then immersed in 100ml 1M HCl overnight (c.18 hours) to dissolve the phosphate. Completion of this stage was identified when the bone texture became "spongy" due to loss of the phosphate into solution. No heat was applied during this phase as this would denature the collagen and result in its dissolution. The liquid fraction containing the phosphate and organic contaminants was decanted off and the residue heated gently in 100 ml distilled water. Due to residual acid the heated solution remained slightly acidic, which denatured and dissolved the collagen through hydrolysis of the proteinic chains. Once the majority of the bone structure had dissolved, the solution was filtered and the collagen freeze-dried.

Marine mollusc shell

The majority of mollusc shell structure consists of $CaCO_3$ crystals bonded within an organic matrix by a protein (conchiolin), that itself comprises <10% of the shell structure (Aitken, 1990). Carbon contaminants affect the shell surfaces as primary shell carbonates are replaced with secondary carbonates from environmental sources after deposition. Though this contamination can affect exposed shell surfaces, the inner shell layers are considered to be a closed system after formation (Chappell and Polach, 1972; Vita-Finzi and Roberts, 1984), and pre-treatment involves identification of surface exchange and removal of outer shell layers.

Shells were inspected and only hard, non-porous shells that had a fresh surface and preserved textures were selected for analysis (Mangerud, 1972, Mook and Waterbolk, 1985). All physical contaminants that adhered visibly to the shell surface were removed by abrasion and subsequently by cleaning in deionised water in an ultrasonic bath. The shell was then dried and weighed before the outer 20% portion by weight was removed by etching in 1 M HCl (c.f. Heier-Nielsen *et al.,* 1995). The dry pre-treated sample weight was recorded and the shell crushed to obtain a 0.1g homogenised sample of the shell structure for CO_2 extraction. Prior to extraction, a further 20% of the sample surface was removed with 1M HCl to extract any further surface contamination that had occurred during storage after pre-treatment.

4.1.2 CO_2 extraction and conversion to graphite

CO_2 was obtained from the pre-treated carbonised plant material and bone samples by combustion in sealed quartz tubes (Vandeputte *et al.*, 1996) that had been pre-cleaned in air at 850^{0}C for 8 hours. The tubes contained the pre-treated sample with 0.5 g copper oxide (CuO) and a small piece of silver wire, included to remove halides (mainly chlorine) that may prevent effective reduction of CO_2 to C (Buchanan and Corcoran, 1959). The tubes were numbered and evacuated on a vacuum line before being flame sealed. Sample combustion was achieved by heating the tubes at 850^{0}C for 8 hours in a muffle furnace, after which they were cooled slowly and attached to a vacuum line for CO_2 collection. The sample gas was released into the line by cracking in a cracking unit (see Figure 4.1).

For marine mollusc shell, the secondary pre-treatment (see above) was performed in a pre-cleaned Pyrex hydrolysis unit. After completion of the pre-treatment, the unit containing the sample was attached to a vacuum line and 1M HCl injected into the unit through a rubber septum. Sufficient HCl was added for complete hydrolysis of the shell carbonate and the evolved sample CO_2 was then released into the vacuum system.

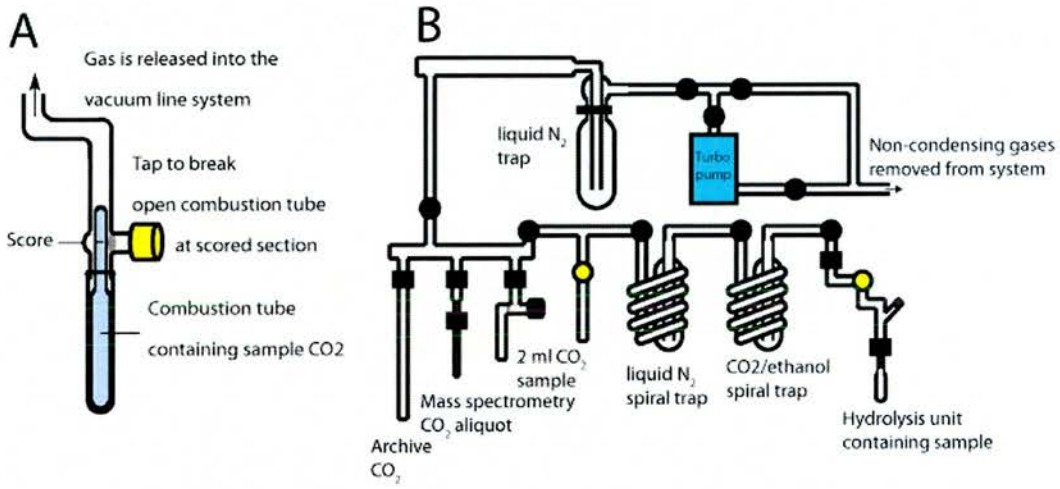

Fig 4.1: A: Cracking unit used for collection of CO_2 from samples of carbonised grain and mammal bone. The unit is attached to the vacuum line (B) and is interchangeable with the hydrolysis unit (used for shell carbonate samples).

The sample CO_2 was then cryogenically purified. Water vapour was removed at -78^{0}C in a spiral trap surrounded by solid CO_2/ethanol, following which the gaseous sample was passed

though a spiral trap surrounded by liquid N_2 (-196^{0}C). At this stage, non-condensing gaseous contaminants were removed by pumping the system under vacuum while the sample CO_2 was frozen with liquid N_2. The purified sample CO_2 yield was measured with a strain gauge and three sub-samples were taken. One 2 ml sample was converted to graphite by the method of Slota *et al.* (1987), for AMS analysis, and the second sub-sample was collected in a clean sealable glass vial for $\delta^{13}C$ analysis. Any remaining sample CO_2 was collected in a glass vial and sealed for possible future analysis.

The 2 ml of purified sample CO_2 was converted to filamentous C (graphite) by reduction to CO using 0.06 g zinc (Zn) as the reaction catalyst at 400^{0}C , followed by reduction to C with 0.003 g iron (Fe) catalyst at 600^{0}C (Vogel *et. al.*, 1987; Lowe and Judd, 1987). The reactions were preformed on a graphitisation unit under vacuum, which consisted of the 2 ml sample CO_2, and two pre-cleaned Pyrex tubes, each containing a catalyst and surrounded by a small furnace. The pressure within the reaction vessel was continuously monitored by a computer-controlled pressure transducer. The measured pressure was converted to a digital value, and this value (input) was displayed on-screen, plotted as a function of time (hours) (see Figure 4.2). As pressure within the reaction vessel fell, the yield of graphite increased. Upon completion of the reaction the sample graphite was collected and pressed into an aluminium sample holder to produce a target suitable for AMS analysis.

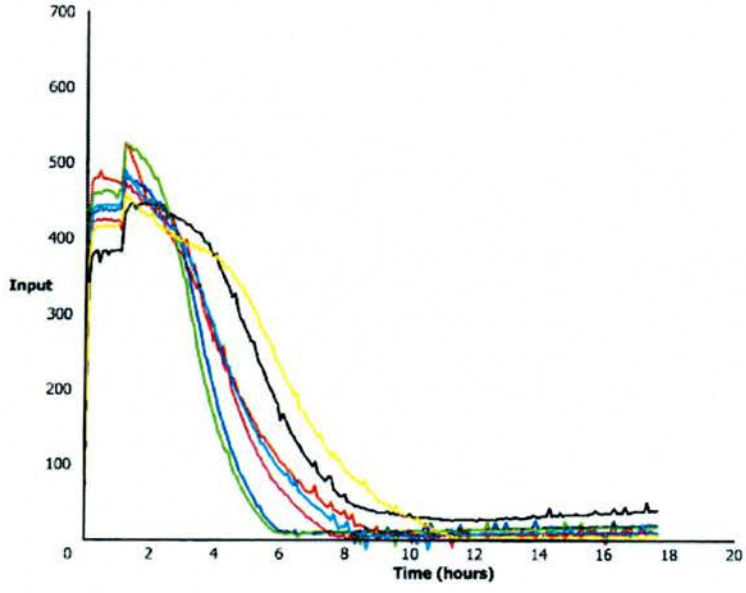

Figure 4.2: Graph output from computer-controlled graphite production showing progress of the reaction. The pressure within the reaction vessel (input) is plotted as a function of time.

4.1.3 Measurement

The prepared graphite targets were inserted into the AMS sample source and measured. A number of samples were measured at the NSF-University of Arizona AMS facility, while the majority were measured using the accelerator facilities at the Scottish Universities Environmental Research Centre (SUERC). The Arizona facility comprised a National Electrostatics Corporation (NEC) 3 MV terminal voltage instrument and measured carbon in the 3+ charge state. The SUERC facility is a NEC 5 MV terminal voltage instrument operated at 4.5 MV, with carbon in the 4+ charge state. At SUERC, a series of measurements were made upon known age material over a period of several months to provide a minimum measurement error of c. ± 35 ^{14}C yr . Wherever possible during measurement, samples from a single context were measured on the same sample wheel to reduce variability introduced by random machine error (RME) and maximize laboratory precision to ±35-50 yr . Sample measurements that were associated with large measurement standard errors were repeated.

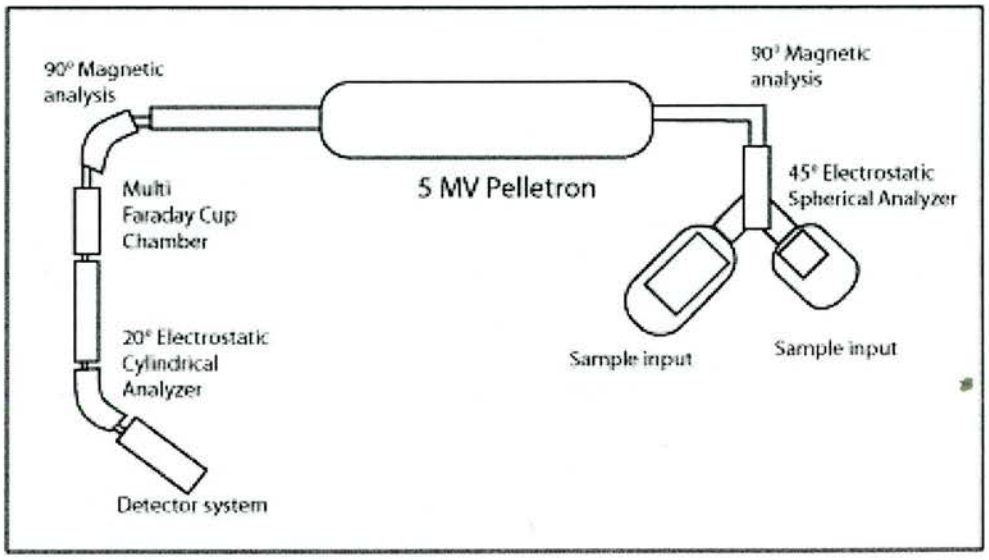

Figure 4.3: Schematic of SUERC AMS facility

The isotopic composition of the CO_2 was measured on a VG SIRA 10 stable isotope mass spectrometer using NBS standards 22 (oil) and 19 (marble) to determine the 45/44 and 46/44 atomic mass ratios, from which a sample $\delta^{13}C$ value could be calculated.

Known age standards

The majority of samples were measured in batches on the SUERC AMS facility. Each batch contained a mixture of unknown age samples and known age standards. The known age standards included modern reference standards (Oxalic acid II) and material that had been used in the third and fourth international radiocarbon intercomparisons (TIRI and FIRI). The aim of the intercomparisons was to provide ^{14}C laboratories with an independent and objective assessment of the quality of their analytical data. Laboratories that took part in the exercise undertook measurements of several core and optional samples. This resulted in the production of reference (consensus) values for the measured samples, which could then be used as known age standards in ^{14}C measurement. The known age standards measured along with unknown age samples that were included in this study were:

1. Modern reference standard. Oxalic acid II produced by the National Institute of Standards and Technology for ^{14}C age calculation and obtained from a 1977 sugar beet molasses harvest.

2. Dendrochronologically-dated Belfast wood. 11.8 kg of dendro-dated wood was provided for the FIRI exercise by the Queen's University of Belfast Dendrochronology laboratory. The wood was a sample of a Scots pine tree from Garry Bog, Co. Antrim, Northern Ireland, grid reference C930074, latitude 54^0 54' N, longitude 6^0 33' W (Scott, 2003). The wood had been pre-treated by the standard acid-alkali-acid method and bleached using sodium hypochlorite solution. Sub-samples of the wood (BC standards) were combusted in sealed quartz tubes and CO_2 extracted following the procedure outlined above. In addition, a large quantity of the wood was combusted to produce a bulk bottled gas, from which aliquots were taken for measurement (BBC standards).

3. Modern Barley mash. This was a core sample in the TIRI exercise and is a by-product from malt whisky production, provided by Glengoyne Distillery. The sample was taken from a single fermentation vat and was well mixed during the industrial process. The sample was force dried and physically mixed before being provided as a TIRI sample (Scott, 2003). Standards were produced by combusting a bulk sample of the barley mash to produce a bulk bottled gas, from which aliquots were taken for measurement (BBM standards).

4. Icelandic Doublespar. The sample was a core sample in the TIRI exercise and is a variety of crystalline calcite, being composed of calcium carbonate and obtained as pure, large, single crystals between basaltic lava sheets. The sample was obtained from the spar-mine at Helgustadir, Iceland and provided by the Museum of Natural History, Iceland. Earlier samples from the spar-mine, after removal of the outer 10%, showed no excess activity to that of freshly cut marble and CO_2 from natural gas (Scott, 2003). Standards were produced by completely hydrolysing the Doublespar to give a bulk bottled gas, from which aliquots were taken for measurement (DS standards).

5. Interglacial age wood. The sample was obtained from Heidelberg and provided by Prof. M. Scott. Measurement of samples of the wood showed no excess activity to that of Icelandic Doublespar. The wood was pre-treated by the standard acid-alkali-acid method and bleached. Sub-samples of the wood were combusted in sealed quartz tubes and CO_2 extracted following the procedure outlined above (BK standards).

Standard	Consensus value	Estimated precision (1σ)
Modern reference	134.07 pMC	0.0019
Belfast wood	4503 BP	6
Barley mash	116.35 pMC	0.0084
Icelandic Doublespar	46, 750 BP 0.18 pMC	208 0.006

Table 4.2: Consensus values for measured standards (Gulliksen and Scott, 1994; Boaretto *et al.*, 2002; Scott, 2003).

4.2 Data analysis

4.2.1 ^{13}C

A $\delta^{13}C$ value was produced for each measurement to allow age correction for isotopic fractionation effects. Where multiple ^{14}C measurements had been made on a single sample the variation in $\delta^{13}C$ values associated with the repeated measurements was examined. Where this was less than the variation between $\delta^{13}C$ values of other (terrestrial or marine) samples for that context, the repeated $\delta^{13}C$ values were averaged. This average was then taken as the overall $\delta^{13}C$ for that sample. The standard deviation of $\delta^{13}C$ values within each

group of terrestrial or marine samples was used to examine the variability in $\delta^{13}C$. This was to establish the typical range in $\delta^{13}C$ that could be expected for measurements from a single context and identify whether measurements from any context showed above-average variation.

4.2.2 Assessing the similarity of multiple sample measurements: The χ^2 test

The sample, site and context selection protocol was designed to maximize the likelihood of obtaining terrestrial and marine material from a context that represented the same calendar interval. Multiple samples of both types were obtained from each context, to improve the accuracy of calculated MRE/ΔR values, and to assess the range in ^{14}C ages of each sample type within a context. If the ^{14}C ages of a group of samples are consistent then this increases the likelihood that the material within a context was deposited over a single short time interval, and that terrestrial and marine material represents the same calendar period.

The consistency of each (terrestrial or marine) group of measured ages from each context was assessed using the chi-squared (χ^2) test (c.f. Ward and Wilson, 1978). Because the MRE means there is an inherent difference between the ^{14}C age of terrestrial and marine material the two sample types were considered separately. The null hypothesis used in the test was that the group of measurements were the same at 95% confidence. The χ^2 test assesses whether the internal variability of a measurement group is consistent with the errors associated with the individual measurements. To avoid biasing the test towards samples that had been measured more than once, multiple measurements of a single sample that were within 2σ error of each other were combined in a weighted mean for that sample. The χ^2 test statistic (*T*) value for 95% confidence of *N* ^{14}C age measurements ($\chi^2_{:0.05} = T$) was compared with the *T* value calculated for each group of ^{14}C ages to determine whether the variability within the measurement groups exceeded what could occur by chance. The *T* statistic for a group of ^{14}C ages is calculated by:

$$T = \sum \frac{(t_i - t)^2}{\sigma_i^2}$$

Equation 4.1

Where: t = the weighted mean of the ^{14}C age group

t_i = the individual ^{14}C measurement

σ = the error on the individual measurement

Where the *T*-statistic was lower than the acceptance value the ages within that group were considered to be contemporaneous. Where the *T*-statistic exceeded the acceptance value the ages within the group were significantly different, and the measurements were examined to determine the source of variation. The ^{14}C measurements that most accurately reflected the age of terrestrial or marine material at the time of context deposition were identified using repeat measurements and reference to other available chronological data. Variation in ^{14}C measurements within a sample group could result from measurement variability, or could reflect real differences in the ages of individual samples. Ages that outlay several similar measurements from separate samples within a group were repeated. In the case of marine mollusc shells, repeat measurements of a single shell are possible as sufficient original material remains after CO_2 extraction and graphitization. This is due to the relatively large mass of the pre-treated samples. Overall measurement reproducibility of marine mollusc shells was assessed using five measurements made using aliquots of a single pre-treated *Patella vulgata* shell from **GA-165**. In the case of carbonised plant material it was usually not possible to repeat measurements due to a lack of remaining material, and additional individual samples were measured instead. Repeated measurements of a single sample that were within error were combined in a weighted mean. The χ^2 test was then applied to all samples within the group, including any additional measurements or weighted mean sample ages. If the ^{14}C ages within the group remained statistically different, the variation is likely to be due to a real difference in the calendar ages of the material within the sample group. The most accurate terrestrial or marine ^{14}C ages for the context were selected according to the degree of coherence with other measurements in the context and with existing archaeological data from the context. This was obtained where available from excavation records.

4.2.3 Assessing ΔR using paired samples

The dataset used for ΔR calculation was derived from a linear interpolation of the Intcal98 atmospheric calibration data and Marine98 modelled marine ^{14}C ages (Stuiver and Braziunas, 1993; Reimer *et al.*, 2002). To calculate ΔR, the upper and lower limits of a terrestrial ^{14}C age (i.e. the age plus and minus 1σ) were converted using the interpolated dataset to upper and lower 1σ modelled marine ^{14}C age bounds. The upper and lower modelled marine bounds were the maximum and minimum intercepts of the terrestrial ^{14}C age bounds with the interpolated data. The average uncertainty in the interpolated calibrated data was incorporated into the standard deviation of these modelled marine ^{14}C age bounds. The midpoint of the upper and lower modelled marine age bounds was then compared with a marine ^{14}C age. The offset of the measured marine ^{14}C age from the midpoint of the

calculated modelled marine age range was the ΔR value. The 1σ error for the ΔR determination ($\sigma_{\Delta R}$) was obtained by combining the error on the marine age (σ_w) and the error on the modelled marine ages (σ_m):

$$\sigma_{\Delta R} = \sqrt{(\sigma_w + \sigma_m)^2}$$

Equation 4.2

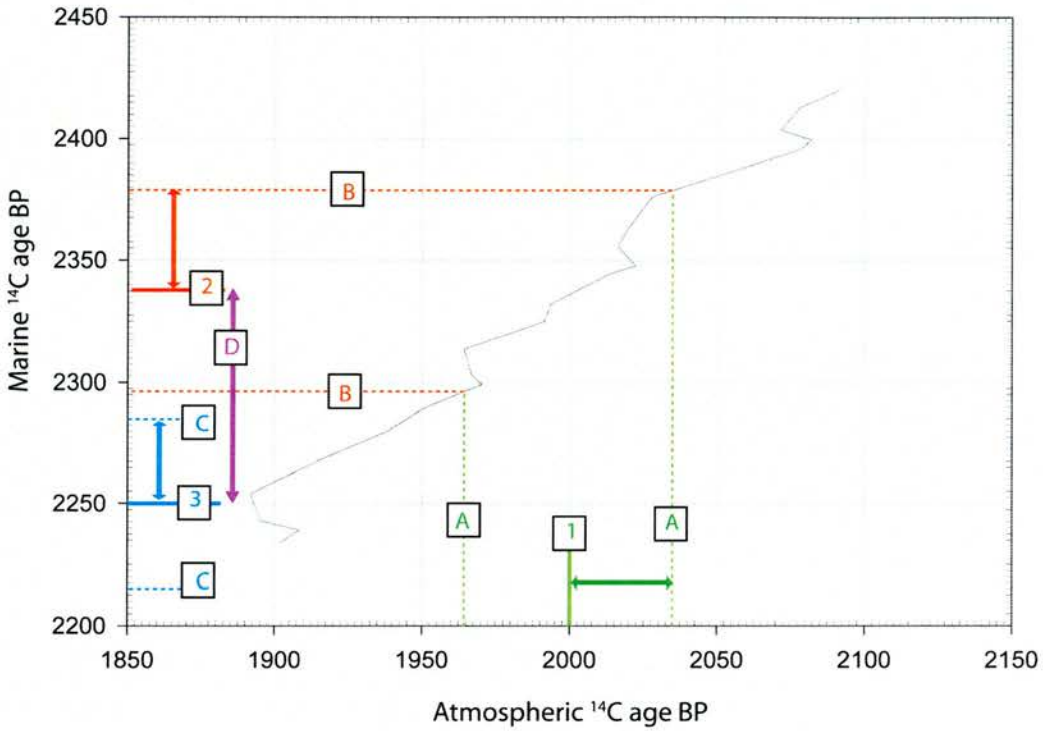

Figure 4.4: Schematic diagram of method used to obtain ΔR values with paired terrestrial/marine samples. 1: Measured terrestrial age; A: error on measured terrestrial age (combined with curve error); B: converted upper and lower modelled marine age bounds; 2: Midpoint of modelled marine age bounds; 3: measured marine age; C: error on measured marine age; D: different between modelled marine age and measured marine age (i. e. ΔR).

A group of terrestrial or marine measurements from a single context that gave a *T*-statistic lower than the acceptance value were used to assess ΔR for each context. The measurements within a group were produced from separate individual samples and therefore have slightly different "underlying" ^{14}C ages. An empirical assessment was made of the variation in ΔR that could be produced over all the terrestrial and marine samples from the context. This was

achieved by considering all possible estimates of ΔR for the group of measured samples from that context by calculating a value of ΔR for each possible pairing of terrestrial and marine ^{14}C ages (see Appendix C). The distribution was summarised by the weighted mean and appropriate standard error for prediction. In this way it is possible to account for any additional variability due to uncertainty about the precise pairing of terrestrial and marine samples.

The weighted mean for a group of values is determined by:

$$t = \frac{\Sigma\, t_i / \sigma_i^2}{\Sigma\, 1 / \sigma_i^2}$$

Equation 4.3

Where: t = the group weighted mean

t_i = the individual value

σ_i^2 = the error on the individual value

By this method, more weight is placed upon values with a smaller associated σ. The standard error of the weighted mean of a group of values was evaluated based upon the measurement uncertainties (Equation 4.4). However, sources of variation that may not be captured by the uncertainty on individual measurements were also assessed (Equation 4.5). The larger of these two uncertainties was taken as the weighted mean for a group of values.

$$\sigma_1 = \sqrt{\frac{1}{\sum 1/s_i^2}}$$

Equation 4.4

Where:

σ_1 = the uncertainty associated with the calculated weighted mean based upon the measured uncertainties associated with individual measurements in the group.

s_i^2 = the error on the individual measurement

$$\sigma_2 = \sqrt{\frac{\sum\left(\left(x_i - \overline{x}\right)^2\right)/n-1}{\sum 1/s_i^2}}$$

Equation 4.5

Where:

σ_2 = the uncertainty associated with the calculated weighted mean taking into account the variation between individual measurements in the group.

x_i = the individual measurement

$\overline{x}$ = the weighted mean

n = number of samples

s_i^2 = the error on the individual measurement

4.2.4 Placing the ΔR values on a temporal scale

One factor that was considered when selecting contexts from which to extract samples for measurement was the likely calendar time period that would be represented. As discussed in chapter 3, an attempt was made to measure samples over as wide a temporal range as possible. To assess the calendar age range that was represented by the 30 measured contexts the terrestrial measurements for each context that were statistically the same on the basis of a χ^2 test were combined in a weighted mean. This was then converted to a calibrated range using the INTCAL04 atmospheric dataset (Reimer *et al.,* 2004) and the OxCal v3.10 calibration program (Bronk Ramsey, 1995; 2001; 2005).

4.2.5 Are ΔR values calculated using different species comparable?

Within this study, the majority of mollusc samples were of *Patella vulgata*, however another shell species was used from five contexts. For these contexts the number of *Patella vulgata* specimens was low relative to that of another shell species, and therefore samples of *Cerastoderma edule* shells were used from **BA-146** and **BA-39**, *Littorina littorea* from **NO-05** and **SC-206**, and *Mytilus edulis* shells from **BE-503**. It has been suggested that significantly different MREs (and therefore ΔR values) could be calculated at a site as a result of species-dependant variations in mollusc shell ^{14}C activity (Forman and Polyak, 1997; Hogg *et al.,* 1998). In contrast, Harkness (1983) found no clear species-dependant

variations in natural enrichment in an assessment of modern UK coastal MRE. Factors that have been suggested as responsible for inter-species ^{14}C activity variations are differences in specific ecological niche, feeding mechanism and food source (e.g. Ingram, 1996). If a specific feeding mechanism or habitat means that carbon incorporated into shell $CaCO_3$ has a different ^{14}C activity to that of other species this would result in different calculated ΔR values using the paired terrestrial/marine sample approach.

Dissolved inorganic carbon (DIC) in the water column is the source of the majority of shell $CaCO_3$, while a variable portion is derived from metabolic sources (Tanaka *et al.*, 1986; Dettman *et al.*, 1999). The amount of metabolically derived carbon appears to be relatively higher within the soft tissues of the organism (Uerpmann, 1990, Dyke *et al*, 1996). At a specific location the DIC is relatively homogeneous, whereas the source of metabolic carbon varies between species due to differences in habitat and feeding mechanism. Mollusc habitats include the hard substrate (eg. bedrock outcrops), the sediment surface (epifaunal position) and below the sediment surface (infaunal position), while feeding mechanisms include grazing upon micro-algae, detritus and seaweeds, or filter feeding on organic material suspended in the water column. Epifaunal grazers (e.g. *Patella vulgata*) consume material such as the microalgal film coating rock surfaces that consists of organic material, diatoms and cyanobacteria (Jenkins and Hartnoll, 2001). Active suspension feeders (e.g. *Mytilus edulis*), consume suspended organic material in the water column that includes bacteria, phytoplankton, detritus, and dissolved organic matter (DOM).

In the absence of local terrestrial inputs, the suspended material (plankton, etc) that is utilised by filter feeders usually has a ^{14}C activity that is close to ocean DIC and may mean that filter feeders, (eg. mussels and oysters) incorporate proportionally lower amounts of atmospheric ^{14}C than herbivorous grazing species (eg. limpets and periwinkles). The latter consume seaweeds that contain carbon derived from the atmosphere when photosynthesis proceeds while the seaweed is exposed at low tide. It is also possible in areas where there is a significant source of geological carbon for this to be incorporated into shell structure during growth, as sedimentary particles are taken up by the mollusc during grazing (Dye, 1994), or while inhabiting carbonate-rich sediments (Forman and Polyak, 1997). Dyke *et al.* (2002) suggest that the elevated ^{14}C age of the deposit-feeding marine mollusc *Portlandia arctica* is the result of its infaunal position and feeding mechanism, while Forman and Polyak (1997) observed that molluscs with sessile habitats and pelagic food sources gave significantly lower MRE offsets (i.e. a younger ^{14}C age).

To examine the effect of interspecies differences in shell ^{14}C activity, multiple samples of shells from five different species were obtained from a single context. This was **HP-201** which contained a particularly high concentration of carbonised cereal grains and marine mollusc shells of several species. Differences between these five mollusc species included shore position, food source and habitat, as shown in Table 4.3. The measurement of shell fragments was avoided to exclude the possibility of inadvertently measuring the same shell twice. For the same reason, only the left-hand shell portions of bivalve species were selected as sample material. A lower number of individual shells were measured for the species *Cerastoderma edule* due to the low density of intact whole shells of this species from the context. The measurements were made on the same sample wheel to minimize variation resulting from measurement process. One shell (201-02J) was measured twice in this wheel to assess any difference in age that resulted from the inner and outer portions of a single mussel shell.

Species	**Range**	**Habitat**	**Feeding mechanism**	**Food source**
Patella vulgata	high shore to sublittoral fringe	On hard substrate	epifaunal grazer	Microalgal film coating rocks
Littorina littorea	high shore to sublittoral fringe	On hard substrate	epifaunal grazer	Microalgal film coating rocks
Mytilus edulis	high intertidal to shallow subtidal	Attached to hard substrate	active suspension feeder	suspended organic debris
Cerastoderma edule	middle to lower intertidal, sometimes subtidally	infaunal position	active suspension feeder	suspended organic debris
Ensis ensis	extreme low water to the shallow sublittoral	infaunal position	active suspension feeder	suspended organic debris

Table 4.3: Mollusc species sampled from **HP-201** showing specific habitat and feeding mechanism

Chapter 5: Results

5.1 ^{14}C measurements

Full details of ^{14}C and ^{13}C measurements for all contexts are contained in Tables 5.1-5.6 below. For convenience, the contexts are grouped by the relevant geographical area (i.e. Areas 1-6) described in Chapter 3. Relative to the majority of contexts, a lower number of samples were measured from **SC-3083** and **NO-5**, due to the amount of available sample material. Two *Hordeum sp.* caryopses were measured from **SC-3083**, as the pre-treatment process destroyed a large number of grains from this context. Typically, this occurred during the alkali or final acid wash and involved break-up and sometimes dissolution of the grain. Loss of grains during pre-treatment was also a problem for samples from **SC-543** and **SC-1269**, but it was possible to obtain four terrestrial measurements at these contexts by combining two grains for a single measurement. The high rate of grain dissolution from these contexts remains unexplained, but may be the result of specific physical or chemical features of the soil matrix that affect structural integrity of the grain. Lower sample numbers were measured from **NO-5** because of the limited availability of hazelnut and *Littorina littorea* fragments that were from distinguishably different individuals.

5.1.1 *Results of ^{14}C measurements for terrestrial and marine sample material from all contexts.*

Area 1: Ireland

	Terrestrial sample material				Marine sample material			
Context	**Sample ID**	**Lab Code**	**Age BP ± 1σ**	**$\delta^{13}C$ (‰)**	**Sample ID**	**Lab Code**	**Age BP ± 1σ**	**$\delta^{13}C$ (‰)**
DL3-19	19-01A	SUERC-1080	1335 ± 35	-23.7	19-02E	SUERC-3188	1605 ± 35	1.1
	19-01B	SUERC-1085	1220 ± 35	-22.9	19-02F	SUERC-1089	1555 ± 35	0.8
	19-01C	SUERC-1086	1225 ± 35	-24.3		SUERC-3545	1475 ± 35	0.3
	19-01D	SUERC-1087	1280 ± 35	-22.2	19-02G	SUERC-1090	1485 ± 125	1.2
						SUERC-3189	1535 ± 35	0.7
					19-02H	SUERC-1091	1630 ± 45	1.2
						SUERC-3190	1555 ± 35	0.7
DL11-2	11-01A	SUERC-1842	1245 ± 50	-24.1	11-02E	SUERC-1850	1590 ± 35	1.2
	11-01B	SUERC-1847	1215 ± 35	-23.7	11-02F	SUERC-1852	1595 ± 40	1.5
	11-01C	SUERC-1848	1200 ± 35	-22.3	11-02G	SUERC-1853	1545 ± 40	2.0
	11-01D	SUERC-1849	1325 ± 35	-22.5	11-02H	SUERC-1854	1535 ± 35	1.4
OI-6	6-01A	SUERC-3226	970 ± 35	-24.3	6-02E	SUERC-1076	1225 ± 35	0.8
	6-01B	SUERC-1073	945 ± 45	-23.6	6-02F	SUERC-1077	1220 ± 40	1.9
	6-01C	SUERC-1074	1050 ± 35	-22.5	6-02G	SUERC-1078	1285 ± 35	1.2
	6-01D	SUERC-1075	980 ± 45	-24.6	6-02H	SUERC-1079	1170 ± 50	0.9

Table 5.1: Results of ^{14}C and ^{13}C measurements of samples from contexts within Area 1.

Area 2: Mainland Scotland

	Terrestrial sample material				Marine sample material			
Context	**Sample ID**	**Lab Code**	**Age BP ± 1σ**	**$\delta^{13}C$ (‰)**	**Sample ID**	**Lab Code**	**Age BP ± 1σ**	**$\delta^{13}C$ (‰)**
SA-013	13-01A	SUERC-3566	7135 ± 35	-21.8	13-02E	SUERC-241	8025 ± 60	1.7
		SUERC-12588	7145 ± 40	-21.8	13-02F	SUERC-242	8028 ± 60	1.1
	13-01B	SUERC-3567	7400 ± 40	-22.3	13-02G	SUERC-3167	7975 ± 40	0.7
		SUERC-12589	7410± 40	-22.3	13-02H	SUERC-3168	8045 ± 40	0.9
	13-01C	SUERC-3543	7600 ± 40	-21.9				
	13-01D	SUERC-3544	7600 ± 35	-22.0				
CMB-XIII	XIII-01A	SUERC-3587	4775 ± 35	-22.7	XIII-02E	SUERC-4947	5330 ± 35	1.4
	XIII-01B	SUERC-3588	4785 ± 45	-25.7	XIII-02F	SUERC-4948	5310 ± 40	1.3
	XIII-01C	SUERC-3592	4785 ± 40	-26.6	XIII-02G	SUERC-4949	5325 ± 40	0.6
		SUERC-4951	4840 ± 35	-26.6	XIII-02H	SUERC-4950	5335 ± 40	0.7
	XIII-01D	SUERC-4952	5070 ± 40	-23.1				
		SUERC-3593	5035 ± 40	-23.1				

Table 5.2: Results of ^{14}C and ^{13}C measurements of samples from contexts within Area 2 (continued below).

	Terrestrial sample material				Marine sample material			
Context	**Sample ID**	**Lab Code**	**Age BP ± 1σ**	**$\delta^{13}C$ (‰)**	**Sample ID**	**Lab Code**	**Age BP ± 1σ**	**$\delta^{13}C$ (‰)**
FL-JM76	JM76-01A	SUERC-1061	950 ± 50	-23.1	JM76-02E	SUERC-1065	1160 ± 47	1.4
	JM76-01B	SUERC-1062	1070 ± 35	-24.5		SUERC-3186	1270 ± 35	1.3
	JM76-01C	SUERC-1063	910 ± 35	-28.1		SUERC-4941	1235 ± 40	1.4
	JM76-01D	SUERC-1064	940 ± 45	-24.4	JM76-02F	SUERC-1066	1179 ± 45	1.3
	JM76-01E	SUERC-3181	870 ± 35	-25.1		SUERC-4942	1170 ± 35	2.1
	JM76-01F	SUERC-3182	920 ± 35	-22.6	JM76-02G	SUERC-1067	1112 ± 49	1.6
						SUERC-3187	1235 ± 40	1.9
					JM7602-H	SUERC-1068	1339 ± 50	1.8
						SUERC-4943	1300 ± 35	1.8
RH-3004	3004-01A	SUERC-254	655 ± 50	-23.3	3004-02E	SUERC-258	1105 ± 60	1.3
	3004-01B	SUERC-255	665 ± 50	-23.2	3004-02F	SUERC-259	1125 ± 55	2.3
	3004-01C	SUERC-256	650 ± 50	-21.8	3004-02G	SUERC-260	1020 ± 50	1.2
	3004-01D	SUERC-257	610 ± 50	-25.1	3004-02H	SUERC-261	1080 ± 50	1.7
RH-3019	3019-01A	SUERC-243	910 ± 45	-23.6	3019-02E	SUERC-247	1210 ± 45	0.6
	3019-01B	SUERC-244	855 ± 45	-24.9	3019-02F	SUERC-248	1175 ± 45	1.6
	3019-01C	SUERC-245	855 ± 50	-27.0	3019-02G	SUERC-249	1220 ± 50	1.2
	3019-01D	SUERC-246	920 ± 50	-25.0	3019-02H	SUERC-253	1200 ± 50	0.5

Table 5.2 (continued): Results of ^{14}C and ^{13}C measurements of samples from contexts within Area 2.

Area 3: Outer Hebrides

	Terrestrial sample material				Marine sample material			
Context	**Sample ID**	**Lab Code**	**Age BP ± 1σ**	**$\delta^{13}C$ (‰)**	**Sample ID**	**Lab Code**	**Age BP ± 1σ**	**$\delta^{13}C$ (‰)**
NO-5	5-01A	AA-50332	7525 ± 80	-24.4	5-02E	AA-53250	7860 ± 45	1.5
	5-01B	AA-50333	7395 ± 45	-23.7	5-02F	AA-53251	7880 ± 45	1.1
	5-01C	AA-50334	7420 ± 45	-24.1				
BA-39	39-01A	AA-52314	2080 ± 45	-21.1	39-02E	AA-52319	2240 ± 45	2.4
	39-01B	AA-52315	1975 ± 45	-20.2	39-02F	AA-52320	2255 ± 45	2.2
	39-01C	AA-52316	2005 ± 45	-21.2	39-02G	AA-52321	2260 ± 45	2.2
	39-01D	AA-52317	1990 ± 45	-23.0	39-02H	AA-52322	2260 ± 45	2.3
BA-146	146-01A	AA-48452	2135 ± 50	-24.5	146-02E	AA-48456	2390 ± 50	2.0
	146-10B	AA-48453	2115 ± 50	-24.9	146-02F	AA-48457	2385 ± 50	2.0
	146-01C	AA-48454	2165 ± 55	-24.5	146-02G	AA-48458	2345 ± 75	1.8
	146-01D	AA-48455	2030 ± 50	-24.3	146-02H	AA-48459	2355 ± 40	1.8
BA-139	139-01A	AA-51177	2290 ± 40	-22.5	139-02E	AA-51180	2540 ± 35	1.2
	139-01B	AA-51178	2220 ± 45	-21.8	139-02F	AA-51181	2540 ± 40	0.9
	139-01C	AA-52318	2255 ± 70	-22.0	139-02G	AA-51182	2535 ± 40	1.2
	139-01D	AA-51179	2245 ± 40	-22.6	139-02H	AA-51183	2480 ± 40	0.8

Table 5.3: Results of ^{14}C and ^{13}C measurements of samples from contexts within Area 3 (continued below).

	Terrestrial sample material				Marine sample material			
Context	**Sample ID**	**Lab Code**	**Age BP ± 1σ**	**$\delta^{13}C$ (‰)**	**Sample ID**	**Lab Code**	**Age BP ± 1σ**	**$\delta^{13}C$ (‰)**
HP-201	201-01A	SUERC-23	2155 ± 40	-24.2	201-02E	SUERC-27	2365 ± 65	0.3
	201-01B	SUERC-24	2120 ± 40	-22.6	201-02F	SUERC-28	2375 ± 40	1.6
	201-01C	SUERC-25	2135 ± 40	-22.8	201-02G	SUERC-29	2385 ± 40	1.5
	201-01D	SUERC-26	2110 ± 80	-24.5	201-02H	SUERC-30	2360 ± 40	1.9
BE-503	503-01A	SUERC-1049	1595 ± 40	-24.2	503-02E	SUERC-1054	1945 ± 35	1.5
	503-01B	SUERC-1050	1725 ± 40	-25.3	503-02F	SUERC-1055	1940 ± 35	0.8
	503-01C	SUERC-1051	1735 ± 40	-23.4	503-02G	SUERC-3179	1980 ± 35	1.1
	503-01D	SUERC-1052	1650 ± 35	-26.0	503-02H	SUERC-1056	2045 ± 40	0.9
	503-01E	SUERC-3176	1630 ± 35	-25.1		SUERC-3180	1990 ± 35	0.6
	503-01F	SUERC-3177	1650 ± 35	-24.8				
BO-64	64-01A	SUERC-1037	1315 ± 40	-23.3	64-02E	SUERC-1041	1365 ± 40	1.0
	64-01B	SUERC-3169	1095 ± 35	-25.1	64-02F	SUERC-1042	1465 ± 35	1.1
	64-01C	SUERC-1038	1150 ± 35	-23.9		SUERC-3171	1475 ± 35	1.1
	64-01D	SUERC-3170	1260 ± 35	-23.7	64-02G	SUERC-1043	1330 ± 40	0.1
	64-01E	SUERC-1039	1120 ± 35	-24.6		SUERC-3172	1435 ± 30	1.3
	64-01F	SUERC-1040	1065 ± 35	-25.0	64-02H	SUERC-4118	1415 ± 35	-0.3

Table 5.3: (Continued):Results of ^{14}C and ^{13}C measurements of samples from contexts within Area 3 (continued below).

	Terrestrial sample material				Marine sample material			
Context	**Sample ID**	**Lab Code**	**Age BP ± 1σ**	**$\delta^{13}C$ (‰)**	**Sample ID**	**Lab Code**	**Age BP ± 1σ**	**$\delta^{13}C$ (‰)**
GA-165	165-01A	AA-48444	1060 ± 50	-25.4	165-02E	AA-53257	1375 ± 35	1.4
	165-01B	AA-48445	1110 ± 55	-25.0		SUERC-4051	1370 ± 35	0.8
	165-01C	AA-48446	1110 ± 50	-24.0		SUERC-4052	1445 ± 35	0.9
	165-01D	AA-48447	1130 ± 50	-25.2		SUERC-4053	1340 ± 35	1.3
						SUERC-4054	1395 ± 35	1.0
					165-02F	AA-53258	1360 ± 40	1.6
					165-02G	AA-53259	1415 ± 35	1.7
					165-02H	AA-53260	1545 ± 35	1.4

Table 5.3: (Continued): Results of ^{14}C and ^{13}C measurements of samples from contexts within Area 3.

Area 4: Orkney Isles

	Terrestrial sample material				Marine sample material			
Context	**Sample ID**	**Lab Code**	**Age BP ± 1σ**	**$\delta^{13}C$ (‰)**	**Sample ID**	**Lab Code**	**Age BP ± 1σ**	**$\delta^{13}C$ (‰)**
SkB-68	68-01A	SUERC-3126	4270 ± 40	-24.2	68-02E	SUERC-3130	4975 ± 40	-0.5
	68-01B	SUERC-3127	4735 ± 40	-24.2	68-02F	SUERC-3131	4995 ± 40	1.2
	68-01C	SUERC-3128	4555 ± 40	-24.5	68-02G	SUERC-3132	4960 ± 45	0.9
	68-01D	SUERC-3129	4605 ± 40	-24.2	68-02H	SUERC-4122	4790 ± 40	-0.7
	68-01E	SUERC-4119	4525 ± 40	-21.8		SUERC-12591	4745 ± 40	1.0
	68-01F	SUERC-4121	4530 ± 35	-21.3				
SkB-26	26-01A	SUERC-3576	4140 ± 40	-22.0	26-02E	SUERC-232	4440 ± 50	1.6
	26-01B	SUERC-4958	4015 ± 40	-21.4	26-02F	SUERC-233	4370 ± 45	0.6
	26-01C	SUERC-3578	4110 ± 35	-21.6	26-02G	SUERC-234	4445 ± 50	0.9
	26-01D	SUERC-3582	4145 ± 45	-21.3	26-02H	SUERC-235	4405 ± 45	0.9
BB-XF	XF-01A	SUERC-3588	3640 ± 35	-22.0	XF-02E	SUERC-221	3920 ± 50	0.6
	XF-01B	SUERC-3572	3645 ± 40	-22.4	XF-02F	SUERC-222	3980 ± 50	1.2
	XF-01C	SUERC-3573	3625 ± 40	-22.3	XF-02G	SUERC-223	4000 ± 50	1.5
	XF-01D	SUERC-3575	3685 ± 40	-22.1	XF-02H	SUERC-224	3956 ± 55	1.5

Table 5.4: Results of ^{14}C and ^{13}C measurements of samples from contexts within Area 4 (continued below).

	Terrestrial sample material				Marine sample material			
Context	**Sample ID**	**Lab Code**	**Age BP ± 1σ**	**$\delta^{13}C$ (‰)**	**Sample ID**	**Lab Code**	**Age BP ± 1σ**	**$\delta^{13}C$ (‰)**
LO-6	LO6-01A	SUERC-1837	3735 ± 40	-23.1	LO6-02E	SUERC-1840	3960 ± 40	1.3
	LO6-01B	SUERC-1838	3690 ± 35	-24.0	LO6-02F	SUERC-1841	3915 ± 35	1.2
	LO6-01C	SUERC-3228	3690 ± 35	-24.9	LO6-02G	SUERC-3137	3950 ± 35	1.0
	LO6-01D	SUERC-1839	3685 ± 40	-24.7	LO6-02H	SUERC-3139	3880 ± 45	1.0
StB-2136	2136-01A	SUERC-107	2050 ± 40	-23.7	2136-02E	SUERC-111	2280 ± 40	1.3
	2136-01B	SUERC-108	2035 ± 45	-24.1	2136-02F	SUERC-112	2325 ± 45	1.3
	2136-01C	SUERC-109	2120 ± 40	-23.5	2136-02G	SUERC-113	2325 ± 90	1.4
	2136-01D	SUERC-110	2035 ± 40	-25.7	2136-02H	SUERC-114	2390 ± 45	1.5
StB-2044	2044-01A	SUERC-115	2085 ± 40	-24.8	2044-02E	SUERC-125	2385 ± 40	0.8
	2044-01B	SUERC-116	2100 ± 40	-24.1	2044-02F	SUERC-126	2360 ± 40	1.1
	2044-01C	SUERC-123	2090 ± 40	-24.0	2044-02G	SUERC-127	2365 ± 40	1.9
	2044-01D	SUERC-124	2070 ± 40	-23.8		SUERC-191	2405 ± 35	1.3
					2044-02H	SUERC-128	2540 ± 40	0.7
						SUERC-4114	2545 ± 35	1.3
StB-1063B	1063-01A	SUERC-129	965 ± 40	-25.0	1063-02E	SUERC-133	1240 ± 40	0.3
	1063-01B	SUERC-130	995 ± 40	-23.9	1063-02F	SUERC-134	1270 ± 40	1.2
	1063-01C	SUERC-131	935 ± 40	-24.8	1063-02G	SUERC-135	1260 ± 40	0.7
	1063-01D	SUERC-132	935 ± 40	-23.5	1063-02H	SUERC-136	1250 ± 40	0.4

Table 5.4: (Continued): Results of ^{14}C and ^{13}C measurements of samples from contexts within Area 4 (continued below).

	Terrestrial sample material				Marine sample material			
Context	**Sample ID**	**Lab Code**	**Age BP ± 1σ**	**$\delta^{13}C$ (‰)**	**Sample ID**	**Lab Code**	**Age BP ± 1σ**	**$\delta^{13}C$ (‰)**
QG-A023	A023-01A	AA-52329	875 ± 45	-24.0	A023-02E	SUERC-3162	1270 ± 35	1.7
	A023-01B	AA-52330	835 ± 40	-24.1		SUERC-4109	1245 ± 35	0.0
	A023-01C	AA-52331	835 ± 40	-22.0	A023-02F	SUERC-4110	1175 ± 35	1.7
	A023-01D	AA-52332	945 ± 55	-22.4	A023-02G	SUERC-3166	1250 ± 30	1.2
	A023-01E	SUERC-3160	940 ± 35	-22.7		SUERC-4111	1210 ± 35	1.1
	A023-01F	SUERC-3161	940 ± 35	-24.5	A023-02H	SUERC-4112	1210 ± 35	0.2
QG-A004	A004-01A	AA-52325	710 ± 80	-23.1	A004-02E	SUERC-3152	1235 ± 40	1.2
	A004-01B	AA-52326	520 ± 40	-24.5	A004-02F	SUERC-3156	1200 ± 35	1.9
	A004-01C	AA-52327	585 ± 65	-25.0	A004-02G	SUERC-3157	1195 ± 35	1.8
	A004-01D	AA-52328	720 ± 40	-28.4	A004-02H	SUERC-3159	1210 ± 35	1.1
	A004-01E	SUERC-3149	980 ± 40	-23.8				
	A004-01F	SUERC-3542	875 ± 35	-24.7				
	A004-01G	SUERC-3150	960 ± 40	-24.7				
	A004-01H	SUERC-3151	925 ± 40	-24.1				

Table 5.4 (Continued): Results of ^{14}C and ^{13}C measurements of samples from contexts within Area 4.

Area 5: Shetland Isles

	Terrestrial sample material				Marine sample material			
Context	**Sample ID**	**Lab Code**	**Age BP ± 1σ**	**$\delta^{13}C$ (‰)**	**Sample ID**	**Lab Code**	**Age BP ± 1σ**	**$\delta^{13}C$ (‰)**
SC-543	543-01A	AA-51153	1740 ± 35	-23.9	543-02E	SUERC-3140	1825 ± 50	1.2
	543-01B	AA-51154	1680 ± 35	-22.1		SUERC-4058	1790 ± 35	0.5
	543-01C	AA-51155	1680 ± 50	-22.0	543-02F	AA-51162	1740 ± 45	1.9
	543-01D	AA-51156	1710 ± 40	-22.6		SUERC-4059	1755 ± 35	0.7
					543-02G	AA-51163	1725 ± 35	1.3
						SUERC-4061	1780 ± 35	1.0
					543-02H	AA-51164	1760 ± 35	1.8
						SUERC-3141	1775 ± 35	1.6
						SUERC-4062	1945 ± 40	1.3
SC-3083	3083-03A	AA-52324	1615 ± 40	-21.3	3083-02E	AA-52310	1925 ± 40	2.1
	3083-03C	AA-52323	1570 ± 55	-22.9	3083-02F	AA-52311	1975 ± 45	1.8
					3083-02G	AA-52312	1955 ± 50	1.4
						SUERC-3147	2055 ± 45	1.6
					3083-02H	SUERC-3148	2080 ± 50	0.9
						SUERC-4960	2005 ± 40	1.2

Table 5.5: Results of ^{14}C and ^{13}C measurements of samples from contexts within Area 5 (continued below).

	Terrestrial sample material				Marine sample material			
Context	**Sample ID**	**Lab Code**	**Age BP ± 1σ**	**$\delta^{13}C$ (‰)**	**Sample ID**	**Lab Code**	**Age BP ± 1σ**	**$\delta^{13}C$ (‰)**
SC-1269	1269-01C	AA-51157	1300 ± 35	-21.7	1269-02E	AA-51165	1580 ± 35	1.7
	1269-03A	AA-51158	1375 ± 35	-22.4	1269-02F	AA-51166	1525 ± 40	1.3
	1269-03B	AA-51159	1280 ± 35	-23.6	1269-02G	AA-51167	1655 ± 35	2.0
	1269-03D	AA-51160	1285 ± 40	-23.3	1269-02H	AA-51168	1580 ± 35	1.7
SC-206	206-01A	AA-51169	815 ± 40	-25.7	206-02E	AA-51173	1180 ± 35	2.3
	206-01B	AA-51170	740 ± 40	-25.9		SUERC-3142	1230 ± 40	2.0
	206-03A	AA-51171	730 ± 45	-25.1	206-02F	AA-51174	1135 ± 35	2.2
	206-03B	AA-51172	840 ± 45	-25.5	206-02G	AA-51175	1230 ± 35	1.8
					206-02H	AA-51176	1325 ± 40	2.4
						SUERC-3146	1325 ± 40	2.9

Table 5.5: (Continued): Results of ^{14}C and ^{13}C measurements of samples from contexts within Area 5.

Area 6: Faroe Isles

	Terrestrial sample material				Marine sample material			
Context	**Sample ID**	**Lab Code**	**Age BP ± 1σ**	**$\delta^{13}C$ (‰)**	**Sample ID**	**Lab Code**	**Age BP ± 1σ**	**$\delta^{13}C$ (‰)**
UJ-23	23-01A	SUERC-3400	1000 ± 40	-23.9	23-02E	SUERC-3404	1410 ± 35	1.5
	23-01B	SUERC-3401	980 ± 40	-26.8	23-02F	SUERC-3407	1460 ± 40	1.6
	23-01C	SUERC-3402	940 ± 45	-26.3	23-02G	SUERC-3408	1445 ± 35	1.4
	23-01D	SUERC-3403	995 ± 35	-24.0	23-02H	SUERC-3409	1440 ± 35	1.3

Table 5.6: Results of ^{14}C and ^{13}C measurements of samples from contexts within Area 6.

5.1.2 Consistency of ^{14}C ages within contexts

Repeat measurements of a single shell from **GA-165** were examined using the χ^2 test to assess the internal variability of the group, and the ages were found not to be significantly different (Table 5.7). The empirical standard deviation on the measurement group was 39 ^{14}C y, which is consistent with the error on the individual measurements of ± 35 ^{14}C y. This indicates that a homogeneous crushed sample is representative of the ^{14}C concentration of the shell. All repeated measurements on mollusc shell samples were within 2 standard deviations of each other and multiple measurements from a single sample were combined in a weighted mean. This allowed a more accurate assessment of the ^{14}C age of the shell where there had been variation in the original marine measurement group from a context. Where the variation had been due to measurement variability a more accurate assessment of individual ages meant that the measurement group including the weighted mean(s) was coherent on the basis of a second χ^2 test. Where the variation was due to differences in the mean ages of the samples, the variation remained evident after additional measurements.

Lab Code ID	**Age BP ± 1σ**	***T*-statistic for group**	**Weighted mean age BP ± 1σ**	**Empirical standard deviation (^{14}C y)**
AA-53257	1375 ± 35			
SUERC-4051	1370 ± 35			
SUERC-4052	1445 ± 35			
SUERC-4053	1340 ± 35			
SUERC-4054	1395 ± 35			
		T= 4.94 ($\chi^2_{:0.05}$ = 9.49)	1385 ± 17	39

Table 5.7: Results of repeat ^{14}C measurements of a single shell from context **GA-165**.

The calculated *T*-statistic for terrestrial and marine sample groups from all contexts are shown in Table 5.8. All measurements made of terrestrial or marine material from a context were used to calculate the relevant *T*-statistics. Where multiple measurements were made of any individual sample, these were combined in a weighted mean prior to calculation of the *T*-statistic for that context. In the majority of instances the *T*-statistic is lower than the critical value for 95% significance, indicating that the ^{14}C ages within these groups are contemporaneous. This supports the assertion that the sample, site and context protocol described in Chapter 3 was effective in selecting contexts within which the terrestrial and marine material was of a comparable calendar age range.

Context	Terrestrial measurement group *T*-statistic	Marine measurement group *T*-statistic
RH-3004	0.70; ($\chi^2_{:0.05}$ = 7.81)	2.28; ($\chi^2_{:0.05}$ = 7.81)
RH-3019	1.06; ($\chi^2_{:0.05}$ = 7.81)	0.52; ($\chi^2_{:0.05}$ = 7.81)
BA-39	3.22; ($\chi^2_{:0.05}$ = 7.81)	0.13; ($\chi^2_{:0.05}$ = 7.81)
BA-146	3.82; ($\chi^2_{:0.05}$ = 7.81)	0.50; ($\chi^2_{:0.05}$ = 7.81)
BA-139	1.43; ($\chi^2_{:0.05}$ = 7.81)	1.65; ($\chi^2_{:0.05}$ = 7.81)
HP-201	0.49; ($\chi^2_{:0.05}$ = 7.81)	0.21; ($\chi^2_{:0.05}$ = 7.81)
NO-5	2.02; ($\chi^2_{:0.05}$ = 5.99)	0.10; ($\chi^2_{:0.05}$ = 3.84)
BE-503	9.69; ($\chi^2_{:0.05}$ = 11.1)	3.84; ($\chi^2_{:0.05}$ = 7.81)
BB-XF	1.24; ($\chi^2_{:0.05}$ = 7.81)	1.42; ($\chi^2_{:0.05}$ = 7.81)
LO-6	1.06; ($\chi^2_{:0.05}$ = 7.81)	2.31; ($\chi^2_{:0.05}$ = 7.81)
StB-2136	3.01; ($\chi^2_{:0.05}$ = 7.81)	3.34; ($\chi^2_{:0.05}$ = 7.81)
StB-1063B	1.55; ($\chi^2_{:0.05}$ = 7.81)	0.31; ($\chi^2_{:0.05}$ = 7.81)
QG-A023	8.82; ($\chi^2_{:0.05}$ = 11.1)	3.99; ($\chi^2_{:0.05}$ = 7.81)
SC-543	1.34; ($\chi^2_{:0.05}$ = 7.81)	1.26; ($\chi^2_{:0.05}$ = 7.81)
SC-1269	4.65; ($\chi^2_{:0.05}$ = 7.81)	6.25; ($\chi^2_{:0.05}$ = 7.81)
OI-6	4.30; ($\chi^2_{:0.05}$ = 7.81)	3.95; ($\chi^2_{:0.05}$ = 7.81)
DL3-19	7.14; ($\chi^2_{:0.05}$ = 7.81)	4.05; ($\chi^2_{:0.05}$ = 7.81)
DL11-2	5.15; ($\chi^2_{:0.05}$ = 7.81)	2.06; ($\chi^2_{:0.05}$ = 7.81)
UJ-23	1.21; ($\chi^2_{:0.05}$ = 7.81)	0.98; ($\chi^2_{:0.05}$ = 7.81)
BO-64	23.62; ($\chi^2_{:0.05}$ = 7.81)	5.82; ($\chi^2_{:0.05}$ = 7.81)
SkB-26	6.60; ($\chi^2_{:0.05}$ = 7.81)	1.64; ($\chi^2_{:0.05}$ = 7.81)
SA-013	156.46; ($\chi^2_{:0.05}$ = 7.81)	1.64; ($\chi^2_{:0.05}$ = 7.81)
QG-A004	114.93; ($\chi^2_{:0.05}$ = 14.1)	0.65; ($\chi^2_{:0.05}$ = 7.81)
SkB-68	72.28; ($\chi^2_{:0.05}$ = 11.1)	16.59; ($\chi^2_{:0.05}$ = 7.81)
FL-JM76	18.86; ($\chi^2_{:0.05}$ = 11.1)	12.81; ($\chi^2_{:0.05}$ = 7.81)
CMB-XIII	57.25; ($\chi^2_{:0.05}$ = 7.81)	0.22; ($\chi^2_{:0.05}$ = 7.81)
GA-165	1.07; ($\chi^2_{:0.05}$ = 7.81)	15.69; ($\chi^2_{:0.05}$ = 7.81)
SC-206	4.78; ($\chi^2_{:0.05}$ = 7.81)	20.04; ($\chi^2_{:0.05}$ = 7.81)
SC-3083	0.44; ($\chi^2_{:0.05}$ = 3.84)	4.30; ($\chi^2_{:0.05}$ = 7.81)
StB-2044	0.29; ($\chi^2_{:0.05}$ = 7.81)	25.26; ($\chi^2_{:0.05}$ = 7.81)

Table 5.8: Calculated *T*-statistics for ^{14}C ages of each group of marine and terrestrial samples from contexts, showing the relevant critical value for 5% significance ($\chi^2_{:0.05}$) for the number of samples (*N*) within the tested group.

The *T*-statistic shows variation in ^{14}C ages within 11 groups (of terrestrial or marine samples) from nine contexts. These groups of measurements were examined to determine the likely cause of variation and the most representative ^{14}C ages from the group. In seven instances, the variation was due to a single measurement that could not be combined legitimately with the remainder of the group. When the outlying data point was removed and the test repeated, the *T*-statistic showed the measurements were indistinguishable at 95% confidence. In four instances, more than one measurement was not consistent with the remaining determinations from a context. In the case of **SkB-68** and **BO-64,** two measurements were not consistent with the remainder of the group or with each other. Here, the group of measurements that comprised the majority of the context was taken as the most accurate representation of the terrestrial age of the context. In the case of **BO-64**, 28 previous ^{14}C measurements from the site range between c.1100-1200 BP (Neighbour, 2001; Church, 2002), and the group of similar ages at c.1100 BP are most likely to represent an accurate terrestrial ^{14}C age for **BO-64**.

The terrestrial measurement group from **SA-013** spans c.500 ^{14}C yr where SUERC-3543 (7600 ± 40 BP) and SUERC-3544 (7600 ± 35 BP) are consistent with each other. SUERC-3567/4957 (7405 ± 28 BP) and SUERC-3566/4953 (7139 ± 26 BP) are not consistent with these measurements or each other. Only SUERC-3543 and SUERC-3544 are consistent on the basis of a χ^2 test with previous measurements of deer bone and charcoal submitted by the site excavators from contexts that underlay **SA-013** (Finlayson *et al.*, 1999; Hardy and Wickham-Jones, 2003; 2004; in press). These ages were chosen to most accurately represent the terrestrial age of **SA-013**.

Four measurements from **QG-A004** are consistent with each other, while the remaining four measurements can be separated into two groups of ^{14}C ages, each internally consistent, but each different from the other and from the remaining measurements from the context. The group of four measurements are consistent with ^{14}C ages from three other contexts in the same midden sequence. These include two contexts (**QG-A005** and **QG-A023**) in the same sample column as **QG-A004**, and one from basal deposits (**QG-022/EO30**) in another area of the same midden. Measurements from **QG-A005** and **QG-022/EO30** were submitted by the site excavators (Barrett and Gerrard, 2002), while measurements from **QG-A023** were performed as part of this project. **QG-A004** was situated in the upper layers of a coastal midden, where the overlying deposits showed signs of mixing and bioturbation. It is possible that these effects have also influenced the contents of **QG-A004**.

Context	Group	1st *T* value	Consistent measurements	Age BP ± 1σ	Inconsistent measurements	Age BP ± 1σ	2nd *T* value
SA-013	Terrestrial	156.46;($\chi^2_{:0.05}$ = 7.81)	SUERC-3543	7600 ± 40	SUERC-3567/4957	7139 ± 26	0.00 ($\chi^2_{:0.05}$ = 3.84)
			SUERC-3544	7600 ± 35	SUERC-3566/4953	7405 ± 28	
CMB-XIII	Terrestrial	57.25; ($\chi^2_{:0.05}$ = 7.81)	SUERC-3587	4775 ± 35	SUERC-3593/4952	5053 ± 28	0.96 ($\chi^2_{:0.05}$ = 5.99)
			SUERC-3588	4785 ± 45			
			SUERC-3592/4951	4816 ± 27			
SkB-68	Terrestrial	72.28; ($\chi^2_{:0.05}$ = 11.1)	SUERC-3128	4555 ± 40	SUERC-3126	4270 ± 40	2.61 ($\chi^2_{:0.05}$ = 7.81)
			SUERC-3129	4605 ± 40	SUERC-3127	4735 ± 40	
			SUERC-4119	4525 ± 40			
			SUERC-4121	4530 ± 35			
SkB-68	Marine	16.59; ($\chi^2_{:0.05}$ = 7.81)	SUERC-3130	4975 ± 40	SUERC-4122/4959	4768 ± 28	0.35($\chi^2_{:0.05}$ = 5.99)
			SUERC-3131	4995 ± 40			
			SUERC-3132	4960 ± 45			
StB-2044	Marine	25.26; ($\chi^2_{:0.05}$ = 7.81)	SUERC-125	2385 ± 40	SUERC-128/4114	2543 ± 26	0.36($\chi^2_{:0.05}$ = 5.99)
			SUERC-126	2360 ± 40			
			SUERC-127/191	2388 ± 26			
QG-A004	Terrestrial	114.93;($\chi^2_{:0.05}$ = 14.1)	SUERC-3149	980 ± 40	AA-52325	710 ± 80	4.61($\chi^2_{:0.05}$ = 17.81)
			SUERC-3542	875 ± 35	AA-52326	520 ± 40	
			SUERC-3150	960 ± 40	AA-52327	585 ± 65	
			SUERC-3151	925 ± 40	AA-52328	720 ± 40	

Table 5.9: (Continued below): Data for contexts that contained measurements that were inconsistent on the basis of a χ^2 test, showing consistent and inconsistent measurements. Consistent measurements were used to calculate values of ΔR and the *T*-statistics for consistent measurement groups are shown.

Context	Group	1st T value	Consistent measurements	Age BP ± 1σ	Inconsistent measurements	Age BP ± 1σ	2nd T value
BO-64	Terrestrial	23.62; ($\chi^2_{:0.05}$ = 7.81)	SUERC-3169	1095 ± 35	SUERC-1037	1315 ± 40	3.2($\chi^2_{:0.05}$ = 17.81)
			SUERC-1038	1150 ± 35	SUERC-3170	1260 ± 35	
			SUERC-1039	1120 ± 35			
			SUERC-1040	1065 ± 35			
FL-JM76	Terrestrial	18.86; ($\chi^2_{:0.05}$ = 11.1)	SUERC-1061	950 ± 50	SUERC-1062	1070 ± 35	2.46($\chi^2_{:0.05}$ = 9.49)
			SUERC-1063	910 ± 35			
			SUERC-1064	940 ± 45			
			SUERC-3181	870 ± 35			
			SUERC-3182	920 ± 35			
FL-JM76	Marine	12.81; ($\chi^2_{:0.05}$ = 7.81)	SUERC-1065/3186/4941	1232 ± 31	SUERC-1068/	1313 ± 29	2.04 ($\chi^2_{:0.05}$ = 5.99)
			SUERC-1066/4942	1173 ± 28	SUERC-3187		
			SUERC-1067/3187	1186 ± 60			
GA-165	Marine	15.69; ($\chi^2_{:0.05}$ = 7.81)	AA-53257/SUERC-4051/	1385 ± 17	AA-53260	1545 ± 35	1.09 ($\chi^2_{:0.05}$ = 5.99)
			4052/4053/4054				
			AA-53258	1360 ± 40			
			AA-53259	1415 ± 35			
SC-206	Marine	20.04; ($\chi^2_{:0.05}$ = 7.81)	AA-51173/SUERC-3142	1202 ± 26	AA-51176/	1325 ± 28	3.98 ($\chi^2_{:0.05}$ = 5.99)
			AA-51174	1135 ± 35	SUERC-3146		
			AA-51175	1230 ± 35			

Table 5.9: (Continued): Data for contexts that contained measurements that were inconsistent on the basis of a χ^2 test, showing consistent and inconsistent measurements. Consistent measurements were used to calculate values of ΔR and the *T*-statistics for consistent measurement groups are shown.

5.1.3 The temporal range of measured contexts

The 2σ calibrated ranges of the contexts are used to assess the temporal coverage of the data. The calibrated ages of the 31 contexts used in the study cover a time period from c. BC 6500 to c. AD 1400. The calibrated age ranges of the contexts studied do not continuously cover this interval, which is a result of the lower number of suitable contexts from older sites that were available. As can be seen from Figure 5.1, in several instances the calibrated age range of several contexts are similar for a given time period. However at other points there are gaps in the temporal coverage of the data. The largest of these are gaps in the 2σ calibrated age ranges in the periods 6230-3650 BC (2580 cal. y), 3110-2870 BC (240 cal. y), 2500-2190 BC (310 cal. y), 1940-400 BC (1540 cal. y), 60-250 AD (190 cal. y), 540-650 AD (110 cal. y), and 810-890 AD (80 cal. y). The largest time periods for which no material was measured was the earliest, a 2580 cal. yr gap between **SA-013/ NO-5** and **CMB-XIII**. The next largest gap in the temporal coverage of the material is 1540 cal. yr (1940-400 BC).

Context	Terr. weighted mean age BP ± 1σ	1σ cal. range	Range (cal. y)	2σ cal. range	Range (cal. y)
SA-013	7600 ± 26	6465-6435 BC	30	6480-6420 BC	60
NO-5	7424 ± 30	6360-6240 BC	120	6390-6230 BC	160
CMB-XIII	4798 ± 19	3640-3530 BC	110	3650-3520 BC	130
SkB-68	4552 ± 19	3370-3130 BC	240	3370-3110 BC	260
SkB-26	4101 ± 29	2840-2570 BC	270	2870-2500 BC	370
LO-6	3699 ± 19	2135-2035 BC	100	2190-2020 BC	170
BB-XF	3648 ± 19	2120-1960 BC	160	2130-1940 BC	190
BA-139	2254 ± 26	390-230 BC	160	400-200 BC	200
BA-146	2109 ± 29	180-60 BC	120	210-40 BC	170
HP-201	2135 ± 22	205-110 BC	95	350-50 BC	300
StB-2044	2086 ± 20	160-50 BC	110	170-40 BC	130
StB-2136	2061 ± 21	110-40 BC	70	170 BC -0 AD	170
BA-39	2013 ± 23	45 BC -20 AD	65	90 BC-60 AD	150
SC-543	1706 ± 19	260-390 AD	130	250-400 AD	150
BE-503	1661 ± 21	350-420 AD	70	330-430 AD	100
SC-3083	1599 ± 21	420-540 AD	120	410-540 AD	130
SC-1269	1312 ± 23	660-770 AD	110	650-770 AD	120
DL3-19	1265 ± 27	685-775 AD	90	660-820 AD	160
DL11-2	1264 ± 25	690-775 AD	85	660-810 AD	150
BO-64	1108 ± 18	895-975 AD	80	890-985 AD	95
GA-165	1102 ± 15	895-980 AD	85	890-990 AD	100
OI-6	992 ± 23	1010-1150 AD	140	990-1160 AD	170
UJ-23	982 ± 20	1010-1150 AD	140	1010-1160 AD	150
StB-1063B	958 ± 20	1020-1150 AD	130	1020-1160 AD	140
QG-A004	931 ± 24	1030-1160 AD	130	1020-1160 AD	140
FL-JM76	912 ± 17	1040-1160 AD	120	1030-1170 AD	140
QG-A023	896 ± 22	1040-1190 AD	150	1040-1220 AD	180
RH-3019	885 ± 24	1050-1210 AD	160	1040-1220 AD	180
SC-206	781 ± 27	1220-1270 AD	50	1215-1280 AD	65
RH-3004	645 ± 25	1290-1390 AD	100	1280-1400 AD	120

Table 5.10: Calibrated age ranges for all contexts, calculated from the weighted mean terrestrial age. The size of the age range in calibrated years is shown for both the 1σ and 2σ intervals. The average 1σ range is 109 y; the average 2σ range is 154 y.

Context	2σ calibrated age range	Approximate archaeological period
SA-013	6480-6420 BC	Mesolithic
NO-5	6390-6230 BC	Mesolithic
CMB-XIII	3650-3520 BC	Neolithic
SkB-68	3370-3110 BC	Neolithic
SkB-26	2870-2500 BC	Neolithic
LO-6	2190-2020 BC	Bronze Age
BB-XF	2130-1940 BC	Bronze Age
BA-139	400-200 BC	Early Iron Age
BA-146	210-40 BC	Iron Age
HP-201	350-50 BC	Iron Age
StB-2044	170-40 BC	Iron Age
StB-2136	170 BC -0 AD	Iron Age
BA-39	90 BC-60 AD	Iron Age
SC-543	250-400 AD	Late Iron Age/Pictish
BE-503	330-430 AD	Late Iron Age/Pictish
SC-3083	410-540 AD	Late Iron Age/Pictish
SC-1269	650-770 AD	Norse
DL3-19	660-820 AD	Norse/Christian
DL11-2	660-810 AD	Norse/Christian
BO-64	890-985 AD	Norse
GA-165	890-990 AD	Norse
OI-6	990-1160 AD	Norse
UJ-23	1010-1160 AD	Norse
StB-1063B	1020-1160 AD	Norse
QG-A004	1020-1160 AD	Norse
FL-JM76	1030-1170 AD	Norse
QG-A023	1040-1220 AD	Norse
RH-3019	1040-1220 AD	Norse
SC-206	1215-1280 AD	Historic/Medieval
RH-3004	1280-1400 AD	Historic/Medieval

Table 5.11: Contexts ordered according to archaeological period subdivisions (described in section 3.2.2, Chapter 3).

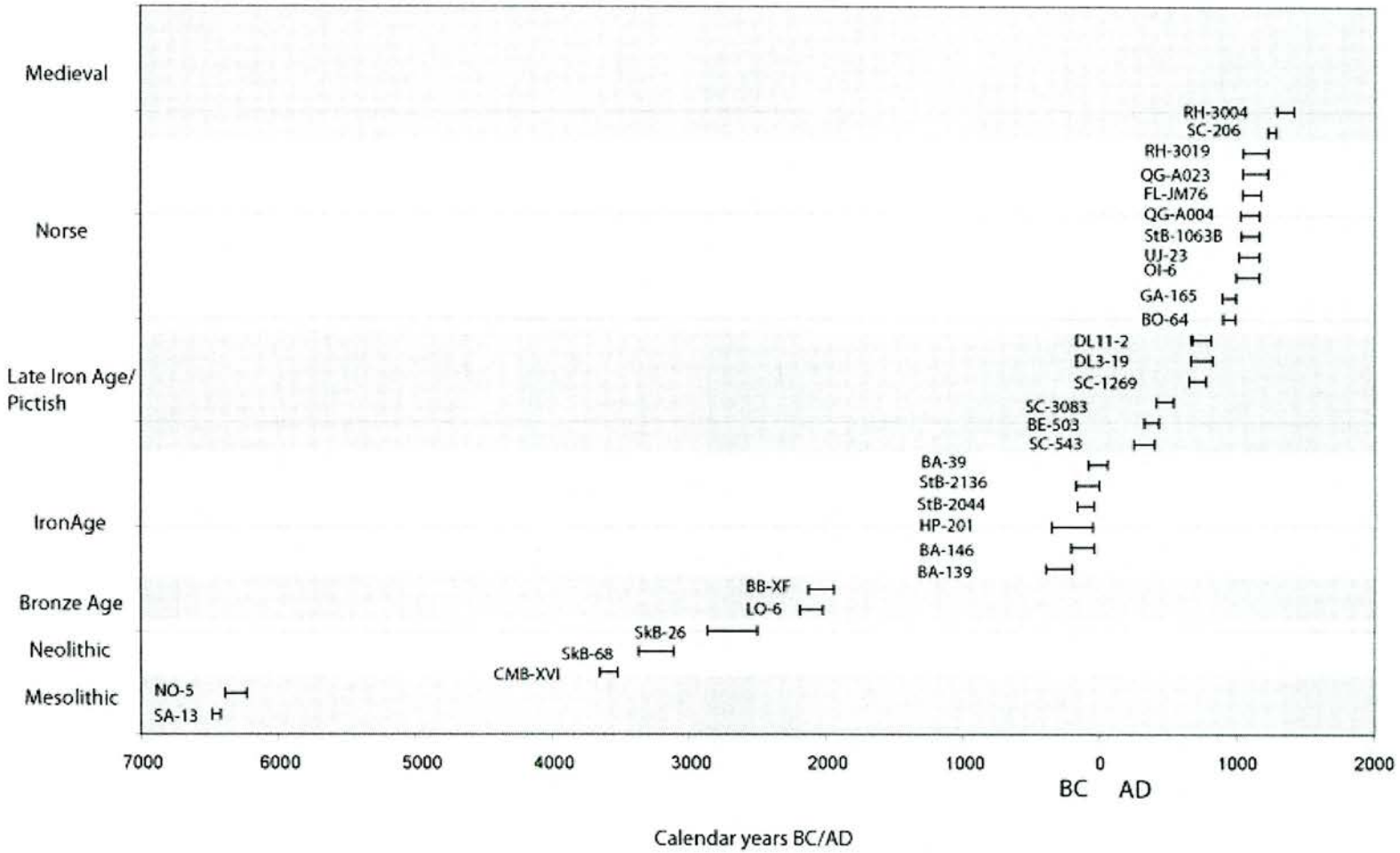

Figure 5.1: Calibrated age ranges of all contexts showing archaeological period.

5.2 ΔR values calculated from the contexts

The ΔR values shown in Table 5.12 below were calculated from the data according to the method described in section 4.2.3, Chapter 4. The values are ordered in the table primarily according to geographic area of the context and secondly in order of calibrated age range.

Context	Cal time period	ΔR
DL3-19	660-820 AD	-107 ± 18
DL11-2	660-810 AD	-69 ± 17
OI-6	990-1160 AD	-142 ± 16
SA-013	6480-6420 BC	46 ± 17
CMB-XIII	3650-3520 BC	148 ± 20
FL-JM76	1030-1170 AD	-84 ± 15
RH-3019	1040-1220 AD	-50 ± 18
RH-3004	1280-1400 AD	30 ± 21
NO-5	6390-6230 BC	78 ± 31
BA-139	400-200 BC	-75 ± 21
BA-146	210-40 BC	-71 ± 21
HP-201	350-50 BC	-116 ± 21
BA-39	90 BC-60 AD	-101 ± 16
BE-503	330-430 AD	-27 ± 10
BO-64	890-985 AD	-57 ± 14
GA-165	890-990 AD	-89 ± 17
SkB-68	3370-3110 BC	28 ± 23
SkB-26	2870-2500 BC	-27 ± 21
LO-6	2190-2020 BC	-96 ± 17
BB-XF	2130-1940 BC	-9 ± 18
StB-2044	170-40 BC	-50 ± 17
StB-2136	170 BC -0 AD	-60 ± 17
StB-1063B	1020-1160 AD	-96 ± 16
QG-A004	1020-1160 AD	-98 ± 17
QG-A023	1040-1220 AD	-42 ± 13

Table 5.12: ΔR values calculated for each context from the data in Tables 5.1-5.6 and Table 5.9 (continued below).

Context	Cal time period	ΔR
SC-543	250-400 AD	-290 ± 16
SC-3083	410-540 AD	50 ± 25
SC-1269	650-770 AD	-121 ± 16
SC-206	1215-1280 AD	35 ± 15
UJ-23	1010-1160 AD	64 ± 13

Table 5.12: (Continued): ΔR values calculated for each context from the data in Tables 5.1-5.6 and Table 5.9.

5.2.1 Are ΔR values calculated using different mollusc species comparable?

Full details of the measured ages for each of the five different mollusc species included in this assessment from **HP-201** are given in Table 5.13. There was no significant difference in age between the inner and outer portions of shell 201-02J, therefore, the two measurements were combined to give a weighted mean age. The $\delta^{13}C$ values were also combined. These are the values that are given in Table 5.13 below.

Lab Code ID	Sample ID	Species	Age BP ± 1σ	$\delta^{13}C$
SUERC-93	201-01A	*Hordeum sp*	2155 ± 40	-24.2
SUERC-94	201-01B	*Hordeum sp*	2120 ± 40	-22.6
SUERC-95	201-01C	*Hordeum sp*	2135 ± 40	-22.8
SUERC-96	201-01D	*Hordeum sp*	2110 ± 80	-24.5
SUERC-3208	201-02Q	*Patella vulgata*	2435 ± 45	0.3
SUERC-3209	201-02R	*Patella vulgata*	2485 ± 45	1.9
SUERC-4113	201-02S	*Patella vulgata*	2410 ± 35	1.4
SUERC-3211	201-02T	*Patella vulgata*	2335 ± 35	1.1
SUERC-3196	201-02I	*Mytilus edulis*	2440 ± 35	1.3
SUERC-3197	201-02J	*Mytilus edulis*	2453 ± 43	1.2
SUERC-3199	201-02K	*Mytilus edulis*	2395 ± 35	1.6
SUERC-3200	201-02L	*Mytilus edulis*	2475 ± 35	0.6
SUERC-3201	201-02M	*Littorina littorea*	2400 ± 35	2.2
SUERC-3202	201-02N	*Littorina littorea*	2390 ± 35	2.4
SUERC-4123	201-02O	*Littorina littorea*	2415 ± 35	1.6
SUERC-3207	201-02P	*Littorina littorea*	2585 ± 35	2.1
SUERC-3212	201-02U	*Ensis ensis*	2520 ± 35	-0.4
SUERC-3216	201-02V	*Ensis ensis*	2455 ± 35	-0.1
SUERC-3217	201-02W	*Ensis ensis*	2425 ± 35	0.5
SUERC-3219	201-02X	*Ensis ensis*	2370 ± 35	0.4
SUERC-3220	201-02Y	*Cestroderma edule*	2505 ± 35	2.4
SUERC-3221	201-02Z	*Cestroderma edule*	2440 ± 35	2.3
SUERC-3222	201-02A	*Cestroderma edule*	2420 ± 40	0.6

Table 5.13: ^{14}C and $\delta^{13}C$ results for samples measured for assessment of inter-species differences.

Species	**Mean ^{14}C age ± 1σ***	***T*-statistic for species group**
Hordeum sp.	2135 ± 22	0.49 ($\chi^2_{:0.05}$ = 7.81)
Patella vulgata	2405 ± 31	7.63 ($\chi^2_{:0.05}$ = 7.81)
Mytilus edulis	2441 ± 18	2.74 ($\chi^2_{:0.05}$ = 7.81)
Littorina littorea	2448 ± 46	20.84 ($\chi^2_{:0.05}$ = 7.81)
Ensis ensis	2443 ± 31	9.57 ($\chi^2_{:0.05}$ = 7.81)
Cestroderma edule	2458 ± 26	2.97 ($\chi^2_{:0.05}$ = 5.99)

* all age measurements included in calculations

Table 5.14: Mean age ± 1σ and *T* –values for the six species measured.

Within the groups of measurements of *Littorina littorea* and *Ensis ensis* there were significant differences in ^{14}C age, as shown by the larger standard deviations and the calculated values of *T* (Table 5.14). In both cases, the higher *T*-statistics were mainly derived from single measurements. In the group of four measurements of *Littorina littorea* shells, SUERC-3207 is significantly older than the other measurements and responsible for the high *T* value. Similarly, in the group of *Ensis ensis* measurements, SUERC-3212 is older than the remaining measurements of this species. These outlying ages may represent either material of an older age that was incorporated into the deposit during formation, or they may represent measurement variability. If SUERC-3207 and SUERC-3212 are excluded from the measurement groups, the values of *T* for these groups become $T = 0.26$ ($\chi^2_{:0.05} = 5.99$) and $T = 3.03$ ($\chi^2_{:0.05} = 5.99$), respectively, indicating that the other measurements were indistinguishable at 95% confidence.

5.3 Measurement of standards

Table 5.16 below shows the average values of known age samples measured during the course of this research. The average measurements are comparable to the international consensus values for the five standard materials.

Standard	Consensus value	Mean of measured values
SRM-4990C (OxII)	134.07 ± 0.19 pMC	134.1 ± 0.28 pMC
Belfast wood	4485 ± 5 BP	4494 ± 46 BP
Belfast wood (bulk gas)	4485 ± 5 BP	4503 ± 39 BP
Barley mash	116.35 ± 0.0084 pMC	116.50 ± 0.59 pMC
Icelandic Doublespar	46, 750 ± 208 BP 0.18 ± 0.006 pMC	0.23 ± 0.0006 pMC
Interglacial wood	No consensus value available	0.18 ± 0.07

Table 5.15: Comparison of international standard consensus values with the average measurement from all batches in this project (Gullikssen and Scott, 1994; Boaretto *et al.*, 2002; Scott, 2003).

5.4 $\delta^{13}C$ values of measured samples

The $\delta^{13}C$ values of all samples fell within the typical ranges for terrestrial plants, terrestrial mammal bone and marine mollusc shell (Aitken, 1990). The mammalian bone samples from three contexts (**SA-013**, **SkB-26**, and **BB-XF**) were typical of bone collagen from animals existing on terrestrial C3 plant material, showing that the animals had consumed a homogeneous diet that did not include any significant amount of marine carbon. Table 5.17 shows the variation in $\delta^{13}C$ values of samples from individual contexts, and the variation in the average $\delta^{13}C$ values between contexts. Variation in $\delta^{13}C$ values of terrestrial or marine samples within each context was relatively low, with the maximum variation shown in terrestrial plant material. The variation in average $\delta^{13}C$ values between contexts was higher than the within-context figure. Full details of all measured $\delta^{13}C$ values are contained in Tables 5.1-5.6.

Material	$\delta^{13}C$ values (‰) for terrestrial plants	$\delta^{13}C$ values (‰) for mammalian bone	$\delta^{13}C$ values (‰) for marine mollusc shell
Typical range (Aitken, 1990)	-25 ± 3	-20 ± 2	0 ± 3
Maximum value	-21.4	-21.6	2.3
Minimum value	-25.6	-22.2	0.1
Range	4.2	0.8	2.2
Max range within any context	2	0.3	0.8

Table 5.16: Summary of variability in measured $\delta^{13}C$ values both within samples from a context and between average values for all contexts.

Chapter 6: Interpretations

The following chapter discusses the implications of the results presented in Chapter 5 for understanding the North Atlantic MRE during the Holocene. The data were examined within both a spatial and temporal framework, and related to climate and oceanographic changes in palaeoenvironmental records that have been previously identified as potential mechanisms for producing variation in ΔR.

6.1 Influence of mollusc species on ΔR values

As discussed in Chapter 4 (section 4.2.4), it is possible that species-dependant variability in mollusc shell ^{14}C could limit the extent to which ΔR values calculated using different species are comparable (Forman and Polyak, 1997; Hogg *et al.,* 1998). This provided the rationale for an assessment of ΔR values using multiple samples of shells from five different species from a single context, **HP-201**. Measurements of shells from a single species that were statistically indistinguishable were combined to produce a weighted mean age (Table 6.1). When the weighted mean ages for the five mollusc species were compared, no significant differences were observed. The *T*-value of the five ages was $T = 4.15$ ($\chi^2_{:0.05} = 9.49$). Similarly, $T = 22.22$ ($\chi^2_{:0.05} = 26.3$) for the entire group of ages, excluding SUERC-3207 and SUERC-3212. The calculated values of ΔR for the different species are detailed in Table 6.1 and again, a χ^2 test indicates no significant difference in ΔR value between the mollusc species ($T = 3.87$ ($\chi^2_{:0.05} = 9.49$)).

Species	**Weighted mean ^{14}C age ± 1 std dev**	**ΔR**
Patella vulgata	2405 ± 31	-74 ± 20
Mytilus edulis	2440 ± 18	-47 ± 20
Littorina littorea	2402 ± 20	-85 ± 22
Ensis ensis	2417 ± 25	-71 ± 23
Cestroderma edule	2458 ± 26	-32 ± 23

Table 6.1: Weighted mean ages (excluding 2 outliers) and ΔR values for the five mollusc species from **HP-201**.

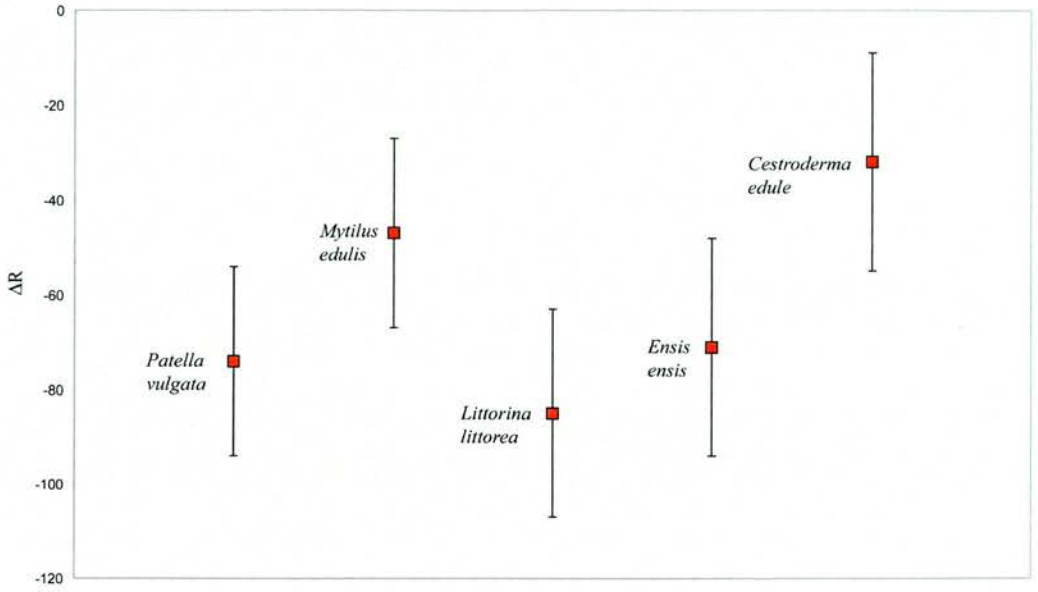

Figure 6.1: ΔR values from five mollusc species from **HP-201**.

Despite the differences in food sources and the ecological niches that the five mollusc species occupy, the variation in measured ^{14}C ages from a single, secure archaeological context does not exceed that which would be expected to result from measurement variability alone. The main conclusion that can be drawn from these results is that at **HP-201**, where there are no large-scale sources of carbon that may be selectively incorporated into specific mollusc species (*eg.* the presence of carboniferous rocks or a significant freshwater input), no observable species-dependant variations in ^{14}C age were observed. This indicates that differences in habitat and feeding behaviour between the species that were studied do not have a significant influence upon the ^{14}C activity of precipitated shell carbonate. The assessments of surface ΔR made with the various mollusc species used in this study are therefore comparable, and no correction for species-dependant variation is required.

The implications of these results may be extended to contexts from other sites that have been selected according to the same criteria as **HP-201**. This means that it is legitimate to compare ΔR values from contexts that have been calculated using measurement of different mollusc shell species that have been examined in the **HP-201** study. The majority of ΔR values in this thesis were calculated using measurements of *Patella vulgata*, however in five instances alternate shell species were used due to a lack of sufficient numbers of suitable *Patella vulgata* specimens.

Context	Mollusc shell species measured
BA-146	Cockle (*Cerastoderma edule*)
BA-39	Cockle (*Cerastoderma edule*)
SC-206	Periwinkle (*Littorina littorea*)
NO-5	Periwinkle (*Littorina littorea*)
BE-503	Mussel (*Mytilus edulis*)

Table 6.2: Contexts for which ΔR values were calculated using other mollusc species than *Patella vulgata*, showing species used.

6.2 Features of the Holocene MRE within the study area

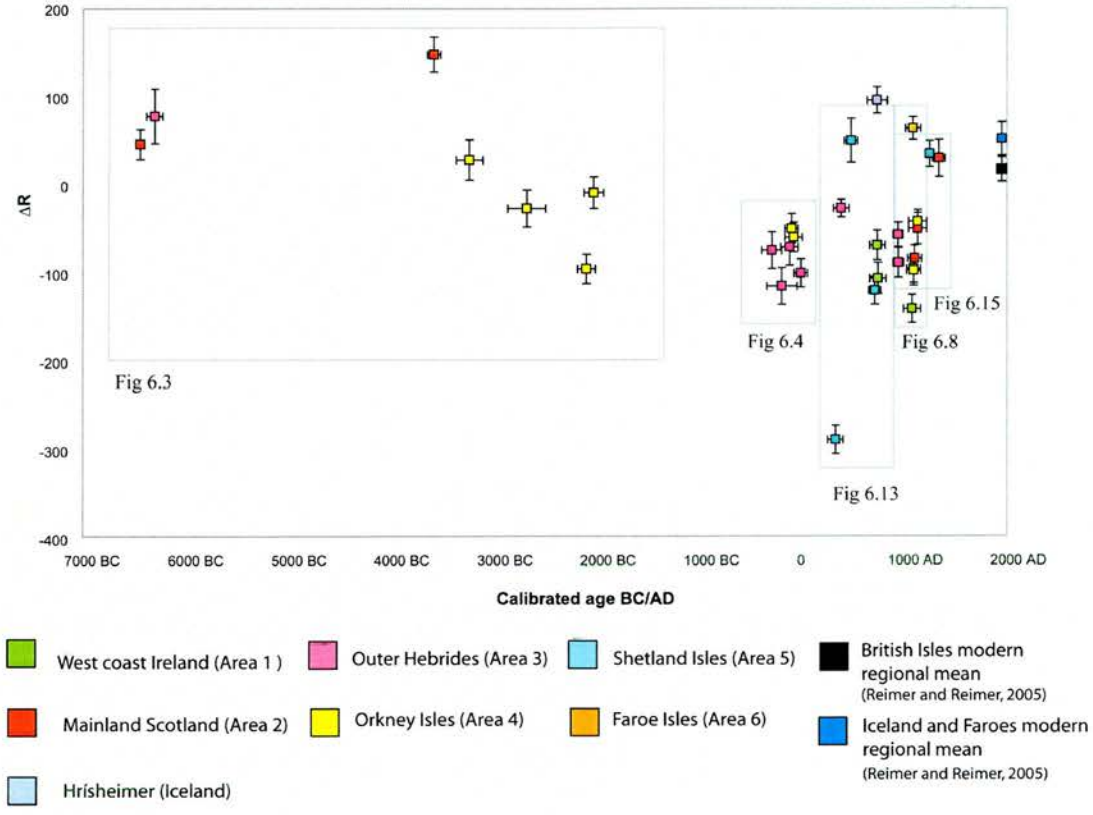

Figure 6.2: ΔR values for all contexts on a temporal scale showing the relevant geographic area for each context. Sections of the overall data are incorporated into figures in the following text, indicated by boxes.

As can be seen from Figure 6.2 above, the overall data suggest a non-zero ΔR has applied within the study area during the Holocene. Positive deviations extend to ΔR = 148 ± 20 ^{14}C yr, and negative deviations to ΔR = -290 ± 16 ^{14}C yr. This latter value may be an anomaly, as it outlies the remainder of the measurements by some way and is significantly different from the remainder of the dataset. The next most negative deviation is ΔR = -142 ± 16 ^{14}C yr, and these results suggest a variability of c.290 ^{14}C yr during the Holocene period within the study area that may have both spatial and temporal aspects. Because the data do not provide entirely continuous temporal and spatial coverage, this has an impact upon the level to which trends in the data can be observed. This means in certain instances that it is difficult to satisfactorily resolve uncertainties. However certain characteristics are apparent in this dataset and are considered in the following sections.

In subsequent sections, where ΔR values are plotted against site age, the midpoint of the calibrated 2σ range of the weighted mean terrestrial age is used. Associated error bars demonstrate the upper and lower limits of the range for each context data point.

6.2.1 The Early Holocene period

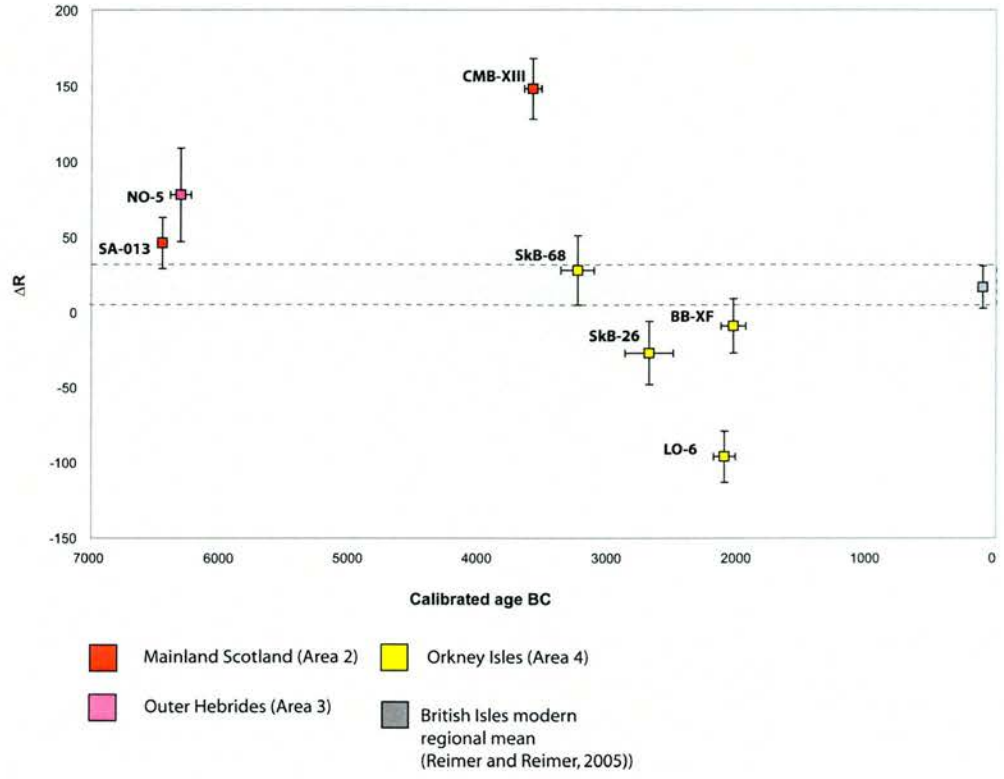

Figure 6.3: Graph showing ΔR values for earlier Holocene contexts (6480-1940 BC) showing geographic area of individual contexts.

The temporal coverage of the data is limited for earlier periods relative to that of the later Holocene. This is due to a limitation of the methodological approach, identified in Chapter 2 (section 2.6.4), ie. there is a lower density of archaeological deposits that meet the sample selection protocol from earlier periods. The period c.6480-1940 BC (c.4540 cal yr) is discontinuously covered by seven contexts (Figure 6.3) located in Areas 2, 3 and 4, for which the ΔR values are significantly different ($T = 100.38$ ($\chi^2_{:0..05} = 12.59$)).

When examined relative to the remainder of the data, ΔR values from the earliest contexts (**SA-13** (46 ± 17 ^{14}C yr), **NO-5** (78 ± 31 ^{14}C yr) and **CMB-XIII** (148 ± 20 ^{14}C yr)) are significantly greater than the majority of values for all later periods. In later periods the ΔR values are predominantly negative and when the correspondence between ΔR values from these early contexts and those from later periods is examined, there are few values that are statistically similar. **SA-13** and **NO-5** are similar only to **SkB-68** (28 ± 23 ^{14}C yr), **SC-3083** (50 ± 25 ^{14}C yr), **UJ-23** (64 ± 13 ^{14}C yr), **SC-206** (35 ± 15 ^{14}C yr), and **RH-3004** (30 ± 21

^{14}C yr), while the ΔR value from **CMB-XIII** is significantly greater than all other later determinations. The ΔR values for the two earliest contexts, **SA-13** and **NO-5** are similar (T = 0.82 ($\chi^2_{:0.05}$ = 3.84)), as are **NO-5** and **CMB-XIII** (T = 3.60 ($\chi^2_{:0.05}$ = 3.84)), while the **SA-13** ΔR value is significantly smaller than that from **CMB-XIII**. With the exception of **UJ-23**, these ΔR values from the early Holocene are the largest of any made within this study.

As well as the potential for temporal effects to influence ΔR, it is also important to consider the potential influence of spatial effects. There is an absence of contexts in close proximity to **SA-013** and **CMB-XIII** within this study that correspond to later time periods. However **NO-5** is located in an exposed location in Area 3 (see Figure 3.5, Chapter 3), and can be compared to several contexts within this area (Outer Hebrides) for later periods. Within Area 3 ΔR values are available for sites covering a maximum range of 6390 BC – 990 AD at 2σ. Determinations are available from eight contexts at six sites from Uist, Harris and Lewis. The value from **NO-5** is substantially older (by a min of c.5830 cal. yr) than the next youngest context, **BA-139**, and the ΔR at **NO-5** is significantly greater than all later determinations within Area 3. These were made at sites within a radius of c.80 km from **NO-5**, a distance that also includes **SA** on the mainland to the east. The closest sites to **NO-5** were **BA** and **HP** on the Uist Isles, located c.35 km southwest of **NO-5**. Three ΔR values from **BA** and one from **HP** are similar to one another, (T = 3.28 ($\chi^2_{:0.05}$ = 7.81)), with a weighted mean for four determinations of -92 ± 10, significantly smaller than the value from **NO-5**. This suggests that the smaller values in Area 3 and on the west coast of Area 2 for the earlier Holocene are not the result of spatial variation.

CMB-XIII is separated by a time span of 540-150 cal. yr from the next oldest context, **SkB-68,** which is located in Area 4 (Orkney Isles). The ΔR value from **SkB-68** (28 ± 23 ^{14}C yr) is significantly lower than that of **CMB-XIII** (148 ± 20 ^{14}C yr) (T = 15.5 ($\chi^2_{:0.05}$ = 3.84)), but is similar to the values from **SA-13** (46 ± 17 ^{14}C yr) and **NO-5** (78 ± 31 ^{14}C yr) (T = 1.68 ($\chi^2_{:0.05}$ = 5.99)). Although nine contexts are located within Area 4, the ΔR value from **SkB-68** is only similar to two other early values, from **SkB-26** (-27 ± 21 ^{14}C yr) (T = 3.12 ($\chi^2_{:0.05}$ = 3.84)), and **BB-XF** (-9 ± 18 ^{14}C yr) (T = 1.60 ($\chi^2_{:0.05}$ = 3.84)). The contexts **SkB-68** (3370-3110 BC) and **SkB-26** (2870-2500 BC) are separated by between 870-240 cal. yr, and the two ΔR values differ by c.55 ^{14}C yr. As the two values cannot be distinguished statistically it is not possible to identify a temporal trend in the data at this site, however there is a difference in the correspondence between each of the ΔR values from **SkB-68** and **SkB-26** with values from later contexts both within Area 4 and from other areas. The ΔR value from **SkB-68** is similar to a smaller number of later contexts (5) than **SkB-26** (11). The values

from **SkB-26** (2870-2500 BC) and **BB-XF** (2130-1940 BC) are both statistically lower than values from **SA-13**, **NO-5**, and **CMB-XIII**, giving possible support to a trend of falling values from the early Holocene onwards. The *T*-statistic for the nine determinations for the Orkney Isles area is 41.29 ($\chi^2_{:0.05}$ = 15.50). The highest contribution to this value is that of **SkB-68**, the earliest determination.

Both ΔR values from **SkB-68** and **SkB-26** are similar to that from **BB-XF** (-9 ± 18 ^{14}C yr), (*T* =3.21 ($\chi^2_{:0.05}$ = 5.99)). **BB-XF** is later than **SkB-26** by between 850-310 cal. yr. Another site within Area 4 (**LO-6**) covers a very similar time period to **BB-XF**, where the calibrated age ranges of the contexts are indistinguishable and cover a range of 2130-2020 BC. Here there are significant differences in the ΔR values between the two contexts (ie. **BB-XF** and **LO-6**) (*T* =12.35 ($\chi^2_{:0.05}$ = 3.84)), with a difference of c.87 ^{14}C yr in the two values. It is difficult to interpret the differences between ΔR at **LO-6** and **BB-XF**, and this highlights the lack of spatial and temporal data coverage at this point in time. It is possible that such differences in values can be observed across a relatively small area at a single point in time. The sites are located <50 km apart, and it is also possible that the data from the two sites relates to different points within the calibrated age range of c.110 cal. yr. In this instance it could be that both ΔR values were experienced at **LO-6** and **BB-XF** where one is the ΔR that applied during the earlier part of the age range, and one to the later. It may be that this was a period of rapid fluctuations in surface water ^{14}C at the sites that has resulted in the apparent differences in ΔR values from the two contexts. Therefore, the difference in ΔR values may be either a reflection of differences in the ^{14}C content of the surface water at the two sites, or may be a product of the resolution to which the methodology can determine ΔR in this instance. In the former case this could result from local circulation differences or variation in the input of terrestrial water components to surface water around the site. During the course of this thesis a preliminary study was undertaken to provide further information on potential differences in water characteristics across the study region. This was achieved by examining δ^{18}O of modern coastal water and shell samples, and the study is described in Appendix A. On the basis of these data, the δ^{18}O of both water and mollusc shell appears significantly higher at **LO** in a modern setting that that found at **BB**. Higher values of δ^{18}O can relate to lower temperatures or to higher salinity in the water, and the results may be indicative of a difference in water characteristics at the two sites due to unaccounted factors.

6.2.2 The implications of a higher ΔR value for the early Holocene

The suggestion of an overall decrease in ΔR from the early Holocene is apparent within the data from this study. However, due to the lack of continuous temporal and spatial coverage these data are indicative rather than definitive. Although it is not possible on this basis to state a definitive correction for the early Holocene, the weighted mean ΔR value from contexts analysed for this time period shows ΔR = 53 ± 15 ^{14}C yr (**SA-013** and **NO-5**) for the west coast of Scotland and the Outer Hebrides c.6480-6230 BC. This may increase to a weighted mean of 127 ± 32 ^{14}C yr for some or all of the period 6360-3530 BC (**NO-5** and **CMB-XIII**), subsequently reducing to near 0 ^{14}C yr for 3370-2570 BC on the Orkney Isles. A potential decrease in ΔR from the Early Holocene around the British Isles was also proposed by Reimer *et al.* (2002), but again this interpretation was limited by data availability. As discussed in Chapter 2 (section 2.8.2), available data from the pre-Holocene period suggests that the MRE was substantially raised relative to present, and that this effect continued into the Early Holocene with MRE values of 690 ^{14}C yr off the west coast of Norway, and 730 ^{14}C yr off the North Icelandic coast at c.9000 ^{14}C yr BP (c.8300-7970 BC) (Haflidason *et. al.*, 2000).

An elevated ΔR in the study area in the early Holocene could be derived from a number of palaeoclimatic forcing mechanisms documented in proxy records for this period. The most important of these within the Holocene appears to be the "8.2 kyr event" at c. 7650-7200 ^{14}C yr BP (8200-8000 cal. yr BP) (c.6500-6100 BC). This period encompasses **SA-013** and **NO-5**. Palaeoclimatic evidence (Alley *et al.*, 1997) and modelling studies (Renssen *et al.*, 2001; 2002) suggest that the 8.2 kyr event was stimulated by a freshwater pulse into the North Atlantic from the waning Laurentide ice sheet. This freshwater pulse may have lowered the surface water density in the Nordic Seas below a critical threshold and resulted in perturbation of deepwater formation and northward heat transport. The climatic cooling which is a signature of the 8.2 kyr event may also have been associated with an increase in sea ice extent in northern latitudes. The combination of a decrease in influence of the North Atlantic current surface waters and increase in sea ice cover on a centennial scale (the event is estimated as being of c.500 cal. yr duration (Rohling and Pälike, 2005)) provides a potential mechanism for relative depletion of surface ocean ^{14}C, and consequent raising of the MRE during and subsequent to this period.

As discussed previously, careful critical assessment is required when suggesting causal links between evidence of palaeoclimatic changes and evidence of MRE variations when the two

appear to coincide. At present there is a lack of quantitative data concerning the impact of specific palaeoclimatic changes upon MRE values, and also of continuous time-series of reliable calculations of pre-modern MRE characteristics. In addition it is important to consider the implication that many of the palaeoclimatic variations that can provide potential forcing mechanisms for MRE change are themselves placed on an absolute timescale using ^{14}C measurements of marine material (e.g. from marine cores). The accuracy of the palaeoclimate chronology constructed from these measurements depends upon several factors, including the accuracy of the correction for the MRE. The implication is that an inaccurate MRE correction may lead to inaccuracies in correlation of palaeoclimate events and interpretations involving forcing mechanisms and their effects. The timing of events that is inferred from palaeoclimatic proxy data for the early Holocene is often relatively rapid. For example during the climate transition from the Younger Dryas to the Holocene, factors such as wind speeds, precipitation, temperatures, and sea ice appear to have changed throughout the Northern Hemisphere on sub decadal time scales (Taylor *et al.*, 1997). Although a calendrical chronology can be confidently ascribed with c.1% precision from ice core data for this period (Alley, 2000), identification of coinciding rapid changes in marine cores highlights the need for both accurate and precise ^{14}C measurements of marine material to support interpretations.

The evidence for climatic and oceanic changes in the early Holocene is an area of intense interest for palaeoclimatic research as these are key to an understanding of how the climate system operates in the North Atlantic. This is particularly relevant given the current focus upon the impact of climate changes and links to possible variations in the thermohaline circulation system. An important difficulty for palaeoclimate investigation in the early Holocene therefore remains the most accurate and precise correction that should be applied to marine samples. As yet there is no definitive correction or universally accepted standardised approach to the problem, and a critical review is required. There is a growing body of evidence, which data from this study may support, that the ocean-atmosphere offset in ^{14}C age was greater for the early Holocene than present. However, the data remain indicative rather than definitive. A major question that remains unaddressed is to what level of precision it is in practice possible to determine the MRE for the early Holocene and previous periods. This is mainly due to the lack of sample types that would provide the desired level of accuracy and precision. The use of unsuitable data in an attempt to define the MRE for this important palaeoclimatic period would be counter-productive and merely serve to increase uncertainty. The question therefore remains over the most practical approach to take to integrating palaeoclimatic evidence dated using marine material within a wider

framework including terrestrial and ice-core records. It is conceivable that some of the interpretations and correlations that have been made on the basis of ^{14}C measurements of marine material for the early Holocene and previous periods may contain additional chronological uncertainties that have not yet been accounted for.

6.2.3 The North Atlantic MRE c.400 BC – 60 AD (during the Iron Age)

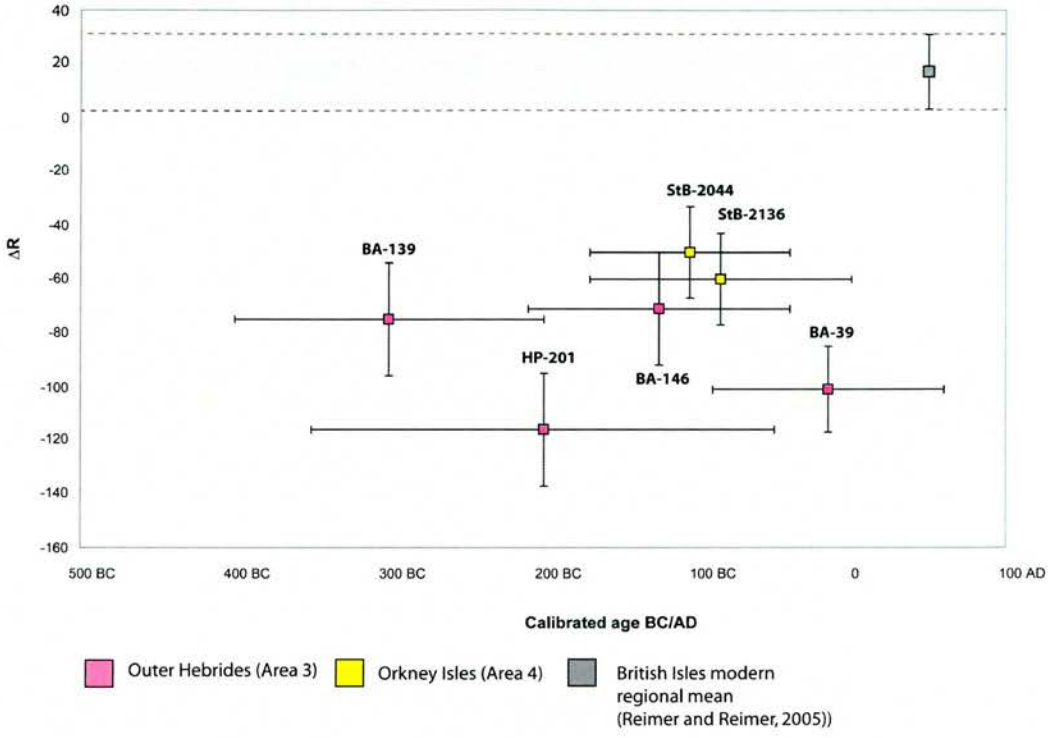

Figure 6.4: ΔR values for six contexts for the calibrated age period 400 BC – 60 AD showing geographic location of individual contexts.

Following the early Holocene, a period of 1930-1540 cal yr separates **BB-XF** from the next youngest context, **BA-139**. This context represents part of a group of six ΔR values from three sites at c.400 BC – 60 AD (c.460 cal. yr), two of which are located in Area 3 and one in Area 4 (Figure 6.4). Data from contexts at the sites shows that ΔR values throughout this time appear to represent a consistent, reduced offset between atmospheric and surface ocean ^{14}C relative to the present day value of ΔR= c.0 ^{14}C yr. In Area 3, **BA-139** is older than **BA-146** and **BA-39**, while the 2σ calibrated age ranges from **BA-146** and **BA-39** overlap. The age ranges from all three sites overlap with that of **HP-201**. The ΔR values from all four contexts in Area 3 are statistically similar to each other ($T = 3.28$ ($\chi^2_{:0.05} = 7.81$)), and also to ΔR values from two contexts (**StB-2136** and **StB-2004**) in Area 4 for an equivalent time

period (170 BC – 0 AD). The ΔR values from **StB-2136** and **StB-2004** are similar to each other (T = 0.17 ($\chi^2_{:0.05}$ = 3.84)), and the T-statistic for these values and the four determinations from Area 3 is T = 9.31 ($\chi^2_{:0.05}$ = 11.1)). The range of ΔR values from the six contexts is from –116 ± 21 ^{14}C yr to –50 ± 17 ^{14}C yr, with a weighted mean value for the whole group of –79 ± 10 ^{14}C yr. This compares to commonly used values of ΔR = c.0 ^{14}C yr for UK waters, e.g.: 17 ± 14 ^{14}C yr (Reimer and Reimer 2005), and a MRE for the region of 405 ^{14}C years BP (Harkness, 1983). The results from these sites therefore indicate a suppression of the MRE and consequently an elevation of the ^{14}C content in surface ocean waters around the sample sites between c.400 BC – 60 AD, an age range that corresponds to the archaeological period known as the Iron Age.

6.2.4 Implications of a revised ΔR value for the Iron Age.

The Scottish Iron Age period, conventionally defined as lasting from c.800 BC to c.800 AD (Table 3.2; Armit and Ralston, 2003), was one when environmental changes coincided with extensive cultural changes, including architectural developments. The ΔR values from six contexts suggest that during this time the ocean environment with respect to ^{14}C was comparable on the Outer Hebridean and Orkney west coasts. The increased ^{14}C content of surface ocean waters that is implied by the data could be the product of a variety of possible mechanisms. The period 400 BC – 60 AD corresponds to c.2000 cal. BP. The millennial-scale events identified by Bond *et al.*, (1997) in Holocene ocean sediments show apparent peaks in ice-rafted debris (IRD) at 1400 and 2800 years ago, whereas c.2000 BP corresponds to an IRD minimum in cores across the North Atlantic (core ^{14}C ages corrected for 400-500 yr MRE). Times of lower IRD concentrations were interpreted in this study as corresponding to warmer sea surface temperatures and similar circulation to present, while IRD peaks correspond to southward or southwestward advection of surface waters from the Greenland-Iceland seas. Warmer climatic conditions linked to ocean circulation at c.2000 BP are also identified by Bianchi and McCave (1999), (see Figure 6.4) when a faster rate of Iceland-Scotland Overflow Water at depth is correlated with warming of the northern European climate (during the "Roman Warm Period").

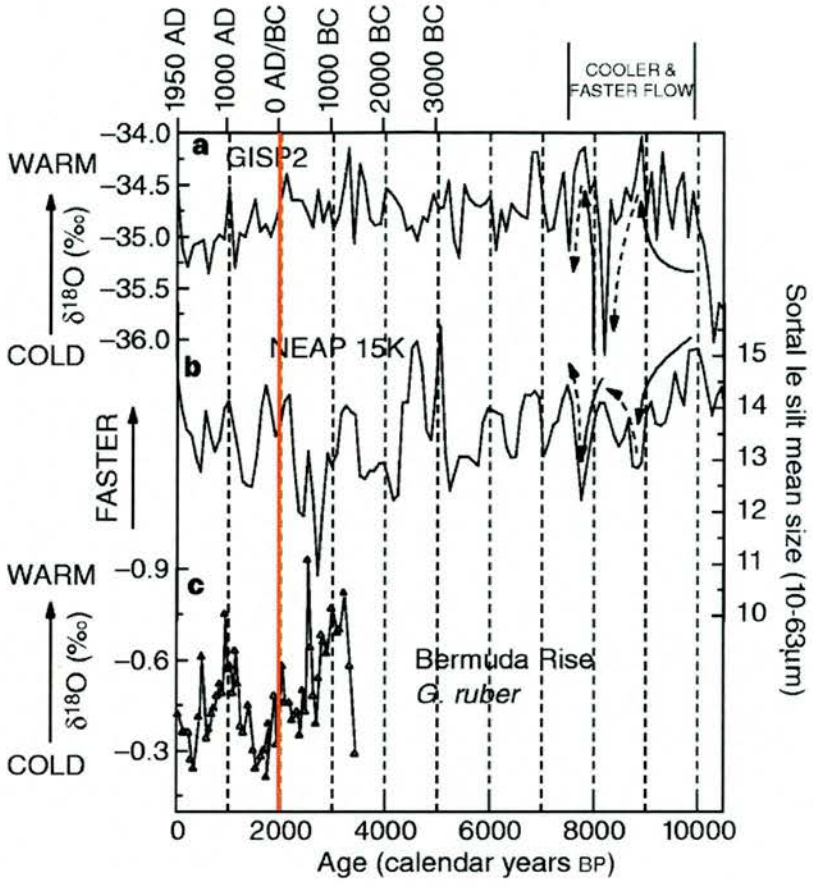

Figure 6.5: Variability in GISP2 $\delta^{18}O$ record and speed of Iceland-Scotland Overflow Water through the Holocene (Bianchi and McCave, 1999), showing the time period c.0 AD/BC within the Scottish Iron Age.

Identification of ΔR values that differ from present regional mean values has important implications for archaeological interpretations. This is well illustrated by examining the example of a revised ΔR for the Scottish Iron Age. Here, the environmental changes during the Iron Age coincided with extensive cultural changes, including architectural developments; meaning chronological accuracy has a critical effect upon archaeological interpretations for this time. In particular, the timing of rapid transitions between several distinct building styles in different regions is currently far from clear, as is the extent to which a cultural change in settlement practice was a response to environmental variations. Two of the architectural styles in question are "brochs" and "wheelhouses". The term 'broch' is traditionally used to define a group of prehistoric drystone-built roundhouses with a range of characteristic internal features including hollow walls, intramural stairs and galleries (Armit 2003). Some of them are tower-like and, for example, Mousa in Shetland is over 13m high, but most are now ruinous and the tower-like structures may always have

been exceptional (Fojut 1981). Wheelhouses, in contrast, are architecturally much less impressive. While they often enclose spaces that are as large as those found within brochs they are often dug into the landscape, especially into sandy deposits and were visually unimpressive. Both site types had complex internal subdivision, usually radially arranged, and this became the dominant feature of the wheelhouse where radial dividing walls suggest the spokes of a wheel, giving rise to the site-type designation. The traditional interpretation is that the construction of wheelhouses post-dates that of the brochs, however, an accurate chronology of these architectural forms across the region is needed to determine whether the developments were part of an ordered sequence progression or a more complex regional pattern of co-existence.

Archaeological interpretations such as the relationship between brochs and wheelhouses are often dependant upon the chronology of apparently successive events and processes. The dominance of ^{14}C measurements in construction of absolute chronologies upon which such interpretations are based leads to the requirement of accurate and precise MRE corrections where marine sample material is measured. A series of wheelhouses at **HP** were placed upon an absolute (^{14}C) chronology using 10 bulk radiometric ^{14}C measurements of marine shells (Barber, 2003). Human occupation at **HP** is estimated to span no more than 330 ^{14}C yrs. The activity consists of a complicated and intensive series of building phases where later structures often involved the use of material from earlier buildings and several wheelhouses were constructed, occupied, and abandoned over a short period. The ^{14}C measurements from **HP** were calibrated with the atmospheric INTCAL98 curve on the basis of a site-specific assessment of the MRE instigated by the site excavators. Here, the MRE was assessed using a comparison of the ^{14}C age BP of six radiometric measurements on terrestrial material (either carbonised plant material or large animal bones) with equivalent marine shell samples. The sample pairs were obtained from both Hornish Point (2 samples) and the nearby site of Baleshare (4 samples). Due to the large volume of material required for each age measurement, it was only possible to obtain marine and terrestrial material from the same deposit in one instance, and other comparisons were made using samples from deposits that were in close proximity. In two instances, the terrestrial sample was composed of material from several immediately adjacent deposits, again due to the sample masses required. In these cases, the equivalent shell age was calculated by interpolating between two measurements made on marine shells from deposits directly above and below the bulk of the terrestrial sample, assuming a known sedimentation rate for all deposits.

Using this methodology, the calculated differences between the marine and terrestrial ^{14}C ages of the six sample pairs ranged from +121 years to –405 years, a total range of 526 ^{14}C

yr at a single site. Using the Students t-test, the differences, taken as a group, were not found to be significantly different from zero at 95% confidence. On the basis of these results, the authors elected to calibrate all ^{14}C measurements in the report using the standard atmospheric INTCAL98 curve. In contrast, the values of ΔR calculated within this study for **HP** and **BA** are highly consistent, with a range of c.45 ^{14}C yr where the four values are statistically similar ($T = 3.28$ ($\chi^2_{:0.05} = 7.81$)).

The approach to MRE correction used by the site excavators means that the ranges of calibrated ages from the Hornish Point wheelhouse phases appear substantially older than those obtained using the marine calibration curve and a ΔR of -79 ± 10 ^{14}C yr (Figure 6.6). These older age ranges for **HP** could imply that the wheelhouses were being constructed and used at the same time as some of the earliest brochs in Scotland.

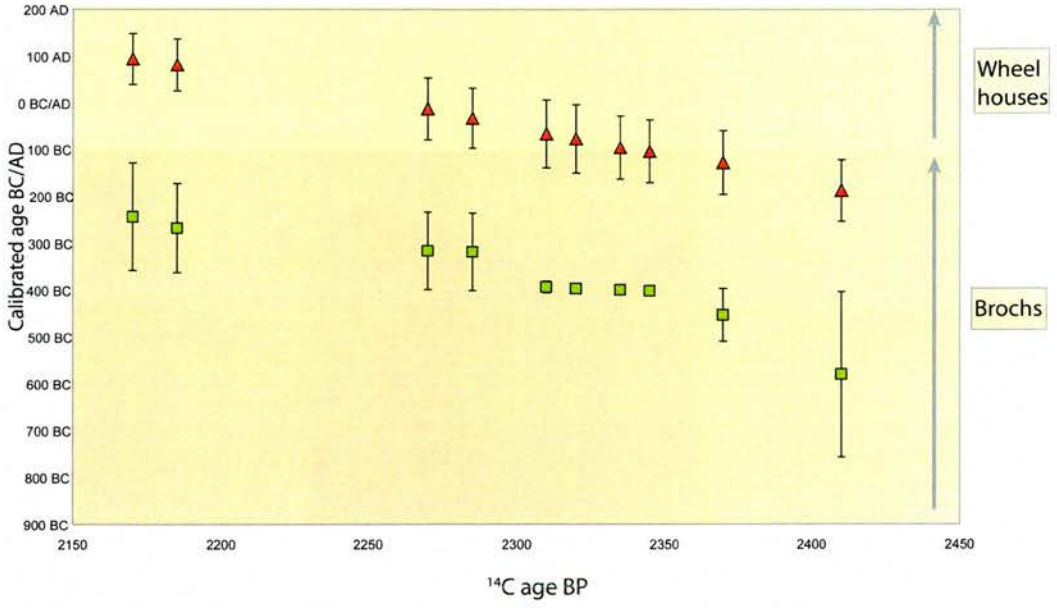

Figure 6.6: Comparison of calibrated age ranges obtained using 10 ^{14}C measurements of marine shells from wheelhouse phases at **HP** with the INTCAL98 atmospheric calibration curve (squares; data from Barber, 2003) and with the MARINE 98 calibration curve and a ΔR of -79 ± 10 ^{14}C yr (triangles). The traditional approximate phases of the broch and wheelhouse architectural phases are indicated by shading.

The previously derived ^{14}C measurements from **HP** were calibrated using the marine INTCAL98 curve, firstly with a ΔR of 0 ^{14}C yr, and then with ΔR of -79 ± 10 ^{14}C yr. The shift in calibrated age ranges of the measurements when the revised ΔR is applied is shown in Figure 6.7. Because the majority of ^{14}C determinations at the site were made on marine

mollusc shells, the assessment of the relative duration and age of phases on this individual site should not change radically through application of a revised ΔR value. However, the position of various activity phases at Hornish Point on an absolute timescale, relative to that of many other sites (including broch and wheelhouse structures), is significantly altered.

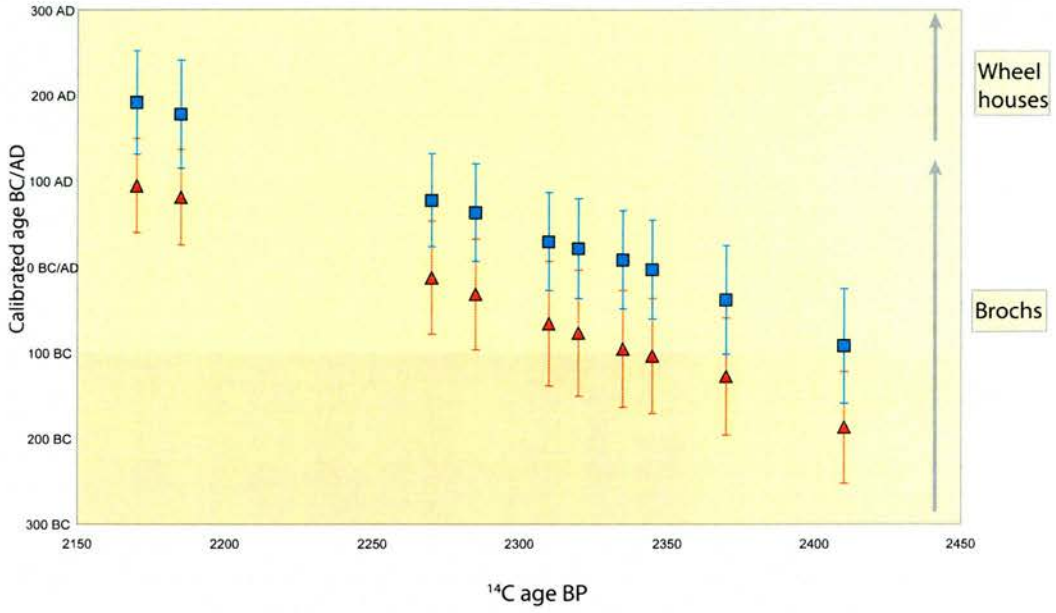

Figure 6.7: Comparison of calibrated age ranges obtained using 10 ^{14}C measurements of marine shells from wheelhouse phases at **HP** with the MARINE98 calibration curve and ΔR = –79 ± 10 ^{14}C yr (triangles) and calibrated with ΔR = 0 ^{14}C yr (squares). The traditional approximate phases of the broch and wheelhouse architectural phases are indicated by shading.

The revised data, re-calibrated with the marine curve and a ΔR of -79 ± 10 ^{14}C yr, indicates that the Hornish Point wheelhouses were constructed during a later period than that indicated by previous assessment. This highlights the importance of a critical assessment of the MRE when using measurements of marine material. The revised ΔR has important implications for our understanding of the nature of the relationship between both monument types when the ages are calibrated using the marine curve. The chronology of the wheelhouses at Hornish Point, based on a ΔR of 0 ^{14}C yr, places these sites in a chronological span ranging from about 158 BC to AD 252 – at the extremes of the calibrated ranges. However, using the revised ΔR of -79 ± 10 ^{14}C yr, this range is revised to 252 BC to 149 AD. Traditionally, wheelhouses were viewed as humble successors that evolved from brochs at a time when the latter were effectively extinct, albeit that some brochs, especially those in the south of

Scotland, persisted in use and construction into the first century AD. The Hornish Point dates imply that there is a significant overlap in construction dates of brochs and wheelhouses. This implies sophistication in the social landscape with impressive structures of several types being built, perhaps for individuals of differing social status or for other functions.

6.2.5 Spatial variation at c.1000 AD

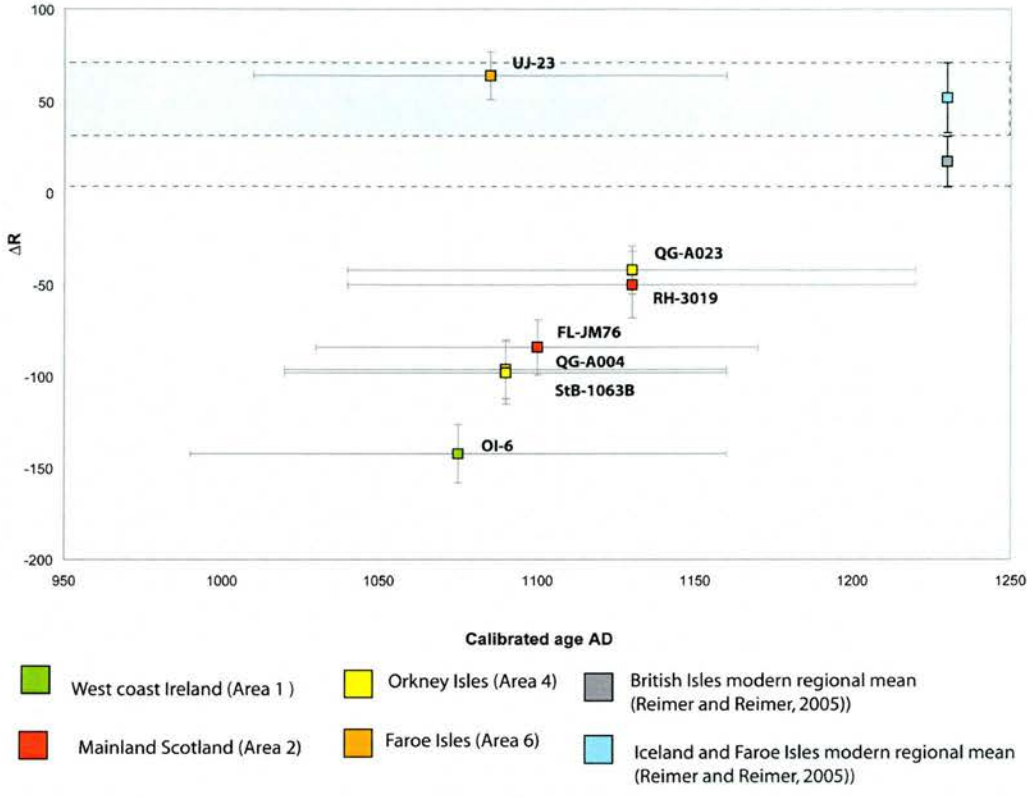

Figure 6.8: ΔR values for contexts with highly similar calibrated age ranges c.1000-1200 AD, showing relevant geographic location of contexts.

A total of seven contexts are available for the period c.1000 AD to c.1200 AD that covers a wide latitudinal range in Areas 1, 2, 4, and 6. The ΔR values for these contexts are significantly different ($T = 30.3$ ($\chi^2_{0.05} = 12.60$)), indicating that a single MRE offset did not apply across the study area during this period. The highest and lowest ΔR values from this group are located in the most northerly and southerly areas respectively (see Table 6.3 and Figure 6.8).

Context	Area	2σ cal. age range	ΔR
OI-6	Area 1	990-1160 AD	-142 ± 16
UJ-23	Area 6	1010-1160 AD	64 ± 13
StB-1063B	Area 4	1020-1160 AD	-96 ± 16
QG-A004	Area 4	1020-1160 AD	-98 ± 17
FL-JM76	Area 2	1030-1170 AD	-84 ± 15
QG-A023	Area 4	1040-1220 AD	-42 ± 13
RH-3019	Area 2	1040-1220 AD	-50 ± 18

Table 6.3: Contexts with calibrated age ranges c.1000 AD showing location within the study area and ΔR values.

Within Area 2, the ΔR values for **FL-JM76** and **RH-3019** are statistically similar (T = 2.11($\chi^2_{:0.05}$ = 3.84)), being separated by c.34 ^{14}C yr with a weighted mean of ΔR = -70 ± 17 ^{14}C yr. In Area 4, the ΔR values from **StB-1063B** and **QG-A004** are similar to those from Area 2 (T = 4.80 ($\chi^2_{:0.05}$ = 7.81)), however the ΔR from **QG-A023** is significantly higher than **StB-1063B** and **QG-A004**. (T = 9.92 3 ($\chi^2_{:0.05}$ = 5.99)), and is separated from **QG-A004** by c.56 ^{14}C yr. This variability could be the result of several factors. It is possible that although the calibrated age ranges are similar, the two contexts represent different points over this 200 cal. yr interval, during which the ΔR values at the site were significantly different. Alternatively, it is possible that the variability in ΔR values at **QG** is the result of additional uncertainties that have not been identified and are related to this context or site. In this instance it would not be possible to identify ΔR more precisely at this site from these two contexts. Due to the similarity of **QG-A004** to other values from Area 4 for this time period and the consistency with other measurements from Area 2, **QG-A023** is identified as an outlying value from this dataset.

Excluding **QG-A023** gives a weighted mean ΔR for Areas 2 and 4 of -83 ± 10 for the period c.1000-1200 AD, and the similarity of the measurements indicates that surface water ^{14}C at sites in Areas 2 and 4 was comparable at this time. In contrast, these consistent determinations from Areas 2 and 4 cannot be combined with those from Area 1 (T = 15.45 ($\chi^2_{:0.05}$ = 9.49)) or Area 6 (T = 96.76 ($\chi^2_{:0.05}$ = 9.49)) for this period.

6.2.6 Possible mechanisms and implications of spatial ΔR variation c.1000 AD

As discussed in Chapter 2 (section 2.7.2), presently available assessments of the MRE for the UK demonstrate a regional MRE of 405 ^{14}C yrs and a pre-industrial ΔR value of 17 ± 14 ^{14}C yrs (Reimer and Reimer, 2005). Available results from the Faroe Isles are limited to an MRE value of 370 ± 99 ^{14}C yrs and ΔR of 19 ± 99 ^{14}C yrs, based upon measurement of known age mussel shells (*Mytilus edulis*) from Sörvåg (Krog and Tauber, 1974). This is included in the calculation of a regional mean ΔR value for the Faroes and Iceland for modern pre-bomb samples of 52 ± 19 ^{14}C yrs (Reimer and Reimer, 2005). This data corresponds with the present general northward increase in MRE (and therefore in ΔR), interpreted as due to the relative distribution of Atlantic and Arctic surface water masses in the North Atlantic. The resulting spatial MRE variation is seen in gradients of apparent surface-water ages across frontal systems such as the Polar Front that reflect climatic and oceanographic gradients (Eiríksson *et al.*, 2004). The relative position of the Polar Front (presently located north of Iceland) is strongly correlated with records of climatic and oceanographic changes (Ruddiman and McIntyre, 1981; Dansgaard *et. al.*, 1993; Haflidason *et. al.*, 1995), and such changes within the study area during the Holocene include significant shifts in the location and intensity of surface and deep-water currents. For example, during colder phases, features such as increased sea-ice cover may surround areas including the Faroes as a body of cold polar waters, (from north of the Iceland-Faroes Front) extends southwards from the East Iceland Current towards the Faroes (Moros *et al.*, 1997; Humlum, 1998; Kuijpers *et al.*, 1998; 2002). Variability in the relative influence of Atlantic and Arctic waters around Iceland has also been identified over short timescales (Knudsen *et al.*, 2004). Also identified is a relationship between variability in the influence of Arctic and Atlantic water masses and MRE values on the North Iceland shelf over the past c.4000 years (Knudsen and Eiríksson, 2000b; Larsen *et al.*, 2002; Eiríksson *et al.*, 2004). Here, higher MRE values are associated with periods of increased influence of Arctic waters (Larsen *et al.*, 2002), whereas the period between c. 750 and c. 1150 cal AD is characterised by dominance of Atlantic waters and a lower offset between atmospheric and ocean surface apparent ages.

Differences in the oceanography of areas 1, 2, 4, and 6 (described in Chapter 3 (section 3.2.2), provide a potential mechanism for spatial variations in MRE. The strong influence of North Atlantic Current (NAC) waters is linked to lower values of MRE, and around the western coast of the British Isles, a branch of the NAC flows northwards. A mainly Atlantic water origin is indicated by ocean salinities off the west coast of Ireland (Area 1), within which **OI-6** is located (OSPAR, 2000). The sites **FL** and **RH** within Area 2 are located in the

eastern area of the northern Scottish mainland coast (see Figure 6.9). The surface water in both Area 2 and Area 4 is derived from the northward flow of the Scottish Coastal Current (SCC) clockwise into the North Sea. The SCC is derived as the NAC forms coastal water that flows up the west coast of Scotland, reinforced by lower-salinity water from the major west coast Firths (McKay *et al.*, 1996). It is possible that the apparent similarity in ΔR values at c.1000 AD at sites in areas 2 and 4 is due to the common dominance of surface waters in these locations by a strong SCC that is not significantly modified by local effects.

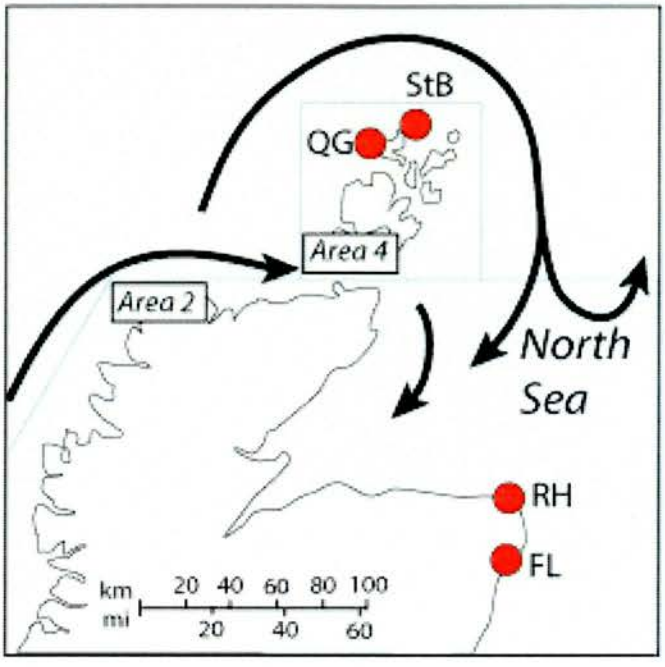

Figure 6.9: Location of sites in Areas 2 and 4 from which contexts are available for the period c.1000 AD, showing major modern surface circulation patterns.

To the north, the Faroe Isles are influenced by a further branch of the NAC, forming the Faroes current, and surface waters consist of modified North Atlantic water as terrestrial freshwater input mixes with NAC water input (Hansen and Østerhus, 2000). The Faroes are situated in proximity to the Iceland-Faroe Front, presently located to the north of the Isles (see Figure 6.10). This front represents the boundary between Arctic-influenced waters of the East Icelandic Current and Atlantic waters derived from the North Atlantic Current. Hydrographic observations over the past 100 years show the Iceland-Faroe Front is north of the Faroes, though cold intrusions from the frontal region may occasionally reach the shelf region (Hansen and Meincke, 1979). Over longer timescales however, it is possible that the

position of frontal systems such as the IFF have varied in response to palaeoclimatic forcing mechanisms.

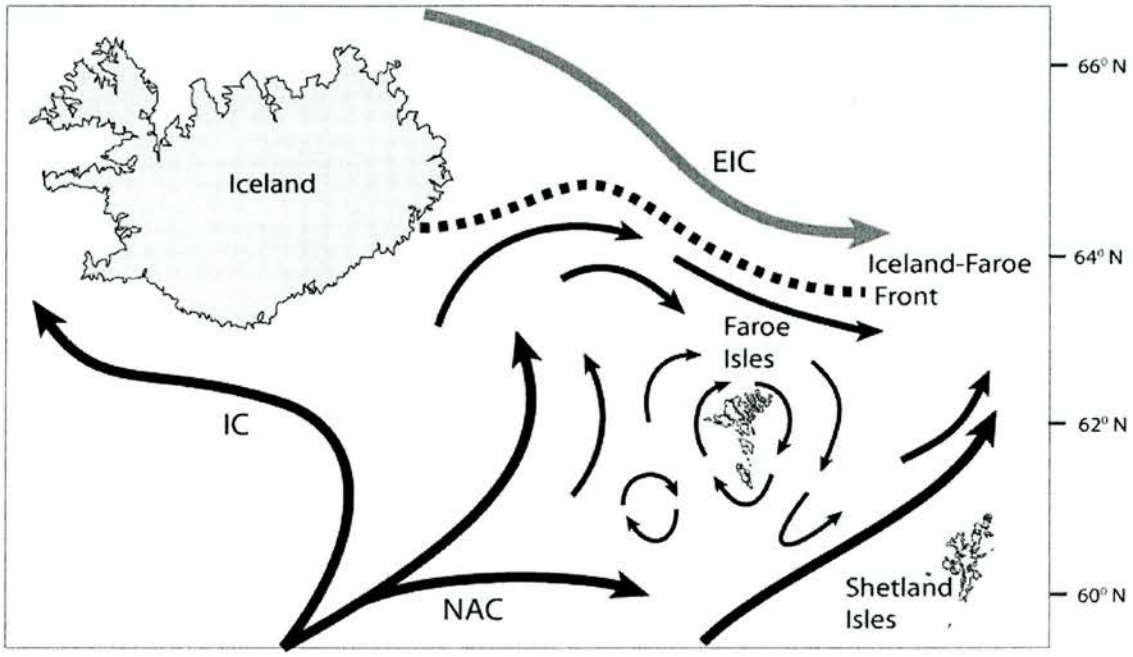

Figure 6.10: Modern surface circulation around the Faroe Isles showing Atlantic dominated (black) currents and Arctic dominated (grey) currents, together with the location of the Iceland-Faroes Front (after Hansen and Meincke, 1979).

The results of the ΔR values for the period c.1000 AD across the study area are indicative of possible spatial variability in the ^{14}C content of North Atlantic surface waters at this period that is significant with respect to the precision of the ^{14}C method. This includes an overall increase of c.200 ^{14}C years in ΔR between the west coast of Ireland and the Faroe Islands. The results suggest a reduced offset between atmospheric and surface ocean ^{14}C relative to the present day at sites on the west coast of Ireland, northern Scotland and the Orkney Isles. The lack of data from the Faroe Isles from modern samples precludes a rigorous comparison, however the ΔR from **UJ-23** is similar to the current regional mean for Iceland and the Faroe Isles ($T = 0.27$ ($\chi^2_{:0.05} = 3.84$)). When compared to the spatial distribution of modern North Atlantic MRE data, such a trend could imply that the relative differences in oceanic and climatic regimes between the geographic locations are comparable to those that operate today, and that surface ^{14}C in areas of the North Atlantic during this time was raised relative to present. If correct, these interpretations would have important implications for the study of past climate and oceanographic variables in the North Atlantic, during the phase of Norse expansion within the region. The cultural developments at this time are often linked with a set of favourable environmental conditions that permitted the settlement and exploitation of a

wide range of North Atlantic settings, including the initial settlement in the Faroes, Iceland and Greenland (cf. Jones, 1986). It is possible that these conditions were comparable to the present climatic situation, and that the subsequent retraction of settlements, such as the termination of the Greenland and Labrador settlements, was linked to deterioration in environmental conditions (cf. Davis *et al.*, 1988; McGovern, 1991). The period represented at c.1000 AD corresponds to a climatic warming that is known as the Mediaeval Warm Period (MWP) and is identified in many palaeoclimatic records. This climatic phase peaked at different times in various regions surrounding the North Atlantic basin between AD 900 to 1250 (c.750 - 1,050 cal. yr BP) (Lamb, 1985; Grove and Switsur, 1994). The characteristics of the MWP have been linked to the strength of the North Atlantic limb of the global thermohaline circulation (Broecker, 2001), and variation in the relative distribution of Atlantic and Arctic water masses. For example, ocean changes in proximity to the study area for this period include incursion of Atlantic water onto the Icelandic shelf (Knudsen *et al.*, 2004).

6.2.7 Correlation of values c.1000 AD with preceding periods

c.778 – 990 AD: The Outer Hebrides and Iceland

The consistent ΔR values for areas 2 and 4 at c.1000 AD are similar to the measurements for areas 3 and 4 for the period c.400 BC – 60 AD, where the *T*-statistic for all these values (N = 10) is $T = 12.47$ ($\chi^2_{:0.05} = 15.5$). In Area 4, ΔR values are available for a single site in both time periods, and again values from these three contexts (**StB-1063B** (-96 ± 16 ^{14}C yr), **StB-2136** (-60 ± 17 ^{14}C yr) and **StB-2004** (-50 ± 17 ^{14}C yr)) are similar ($T = 4.37$ ($\chi^2_{:0.05} = 5.99$). These results suggest comparable oceanographic conditions at sites in Area 4 during both the Iron Age and Norse periods. In both palaeoclimatic and archaeological records, these two periods are interpreted as ones in which warmer climatic conditions (linked in palaeoclimatic evidence to oceanographic characteristics) appear to have prevailed. The similarity of ΔR values at c.400 BC – 60 AD in Areas 3 and 4 to ΔR values in Areas 2 and 4 at c.1000-1200 AD may mean that ΔR values in Area 3 at c.1000-1200 AD were comparable to those in Areas 2 and 4. By extension of this hypothesis, it may be that ΔR values during c.400 BC – 60 AD in Area 2 were comparable to those in Areas 3 and 4. Although no ΔR values are available for c.1000 AD from Area 3 (Outer Hebrides), two values are available for the preceding period, c.890- 990 AD from two sites within Area 3. These are **BO-64** (-57 ± 14 ^{14}C yr) and **GA-165** (-89 ± 17 ^{14}C yr), and the ΔR values from these contexts are similar ($T = 2.11$ ($\chi^2_{:0.05} = 3.84$). The values from these two contexts are also statistically similar to the

consistent measurements from Areas 2 and 4 for c.1000 AD ((*T* = 7.89 ($\chi^2_{:0.05}$ = 11.1)). These results from **BO-64** and **GA-165** indicate that during the period c.890- 990 AD, ΔR values on the Outer Hebrides (Area 3), were comparable to ΔR values in this area during c.400 BC- 60 AD.

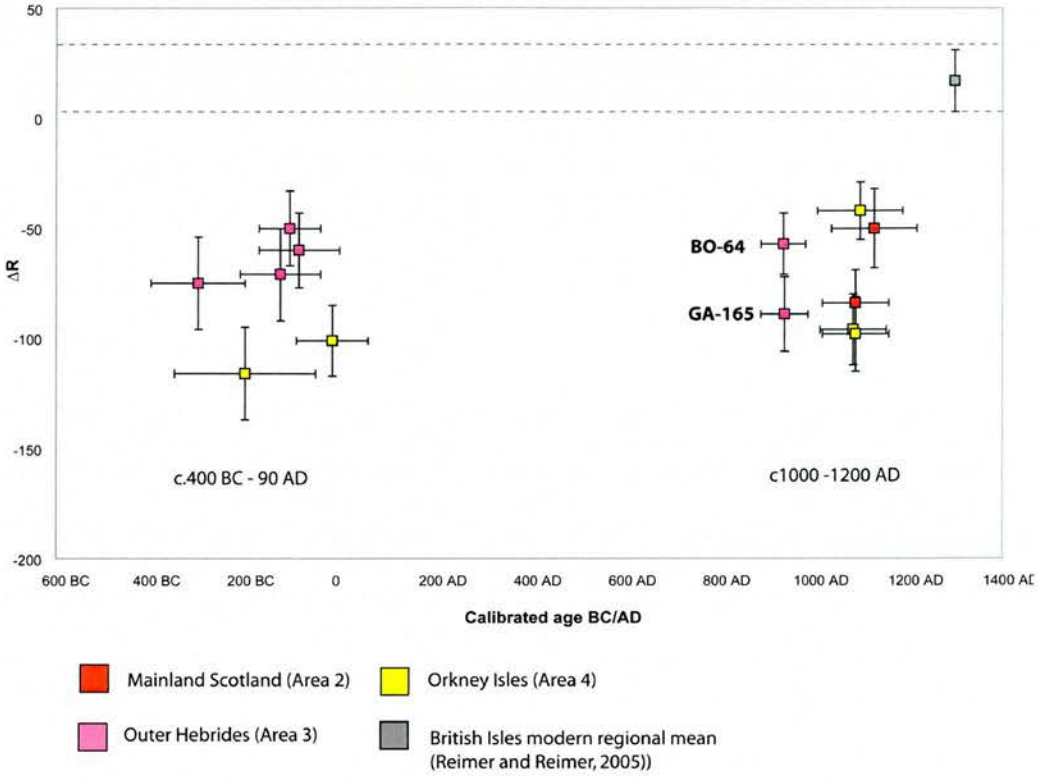

Figure 6.11: Comparison of ΔR values for Areas 2, 3 and 4 for two time periods c.400 BC- 60 AD and c.1000-1200 AD, showing the values from **BO-64** and **GA-165** for the period c.890- 990 AD in Area 3. Relevant geographic locations of contexts are indicated.

During the course of this thesis, an opportunity became available to collect data from contexts at a site in Iceland, Hrísheimar (**HR**). The relevant context and site details for marine and terrestrial samples obtained from Hrísheimar are contained within Appendix B. As a result, samples of *Mytilus edulis* shells and neo-natal cow bones were obtained from a single, stratified midden deposit (**HR-45**) according to the context selection protocol described in Chapter 3, in order to assess a ΔR value from this material. These samples were measured at SUERC and pre-treatment and measurement followed the procedures described in Chapter 4. As the *T*-statistics of the terrestrial and marine samples were $T = 6.78$ ($\chi^2_{:0.05}$ =

7.81) and $T = 1.11$ ($\chi^2_{:0.05} = 7.81$) respectively, these were used according to the procedure described in Chapter 4 to calculate $\Delta R = 96 \pm 15$ ^{14}C yr for (**HR-45**).

The weighted mean terrestrial ^{14}C age at (**HR-45**) is 1165 ± 26 BP ($T = 6.78$ ($\chi^2_{:0.05} = 7.81$)), giving a 2σ calibrated age range of 778-970 AD, which is similar to that of the period covered by **BO-64** and **GA-165** (c.890- 990 AD). This enables an assessment of spatial variability in ΔR for the period c.778 – 990 AD from the Outer Hebrides to Iceland. The value from **HR-45** (96 ± 15 ^{14}C yr) is significantly higher ($T = 82.67$ ($\chi^2_{:0.05} = 5.99$) than the ΔR values from **BO-64** (-57 ± 14 ^{14}C yr) and **GA-165** (-89 ± 17 ^{14}C yr). When compared with the value for the current modern Iceland and Faroe Isles region (52 ± 19 ^{14}C yr), the ΔR from **HR-45** appears to be similar ($T = 3.30$ ($\chi^2_{:0.05} = 3.84$)). In addition, the ΔR from **HR-45** is also similar to that of **UJ-23** ($T = 2.60$ ($\chi^2_{:0.05} = 3.84$)). When correlated with the data described above for c.1000 AD, these results suggest that spatial variability with a northward increase in ΔR was also present in the North Atlantic within the study area for the period preceding c.1000 AD.

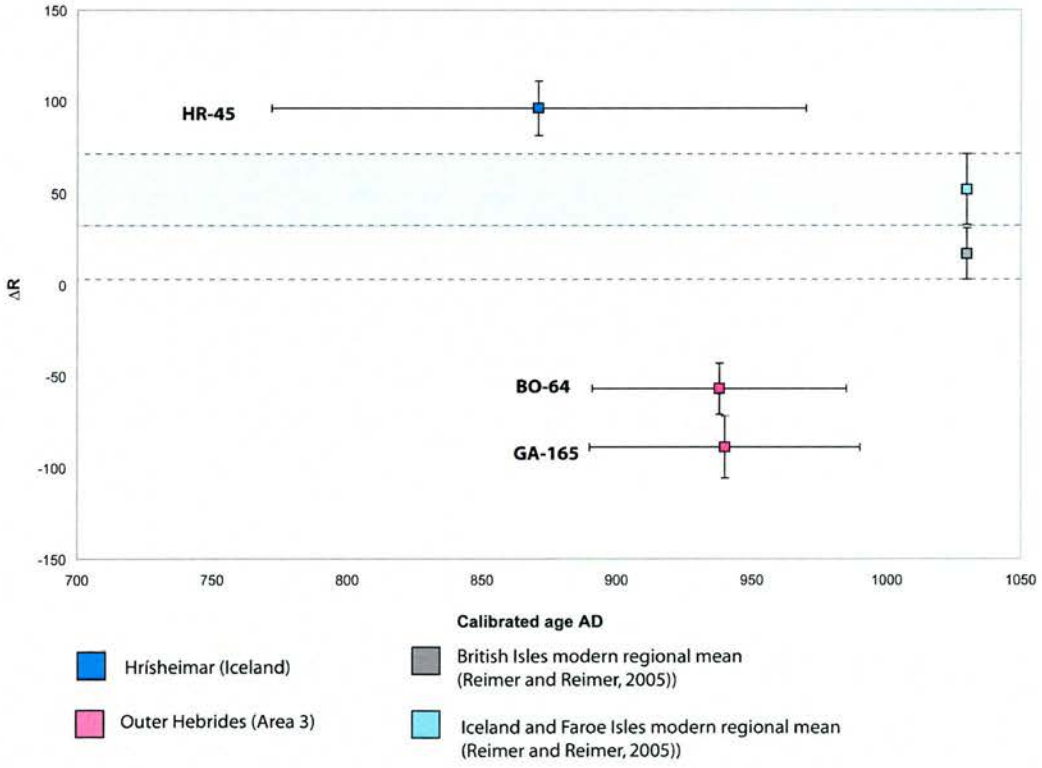

Figure 6.12: Comparison of ΔR values from the Outer Hebrides and Iceland c. 750 – 1000 AD.

c.250 – 820 AD: The Outer Hebrides, western Ireland and Shetland

Results from Area 3 for the periods c.400 BC- 60 AD and c.890- 990 AD suggest consistency in ocean ^{14}C content for these periods. As discussed above (section 6.2.1), these data are not consistent with those of the Early Holocene for this Area. A ΔR value is available from Area 3 for the period 330-430 AD (from **BE-503**) that is also not consistent with other values in Area 3 during c.400 BC- 60 AD and c.890- 990 AD. The ΔR from **BE-503** (-27 ± 10) is significantly higher than values during the previous and subsequent time period in Area 3 ($T = 28.00$ ($\chi^2_{:0.05} = 12.6$)), although it is similar to the lowest individual ΔR values from these periods.

Context	2σ cal. age range	ΔR
BA-139	400-200 BC	-75 ± 21
BA-146	210-40 BC	-71 ± 21
HP-201	350-50 BC	-116 ± 21
BA-39	90 BC-60 AD	-101 ± 16
BE-503	330-430 AD	-27 ± 10
BO-64	890-985 AD	-57 ± 14
GA-165	890-990 AD	-89 ± 17

Table 6.4: Available ΔR values from Area 3 for the time periods preceding and succeeding that of **BE-503**.

This makes interpretation of the ΔR from **BE-503** difficult, and there are two main possibilities. One is that the ΔR value for this period within Area 3 is consistent with the previous and subsequent periods (i.e. c.400 BC- 60 AD and c.890- 990 AD), and the value from **BE-503** is an outlier that is the result of unknown sources of variability. Alternatively **BE-503** could be representative of an increased ΔR in Area 3 for 330-430 AD relative to c.400 BC- 60 AD and c.890- 990 AD. To investigate this further, **BE-503** was compared with two contexts from Area 5 **SC-543** and **SC-3083**. These have 2σ calibrated age ranges that are similar to **BE-503** of 250-400 AD (**SC-543**), and 410-540 AD (**SC-3083**). The ΔR values from the three contexts are not similar ($T = 226.96$ ($\chi^2_{:0.05} = 5.99$)) (see Figure 6.13), and it is not possible to make a definitive statement from the data. The ΔR value from **SC-3083** (-121 ± 16 ^{14}C yr) also appears to be increased relative to preceding and subsequent values, and is significantly greater than **BE-503**. This could support an interpretation of spatial variability in ΔR that corresponds to the northward increase observed at c.1000 AD in

the data, and also possibly an increased ΔR within the study area at c. 330-540 AD. However, the value from **SC-543** does not correlate with these values, being at -290 ± 16 ^{14}C yr, the lowest value in the dataset. This value is not similar to any other value in this study from any context, and is 142 yr lower than any other ΔR offset. This value may represent a significant increase in surface ocean ^{14}C either in the area surrounding the site, or within the wider study area at a time within the period 250-400 AD. Alternatively, it is possible that the value from **SC-543** is an anomaly and produced by sources of variability that may be associated with the archaeological sample provenance that have not been identified. The ΔR value from **SC-543** and potential variability over this time period suggested by this value means that it is therefore not possible to state definitively from the data whether **BE-503** and **SC-3083** represent a period of raised MRE values at c. 330-540 AD.

The variability between ΔR values from **SC-543** and **SC-3083** may be representative of an area that is sensitive to changes in factors that underlie specific MRE changes. Alternatively the period 250-540 AD may be one in which these factors were highly variable across the wider study region. This would contrast with the previous apparent c.400 yr stability in conditions on the Western Isles and Orkney. Subsequent to increased ΔR values in Area 5 at 410-540 AD (**SC-3083**), the value from **SC-1269** (-121 ± 16 ^{14}C yr) shows a significantly different ΔR value at the site for the period 650-770 AD from both **SC-543** and **SC-3083** (T= 142.48 ($\chi^2_{:0.05}$ = 5.99)). The ΔR from **SC-1269** can also be compared with two values (at **DL3-19** (-107 ± 18 ^{14}C yr) and **DL11-2** (-69 ± 17 ^{14}C yr)) from Area 1, which together cover a comparable calibrated 2σ age range to **SC-1269** (i.e. 660-820 AD).

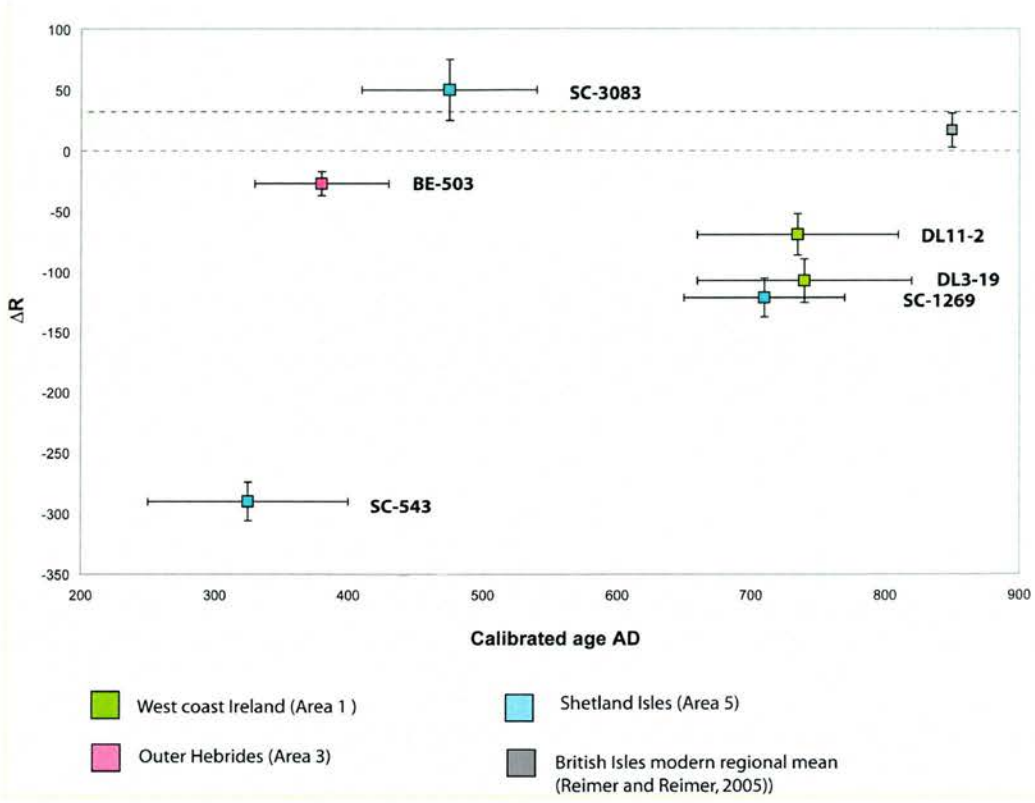

Figure 6.13: Comparison of values from Areas 1, 3 and 5 for the period c.250-540 AD and c. 650 – 820 AD.

To examine ΔR within Area 1, values from **DL3-19** and **DL11-2** can be compared with the later value from Area 1, **OI-6** (Figure 6.13). Here, only the higher value (**DL3-19** ΔR = -107 ± 18 ^{14}C yr) is similar to **OI-6** (T = 2.11 ($\chi^2_{:0.05}$ = 3.84)). It is possible that the ΔR for this area was consistent in the two time periods and **DL11-2** represents an outlying value, or that ΔR values became smaller in this area between the period 660-820 AD and 990-1160 AD. It is also possible that **OI-6** represents an anomalously low value for this area, and ΔR values were closer to those at Scottish sites than could otherwise be supposed. Previous assessments of ΔR values were performed using measurements made of charcoal and shell pairs from contexts at **OI** and **DL11** by Reimer *et al.*, (2002). Three ΔR values from contexts at **OI** (two for c.1000 AD and one for c.2350-1910 BC) are similar (T = 1.68 ($\chi^2_{:0.05}$ = 5.99)), and give a weighted mean ΔR of -135 ± 39. A ΔR from **DL11** (660-810 AD) gave -110 ± 50. This data was excluded from an assessment of a regional mean ΔR for the British Isles due to the possibility at archaeological sites that charcoal samples represent re-use of old wood. However, these values are noted here as they may indicate that the low ΔR values calculated in Area 1 during this study are supported by other assessments.

The ΔR values from **DL3-19** (-107 ± 18 ^{14}C yr) and **DL11-2** (-69 ± 17 ^{14}C yr) are similar to each other (T = 2.36 ($\chi^2_{:0.05}$ = 3.84)). When these are compared to the ΔR value from **SC-1269** (-121 ± 16 ^{14}C yr) the three values are similar (T = 5.20 ($\chi^2_{:0.05}$ = 5.99)). The results from these three contexts therefore do not indicate a spatial variation in ΔR over the study period at 650-820 AD. It is possible however to compare these results with the value from **HR-45** (96 ± 15 ^{14}C yr), which has a 2σ calibrated age range that within its lower range is similar to **DL3-19** and **DL11-2**. The ΔR from **HR-45** for this time is higher than at the sites from Ireland (see Figure 6.14), where T = 90.93 ($\chi^2_{:0.05}$ = 5.99). This may therefore indicate a latitudinal variation in ΔR between the west coast of Ireland and the north east coast of Iceland for this time period.

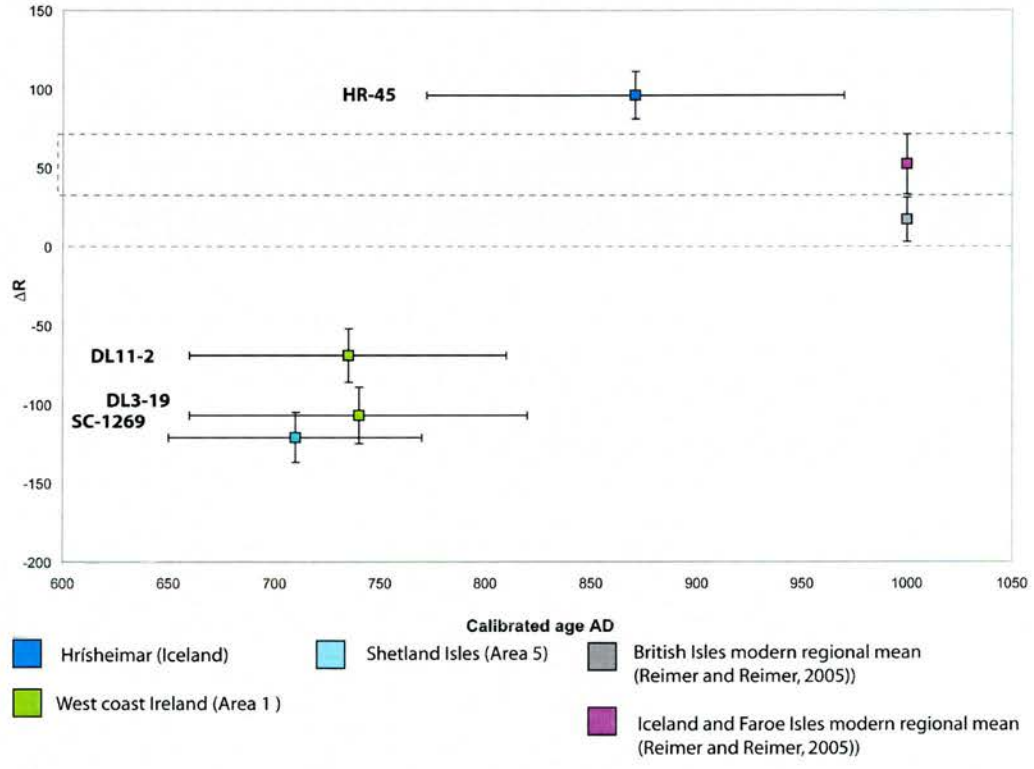

Figure 6.14: Comparison of ΔR values from Shetland, Ireland and Iceland for c.650-1000 AD, showing modern regional mean ΔR values for the British Isles and Iceland.

6.2.8 ΔR values for the later Holocene: c.1200-1400 AD

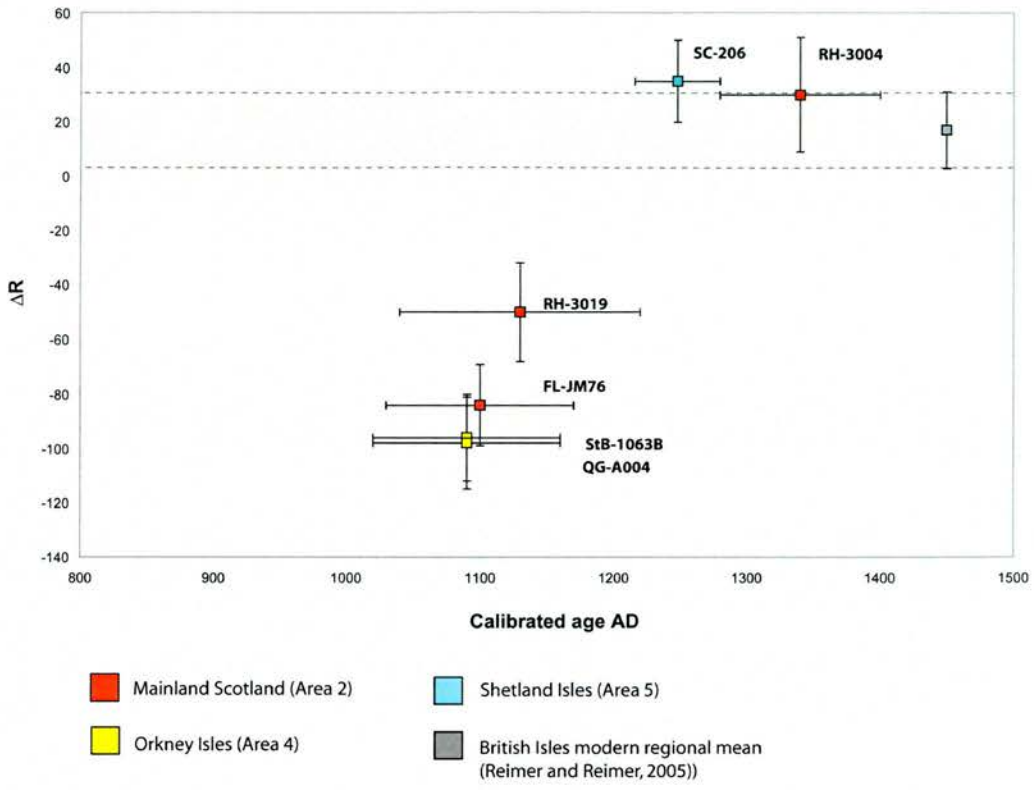

Figure 6.15: ΔR values for the later Holocene, within the study area, showing geographic location of individual contexts.

Two contexts cover the period c.1200-1400 AD, located in Area 2 (**RH-3004** (30 ± 21 ^{14}C yr)) and Area 5 (**SC-206** (35 ± 15 ^{14}C yr)). The ΔR values from these contexts are similar (T = 0.04 ($\chi^2_{:0.05}$ = 3.84)), and both are significantly larger than the majority of preceding determinations. At the same site as **RH-3004,** the ΔR value from an earlier context **RH-3019**, is significantly smaller than **RH-3004** (T = 8.37 ($\chi^2_{:0.05}$ = 3.84)) where the two contexts are separated by a maximum of c.360 cal. yr at 2 σ (Figure 6.15). A rise in ΔR relative to the next oldest value is also seen at **SC-206**, where the ΔR value (35 ± 15 ^{14}C yr) is higher than the previous determination from **SC-1269** (-121 ± 16 ^{14}C yr), (T = 50.59 ($\chi^2_{:0.05}$ = 3.84)). The ΔR from **SC-206** is however similar to that from **SC-3083** (T = 0.26 ($\chi^2_{:0.05}$ = 3.84)), which is during a phase of possible increased ΔR values relative to other periods. It is therefore possible that the ΔR values from the youngest contexts within this study could indicate a rise in ΔR within the study area for the period post-1200 AD. The data are

however indicative only of this possibility, and a larger number of measurements would be required to show whether this hypothesis is supported.

If within the study area ΔR values increased in the period post 1200 AD, a potential mechanism is the Little Ice Age (LIA) that appears to have succeeded the Medieval Warm period from c.1300-1400 AD. The LIA corresponds to a period of significant climatic cooling within both the North Atlantic, and wider global areas that lasted c.500 yr and was only definitively ended by 20th century climatic warming (Lamb, 1985). Palaeoclimatic factors identified as potential mechanisms for the LIA cooling include variation in ocean circulation features. For example Broecker (2000) proposed that features of the LIA could be linked to oceanographic variations in the thermohaline circulation system, and Knudsen *et al.* (2004), identified an increasing influence of water from the East Greenland Current on the North Icelandic shelf from 700-800 yr BP (c.1200-1300 AD).

6.3 Assessment of the methodological approach

The above interpretations were produced on the basis of c.300 ^{14}C measurements of terrestrial and marine samples that were selected from 30 contexts at 20 sites according to a new multi-paired sample methodological protocol (described in Chapters 3 and 4) developed within this thesis. This approach was designed to maximize the accuracy and precision of ΔR values that were produced as this would achieve the aim of examining the North Atlantic MRE to a high level of resolution. The efficacy of the methodological approach in achieving this can be assessed by examining the results of the χ^2-test upon samples from individual contexts (Table 5.8). These data show that for a large number of contexts the *T*-statistic for a group of terrestrial or marine measurements was below the critical test value for 95% significance ($\chi^2_{:0.05}$) for the appropriate number of samples (*N*) in a tested group. This result demonstrates that the methodological protocol successfully achieved the aims for which it was designed, and is a robust way of selecting samples with which to examine the MRE in areas where suitable (archaeological) terrestrial deposits are available. The use of this methodology has effectively reduced uncertainty over the association between terrestrial and marine sample material, and enabled the production of a coherent dataset.

Chapter 7: Conclusions

The overall aim of this thesis was to examine spatial and temporal characteristics of the ^{14}C marine reservoir effect (MRE) in the North Atlantic over the Holocene. This has resulted in the determination of 30 ΔR values at 20 sites over an area including the island belts of Northern and Western Scotland, the western and northern Scottish mainland coast, Western Ireland and the Faroe Isles, with additional data from Iceland. These data cover a temporal range from c.6500 BC to c.1400 AD, a total of c.8000 cal. yr and provide an assessment of ΔR for this time period across the study area that has a high degree of both precision and accuracy. A number of conclusions are drawn from this:

1. The sample selection protocol developed in this thesis is an effective way to optimise the precision and accuracy of ΔR values produced using the paired sample approach

2. It is possible using such a strict sample methodology to obtain the required level of resolution to observe ΔR variations relative to present in the North Atlantic over the Holocene

3. These potential variations include:
    i. Higher ΔR values in the earlier Holocene
    ii. Reduced ΔR values at c.400 BC – 90 AD
    iii. Reduced ΔR values at c.1000 AD in Scottish waters
    iv. Potential spatial variation in ΔR across the study area (e.g. at c.1000 AD)
    v. Higher ΔR values from c.1200 – 1400 AD

4. It is possible to correlate spatial and temporal features of Holocene ΔR values in the North Atlantic with climatic and oceanographic changes from palaeoclimatic records.

The implications of this thesis for determining ΔR values

Increasing the accuracy and precision of available ΔR values is an important aim in order to place ^{14}C measurements from a wide range of geographical areas and time periods within a common chronological framework. As discussed in this thesis this aim is of particular relevance in palaeoenvironmental and archaeological investigations at times of rapid climatic

or cultural transitions, when chronological resolution becomes more critical. In light of this, the conclusions outlined above have important implications. Firstly, the dataset produced in this study allows a more precise and accurate assessment of ΔR for the study region over the Holocene period. This facilitates use of marine samples within research areas where these samples are the optimal, or the only material available for ^{14}C measurement. Both the accuracy and precision of a calculated ΔR value are highly influenced by the particular samples upon which the assessment has been made. Because of this, it is crucial that effective sample selection protocols are developed and applied. If inappropriate samples are used to produce ΔR or MRE assessments, the resulting data may be counter-productive, giving inaccurate values that lead to inaccurate palaeoenvironmental or archaeological interpretations. The efficacy of the sample selection protocol developed in this thesis therefore highlights important considerations for the future development of such protocols:

- Samples for ΔR determination should be in as close association as possible within a single deposit

- This deposit should exhibit several features:
  i. A short (e.g. ideally < 20 yr) accumulation period
  ii. A lack of post-depositional bioturbation or other disturbance
  iii. A large volume of dateable material relative to the deposit size

- Multiple samples should be measured from each deposit

- It is important to consider the site microenvironment and potential for on-site contamination, including groundwater runoff and input of geological carbonate. For example, sampling in sheltered locations, bays, estuaries and inlets, and areas with a high proportion of fresh water and sediment run off, should be avoided.

- Results of a study within this thesis suggest that at sites selected according to the protocol described in Chapter 3, any of several marine mollusc species may be used to accurately determine ΔR. However, consideration of organism behaviour (both terrestrial and marine), and in particular feeding mechanisms, should be incorporated into research strategies and possible interspecies variability in ^{14}C content should be considered.

The implications of this thesis for understanding of the North Atlantic MRE in the Holocene

The variations in ΔR that are identified in this thesis allow a more coherent picture to be developed of changing ocean ^{14}C content within the study area over the Holocene. Throughout the time period covered by the dataset there are fluctuations in values relative to the current regional mean ΔR for the British Isles. These Holocene variations occur on a reduced scale relative to the MRE changes identified in pre-Holocene datasets (e.g. the Younger Dryas). This is consistent with the evidence that variations in palaeoclimatic forcing mechanisms thought to dictate the size of ΔR values occur at a lower amplitude during the Holocene than previously. As identified in point 4 above, variations in these mechanisms over the Holocene can be correlated with features of the ΔR observed in this study, particularly with respect to oceanographic features. The reduced ΔR values relative to present on the Outer Hebrides, Northern Scottish mainland and Orkney for c.400 BC – 90 AD and c.1000 AD for example, occur during two climatic periods for which palaeoclimatic and archaeological evidence suggest ameliorating conditions. These conditions are linked to factors including warming sea surface temperatures, reduced sea ice extent and strengthened inflow of Atlantic waters, and the consistency of ΔR values at sites for these periods suggests that the palaeoclimatic factors determining ΔR were comparable for the two time intervals. Although it is outwith the scope of this study to provide quantitative relationships between the strength of palaeoclimatic forcing mechanisms and ΔR values, the results give considerable support for a relationship between specific features of the North Atlantic palaeoclimatic record and ΔR values. These correlations highlight the potential to gain a better understanding of the nature and mechanisms of the MRE itself through using standardised methodologies and rigorous sample protocols to define ΔR values. The results of this study suggest that if a better understanding of the links between palaeoclimate and MRE variation is gained, it is possible that variations in the marine ^{14}C record could be themselves employed as a proxy record of palaeoenvironmental change.

The implications of this thesis for application of ΔR corrections for North Atlantic samples and potential future research directions

This thesis has resulted in the production of a unique large dataset of ΔR values that are applicable to the study area of western Ireland, northern and western Scotland and the Faroe Isles. The temporal range of the data over c.6500 BC – 1400 AD is discontinuously covered by the data, however there are ranges where several determinations coincide. As outlined in

point 3 above, several distinct features of ΔR can be identified in the dataset. The current regional mean correction values for the study area include ΔR = 52 ± 19 ^{14}C yr for the Faroes and Iceland and ΔR = 17 ± 14 ^{14}C yr for the British Isles (Reimer and Reimer, 2005). The reproducibility of ΔR data generated within this thesis for specific intervals leads to the recommendation of a revised correction value for specific areas at specific time periods. These include the value of -79 ± 10 ^{14}C yr for Scottish coastal waters during the Middle Iron Age period, derived from samples covering c.400 BC – 60 AD. These values can be used with calibration programs such as OxCal (Bronk-Ramsey, 1995; 2001) and CALIB (Stuiver and Reimer, 1993) to correct marine samples for the MRE. However, there are also intervals where results are less conclusive and it is more difficult to definitively interpret the data. For example, the variability observed in ΔR values for the period 250-540 BC at sites from the Outer Hebrides and Shetland. At such intervals there is a need for more data to support interpretations before any correction can be confidently ascribed. An important implication of the MRE for ^{14}C measurement of samples is that it is preferable where possible to use samples that consist entirely of terrestrial-derived carbon. This removes the need to correct for the MRE and ΔR values which have an associated level of uncertainty. Where it is not possible to avoid measurement of samples containing marine-derived carbon, a careful assessment must be made of the most appropriate correction value to be applied for the samples geographic location and temporal period where relevant. At all times it is crucial that full details are provided by authors of the method by which calibrated age ranges have been obtained for samples containing marine carbon.

At present there is a growing recognition of the importance and potential of the MRE, and correspondingly, an increased research effort to define and understand the effect. Refinement of existing ΔR corrections in the North Atlantic would enable the re-evaluation or confirmation of previous environmental and archaeological interpretations and ultimately lead to an improvement in the datasets and methodology used in these research disciplines. This thesis has resulted in the production of a unique dataset from which it is hoped future research directions can be developed to enhance our understanding of the MRE on both a regional and global scale.

Appendix A: A preliminary assessment of $\delta^{18}O$ in coastal water and mollusc shell carbonates.

A.1 Introduction

This thesis examines characteristics of the ^{14}C concentration of surface ocean water at a range of study sites over the Holocene, using marine mollusc shells as a proxy record. During this work the opportunity became available to examine modern features of surface ocean water in proximity to the majority of archaeological sites that had been included in the thesis. These features included the temperature and salinity of coastal water, and this was achieved using $\delta^{18}O$ measurements of coastal surface water and marine mollusc shell carbonates.

Water $\delta^{18}O$ ($\delta^{18}O_w$) is dependant upon rates of evaporation and freshwater input. Evaporation raises water salinity and $\delta^{18}O_w$ (as ^{16}O is preferentially removed) while freshwater input lowers both the $\delta^{18}O_w$ and salinity of the water. Freshwater input to surface coastal water is derived from terrestrial runoff, resulting from meteoric precipitation. The typical $\delta^{18}O$ range of meteoric precipitation over Western Europe is between -5 and -15‰, with decreasing values at higher latitudes (Bowen and Wilkinson, 2002). In contrast, observations of the relationship between salinity and $\delta^{18}O_w$‰ in the Northeast Atlantic Ocean give a typical surface $\delta^{18}O_w$ of c. 0.0‰ for these waters, which have salinities of c. 35‰ (Östlund *et al.*, 1987). Measurements of coastal water $\delta^{18}O_w$ within this preliminary study therefore allowed an assessment of the terrestrial freshwater input to the surface ocean close to a sampled site. A feature of the selection criteria for archaeological sites from which to obtain samples for ^{14}C dating was the absence of any significant freshwater input. This was because such an input may alter the surface water ^{14}C concentration in a specific location. This study enabled the degree to which this criterion had been met to be identified at 19 sampled sites. The use of mollusc shell carbonates as a record of $\delta^{18}O_w$ variations is possible as molluscs generally precipitate their shell carbonate in equilibrium with water $\delta^{18}O$ and the shells therefore provide an isotopic record of the ambient water at the time of precipitation (Epstein *et al.*, 1953). The $\delta^{18}O$ of biologically precipitated marine carbonates ($\delta^{18}O_c$) is dependent upon the isotopic composition and temperature of the ambient water. This means that a quantifiable relationship exists between these three variables (Grossman and Ku, 1986). The carbonate shells of different species of marine organism may have different values of $\delta^{18}O_c$ even though the organisms inhabit the same environment. This is due to factors such as species-

specific biogenic effects and season of shell growth. To investigate the relationship between surface water isotopic composition and the shell $CaCO_3$ precipitated by *Patella vulgata* inhabiting these waters, measurements of $\delta^{18}O_w$ and $\delta^{18}O_c$ at the 19 sample sites were compared. The record of $\delta^{18}O_w$ contained within carbonates precipitated by marine organisms has proved particularly useful in palaeoclimatic studies as a proxy for oceanographic changes such as water temperature and salinity. A final part of this preliminary study therefore investigated whether any difference could be identified in the $\delta^{18}O_c$ of modern and fossil shells within the study area. This was achieved by comparison of $\delta^{18}O_c$ measurements made of *Patella vulgata* shells from both the modern shoreline and archaeological contexts at six sites.

A.2 Methodology

Modern samples of coastal water and *Patella vulgata* shells were collected for $\delta^{18}O$ measurement from 19 locations (Figure A.1). Of the sampled sites, 16 were close (<0.5 km) to archaeological sites from which samples had been obtained for ^{14}C measurement. Two other sites (Lochmaddy (**LM**) and Skapa Flow (**SF**)) were close to coastal water monitoring stations of the Fisheries Research Services (FRS), an agency of the Scottish Executive Environment and Rural Affairs Department. At these sites water temperature is recorded every 30 minutes and water salinity and nutrients are recorded weekly. The annual range of sea surface temperature (SST) and sea surface salinity (SSS) was obtained from FRS records at four monitoring stations within the study area, including **LM** and **SF**.

Site	**Lochmaddy**	**Skapa Flow**	**Fair Isle**	**Scalloway**
Location	57°35'N, 07°09'W	58°57'N 002°58'W	59°32'N, 01°36'W	60°07'N, 001°16'W
SSS measurements	2 years available	6 years available	Not available	5 years available
SST measurements	1 year available	5 years available	22 years available	4 years available

Table A.1: locations and available monitored data from FRS monitoring sites in the study area.

In addition to samples of coastal water, $\delta^{18}O_w$ measurements were made on terrestrial run-off water from a stream which was situated at the east of Skapa Flow, <0.5 km from the coastal water sample site (**SF**). This was in order to assess the $\delta^{18}O_w$ of terrestrial (meteoric) freshwater runoff for a typical location within the study area, which could then be compared

with the measured coastal $\delta^{18}O_w$, and typical values for Western Europe meteoric water $\delta^{18}O$ (-5 to -15‰).

Sample site	Identifier code
Carding Mill Bay	**CMB**
Lochmaddy	**LM**
Hornish Point	**HP**
Baleshare	**BA**
Northton	**NO**
Berie	**BE**
Bostadh	**BO**
Galson	**GA**
Sand	**SA**
Skara Brae	**SkB**
Birsay Bay	**BB**
Quoygrew	**QG**
St. Boniface	**StB**
Lopness	**LO**
Pool Bay	**PB**
Skapa Flow	**SF**
Roberts Haven	**RH**
Freswick Links	**FL**
Undir Junkarinsfløtti	**UJ**

Table A.2: Identifier codes used in the text for sites from which samples of modern coastal water and *Patella vulgata* were obtained.

The molluscs were obtained from the shoreline and where relevant in close proximity to the excavated archaeological remains. Molluscs were removed live in small quantities (4 individuals per site) from the rocky foreshore when exposed by low tide. The shells were immersed in boiling water for 2-3 minutes after which the flesh was removed and the dry shells placed in labelled bags for transport to the laboratory. Water samples were collected in 1 litre plastic sample bottles then decanted into 12 ml Exetainer ™ vials and labelled. Samples of coastal water were obtained from the surface water where the depth of the water was c.1m. Samples were taken in clean 1 litre plastic containers, which were washed out with the surface water three times before being filled. Water from the containers was then decanted into 12 ml Exetainers, capped and labelled.

Six archaeological contexts were chosen from which to obtain measurements of mollusc shell $\delta^{18}O$. From each context, four shells were selected that had been measured for ^{14}C within this thesis for assessment of the MRE and the ^{14}C ages of the shells within each context were statistically similar on the basis of a χ^2 test (Table A.3). A 2σ calibrated age

range was provided for each context by ^{14}C measurement of terrestrial material from within the context.

Site	***T*-statistic for ^{14}C measurements of mollusc shells from contexts**	**Context 2σ cal. age range**
SkB-26	1.64; ($\chi^2_{:0.05} = 7.81$)	2840-2570 BC
BB-XF	1.42; ($\chi^2_{:0.05} = 7.81$)	2120-1960 BC
BA-139	1.65; ($\chi^2_{:0.05} = 7.81$)	390-230 BC
HP-201	0.21; ($\chi^2_{:0.05} = 7.81$)	205-110 BC
StB-1063B	0.31; ($\chi^2_{:0.05} = 7.81$)	1020-1150 AD
RH-3019	0.52; ($\chi^2_{:0.05} = 7.81$)	1050-1210 AD

Table A.3: Archaeological contexts from which samples of *Patella vulgata* were taken for $\delta^{18}O$ measurement showing calibrated 2σ age ranges (calculated from ^{14}C measurements of terrestrial material within the context), and *T*-statistics for groups of measured mollusc shell ^{14}C ages.

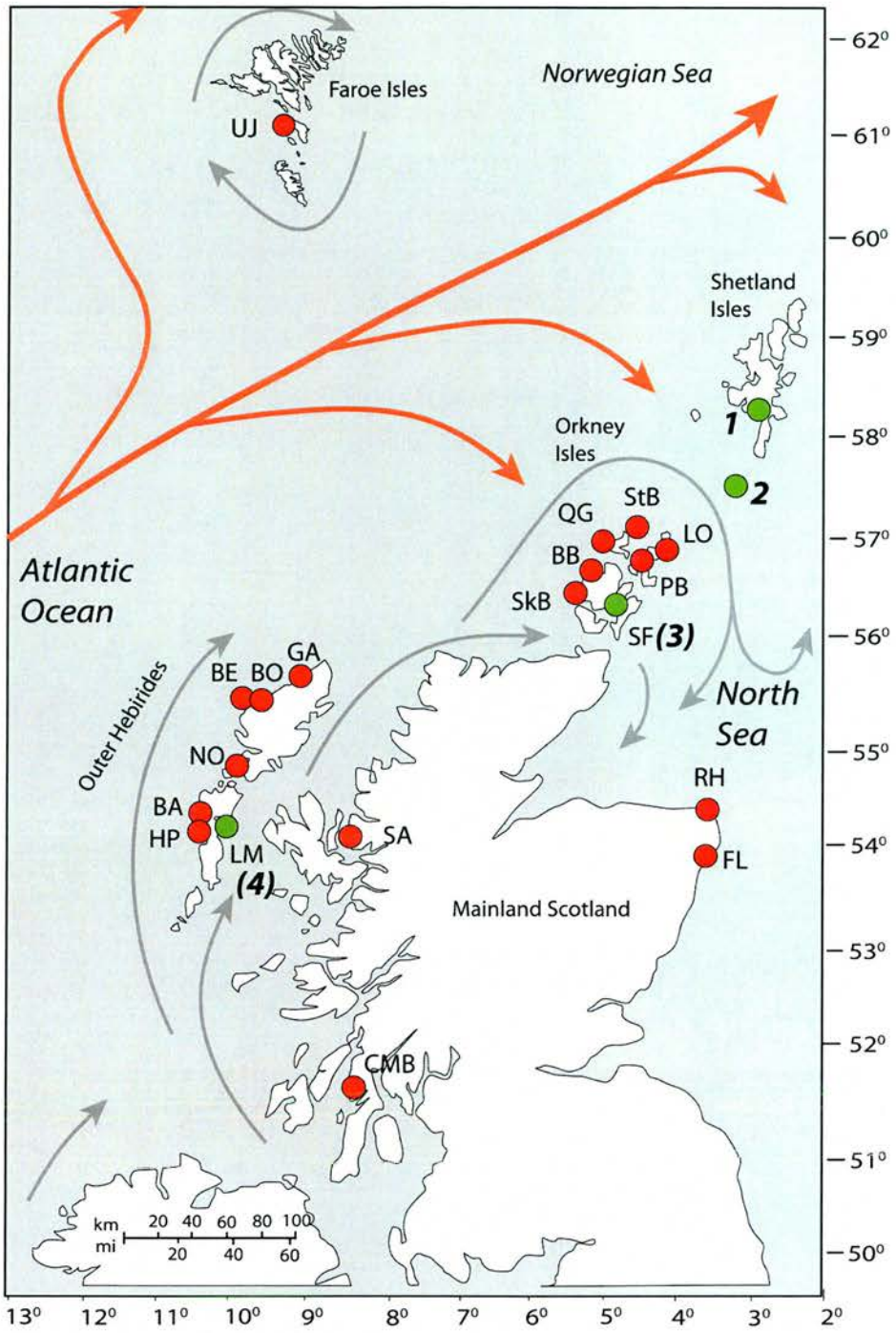

Figure A.1: The study area: Red circles show the location of sites sampled for modern coastal water and *Patella vulgata*. Atlantic Ocean waters are shown as red arrows and coastal water currents as grey arrows. The identifier codes for sites are given in Table A.2. Green circles show the location of four FRS water-monitoring stations (1: Scalloway, 2: Fair Isle, 3: Skapa Flow, 4: Lochmaddy).

Mollusc shell samples for ^{18}O measurement from contexts at archaeological sites were those that had also been measured for ^{14}C. These shells had therefore been subjected to the pre-treatment method described in Chapter 4 (section 4.1.1), and a sub-sample of each pre-treated shell was taken for ^{18}O measurement. Post-depositional isotopic exchange would not have affected the modern mollusc shells as these were collected from live specimens, making surface removal unnecessary. A homogenised sample was obtained from each archaeological or modern shell by crushing the shell to a powder. The organic component of living shells is significantly higher than that of archaeological shell samples, as the shell is covered by a further organic (proteinacious) layer, known as the periostractum, and it is possible for a quantity of soft tissue to adhere to the shell after removal of the mollusc body. It is necessary to remove this organic component from modern shells as the isotopic composition of organic proteins may be significantly different to that of the shell carbonate. The crushed samples of modern mollusc shells were therefore placed in a Biorad Polaron plasma asher for a minimum of 5 hours to remove organic material. The plasma asher bonds organic material from the shell $CaCO_3$ with an O_2 plasma at 10^{-1} millibars pressure, which converts the organic component to CO_2 and H_2O at room temperature without destruction of the shell carbonate structure.

Samples of coastal water were prepared using 1 ml aliquots of sample water in 12 ml Exetainers where 300 µl of CO_2 gas was then equilibrated with the water bicarbonate (CO_3^{2-}) in helium over 10 days. Two aliquots were measured from each water sample.

The stable isotopic ratio of shell carbonate was measured using a VG Isogas Prism II dual inlet stable isotope mass spectrometer at SUERC, East Kilbride. The apparatus incorporated a VG Isocarb common acid bath automated carbonate dissolution system. Between 1 and 1.5 mg of crushed sample shell was used for each measurement. The shell $CaCO_3$ was dissolved at 90^0C in "103"% phosphoric acid, produced with partially polymerized orthophosphoric acid and having a specific gravity of 1.92 at standard temperature and pressure. The samples were sequentially introduced to the acid bath and the evolved CO_2 passed across a water trap before being frozen and collected. The measurement results were expressed using the δ-notation (Craig, 1957) as per mille deviation from the VPDB standard, calibrated using the IAEA CO1 (Carrara marble) international standard. The internal analytical precision of the standards was 0.04‰ for $\delta^{13}C$ and 0.08‰ for $\delta^{18}O$.

Coastal water samples were measured using an Analytical Precision AP2003 stable isotope mass spectrometer with Gas Preparation Interface. A reference sample of pre-calibrated CO_2 gas was measured with each sample. Isotopic ratios were calculated with known standards using standard linear regression (r2 for $\delta^{18}O$ and δD = 1.000). The external precision (as stated by the manufacturer) was ± 0.15 ‰ at natural abundance. The samples were run twice with a five-day gap to exclude any influence induced by water salinity upon equilibrium. The measurement results were expressed using the δ-notation (Craig, 1957) as per mille deviation from the VSMOW standard, calibrated using Vienna Standard Light Antarctic Precipitate (VSLAP) and Greenland Ice Sheet Precipitate (GISP) international standards.

The variation in $\delta^{18}O_w$ of samples measured at one site was assessed by examining the average and standard deviation of two measured aliquots from each water sample. The average of the two aliquots was then taken as the $\delta^{18}O_w$ value for a single site. These values represent only the summer $\delta^{18}O_w$ and are not the result of continual monitoring, therefore can only be taken as an estimate of the summer water $\delta^{18}O_w$. The variation in shell $\delta^{18}O$ ($\delta^{18}O_c$) at each site was assessed by examining the standard deviation of $\delta^{18}O_c$ measured on different shells from a single site. This assessment included both modern shell samples and samples from specific archaeological deposits. The variation in values of $\delta^{18}O_c$ between the modern samples at measured sites was then examined to determine if any variation existed which exceeded the average variation for measured shells at a single site. To examine the variability on a single shell, 10 measurements were made of one shell from Roberts Haven (^{14}C sample code GU-10929). The average $\delta^{18}O_c$ measured for shells from the archaeological deposits was then compared to the measured values for the modern samples from each of the six sites.

The relationship between temperature, water $\delta^{18}O$ and shell $\delta^{18}O$ is different for the two main species of carbonate, aragonite and calcite. Analysis of *Patella vulgata* using X-Ray diffraction showed that the shells of this species are composed of calcite. The relationship between biogenic calcite $\delta^{18}O$ ($\delta^{18}O_c$), water $\delta^{18}O$ ($\delta^{18}O_w$) and water temperature (T) is given by:

$$T = 16.9 - 4.38(\delta^{18}O_c - \delta^{18}O_w) + 0.10(\delta^{18}O_c - \delta^{18}O_w)^2$$

(Equation A.1 (O'Neil *et al.*, 1969; Wefer and Berger, 1991))

Both $\delta^{18}O_c$ and $\delta^{18}O_w$ values are expressed relative to VPDB, where $\delta^{18}O_w$ was converted from the VSMOW to the VPDB scales using a correction value of -0.27‰ (Hut, 1987; Bemis *et al.*, 1998).

$$\delta^{18}O_{w\,(VPDB)} = \delta^{18}O_{w\,(SMOW)} - 0.27$$

(Equation A.2)

By using Equation A.2 and a rearranged version of Equation A.1 (Equation A.3) it is possible to calculate a predicted value of *Patella vulgata* $\delta^{18}O_c$ that is based upon the measured values of $\delta^{18}O_w$ together with the water temperature values from the FRS monitoring station closest to each site.

$$\delta^{18}O_c = \left(\left(\frac{16.9 - T}{4.38}\right) + \delta^{18}O_w\right)$$

(Equation A.3)

For each site the maximum (ie. indicating warmest/most saline conditions) and minimum (ie. indicating coldest/least saline conditions) predicted values of $\delta^{18}O_c$ were calculated. These were then compared with the average of the two measured samples at each site. This allowed an examination of whether the relationship between measured $\delta^{18}O_w$ and $\delta^{18}O_c$ at the sampled sites corresponded to that predicted by the palaeotemperature equation (Equation A.1). It must be noted that within this assessment only the summer $\delta^{18}O_w$ values had been measured at the sample sites. The relationship between $\delta^{18}O_w$ and temperature generally means that at lower (i.e. winter) atmospheric temperatures, the $\delta^{18}O_w$ of coastal water is higher. The predicted range of $\delta^{18}O_c$ at equilibrium calculated within this study for the sample sites is therefore a preliminary assessment.

A.3 Results

Coastal water characteristics across the study area

The average range in sea surface temperature (SST) and sea surface salinity (SSS) for the four FRS monitoring stations shows an overall northward decrease in both variables (Table A.4). In comparison to open ocean waters of the North Atlantic Current (NAC) between 50°-64°N and 10°-30°W, the annual range in SST is comparable to that of open ocean waters, while the SSS's are lower than values measured for the NAC.

	SST (^{0}C)			**SSS (‰)**		
Site	**Max**	**Min**	**Range**	**Max**	**Min**	**Range**
NAC	Between 18-12	Between 12-6	6.00	35.7	35.2	0.5
Scalloway	13.45	5.86	7.59	35.13	33.6	1.53
Fair Isle	12.07	6.66	5.41	N/A	N/A	N/A
Skapa Flow	13.78	6.09	7.69	34.79	34.19	0.6
Lochmaddy	13.9	N/A	N/A	34.64	32.83	1.81

Table A.4: Calculated mean SST and SSS for sites monitored by the Scottish Fisheries Research Centre (FRS). Data from FRS, data for NAC waters from Levitus, (1982); Levitus, and Boyer (1994); Rossby *et al.,* 1998.

For the samples of coastal water, the average of the measured $\delta^{18}O_w$ values at the 19 sample sites range from -0.3‰ to 0.5‰ (a range of 0.8‰). The average range in measured values of $\delta^{18}O_w$ at a single site is 0.4‰. The variability in $\delta^{18}O_w$ at a single site is higher than average at seven sites, of which four sites (**LO**, **PB**, **StB**, and **BB**) show variability on two measurements of greater than 0.7‰. The average variability on measurements at individual sites excluding these four sites is 0.2‰. This effect remains unexplained, and may be the result of measurement variability or non-homogeneity within the measured samples.

Site	Aliquot 1 $\delta^{18}O_w$ (SMOW)	Aliquot 2 $\delta^{18}O_w$ (SMOW)	Average $\delta^{18}O_w$ (SMOW)	Range of measured $\delta^{18}O_w$ (SMOW)
UJ	-0.5	-0.1	-0.3	0.4
LO	1.0	-0.1	0.5	1.1
PB	0.7	-0.1	0.3	0.8
StB	0.8	-0.2	0.3	1.0
QG	-0.1	-0.5	-0.3	0.4
BB	-1.0	-0.2	-0.6	0.8
SkB	-0.3	-0.2	-0.3	0.1
SF	-0.0	0.5	0.3	0.5
GA	0.1	0.0	0.1	0.1
BO	0.0	0.0	0.0	0.0
BE	0.1	0.2	0.2	0.1
NO	0.1	-0.1	0.0	0.2
HP	0.2	0.4	0.3	0.2
BA	0.4	0.3	0.4	0.1
LM	0.4	0.3	0.4	0.1
RH	0.3	0.2	0.3	0.1
FL	-0.0	-0.2	-0.1	0.2
SA	0.1	0.2	0.2	0.1
CMB	-0.2	0.4	0.1	0.6

Table A.5: Measured July values of $\delta^{18}O_W$ (SMOW).

The $\delta^{18}O$ terrestrial freshwater from a stream at the east of Skapa Flow gave an average $\delta^{18}O_w$ of -7.4‰. This indicates that the terrestrial freshwater end member for the study area conforms to typical values for meteoric precipitation for Western Europe (-5 to -15‰).

Site	Aliquot 1 $\delta^{18}O_w$ (SMOW)	Aliquot 2 $\delta^{18}O_w$ (SMOW)	Average $\delta^{18}O_w$ (SMOW)	Range of measured $\delta^{18}O_w$ (SMOW)
SF (terrestrial freshwater)	-7.6	-7.3	-7.4	0.30

Table A.6: Measured values of $\delta^{18}O$ for terrestrial freshwater runoff water in proximity to Skapa Flow.

In comparison to typical open ocean $\delta^{18}O_w$ values and the typical and measured terrestrial (meteoric) freshwater $\delta^{18}O_w$, the coastal water samples correlate more closely with a marine end member. This can be shown by calculating a salinity (S) value from the average measured $\delta^{18}O_w$ at each site using the regional salinity: $\delta^{18}O_w$ mixing line between fully fresh and fully marine water for Scottish west coast waters calculated by Austin and Inall, (2002). This is defined by the relationship:

$$\delta^{18}O_w = S*0.18 - 6.0$$

(Equation A.4)

The salinity values for all 19 coastal sites calculated from the average measured $\delta^{18}O_w$ values using the above relationship appear to be more consistent with a dominantly marine water end member (see Figure A.2). It was possible to plot measured values of both salinity and $\delta^{18}O_w$ from two sites, **LM** and **SF**, using the available FRS salinity monitoring data from these sites. These data appear to be in good agreement with the relationship predicted by the Austin and Inall, (2002) mixing line

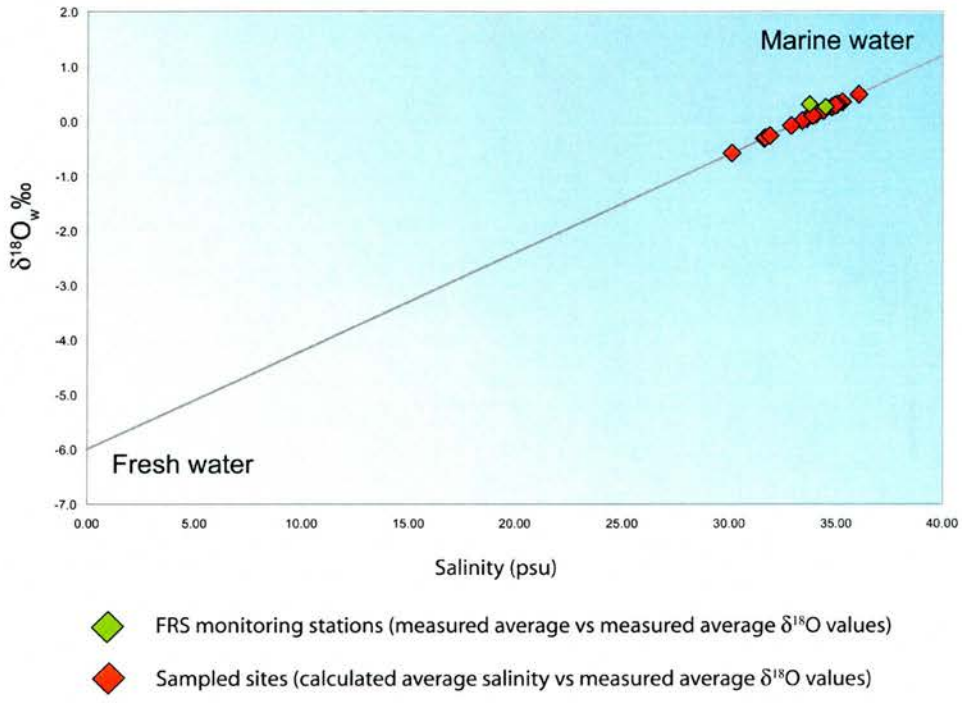

Figure A.2: Red diamonds show measured average $\delta^{18}O_w$ values for sampled sites versus salinities calculated using the Austin and Inall, (2002) regional salinity: $\delta^{18}O_w$ mixing line for Scottish west coast waters. The green diamonds indicate measured average annual salinity versus the average $\delta^{18}O_w$ values measured in this study at FRS monitoring sites **LM** and **SF**. The Austin and Inall, (2002) mixing line is indicated on the graph.

Although the measurement reproducibility discussed above limits the resolution to which potential differences in $\delta^{18}O_w$ between sampled sites can be identified, the values show some variation between 4 main areas. In Area A (mainland Scotland) the $\delta^{18}O_w$ at **RH** (0.3‰) is similar to that of values on the west coast at **SA** (0.1‰) and **CMB** (0.6‰) within the average measurement reproducibility (0.4‰). The $\delta^{18}O_w$ at **FL** (-0.1‰) appears to be lower than that

of **CMB**, though similar to the other two sites from this area. In Area B (Outer Hebrides), the variability in $\delta^{18}O_w$ over seven sites shows a low level of variability, ranging from 0.0‰ (**NO** and **BO**) to 0.4‰ (**LM** and **BA**). This contrasts with the variation within Area C (Orkney Isles), where the $\delta^{18}O_w$ over seven sites ranges between -0.6‰ (**BB**) and 0.5‰ (**LO**). The three lower $\delta^{18}O_w$ values in Area C (**BB** (-0.6‰), **SkB** (-0.3‰) and **QG** (-0.3‰)) are located on the western coastline of the mainland and Westray, whereas the four higher $\delta^{18}O_w$ values in this area (**LO** (0.5‰), **PB** (0.3‰), **StB** (0.3‰) and **SF** (0.3‰) are located further east within the Orkney Island group. The $\delta^{18}O_w$ value for **UJ** within Area D (Faroe Isles) is -0.3‰ and therefore appears to be similar to that of lower values from the Orkney Isles.

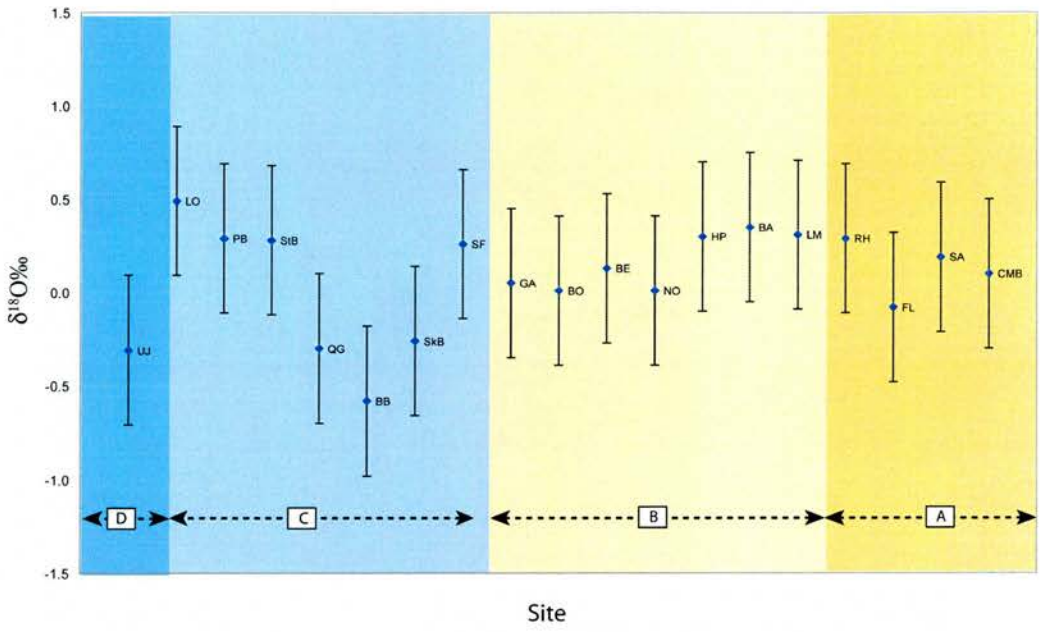

Figure A.3: variation in $\delta^{18}O_w$ at sampled sites showing average variation in values at a single site. Shaded areas indicate different geographic areas (see Figure A.1), A: mainland Scotland; B: Outer Hebrides; C: Orkney Isles; D: Faroe Isles.

Modern $\delta^{18}O_c$ of Patella vulgata shells across the study area

The average measured $\delta^{18}O_c$ values at the 19 modern sampled sites ranged between 3.5‰ to 1.7‰ (range of 1.8‰). The average difference in measured values from two individual shells from each of these sites was 0.2‰. At two sites (**LO** and **HP**) however, a difference of 0.6‰ was observed between two measured shells from each site. The average difference between measurements from the remainder of the sites was 0.1‰. During the course of

sample measurement, 10 repeat analyses were performed upon a single shell from an archaeological deposit at **RH**. The standard deviation in $\delta^{18}O_c$ of these measurements was 0.3‰. This apparent variability in repeat measurements of an individual shell appears to be relatively large, and it is possible that this could represent heterogeneity in $\delta^{18}O_c$ across an individual *Patella vulgata* specimen that has not been resolved by homogenising a larger section of the shell for measurement. More detailed investigation of this effect is outwith the scope of this preliminary study but it is possible that seasonal variations in $\delta^{18}O_w$ of the ambient water are recorded in the $\delta^{18}O_c$ of *Patella vulgata* that may be resolved by further study.

The average $\delta^{13}C$ of the measured shell carbonates ($\delta^{13}C_c$) from the 19 sample sites ranges from -0.8‰ to 0.9‰ (range of 1.7‰), with an average difference between measurements at a single site of 0.5‰. The variability in $\delta^{13}C_c$ at the sampled sites appears to be much greater than that of $\delta^{18}O_c$ measurements upon the same shells, and at two sites (**PB** and **LM**) the difference in $\delta^{18}O_c$ on two shells is greater than 1‰.

Site	Average $\delta^{18}O$‰	Difference	Average $\delta^{13}C$‰	Difference
UJ	3.0	0.0	0.9	0.0
LO	3.5	0.6	-0.2	0.2
PB	2.6	0.2	-0.5	1.2
StB	2.9	0.0	-0.5	0.5
QG	2.0	0.0	-0.1	0.7
BB	2.6	0.2	0.0	0.3
SkB	2.5	0.1	-0.4	0.6
SF	2.6	0.4	0.2	0.4
GA	2.7	0.2	1.5	0.6
BO	2.1	0.1	0.3	0.2
BE	2.4	0.2	-0.3	0.1
NO	1.7	0.0	-0.6	0.5
HP	2.5	0.6	-0.8	0.5
BA	2.5	0.0	-0.3	0.5
LM	2.7	0.2	0.5	0.1
RH	2.1	0.0	-0.2	1.0
FL	1.7	0.1	-0.6	0.4
SA	2.3	0.3	0.0	0.4
CMB	2.3	0.0	-0.4	0.5

Table A.7: Measured values of $\delta^{18}O_c$ for sampled sites. Each value and associated difference is produced from the measured values of two individual shells from each site.

In contrast to the measured $\delta^{18}O_w$ values the variation in $\delta^{18}O_c$ between the 19 sampled sites appears to include greater variability within all sampled areas. The most homogeneous

geographical zone appears to be that of Mainland Scotland, where the $\delta^{18}O_c$ values of **SA** (2.3‰), **CMB** (2.3‰) and **RH** (2.1‰) are similar, and the value from **FL** is lower (1.7‰). In the Outer Hebrides region the $\delta^{18}O_c$ of five sites (**LM**, **BA**, **HP**, **BE** and **GA**) range between 2.7‰ and 2.4‰, with lower values at **NO** (1.7‰) and **BO** (2.1‰). On the Orkney Isles the variability is higher then in other areas, with four sites (**SF**, **SkB**, **BB**, and **PB**) ranging between 2.5 and 2.6, while a lower value is recorded at **QG** (2.0‰) and higher values at **StB** (2.9‰) and **LO** (3.5‰). A higher than average value compared to other geographical areas is also recorded on the Faroe Isles at **UJ** (3.0‰).

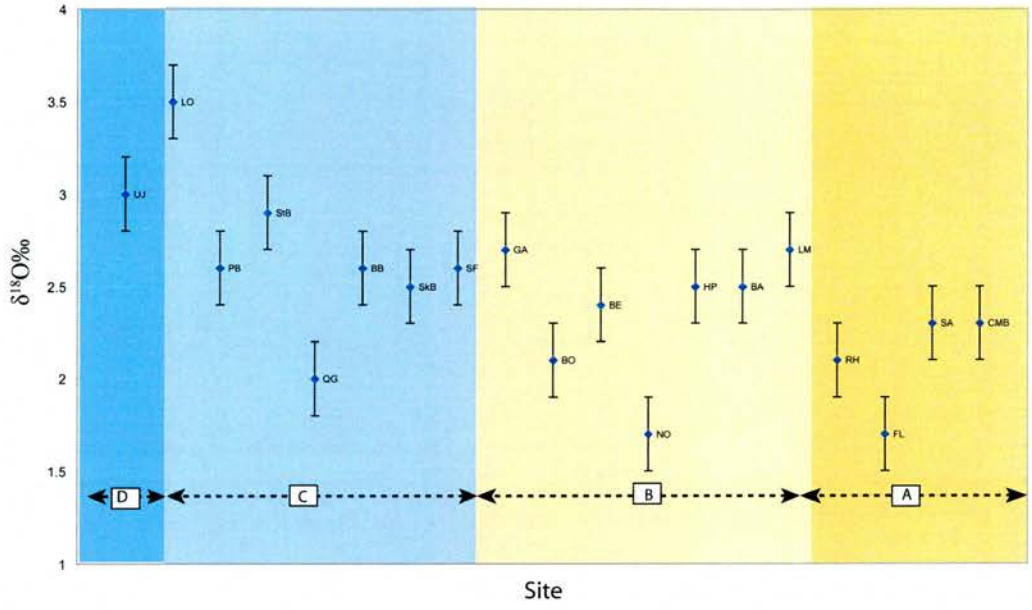

Figure A.4: variation in $\delta^{18}O_c$ of modern samples at sites showing average difference in values at a single site.

Calculation of predicted $\delta^{18}O_c$ using measured $\delta^{18}O_w$ and comparison with measured $\delta^{18}O_c$

	Measured $\delta^{18}O_c$	Predicted $\delta^{18}O_c$		Water temperature		$\delta^{18}O_w$
Site	**Average**	**Min**	**Max**	**Min**	**Max**	**Average**
UJ	3.0	0.2	2.0	13.45	5.86	-0.3
LO	3.5	0.9	2.7	6.09	13.78	0.5
PB	2.6	0.7	2.5	6.09	13.78	0.3
StB	2.9	0.7	2.5	6.09	13.78	0.3
QG	2.0	0.1	1.9	6.09	13.78	-0.3
BB	2.6	-0.2	1.6	6.09	13.78	-0.6
SkB	2.5	0.1	1.9	6.09	13.78	-0.3
SF	2.6	0.7	2.5	6.09	13.78	0.3
GA	2.7	0.5	2.3	6.09	13.9	0.1
BO	2.1	0.4	2.2	6.09	13.9	0.0
BE	2.4	0.6	2.4	6.09	13.9	0.2
NO	1.7	0.4	2.2	6.09	13.9	0.0
HP	2.5	0.7	2.5	6.09	13.9	0.3
BA	2.5	0.8	2.6	6.09	13.9	0.4
LM	2.7	0.8	2.6	6.09	13.9	0.4
RH	2.1	0.7	2.5	6.09	13.9	0.3
FL	1.7	0.3	2.1	6.09	13.9	-0.1
SA	2.3	0.6	2.4	6.09	13.9	0.2
CMB	2.3	0.5	2.3	6.09	13.9	0.1

Table A.8: Measured versus predicted values of $\delta^{18}O_c$‰ for modern marine molluscs

As the maximum (low water temperature) values of predicted $\delta^{18}O_c$ are calculated using summer measured $\delta^{18}O_w$ values, these appear somewhat higher than would be the case if they had been calculated using measurements of low temperature $\delta^{18}O_w$ from the sample sites. It is possible, using the salinity: $\delta^{18}O_w$ mixing line equation of Austin and Inall, (2002) to predict a low temperature value of $\delta^{18}O_w$ for the three FRS monitoring stations (Lochmaddy, Skapa Flow and Scalloway) where water temperature and salinity data are available (see Table A.4). These predicted values can be used to estimate a low temperature $\delta^{18}O_c$ for the general areas of i. Mainland Scotland and the Outer Hebrides, ii. the Orkney Isles and iii. the Faroe Isles, and these are shown in Figure A.5 as a dashed line. The predicted $\delta^{18}O_c$ values based upon measured $\delta^{18}O_w$ from the sample sites are however presented in Figure A.5 and used in interpretation as these data allow higher resolution variation in $\delta^{18}O_w$ between the sample sites to be preserved.

The pattern of site-to-site variation in the equilibrium values of $\delta^{18}O_c$ predicted from measurements of $\delta^{18}O_w$ at 19 sites appears to be in agreement with the average values of $\delta^{18}O_c$ measured on *Patella vulgata* specimens from these sites (Figure A.5). The measured values of $\delta^{18}O_c$ from the 19 sample sites all appear closer to the maximum predicted $\delta^{18}O_c$ values, indicating that the measured shells were precipitated at lower water temperatures.

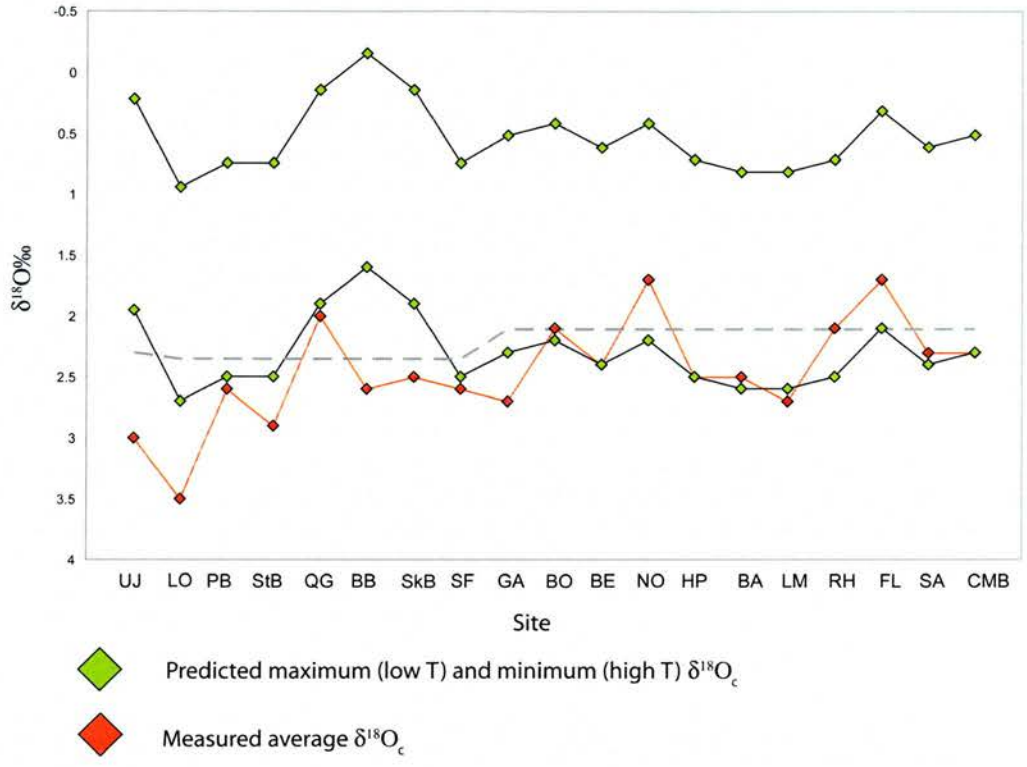

Figure A.5: Predicted equilibrium values of $\delta^{18}O_c$ for the sample sites showing the average measured value of $\delta^{18}O_c$ at each site. The dashed line indicates low temperature $\delta^{18}O_c$ based upon salinity measurements from three FRS monitoring stations and the Austin and Inall, (2002) salinity: $\delta^{18}O_w$ mixing line.

Comparison of modern and fossil $\delta^{18}O_c$ data

	Modern samples	Archaeological samples	
Site	**Average $\delta^{18}O_c$**	**Average $\delta^{18}O_c$**	**Cal. age range BC/AD**
SkB	2.5 ± 0.1	2.4 ± 0.1	2870-2500 BC
BB	2.6 ± 0.2	2.4 ± 0.2	2130-1940 BC
BA	2.5 ± 0.0	2.9 ± 0.2	400-200 BC
HP	2.5 ± 0.6	2.6 ± 0.2	350-50 BC
StB	2.9 ± 0.0	2.7 ± 0.1	1020-1160 AD
RH	2.1 ± 0.0	2.5 ± 0.4	1040-1220 AD

Table A.9: Comparison of mean $\delta^{18}O_c$ from modern and archaeological shells from 6 sites.

The average $\delta^{18}O_c$ of the archaeological *Patella vulgata* samples from six sites ranges from 2.4‰ (**SkB** and **BB**) to 2.9‰ (**BA**), while the average $\delta^{18}O_c$ of modern *Patella vulgata* samples from the same sites ranges between 2.1‰ (**RH**) to 2.9‰ (**StB**). The average variability on the archaeological shell samples is 0.2‰ and the average variability on the modern shell samples is 0.1‰. At four sites, (**SkB**, **BB**, **HP** and **StB**) the difference between average $\delta^{18}O_c$ values of modern and fossil shells is 0.2‰ or less, however at **RH** and **BA** the average archaeological and modern $\delta^{18}O_c$ values differ by 0.4‰.

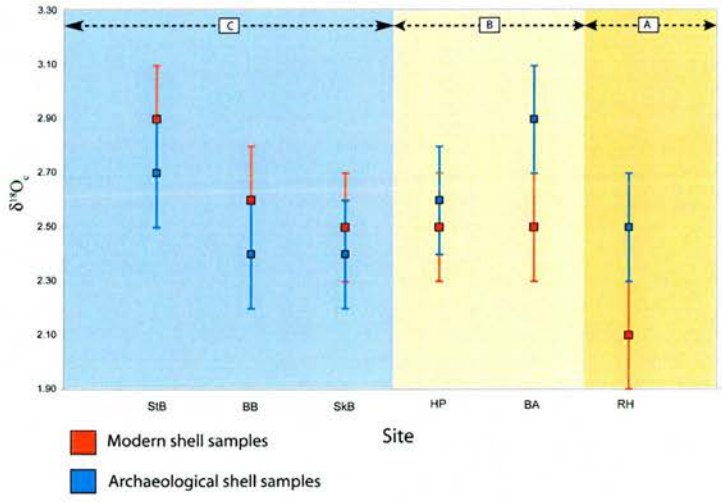

Figure A.6: Comparison of mean $\delta^{18}O_c$ measured at six sites from archaeological and modern *Patella vulgata* specimens. Modern values are shown in red and archaeological

values in blue. The larger of the average variability on the archaeological and modern shell samples is shown.

A.4 Interpretations

Coastal water characteristics across the study area

The overall northward decrease in annual SST range at the FRS monitoring sites reflects known climatic gradients in the North Atlantic, where annual atmospheric temperatures decrease with increasing latitude. Coastal water salinities are generally reduced relative to open ocean values because a component of coastal water is derived from terrestrial (meteoric) runoff, which is reflected in the SSS values at the monitoring stations, which are lower than those of the NAC (Table A.4). A dominantly marine end member at all of the 19 measured sample sites is however indicated by the average $\delta^{18}O_w$ values and the corresponding water salinities calculated from these. At no site is an anomalously large freshwater input to the coastal water indicated from these data, suggesting that the surface water in these locations is representative of typical coastal water composition. The protocol by which archaeological sites were selected within this thesis for ^{14}C measurement therefore appears to have been effective in excluding sites where the modern surface water isotopic composition is significantly influenced by freshwater sources away from typical coastal water values.

Although the average $\delta^{18}O_w$ values from the sampled sites appear typical of coastal water, variability in these values is apparent between the sampled sites. The relative homogeneity of samples from mainland Scotland and the Outer Hebrides may reflect consistency in coastal water characteristics at these sites, while the greater variation in $\delta^{18}O_w$ between sites within the Orkney Isles indicates differences in coastal water temperature and/or salinity exist at the samples sites in this area. Overall, the highest values of sampled sites are recorded in the north of the study area on the Orkney Isles. A northward increase in $\delta^{18}O_w$ is consistent with decreasing temperatures at higher latitudes.

The three lower $\delta^{18}O_w$ values within the Orkney Isles are located on more exposed west Island coasts, in comparison to **LO**, **PB**, **StB** and **SF**, which are located further east within the island group. However, this difference does not readily explain the differences in measured $\delta^{18}O_w$ values, as the coastal water that influences **QG**, **SkB** and **BB** would be expected to be cooler and more saline than the eastern sites being derived more directly from

the eastward flow of open ocean waters. The preliminary nature of this study limits the resolution to which these potential site-specific variations can be assessed, particularly as the temporal record of $\delta^{18}O_w$ at the sites is restricted to individual summer measurements. It is desirable to examine these effects in more detail however, and a longer-term average record of $\delta^{18}O_w$ values from the sites is required in order to achieve this.

Modern $\delta^{18}O_c$ of Patella vulgata shells across the study area

The general pattern in $\delta^{18}O_w$ is consistent with that observed in the $\delta^{18}O_c$ measurements from the 19 sample sites. This correlation indicates that *Patella vulgata* precipitates its shell carbonate in equilibrium with the ambient water, and that both the $\delta^{18}O_w$ and $\delta^{18}O_c$ measurements within this study are valid assessments of the isotopic composition of coastal water and shell carbonates from the sample sites. The data suggest an overall northward increase in $\delta^{18}O_c$ similar to that in the $\delta^{18}O_w$ measurements from the sample sites. Along with the influence of increasing $\delta^{18}O_w$ in the ambient water, increasing $\delta^{18}O_c$ is also a function of decreasing temperatures, which is consistent with the northward climatic gradient in the North Atlantic.

Calcareous organisms may precipitate their shell carbonate in isotopic disequilibrium with that of the ambient water due to metabolic effects that may be specific to species, and these effects appear to be common with respect to carbon isotopes (Wefer and Berger, 1991). The apparently high variability in measured $\delta^{13}C_c$ at the measured sites indicates that along with the isotopic composition of the ambient water, biological effects influence the $\delta^{13}C_c$ of *Patella vulgata*.

Calculation of predicted $\delta^{18}O_c$ using measured $\delta^{18}O_w$ and comparison with measured $\delta^{18}O_c$

The indication (from measured $\delta^{18}O_w$ and $\delta^{18}O_c$) that *Patella vulgata* within the study area precipitates its shells in isotopic equilibrium with the ambient water is supported by the results of predicted $\delta^{18}O_c$ from the sample sites. From Figure A.5 it can be seen that the measured values are similar to the equilibrium values predicted from the modified palaeotemperature equation (Equation A.3). However, the measured $\delta^{18}O_c$ values lie much closer to the maximum predicted values, which reflect lower water temperatures, however, the fastest season of growth for *Patella vulgata* appears to be the summer (Hill, 2000). The results of the predicted and measured $\delta^{18}O_c$ within this study may therefore be the result of

two factors. Firstly, it is possible that rather than precipitating shell material in isotopic equilibrium, there is a positive offset in *Patella vulgata* $\delta^{18}O_c$. These effects have been identified in other marine organisms (e.g. corals). For example, Burman and Schmitz, (2005) found that $\delta^{18}O_c$ precipitated by *Littorina littorea*, another intertidal gastropod in Denmark fjord sites was enriched by c.2‰ relative to theoretical $\delta^{18}O$ isotopic equilibrium. Such an offset would shift the measured $\delta^{18}O_c$ values significantly closer to the values predicted from the maximum water temperatures (i.e. summer values) from the FRS monitoring station data. Secondly, from examination of the water temperature data at the monitoring stations (Table A.9), low temperatures persist in these locations until the month of April, rising above 10^0C from June onwards. It is possible that at the study region latitudes *Patella vulgata* grows a larger portion of its shell material (in equilibrium) during the spring time than is otherwise assumed, and that this is reflected in the measured $\delta^{18}O_c$ of shells from the study sites.

Month	**Lochmaddy water temp (^{0}C)**	**Skapa Flow water temp (^{0}C)**	**Fair Isle water temp (^{0}C)**	**Scalloway water temp (^{0}C)**
January	N/A	6.83	7.25	6.63
February	N/A	6.09	6.66	5.86
March	7.9	6.59	6.96	6.25
April	8.7	7.77	7.54	7.64
May	9.9	9.56	8.73	9.66
June	11.6	11.57	10.24	11.38
July	12.9	12.59	11.28	12.61
August	13.9	13.78	12.07	13.45
September	13.6	13.31	11.89	12.45
October	11.9	11.60	10.95	10.78
November	11.1	9.64	9.45	8.86
December	10.3	8.05	8.19	7.82

Table A.10: Monthly average water temperature data from the FRS monitoring stations within the study area.

Comparison of modern and fossil $\delta 18O_c$ data

The assessment of $\delta^{18}O_c$ from modern and archaeological *Patella vulgata* shells at six sites shows a difference of 0.4‰ at two sites (**BA** and **RH**), while the $\delta^{18}O_c$ of shells from the other four sites are indistinguishable at the resolution afforded within this study. These data indicate that the average SST and/or SSS at the archaeological sites at the time the shells were precipitated were comparable to modern values on the Orkney Isles for the periods 2870-2500 BC (**SkB**), 2130-1940 BC (**BB**) and 1020-1160 AD (**StB**). The apparent

difference in $\delta^{18}O_c$ between modern and fossil shells on the Outer Hebrides (at **BA**) for the period 400-200 BC is however not reflected in the data for **HP**, which is located in close proximity and relates to the comparable time period 350-50 BC. The archaeological samples from **RH** are dated to a comparable time period (1040-1220 AD) to that of **StB**, where no difference in archaeological and modern $\delta^{18}O_c$ can be identified. It is difficult therefore to state to what extent variations between the $\delta^{18}O_c$ of modern and archaeological shells from the sites are extant. The measurements were produced from homogenised whole shells samples, meaning that seasonal variations in $\delta^{18}O_c$ are not resolved in these data. Examination of such seasonal variations within *Patella vulgata* was outwith the scope of this study; however it is possible that an investigation of these characteristics could identify differences in the seasonal temperature and/or salinity ranges between modern and archaeological shells at the sample sites.

A.5 Conclusions

The results of this preliminary study demonstrate the potential for added value to be obtained from marine mollusc shells from archaeological sites, and of the value of further investigation of coastal $\delta^{18}O_w$ and $\delta^{18}O_c$ within the climatically sensitive study area. The results of the investigation indicate that the site selection protocol by which samples were obtained within this thesis for ^{14}C measurement was successful in excluding sites at which there is an anomalously high freshwater input. The limited nature of the investigation precludes a detailed interpretation of $\delta^{18}O_w$ and mollusc shell $\delta^{18}O_c$ across the study area; however it does highlight potential variation in $\delta^{18}O_w$ and $\delta^{18}O_c$ across this region. This suggestion could be further investigated by a more intensive assessment that could incorporate information concerning annual variations in $\delta^{18}O_c$ and $\delta^{18}O_w$. In particular the potential of *Patella vulgata* within such further investigations should be noted, as the prevalence of this species within both modern and prehistoric settings may mean that it is a useful source of palaeoclimatic proxy data.

Appendix B: Calculation of ΔR at Hrísheimar, Iceland.

B.1 Introduction

During the course of this thesis an opportunity arose to obtain samples from Hrísheimar, Iceland, a site at which excavation was being undertaken as part of research programmes funded by the Leverhulme trust and the National Science Foundation of America. The site at Hrísheimar is a farm with associated midden deposits located in the interior highland basin of Lake Mývatn, north Iceland. This afforded the possibility of extending the spatial range of the dataset, particularly with respect to providing additional data to the Faroe Isles site of Undir Junkarinsfløtti.

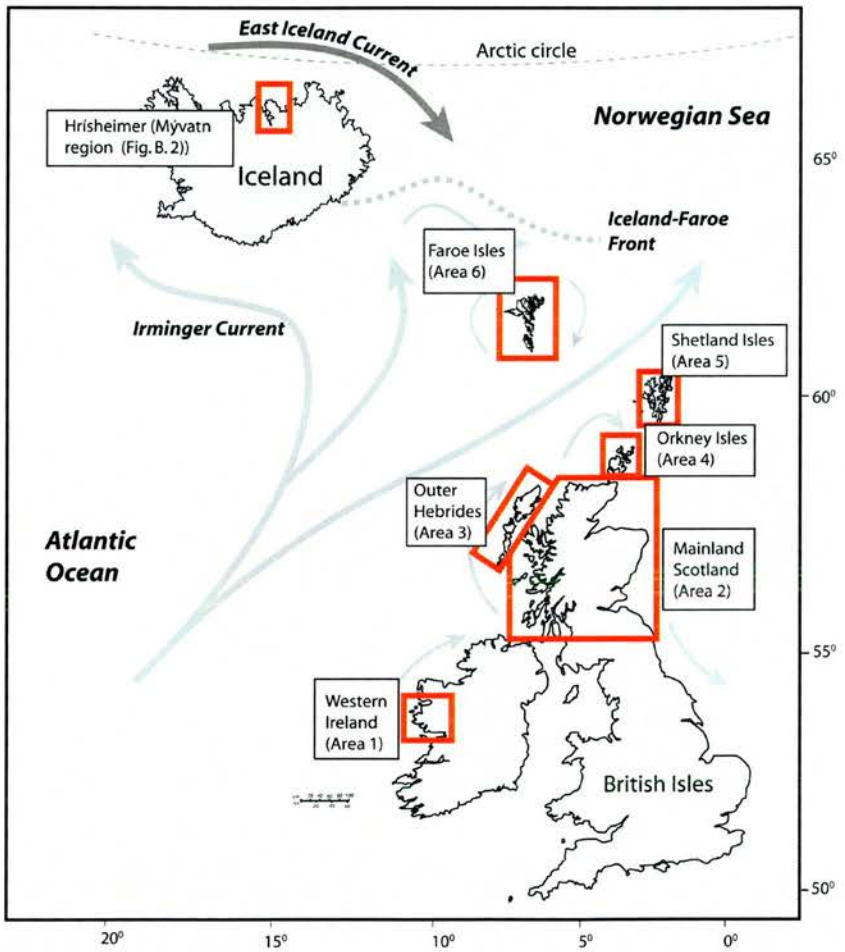

Figure B.1: Location of Hrísheimar relative to the sites from which material for measurement was obtained during this thesis, showing modern surface circulation patterns of Atlantic (grey arrows) and Arctic (black arrows) derived currents.

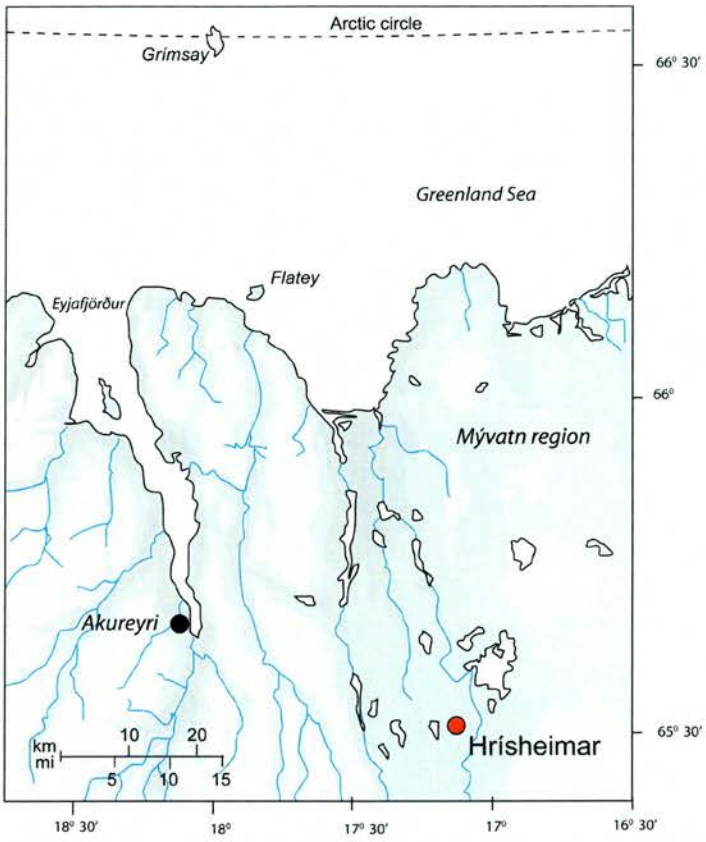

Figure B.2: Location of Hrísheimar within the Mývatn area. (north Iceland).

Modern northern Iceland is a low Arctic environment with a climate that is significantly colder than the south of Iceland due to the influence of the East Icelandic Current (EIC), derived from the southward-flowing Arctic waters of the East Greenland current. The North Iceland shelf is positioned close to the modern Polar Front, which separates the waters of the EIC from the Atlantic-derived waters of the Irminger Current (IC) as it flows clockwise around Iceland. This means that the area contains a series of sensitive oceanographic and climatic fronts, the position of which appears to have fluctuated over the Holocene according to data from both historical and palaeoenvironmental records (Ogilvie, 1996; Knudsen *et al.*, 2004). Hrísheimar forms one of a large number of settlements identified in the Mývatn region (Mývatnssveit), dated to between the 9^{th} – 12^{th} centuries AD (McGovern *et al.*, 2005). Excavations revealed that although Hrísheimar is situated c.60 km from the present coastline, the archaeological fauna that had been incorporated into midden deposits contained a significant proportion of marine resources, including seal bones, marine fish, sea bird bones and mussel shells (McGovern *et al.*, 2005; Perdikaris and McGovern, 2005).

B.2 Methodology

The inland location of Hrísheimar required modifications of the site selection protocols applied to coastal sites. Sample material was obtained from context 45 (**HR-45**), which was a stratigraphically contained midden deposit in the upper site sequence. The material comprised four individual neo-natal cow bones (*Bos sp.*), and four individual mussel shells (*Mytilus edulis*). Sample pretreatment procedures followed those outlined in Chapter 4 for terrestrial mammal bone and marine mollusc shells, as did the evolution of sample CO_2 and production of graphite targets for AMS analysis. The sample $^{14}C/^{13}C$ ratios were measured on the SUERC facility. The contemporaneity of groups of terrestrial and marine sample ^{14}C ages were assessed using the χ^2 test (c.f. Ward and Wilson, 1978), and sample ages that were similar were used to calculate ΔR, following the procedure in Chapter 4 (section 4.2.3). A 2σ calibrated age range was calculated for **HR-45** using a weighted mean value of terrestrial measurements that were statistically the same on the basis of a χ^2 test. The weighted mean terrestrial age BP was then converted to a calibrated range using the INTCAL04 atmospheric dataset (Reimer *et al.*, 2004) and the OxCal v3.10 calibration program (Bronk Ramsey, 1995; 2001).

B.3 Results

	Terrestrial samples			**Marine samples**		
Context	**Lab Code**	**Age BP ± 1σ**	**$\delta^{13}C$ (‰)**	**Lab Code**	**Age BP ± 1σ**	**$\delta^{13}C$ (‰)**
45	6431	1220 ± 35	-21.5	6438	1650 ± 40	0.8
	6432	1200 ± 35	-21.4	6439	1610 ± 35	-0.3
	6433	1120 ± 35	-21.7	6440	1595 ± 35	0.3
	6437	1120 ± 35	-21.6	6441	1615 ± 35	0.6

Table B.1: Measurement results for samples from **HR-45**

T-statistic (Terrestrial)	*T*-statistic (Marine)	Terrestrial weighted mean	Cal. age range (2σ)	ΔR
6.78 ($\chi^2_{:0.05} = 7.81$)	1.11 ($\chi^2_{:0.05} = 7.81$)	1165 ± 26 ^{14}C y	778-963 AD	96 ± 15 ^{14}C y

Table B.2: Calculated *T*-statistics, weighted mean terrestrial ^{14}C age, calibrated age range and ΔR value based upon measurements from **HR-45**

The χ^2 test showed that the groups of marine and terrestrial sample ^{14}C ages were statistically similar with *T*-statistics of $T = 6.78$ ($\chi^2_{:0.05} = 7.81$) for the group of four terrestrial sample ages and $T = 1.11$ ($\chi^2_{:0.05} = 7.81$) for the four marine sample ages. The 2σ calibrated age range for the weighted mean terrestrial ^{14}C age for the group of samples from **HR-45** is 778-963 AD, and calculated ΔR value was 96 ± 15 ^{14}C y.

B.4 Interpretations

The calibrated age range of **HR-45** is consistent with other determinations made from this site, where the calibrated ranges of these measurements at 2σ lay between 770 - 1020 AD (McGovern *et al.*, 2005). These were measured on nine individual samples of cow and pig bone from contexts including midden deposits and a deflated upper site deposit (McGovern *et al.*, 2005). When the 2σ calibrated age range of **HR-45** is compared to other contexts for which ΔR was calculated within this study, it is similar to four individual contexts from the west coast of Ireland (Area 1: contexts **DL3-19** (ΔR = -107 ± 18) and **DL11-2** (ΔR = -69 ± 17)) and the Outer Hebrides (Area 3; contexts **BO-64** (ΔR = -57 ± 14) and **GA-156** (ΔR = -89 ± 17)). The ΔR value from **HR-45** (96 ± 15 ^{14}C y) is compared with the values from these contexts in Chapter 6 (section 6.2.7). This comparison shows a difference in the ΔR from **HR-45**, which is significantly higher than values from both sites in Area 1 for the period 660-820 AD and sites in Area 3 for the period 778 – 990 AD. This may indicate spatial variability in surface ocean ^{14}C between the Areas for these time periods. Such a variation is comparable to that observed at c.1000 AD between Ireland, the Outer Hebrides and the Faroe Isles, which involves an overall northward increase in ΔR, with the highest values located on the Faroe Isles. The ΔR value from **HR-45** is similar to the value for the Faroe Isles at c.1000 AD (**UJ-23**; 64 ± 13 ^{14}C y) where $T = 2.60$ ($\chi^2_{:0.05} = 3.84$)), and also to the current regional mean value for Iceland and the Faroe Isles (52 ± 19 ^{14}C y (Reimer and Reimer, 2005)), where $T = 3.30$ ($\chi^2_{:0.05} = 3.84$). This may represent a spatial variability in ΔR during the period when the Norse settlers colonised Iceland (c.870-930 AD), that is comparable with the variation which exists today.

B.5 Conclusion

An opportunity to perform an assessment of ΔR for the north coast of Iceland is possible based upon measurements of neo-natal cow bones and mussel (*Mytilus edulis*) shells from the archaeological site of Hrísheimar. Material was selected for dating from the context **HR-45**, which gave a terrestrial weighted mean age of 1165 ± 26 ^{14}C y (778-963 AD at 2σ). The

resulting ΔR value from **HR-45** (96 ± 15 ^{14}C y) is similar to both the current regional mean value for Iceland and the Faroe Isles (53 ± 19 ^{14}C y), and a value for the Faroe Isles at c.1000 AD (64 ± 13 ^{14}C y), but is significantly higher than values from the west coast of Ireland and the Outer Hebrides of between -107 ± 18 ^{14}C y and -57 ± 14 ^{14}C y. This indicates that a spatial variation in ΔR existed between these areas for the periods 660-820 AD and 778 – 990 AD comparable to that which is observed in modern regional mean ΔR values within the North Atlantic.

Appendix C: Empirical assessment of ΔR values calculated for individual pairings of marine and terrestrial samples for each measured context.

The methodology used to determine ΔR for each measured context is described in Chapter 4 (section 4.2.3). From each context, terrestrial and marine samples were used to assess ΔR that had been selected on the basis of a χ^2 test for contemporaneity. Although the measurements within a group of terrestrial or marine samples selected on this basis were statistically similar at 95% confidence, the group of measurements were produced from separate individual samples and therefore had slightly different "underlying" ^{14}C ages. To account for any additional variability due to uncertainty about the precise pairing of terrestrial and marine samples, a value of ΔR was calculated for each possible pairing of terrestrial and marine ^{14}C ages from a context. The distribution was summarised by the weighted mean and appropriate standard error for prediction. The full data from these assessments is contained within the following tables, within which the individual contexts are ordered by relevant geographic area and ^{14}C age BP.

C.1 Area 1: Western Ireland

Context: DL3-19

Terrestrial samples		**Marine samples**		
Measurement No. (SUERC-)	**Age BP**	**Measurement No. (SUERC-)**	**Age BP**	**ΔR value (^{14}C y BP)**
1080	1335 ± 35	3188	1605 ± 35	-124 ± 45
1080	1335 ± 35	1089/3545	1515 ± 40	-214 ± 49
1080	1335 ± 35	1090/3189	1531 ± 34	-198 ± 44
1080	1335 ± 35	1091/3190	1583 ± 36	-146 ± 45
1085	1220 ± 35	3188	1605 ± 35	14 ± 69
1085	1220 ± 35	1089/3545	1515 ± 40	-76 ± 72
1085	1220 ± 35	1090/3189	1531 ± 34	-60 ± 69
1085	1220 ± 35	1091/3190	1583 ± 36	-8 ± 70
1086	1225 ± 35	3188	1605 ± 35	11 ± 70
1086	1225 ± 35	1089/3545	1515 ± 40	-79 ± 73
1086	1225 ± 35	1090/3189	1531 ± 34	-63 ± 70
1086	1225 ± 35	1091/3190	1583 ± 36	-11 ± 71
1087	1280 ± 35	3188	1605 ± 35	-61 ± 59
1087	1280 ± 35	1089/3545	1515 ± 40	-151 ± 62
1087	1280 ± 35	1090/3189	1531 ± 34	-135 ± 58
1087	1280 ± 35	1091/3190	1583 ± 36	-83 ± 60
			Weighted mean ΔR	**-107 ± 18**

Table C.1: ΔR values for individual pairings of terrestrial and marine samples for **DL3-19**.

Context: DL11-2

Terrestrial samples		**Marine samples**		
Measurement No. (SUERC-)	**Age BP**	**Measurement No. (SUERC-)**	**Age BP**	**ΔR value (^{14}C y BP)**
1842	1245 ± 50	1850	1590 ± 35	-30 ± 89
1842	1245 ± 50	1852	1595 ± 40	-25 ± 91
1842	1245 ± 50	1853	1545 ± 40	-75 ± 91
1842	1245 ± 50	1854	1535 ± 35	-85 ± 89
1847	1215 ± 35	1850	1590 ± 35	15 ± 58
1847	1215 ± 35	1852	1595 ± 40	20 ± 61
1847	1215 ± 35	1853	1545 ± 40	-30 ± 61
1847	1215 ± 35	1854	1535 ± 35	-40 ± 58
1848	1260 ± 35	1850	1590 ± 35	-67 ± 57
1848	1260 ± 35	1852	1595 ± 40	-62 ± 60
1848	1260 ± 35	1853	1545 ± 40	-112 ± 60
1848	1260 ± 35	1854	1535 ± 35	-122 ± 57
1849	1325 ± 35	1850	1590 ± 35	-102 ± 69
1849	1325 ± 35	1852	1595 ± 40	-97 ± 72
1849	1325 ± 35	1853	1545 ± 40	-147 ± 72
1849	1325 ± 35	1854	1535 ± 35	-157 ± 69
			Weighted mean ΔR	**-69 ± 17**

Table C.2: ΔR values for individual pairings of terrestrial and marine samples for **DL11-2.**

Context: OI-6

Terrestrial samples		**Marine samples**		
Measurement No. (SUERC-)	**Age BP**	**Measurement No. (SUERC-)**	**Age BP**	**ΔR value (^{14}C y BP)**
3226	970 ± 35	1076	1225 ± 35	-107 ± 70
3226	970 ± 35	1077	1220 ± 40	-112 ± 73
3226	970 ± 35	1078	1285 ± 35	-47 ± 70
3226	970 ± 35	1079	1170 ± 50	-162 ± 79
1073	945 ± 45	1076	1225 ± 35	-100 ± 70
1073	945 ± 45	1077	1220 ± 40	-105 ± 73
1073	945 ± 45	1078	1285 ± 35	-40 ± 70
1073	945 ± 45	1079	1170 ± 50	-155 ± 79
1074	1050 ± 35	1076	1225 ± 35	-195 ± 43
1074	1050 ± 35	1077	1220 ± 40	-201 ± 47
1074	1050 ± 35	1078	1285 ± 35	-136 ± 43
1074	1050 ± 35	1079	1170 ± 50	-251 ± 56
1075	980 ± 45	1076	1225 ± 35	-112 ± 74
1075	980 ± 45	1077	1220 ± 40	-117 ± 77
1075	980 ± 45	1078	1285 ± 35	-52 ± 74
1075	980 ± 45	1079	1170 ± 50	-167 ± 82
			Weighted mean ΔR	**-142 ± 16**

Table C.3: ΔR values for individual pairings of terrestrial and marine samples for **OI-6.**

C.2 Area 2: Mainland Scotland

Context: SA-013

Terrestrial samples		**Marine samples**		
Measurement No. (SUERC-)	**Age BP**	**Measurement No. (SUERC-)**	**Age BP**	**ΔR value (^{14}C y BP)**
3566/4953	7600 ± 40	241	8025 ± 60	52 ± 61
3567/4957	7600 ± 35	241	8025 ± 60	59 ± 62
3566/4953	7600 ± 40	242	8028 ± 60	55 ± 61
3567/4957	7600 ± 35	242	8028 ± 60	62 ± 62
3566/4953	7600 ± 40	3167	7975 ± 40	2 ± 42
3567/4957	7600 ± 35	3167	7975 ± 40	9 ± 43
3566/4953	7600 ± 40	3168	8045 ± 40	72 ± 42
3567/4957	7600 ± 35	3168	8045 ± 40	79 ± 43
			Weighted mean ΔR	**46 ± 17**

Table C.4: ΔR values for individual pairings of terrestrial and marine samples for **SA-013.**

Context: CMB-XIII

Terrestrial samples		**Marine samples**		
Measurement No. (SUERC-)	**Age BP**	**Measurement No. (SUERC-)**	**Age BP**	**ΔR value (^{14}C y BP)**
3587	4775 ± 35	4947	5330 ± 35	154 ± 66
3588	4785 ± 45	4947	5330 ± 35	149 ± 70
3592/4951	4816 ± 27	4947	5330 ± 35	137 ± 65
3587	4775 ± 35	4948	5310 ± 40	134 ± 69
3588	4785 ± 45	4948	5310 ± 40	129 ± 73
3592/4951	4816 ± 27	4948	5310 ± 40	117 ± 68
3587	4775 ± 35	4949	5325 ± 40	149 ± 69
3588	4785 ± 45	4949	5325 ± 40	144 ± 73
3592/4951	4816 ± 27	4949	5325 ± 40	132 ± 68
3587	4775 ± 35	4950	5335 ± 40	159 ± 69
3588	4785 ± 45	4950	5335 ± 40	154 ± 73
3592/4951	4816 ± 27	4950	5335 ± 40	142 ± 68
			Weighted mean ΔR	**148 ± 20**

Table C.5: ΔR values for individual pairings of terrestrial and marine samples for **CMB-XIII.**

Context: FL-JM76

Terrestrial samples		**Marine samples**		
Measurement No. (SUERC-)	**Age BP**	**Measurement No. (SUERC-)**	**Age BP**	**ΔR value (^{14}C y BP)**
1061	950 ± 50	3130	1232 ± 23	-95 ± 67
1063	910 ± 35	3130	1232 ± 23	-66 ± 66
1064	940 ± 45	3130	1232 ± 23	-90 ± 66
3181	870 ± 35	3130	1232 ± 23	-4 ± 38
3182	920 ± 35	3130	1232 ± 23	-78 ± 61
1061	950 ± 50	3131	1173 ± 31	-154 ± 70
1063	910 ± 35	3131	1173 ± 31	-125 ± 69
1064	940 ± 45	3131	1173 ± 31	-150 ± 69
3181	870 ± 35	3131	1173 ± 31	-63 ± 43
3182	920 ± 35	3131	1173 ± 31	-137 ± 65
1061	950 ± 50	3132	1186 ± 31	-141 ± 70
1063	910 ± 35	3132	1186 ± 31	-112 ± 69
1064	940 ± 45	3132	1186 ± 31	-136 ± 69
3181	870 ± 35	3132	1186 ± 31	-50 ± 43
3182	920 ± 35	3132	1186 ± 31	-124 ± 65
			Weighted mean ΔR	**-84 ± 15**

Table C.6: ΔR values for individual pairings of terrestrial and marine samples for **FL-JM76.**

Context: RH-3019

Terrestrial samples		**Marine samples**		
Measurement No. (SUERC-)	**Age BP**	**Measurement No. (SUERC-)**	**Age BP**	**ΔR value (^{14}C y BP)**
243	910 ± 45	247	1210 ± 45	-87 ± 83
243	910 ± 45	248	1175 ± 45	-122 ± 82
243	910 ± 45	249	1220 ± 50	-77 ± 85
243	910 ± 45	253	1200 ± 50	-97 ± 85
244	855 ± 45	247	1210 ± 45	-12 ± 62
244	855 ± 45	248	1175 ± 45	-47 ± 62
244	855 ± 45	249	1220 ± 50	-2 ± 66
244	855 ± 45	253	1200 ± 50	-22 ± 66
245	855 ± 50	247	1210 ± 45	-9 ± 65
245	855 ± 50	248	1175 ± 45	-44 ± 65
245	855 ± 50	249	1220 ± 50	1 ± 69
245	855 ± 50	253	1200 ± 50	-19 ± 69
246	920 ± 50	247	1210 ± 45	-95 ± 84
246	920 ± 50	248	1175 ± 45	-130 ± 84
246	920 ± 50	249	1220 ± 50	-85 ± 87
246	920 ± 50	253	1200 ± 50	-105 ± 87
			Weighted mean ΔR	**-50 ± 18**

Table C.7: ΔR values for individual pairings of terrestrial and marine samples for **RH-3019.**

Context: RH-3004

Terrestrial samples		**Marine samples**		
Measurement No. (SUERC-)	**Age BP**	**Measurement No. (SUERC-)**	**Age BP**	**ΔR value (^{14}C y BP)**
254	655 ± 50	258	1105 ± 60	49 ± 87
254	655 ± 50	259	1125 ± 55	69 ± 84
254	655 ± 50	260	1020 ± 50	-36 ± 81
254	655 ± 50	261	1080 ± 50	25 ± 81
255	665 ± 50	258	1105 ± 60	45 ± 88
255	665 ± 50	259	1125 ± 55	65 ± 84
255	665 ± 50	260	1020 ± 50	-40 ± 81
255	665 ± 50	261	1080 ± 50	20 ± 81
256	650 ± 50	258	1105 ± 60	52 ± 87
256	650 ± 50	259	1125 ± 55	72 ± 84
256	650 ± 50	260	1020 ± 50	-33 ± 81
256	650 ± 50	261	1080 ± 50	27 ± 81
257	610 ± 50	258	1105 ± 60	71 ± 87
257	610 ± 50	259	1125 ± 55	91 ± 83
257	610 ± 50	260	1020 ± 50	-14 ± 80
257	610 ± 50	261	1080 ± 50	46 ± 80
			Weighted mean ΔR	30 ± 21

Table C. 8: ΔR values for individual pairings of terrestrial and marine samples for **RH-3004.**

C.3 Area 3: Outer Hebrides

Context: NO-5

Terrestrial samples		**Marine samples**		
Measurement No. (SUERC-)	**Age BP**	**Measurement No. (SUERC-)**	**Age BP**	**ΔR value (^{14}C y BP)**
AA-50332	7525 ± 80	AA-53250	7860 ± 45	-4 ± 105
AA-50332	7525 ± 80	AA-53251	7880 ± 45	16 ± 105
AA-50333	7395 ± 45	AA-53250	7860 ± 45	95 ± 62
AA-50333	7395 ± 45	AA-53251	7880 ± 45	115 ± 62
AA-50334	7420 ± 45	AA-53250	7860 ± 45	65 ± 75
AA-50334	7420 ± 45	AA-53251	7880 ± 45	85 ± 75
			Weighted mean ΔR	**78 ± 31**

Table C.9: ΔR values for individual pairings of terrestrial and marine samples for **NO-5.**

Context: BA-139

Terrestrial samples		**Marine samples**		
Measurement No. (SUERC-)	**Age BP**	**Measurement No. (SUERC-)**	**Age BP**	**ΔR value (^{14}C y BP)**
AA-51177	2290 ± 40	AA-51180	2540 ± 35	-80 ± 79
AA-51177	2290 ± 40	AA-51181	2540 ± 40	-80 ± 82
AA-51177	2290 ± 40	AA-51182	2535 ± 40	-85 ± 82
AA-51177	2290 ± 40	AA-51183	2480 ± 40	-140 ± 82
AA-51178	2220 ± 45	AA-51180	2540 ± 35	-42 ± 78
AA-51178	2220 ± 45	AA-51181	2540 ± 40	-42 ± 81
AA-51178	2220 ± 45	AA-51182	2535 ± 40	-47 ± 81
AA-51178	2220 ± 45	AA-51183	2480 ± 40	-102 ± 81
AA-52318	2255 ± 70	AA-51180	2540 ± 35	-61 ± 94
AA-52318	2255 ± 70	AA-51181	2540 ± 40	-61 ± 96
AA-52318	2255 ± 70	AA-51182	2535 ± 40	-66 ± 96
AA-52318	2255 ± 70	AA-51183	2480 ± 40	-121 ± 96
AA-51179	2245 ± 40	AA-51180	2540 ± 35	-53 ± 82
AA-51179	2245 ± 40	AA-51181	2540 ± 40	-53 ± 84
AA-51179	2245 ± 40	AA-51182	2535 ± 40	-58 ± 84
AA-51179	2245 ± 40	AA-51183	2480 ± 40	-113 ± 84
			Weighted mean ΔR	**-75 ± 21**

Table C.10: ΔR values for individual pairings of terrestrial and marine samples for **BA-139.**

Context: BA-146

Terrestrial samples		**Marine samples**		
Measurement No. (SUERC-)	**Age BP**	**Measurement No. (SUERC-)**	**Age BP**	**ΔR value (^{14}C y BP)**
AA-48452	2135 ± 50	AA-48456	2390 ± 50	-112 ± 99
AA-48452	2135 ± 50	AA-48457	2385 ± 50	-117 ± 99
AA-48452	2135 ± 50	AA-48458	2345 ± 75	-157 ± 114
AA-48452	2135 ± 50	AA-48459	2355 ± 40	-147 ± 95
AA-48453	2115 ± 50	AA-48456	2390 ± 50	-60 ± 78
AA-48453	2115 ± 50	AA-48457	2385 ± 50	-65 ± 78
AA-48453	2115 ± 50	AA-48458	2345 ± 75	-105 ± 96
AA-48453	2115 ± 50	AA-48459	2355 ± 40	-95 ± 72
AA-48454	2165 ± 55	AA-48456	2390 ± 50	-132 ± 102
AA-48454	2165 ± 55	AA-48457	2385 ± 50	-137 ± 102
AA-48454	2165 ± 55	AA-48458	2345 ± 75	-177 ± 116
AA-48454	2165 ± 55	AA-48459	2355 ± 40	-167 ± 97
AA-48455	2030 ± 50	AA-48456	2390 ± 50	23 ± 69
AA-48455	2030 ± 50	AA-48457	2385 ± 50	18 ± 69
AA-48455	2030 ± 50	AA-48458	2345 ± 75	-22 ± 89
AA-48455	2030 ± 50	AA-48459	2355 ± 40	-12 ± 62
			Weighted mean ΔR	**-71 ± 21**

Table C. 11: ΔR values for individual pairings of terrestrial and marine samples for **BA-146.**

Context: HP-201

Terrestrial samples		**Marine samples**		
Measurement No. (SUERC-)	**Age BP**	**Measurement No. (SUERC-)**	**Age BP**	**ΔR value (^{14}C y BP)**
23	2155 ± 40	27	2365 ± 65	-166 ± 92
23	2155 ± 40	28	2375 ± 40	-156 ± 77
23	2155 ± 40	28	2385 ± 40	-146 ± 77
23	2155 ± 40	30	2360 ± 40	-171 ± 77
24	2120 ± 40	27	2365 ± 65	-85 ± 85
24	2120 ± 40	28	2375 ± 40	-75 ± 66
24	2120 ± 40	28	2385 ± 40	-65 ± 68
24	2120 ± 40	30	2360 ± 40	-90 ± 68
25	2135 ± 40	27	2365 ± 65	-130 ± 98
25	2135 ± 40	28	2375 ± 40	-120 ± 84
25	2135 ± 40	28	2385 ± 40	-110 ± 84
25	2135 ± 40	30	2360 ± 40	-135 ± 84
26	2110 ± 80	27	2365 ± 65	-119 ± 125
26	2110 ± 80	28	2375 ± 40	-109 ± 115
26	2110 ± 80	28	2385 ± 40	-99 ± 115
26	2110 ± 80	30	2360 ± 40	-124 ± 115
			Weighted mean ΔR	**-116 ± 21**

Table C. 12: ΔR values for individual pairings of terrestrial and marine samples for **HP-201.**

Context: BA-39

Terrestrial samples		**Marine samples**		
Measurement No. (SUERC-)	**Age BP**	**Measurement No. (SUERC-)**	**Age BP**	**ΔR value (^{14}C y BP)**
AA-51177	2080 ± 45	AA-51180	2240 ± 45	-186 ± 66
AA-51177	2080 ± 45	AA-51181	2255 ± 45	-171 ± 66
AA-51177	2080 ± 45	AA-51182	2260 ± 45	-166 ± 66
AA-51177	2080 ± 45	AA-51183	2260 ± 45	-167 ± 66
AA-51178	1975 ± 45	AA-51180	2240 ± 45	-81 ± 64
AA-51178	1975 ± 45	AA-51181	2255 ± 45	-66 ± 64
AA-51178	1975 ± 45	AA-51182	2260 ± 45	-61 ± 64
AA-51178	1975 ± 45	AA-51183	2260 ± 45	-61 ± 64
AA-52318	2005 ± 45	AA-51180	2240 ± 45	-99 ± 64
AA-52318	2005 ± 45	AA-51181	2255 ± 45	-84 ± 64
AA-52318	2005 ± 45	AA-51182	2260 ± 45	-79 ± 64
AA-52318	2005 ± 45	AA-51183	2260 ± 45	-79 ± 64
AA-51179	1990 ± 45	AA-51180	2240 ± 45	-92 ± 66
AA-51179	1990 ± 45	AA-51181	2255 ± 45	-77 ± 66
AA-51179	1990 ± 45	AA-51182	2260 ± 45	-77 ± 66
AA-51179	1990 ± 45	AA-51183	2260 ± 45	-77 ± 66
			Weighted mean ΔR	**-101 ± 16**

Table C. 13: ΔR values for individual pairings of terrestrial and marine samples for **BA-39.**

Context: BE-503

Terrestrial samples		**Marine samples**		
Measurement No. (SUERC-)	**Age BP**	**Measurement No. (SUERC-)**	**Age BP**	**ΔR value (^{14}C y BP)**
1049	1595 ± 40	1054	1980 ± 35	43 ± 60
1049	1595 ± 40	1055	1945 ± 35	8 ± 60
1049	1595 ± 40	3179	1940 ± 35	3 ± 60
1049	1595 ± 40	1056/3180	2014 ± 27	77 ± 56
1050	1630 ± 35	1054	1980 ± 35	-4 ± 41
1050	1630 ± 35	1055	1945 ± 35	-39 ± 41
1050	1630 ± 35	3179	1940 ± 35	-44 ± 41
1050	1630 ± 35	1056/3180	2014 ± 27	30 ± 34
1051	1725 ± 40	1054	1980 ± 35	-88 ± 64
1051	1725 ± 40	1055	1945 ± 35	-123 ± 64
1051	1725 ± 40	3179	1940 ± 35	-128 ± 64
1051	1725 ± 40	1056/3180	2014 ± 27	-54 ± 59
1052	1650 ± 35	1054	1980 ± 35	-16 ± 41
1052	1650 ± 35	1055	1945 ± 35	-51 ± 42
1052	1650 ± 35	3179	1940 ± 35	-56 ± 42
1052	1650 ± 35	1056/3180	2014 ± 27	18 ± 34
3176	1735 ± 40	1054	1980 ± 35	-95 ± 64
3176	1735 ± 40	1055	1945 ± 35	-129 ± 64
3176	1735 ± 40	3179	1940 ± 35	-134 ± 64
3176	1735 ± 40	1056/3180	2014 ± 27	-60 ± 60
3177	1650 ± 35	1054	1980 ± 35	-16 ± 42
3177	1650 ± 35	1055	1945 ± 35	-51 ± 41
3177	1650 ± 35	3179	1940 ± 35	-56 ± 42
3177	1650 ± 35	1056/3180	2014 ± 27	18 ± 34
			Weighted mean ΔR	**-27 ±10**

Table C. 14: ΔR values for individual pairings of terrestrial and marine samples for **BE-503.**

Context: BO-64

Terrestrial samples		**Marine samples**		
Measurement No. (SUERC-)	**Age BP**	**Measurement No. (SUERC-)**	**Age BP**	**ΔR value (^{14}C y BP)**
3169	1095 ± 35	1041	1365 ± 40	-105 ± 57
1038	1150 ± 35	1041	1365 ± 40	-132 ± 54
1039	1120 ± 35	1041	1365 ± 40	-117 ± 56
1040	1065 ± 35	1041	1365 ± 40	-82 ± 59
3169	1095 ± 35	1042/3171	1470 ± 25	0 ± 48
1038	1150 ± 35	1042/3171	1470 ± 25	-27 ± 44
1039	1120 ± 35	1042/3171	1470 ± 25	-12 ± 47
1040	1065 ± 35	1042/3171	1470 ± 25	23 ± 50
3169	1095 ± 35	1043/3172	1397 ± 50	-73 ± 65
1038	1150 ± 35	1043/3172	1397 ± 50	-100 ± 61
1039	1120 ± 35	1043/3172	1397 ± 50	-86 ± 64
1040	1065 ± 35	1043/3172	1397 ± 50	-50 ± 66
3169	1095 ± 35	4118	1415 ± 35	-55 ± 54
1038	1150 ± 35	4118	1415 ± 35	-82 ± 50
1039	1120 ± 35	4118	1415 ± 35	-68 ± 53
1040	1065 ± 35	4118	1415 ± 35	-32 ± 56
			Weighted mean ΔR	**-57 ± 14**

Table C. 15: ΔR values for individual pairings of terrestrial and marine samples for **BO-64.**

Context: GA-165

Terrestrial samples		**Marine samples**		
Measurement No. (SUERC-)	**Age BP**	**Measurement No. (SUERC-)**	**Age BP**	**ΔR value (^{14}C y BP)**
AA-48444	1060 ± 50	AA-53257/SUERC-4051/4052/4053/4054	1375 ± 35	-72 ± 63
AA-48445	1110 ± 55	AA-53257/SUERC-4051/4052/4053/4054	1375 ± 35	-101 ± 60
AA-48446	1110 ± 50	AA-53257/SUERC-4051/4052/4053/4054	1375 ± 35	-101 ± 58
AA-48447	1130 ± 50	AA-53257/SUERC-4051/4052/4053/4054	1375 ± 35	-111 ± 57
AA-48444	1060 ± 50	AA-53258	1360 ± 40	-87 ± 66
AA-48445	1110 ± 55	AA-53258	1360 ± 40	-116 ± 63
AA-48446	1110 ± 50	AA-53258	1360 ± 40	-116 ± 62
AA-48447	1130 ± 50	AA-53258	1360 ± 40	-136 ± 60
AA-48444	1060 ± 50	AA-53259	1415 ± 35	-32 ± 63
AA-48445	1110 ± 55	AA-53259	1415 ± 35	-61 ± 60
AA-48446	1110 ± 50	AA-53259	1415 ± 35	-61 ± 58
AA-48447	1130 ± 50	AA-53259	1415 ± 35	-70 ± 56
			Weighted mean ΔR	**-89 ± 17**

Table C. 16: ΔR values for individual pairings of terrestrial and marine samples for **GA-165.**

C.4 Area 4: Orkney Isles

Context: SkB-68

Terrestrial samples		Marine samples		
Measurement No. (SUERC-)	**Age BP**	**Measurement No. (SUERC-)**	**Age BP**	**ΔR value (^{14}C y BP)**
3128	4555 ± 40	3130	4975 ± 40	65 ± 92
3129	4605 ± 40	3130	4975 ± 40	-45 ± 62
4119	4525 ± 40	3130	4975 ± 40	81 ± 90
4121	4530 ± 35	3130	4975 ± 40	80 ± 89
3128	4555 ± 40	3131	4995 ± 40	85 ± 92
3129	4605 ± 40	3131	4995 ± 40	-25 ± 62
4119	4525 ± 40	3131	4995 ± 40	101 ± 90
4121	4530 ± 35	3131	4995 ± 40	99 ± 89
3128	4555 ± 40	3132	4960 ± 45	50 ± 94
3129	4605 ± 40	3132	4960 ± 45	-60 ± 65
4119	4525 ± 40	3132	4960 ± 45	66 ± 93
4121	4530 ± 35	3132	4960 ± 45	65 ± 91
			Weighted mean ΔR	**28 ± 23**

Table C. 17: ΔR values for individual pairings of terrestrial and marine samples for **SkB-68.**

Context: SkB-26

Terrestrial samples		Marine samples		
Measurement No. (SUERC-)	**Age BP**	**Measurement No. (SUERC-)**	**Age BP**	**ΔR value (^{14}C y BP)**
3576	4140 ± 40	232	4440 ± 50	-75 ± 96
4958	4015 ± 40	232	4440 ± 50	83 ± 64
3578	4110 ± 35	232	4440 ± 50	-46 ± 96
3582	4145 ± 45	232	4440 ± 50	-78 ± 99
3576	4140 ± 40	233	4370 ± 45	-145 ± 94
4958	4015 ± 40	233	4370 ± 45	13 ± 61
3578	4110 ± 35	233	4370 ± 45	-116 ± 93
3582	4145 ± 45	233	4370 ± 45	-148 ± 96
3576	4140 ± 40	234	4445 ± 50	-70 ± 96
4958	4015 ± 40	234	4445 ± 50	88 ± 64
3578	4110 ± 35	234	4445 ± 50	-41 ± 96
3582	4145 ± 45	234	4445 ± 50	-73 ± 99
3576	4140 ± 40	235	4405 ± 45	-110 ± 94
4958	4015 ± 40	235	4405 ± 45	48 ± 61
3578	4110 ± 35	235	4405 ± 45	-81 ± 93
3582	4145 ± 45	235	4405 ± 45	-113 ± 96
			Weighted mean ΔR	**-27 ± 21**

Table C. 18: ΔR values for individual pairings of terrestrial and marine samples for **SkB-26.**

Context: BB-XF

Terrestrial samples		**Marine samples**		
Measurement No. (SUERC-)	**Age BP**	**Measurement No. (SUERC-)**	**Age BP**	**ΔR value (^{14}C y BP)**
3588	3640 ± 35	221	3920 ± 50	-44 ± 62
3588	3640 ± 35	222	3980 ± 50	16 ± 62
3588	3640 ± 35	223	4000 ± 50	36 ± 62
3588	3640 ± 35	224	3956 ± 55	-8 ± 66
3572	3645 ± 40	221	3920 ± 50	-63 ± 75
3572	3645 ± 40	222	3980 ± 50	-3 ± 75
3572	3645 ± 40	223	4000 ± 50	17 ± 75
3572	3645 ± 40	224	3956 ± 55	-27 ± 78
3573	3625 ± 40	221	3920 ± 50	-11 ± 82
3573	3625 ± 40	222	3980 ± 50	50 ± 82
3573	3625 ± 40	223	4000 ± 50	70 ± 82
3573	3625 ± 40	224	3956 ± 55	26 ± 85
3575	3685 ± 40	221	3920 ± 50	-91 ± 74
3575	3685 ± 40	222	3980 ± 50	-31 ± 74
3575	3685 ± 40	223	4000 ± 50	-11 ± 74
3575	3685 ± 40	224	3956 ± 55	-55 ± 78
			Weighted mean ΔR	**-9 ± 18**

Table C. 19: ΔR values for individual pairings of terrestrial and marine samples for **BB-XF.**

Context: LO-6

Terrestrial samples		**Marine samples**		
Measurement No. (SUERC-)	**Age BP**	**Measurement No. (SUERC-)**	**Age BP**	**ΔR value (^{14}C y BP)**
1837	3735 ± 40	1840	3960 ± 40	-99 ± 67
1837	3735 ± 40	1841	3915 ± 35	-145 ± 65
1837	3735 ± 40	3137	3950 ± 35	-110 ± 65
1837	3735 ± 40	3139	3880 ± 45	-180 ± 70
1838	3690 ± 35	1840	3960 ± 40	-52 ± 67
1838	3690 ± 35	1841	3915 ± 35	-97 ± 64
1838	3690 ± 35	3137	3950 ± 35	-62 ± 64
1838	3690 ± 35	3139	3880 ± 45	-132 ± 70
3228	3690 ± 35	1840	3960 ± 40	-52 ± 67
3228	3690 ± 35	1841	3915 ± 35	-97 ± 64
3228	3690 ± 35	3137	3950 ± 35	-62 ± 64
3228	3690 ± 35	3139	3880 ± 45	-132 ± 70
1839	3685 ± 40	1840	3960 ± 40	-51 ± 68
1839	3685 ± 40	1841	3915 ± 35	-96 ± 65
1839	3685 ± 40	3137	3950 ± 35	-61 ± 65
1839	3685 ± 40	3139	3880 ± 45	-131 ± 71
			Weighted mean ΔR	**-96 ± 17**

Table C. 20: ΔR values for individual pairings of terrestrial and marine samples for **LO-6.**

Context: StB-2136

Terrestrial samples		**Marine samples**		
Measurement No. (SUERC-)	**Age BP**	**Measurement No. (SUERC-)**	**Age BP**	**ΔR value (^{14}C y BP)**
107	2050 ± 40	111	2280 ± 40	-101 ± 56
107	2050 ± 40	112	2325 ± 45	-56 ± 60
107	2050 ± 40	113	2325 ± 90	-56 ± 98
107	2050 ± 40	114	2390 ± 45	9 ± 60
108	2035 ± 45	111	2280 ± 40	-89 ± 61
108	2035 ± 45	112	2325 ± 45	-44 ± 64
108	2035 ± 45	113	2325 ± 90	-44 ± 101
108	2035 ± 45	114	2390 ± 45	21 ± 64
109	2120 ± 40	111	2280 ± 40	-170 ± 68
109	2120 ± 40	112	2325 ± 45	-125 ± 71
109	2120 ± 40	113	2325 ± 90	-125 ± 105
109	2120 ± 40	114	2390 ± 45	-60 ± 71
110	2035 ± 40	111	2280 ± 40	-91 ± 56
110	2035 ± 40	112	2325 ± 45	-46 ± 60
110	2035 ± 40	113	2325 ± 90	-46 ± 98
110	2035 ± 40	114	2390 ± 45	19 ± 60
			Weighted mean ΔR	**-60 ± 17**

Table C. 21: ΔR values for individual pairings of terrestrial and marine samples for **StB-2136.**

Context: StB-2004

Terrestrial samples		**Marine samples**		
Measurement No. (SUERC-)	**Age BP**	**Measurement No. (SUERC-)**	**Age BP**	**ΔR value (^{14}C y BP)**
115	2085 ± 40	125	2385 ± 40	-43 ± 61
116	2100 ± 40	125	2385 ± 40	-50 ± 62
123	2090 ± 40	125	2385 ± 40	-46 ± 62
124	2070 ± 40	125	2385 ± 40	-36 ± 60
115	2085 ± 40	126	2360 ± 40	-68 ± 61
116	2100 ± 40	126	2360 ± 40	-75 ± 62
123	2090 ± 40	126	2360 ± 40	-71 ± 62
124	2070 ± 40	126	2360 ± 40	-61 ± 60
115	2085 ± 40	127/191	2388 ± 26	-40 ± 53
116	2100 ± 40	127/191	2388 ± 26	-47 ± 54
123	2090 ± 40	127/191	2388 ± 26	-43 ± 54
124	2070 ± 40	127/191	2388 ± 26	-33 ± 51
			Weighted mean ΔR	**-50 ± 17**

Table C. 22: ΔR values for individual pairings of terrestrial and marine samples for **StB-2004.**

Context: StB-1063B

Terrestrial samples		**Marine samples**		
Measurement No. (SUERC-)	**Age BP**	**Measurement No. (SUERC-)**	**Age BP**	**ΔR value (^{14}C y BP)**
129	965 ± 40	133	1240 ± 40	-91 ± 74
129	965 ± 40	134	1270 ± 40	-61 ± 74
129	965 ± 40	135	1260 ± 40	-71 ± 74
129	965 ± 40	136	1250 ± 40	-81 ± 74
130	995 ± 40	133	1240 ± 40	-148 ± 47
130	995 ± 40	134	1270 ± 40	-118 ± 47
130	995 ± 40	135	1260 ± 40	-128 ± 47
130	995 ± 40	136	1250 ± 40	-138 ± 47
131	935 ± 40	133	1240 ± 40	-79 ± 71
131	935 ± 40	134	1270 ± 40	-49 ± 71
131	935 ± 40	135	1260 ± 40	-59 ± 71
131	935 ± 40	136	1250 ± 40	-69 ± 71
132	935 ± 40	133	1240 ± 40	-79 ± 71
132	935 ± 40	134	1270 ± 40	-49 ± 71
132	935 ± 40	135	1260 ± 40	-59 ± 71
132	935 ± 40	136	1250 ± 40	-69 ± 71
			Weighted mean ΔR	**-96 ± 16**

Table C. 23: ΔR values for individual pairings of terrestrial and marine samples for **StB-1063B.**

Context: QG-A004

Terrestrial samples		**Marine samples**		
Measurement No. (SUERC-)	**Age BP**	**Measurement No. (SUERC-)**	**Age BP**	**ΔR value (^{14}C y BP)**
3149	980 ± 40	3152	1235 ± 40	-101 ± 75
3542	875 ± 35	3152	1235 ± 40	-26 ± 66
3150	960 ± 40	3152	1235 ± 40	-95 ± 73
3151	925 ± 40	3152	1235 ± 40	-78 ± 72
3149	980 ± 40	3156	1200 ± 35	-136 ± 72
3542	875 ± 35	3156	1200 ± 35	-61 ± 63
3150	960 ± 40	3156	1200 ± 35	-130 ± 70
3151	925 ± 40	3156	1200 ± 35	-114 ± 69
3149	980 ± 40	3157	1195 ± 35	-141 ± 73
3542	875 ± 35	3157	1195 ± 35	-66 ± 63
3150	960 ± 40	3157	1195 ± 35	-135 ± 71
3151	925 ± 40	3157	1195 ± 35	-119 ± 69
3149	980 ± 40	3159	1210 ± 35	-126 ± 73
3542	875 ± 35	3159	1210 ± 35	-51 ± 63
3150	960 ± 40	3159	1210 ± 35	-120 ± 71
3151	925 ± 40	3159	1210 ± 35	-104 ± 70
			Weighted mean ΔR	**-98 ± 17**

Table C. 24: ΔR values for individual pairings of terrestrial and marine samples for **QG-A004.**

Context: QG-A023

Terrestrial samples		**Marine samples**		
Measurement No. (SUERC-)	**Age BP**	**Measurement No. (SUERC-)**	**Age BP**	**ΔR value (^{14}C y BP)**
AA-52329	875 ± 45	3162/4109	1258 ± 25	-9 ± 67
AA-52330	835 ± 40	3162/4109	1258 ± 25	51 ± 49
AA-52331	835 ± 40	3162/4109	1258 ± 25	51 ± 49
AA-52332	945 ± 55	3162/4109	1258 ± 25	-66 ± 71
3160	940 ± 35	3162/4109	1258 ± 25	-64 ± 62
3161	940 ± 35	3162/4109	1258 ± 25	-64 ± 62
AA-52329	875 ± 45	4110	1175 ± 35	-92 ± 71
AA-52330	835 ± 40	4110	1175 ± 35	-32 ± 55
AA-52331	835 ± 40	4110	1175 ± 35	-32 ± 55
AA-52332	945 ± 55	4110	1175 ± 35	-149 ± 75
3160	940 ± 35	4110	1175 ± 35	-147 ± 67
3161	940 ± 35	4110	1175 ± 35	-149 ± 67
AA-52329	875 ± 45	3166/4111	1233 ± 23	-34 ± 66
AA-52330	835 ± 40	3166/4111	1233 ± 23	26 ± 49
AA-52331	835 ± 40	3166/4111	1233 ± 23	26 ± 49
AA-52332	945 ± 55	3166/4111	1233 ± 23	-91 ± 70
3160	940 ± 35	3166/4111	1233 ± 23	-89 ± 61
3161	940 ± 35	3166/4111	1233 ± 23	-89 ± 61
AA-52329	875 ± 45	4112	1210 ± 35	-57 ± 71
AA-52330	835 ± 40	4112	1210 ± 35	3 ± 58
AA-52331	835 ± 40	4112	1210 ± 35	3 ± 55
AA-52332	945 ± 55	4112	1210 ± 35	-114 ± 75
3160	940 ± 35	4112	1210 ± 35	-112 ± 67
3161	940 ± 35	4112	1210 ± 35	-112 ± 67
			Weighted mean ΔR	**96 ± 15**

Table C. 25: ΔR values for individual pairings of terrestrial and marine samples for **QG-A023.**

C.5 Area 5: Shetland Isles

Context: SC-543

Terrestrial samples		**Marine samples**		
Measurement No. (SUERC-)	**Age BP**	**Measurement No. (SUERC-)**	**Age BP**	**ΔR value (^{14}C y BP)**
AA-51153	1740 ± 35	SUERC-3140/4058	1763 ± 35	-323 ± 54
AA-51154	1680 ± 35	SUERC-3140/4058	1763 ± 35	-279 ± 71
AA-51155	1680 ± 50	SUERC-3140/4058	1763 ± 35	-278 ± 63
AA-51156	1710 ± 40	SUERC-3140/4058	1763 ± 35	-296 ± 66
AA-51153	1740 ± 35	AA-51162/SUERC-4059	1749 ± 28	-337 ± 50
AA-51154	1680 ± 35	AA-51162/SUERC-4059	1749 ± 28	-292 ± 59
AA-51155	1680 ± 50	AA-51162/SUERC-4059	1749 ± 28	-293 ± 67
AA-51156	1710 ± 40	AA-51162/SUERC-4059	1749 ± 28	-310 ± 62
AA-51153	1740 ± 35	AA-51163/SUERC-4061	1753 ± 28	-333 ± 50
AA-51154	1680 ± 35	AA-51163/SUERC-4061	1753 ± 28	-288 ± 59
AA-51155	1680 ± 50	AA-51163/SUERC-4061	1753 ± 28	-289 ± 67
AA-51156	1710 ± 40	AA-51163/SUERC-4061	1753 ± 28	-306 ± 62
AA-51153	1740 ± 35	AA-51164/SUERC-3141/4062	1817 ± 56	-169 ± 70
AA-51154	1680 ± 35	AA-51164/SUERC-3141/4062	1817 ± 56	-224 ± 77
AA-51155	1680 ± 50	AA-51164/SUERC-3141/4062	1817 ± 56	-225 ± 83
AA-51156	1710 ± 40	AA-51164/SUERC-3141/4062	1817 ± 56	-242 ± 79
			Weighted mean ΔR	**-290 ± 16**

Table C. 26: ΔR values for individual pairings of terrestrial and marine samples for **SC-543.**

Context: SC-3083

Terrestrial samples		**Marine samples**		
Measurement No. (SUERC-)	**Age BP**	**Measurement No. (SUERC-)**	**Age BP**	**ΔR value (^{14}C y BP)**
AA-52324	1615 ± 40	AA-52310	1925 ± 40	-21 ± 66
AA-52324	1615 ± 40	AA-52311	1975 ± 45	29 ± 69
AA-52324	1615 ± 40	AA-52312/3147	2010 ± 50	64 ± 72
AA-52324	1615 ± 40	3148/4960	2034 ± 37	88 ± 64
AA-52323	1570 ± 55	AA-52310	1925 ± 40	1 ± 70
AA-52323	1570 ± 55	AA-52311	1975 ± 45	51 ± 73
AA-52323	1570 ± 55	AA-52312/3147	2010 ± 50	86 ± 76
AA-52323	1570 ± 55	3148/4960	2034 ± 37	110 ± 68
			Weighted mean ΔR	**50 ± 25**

Table C. 27: ΔR values for individual pairings of terrestrial and marine samples for **SC-3083.**

Context: SC-1269

Terrestrial samples		**Marine samples**		
Measurement No. (SUERC-)	**Age BP**	**Measurement No. (SUERC-)**	**Age BP**	**ΔR value (^{14}C y BP)**
AA-51157	1300 ± 35	AA-51165	1580 ± 35	-100 ± 65
AA-51157	1300 ± 35	AA-51166	1525 ± 40	-155 ± 68
AA-51157	1300 ± 35	AA-51167	1655 ± 35	-25 ± 65
AA-51157	1300 ± 35	AA-51168	1580 ± 35	-100 ± 65
AA-51158	1375 ± 35	AA-51165	1580 ± 35	-175 ± 40
AA-51158	1375 ± 35	AA-51166	1525 ± 40	-230 ± 45
AA-51158	1375 ± 35	AA-51167	1655 ± 35	-100 ± 40
AA-51158	1375 ± 35	AA-51168	1580 ± 35	-175 ± 40
AA-51159	1280 ± 35	AA-51165	1580 ± 35	-86 ± 59
AA-51159	1280 ± 35	AA-51166	1525 ± 40	-141 ± 62
AA-51159	1280 ± 35	AA-51167	1655 ± 35	-11 ± 59
AA-51159	1280 ± 35	AA-51168	1580 ± 35	-86 ± 59
AA-51160	1285 ± 40	AA-51165	1580 ± 35	-91 ± 63
AA-51160	1285 ± 40	AA-51166	1525 ± 40	-146 ± 66
AA-51160	1285 ± 40	AA-51167	1655 ± 35	-16 ± 63
AA-51160	1285 ± 40	AA-51168	1580 ± 35	-91 ± 63
			Weighted mean ΔR	**-121 ± 16**

Table C. 28: ΔR values for individual pairings of terrestrial and marine samples for **SC-1269.**

Context: SC-206

Terrestrial samples		**Marine samples**		
Measurement No. (SUERC-)	**Age BP**	**Measurement No. (SUERC-)**	**Age BP**	**ΔR value (^{14}C y BP)**
AA-51169	815 ± 40	AA-51173/SUERC-3142	1202 ± 26	18 ± 42
AA-51169	815 ± 40	AA-51174	1135 ± 35	-50 ± 48
AA-51169	815 ± 40	AA-51175	1230 ± 35	46 ± 48
AA-51170	740 ± 40	AA-51173/SUERC-3142	1202 ± 26	66 ± 34
AA-51170	740 ± 40	AA-51174	1135 ± 35	-1 ± 41
AA-51170	740 ± 40	AA-51175	1230 ± 35	94 ± 41
AA-51171	730 ± 45	AA-51173/SUERC-3142	1202 ± 26	72 ± 35
AA-51171	730 ± 45	AA-51174	1135 ± 35	5 ± 42
AA-51171	730 ± 45	AA-51175	1230 ± 35	100 ± 42
AA-51172	840 ± 45	AA-51173/SUERC-3142	1202 ± 26	-8 ± 53
AA-51172	840 ± 45	AA-51174	1135 ± 35	-75 ± 58
AA-51172	840 ± 45	AA-51175	1230 ± 35	20 ± 58
			Weighted mean ΔR	**35 ± 15**

Table C. 29: ΔR values for individual pairings of terrestrial and marine samples for **SC-206.**

C.6 Area 6: Faroe Isles

Context: UJ-23

Terrestrial samples		**Marine samples**		
Measurement No. (SUERC-)	**Age BP**	**Measurement No. (SUERC-)**	**Age BP**	**ΔR value (^{14}C y BP)**
3400	1000 ± 40	3404	1410 ± 35	17 ± 44
3400	1000 ± 40	3407	1460 ± 40	67 ± 48
3400	1000 ± 40	3408	1445 ± 35	52 ± 44
3400	1000 ± 40	3409	1440 ± 35	47 ± 44
3401	980 ± 40	3404	1410 ± 35	73 ± 74
3401	980 ± 40	3407	1460 ± 40	124 ± 75
3401	980 ± 40	3408	1445 ± 35	109 ± 73
3401	980 ± 40	3409	1440 ± 35	104 ± 73
3402	940 ± 45	3404	1410 ± 35	88 ± 71
3402	940 ± 45	3407	1460 ± 40	138 ± 73
3402	940 ± 45	3408	1445 ± 35	123 ± 71
3402	940 ± 45	3409	1440 ± 35	118 ± 71
3403	995 ± 35	3404	1410 ± 35	24 ± 40
3403	995 ± 35	3407	1460 ± 40	74 ± 44
3403	995 ± 35	3408	1445 ± 35	59 ± 40
3403	995 ± 35	3409	1440 ± 35	54 ± 40
			Weighted mean ΔR	**64 ± 13**

Table C. 30: ΔR values for individual pairings of terrestrial and marine samples for **UJ-23.**

C.7 Hrísheimer: Iceland

Context: HR-45

Terrestrial samples		**Marine samples**		
Measurement No. (SUERC-)	**Age BP**	**Measurement No. (SUERC-)**	**Age BP**	**ΔR value (^{14}C y BP)**
6431	1220 ± 35	6438	1650 ± 40	59 ± 72
6431	1220 ± 35	6439	1610 ± 35	19 ± 70
6431	1220 ± 35	6440	1595 ± 35	4 ± 70
6431	1220 ± 35	6441	1615 ± 35	24 ± 70
6432	1200 ± 35	6438	1650 ± 40	78 ± 62
6432	1200 ± 35	6439	1610 ± 35	40 ± 58
6432	1200 ± 35	6440	1595 ± 35	45 ± 58
6432	1200 ± 35	6441	1615 ± 35	45 ± 58
6433	1120 ± 35	6438	1650 ± 40	168 ± 56
6433	1120 ± 35	6439	1610 ± 35	128 ± 53
6433	1120 ± 35	6440	1595 ± 35	113 ± 53
6433	1120 ± 35	6441	1615 ± 35	133 ± 53
6437	1120 ± 35	6438	1650 ± 40	168 ± 56
6437	1120 ± 35	6439	1610 ± 35	128 ± 53
6437	1120 ± 35	6440	1595 ± 35	113 ± 53
6437	1120 ± 35	6441	1615 ± 35	133 ± 53
			Weighted mean ΔR	**96 ± 15**

Table C. 31: ΔR values for individual pairings of terrestrial and marine samples for **HR-45.**

Appendix D: Publications arising from this thesis.

Publications

Ascough P. L. Forthcoming. Radiocarbon dating. *In* Neighbour T, Church M. J and Heald, A. A Late Iron Age and Norse settlement and cemetery at Galson: an overview and assessment of a multi-period coastal erosion complex in Lewis, Scotland. submitted to Historic Scotland for comments prior to submission to *Proceedings of the Society of Antiquaries of Scotland*

Ascough P. L, Church, M. J and Neighbour T. Forthcoming. Dating strategy. *In* Neighbour, T and Church, M J. In preparation. A Late Iron Age and Norse village at Bostadh Beach, Great Bernera. Submitted to Historic Scotland for comments prior to publication on *Scottish Archaeological Internet Reports*.

Ascough P. L, Cook G. T and Dugmore, A. J. 2005. Methodological approaches to determining the marine radiocarbon reservoir effect. *Progress in Physical* Geography (in press).

Ascough P, Cook G, Church M. J, Dugmore A. J, Arge S. V and McGovern T. H. Variability in North Atlantic marine radiocarbon reservoir effects at c.1000 AD. *The Holocene* (in press).

Ascough P. L, Cook G. T, Dugmore A. J, Barber J, Higney E and Scott E. M. 2004. Holocene variations in the Marine Radiocarbon Reservoir Effect. *Radiocarbon*, 46 (2), 611-620.

Ascough P. L, Cook G. T, Dugmore A. J, Scott E. M and Freeman S. P. H. T. (2005). Influence of mollusc species on marine ΔR determinations. *Radiocarbon* (in press)

References

Adkins J. F, Cheng H, Boyle E. A, Druffle E. R. M, and Edwards R. L. 1998. Deep-Sea Coral Evidence for Rapid Change in ventilation of the deep North Atlantic 15,400 years ago. *Science* 280, 725-728.

Aitken M. J. 1990. *Science-based dating in archaeology*. Longman Archaeology series. Longman Group, England.

Albero M. C, Angiolini F. E, and Piana E. L. 1986. Discordant ages related to reservoir effect of associated archaeologic remains from the Tunel site, Beagle Channel, Argentine Republic. *Radiocarbon* 28 (2A), 748-753.

Alley R. B. 2000. The Younger Dryas cold interval as viewed from central Greenland. *Quaternary Science Reviews* 19, 213-226.

Alley R. B, Mayewski P. A, Sowers T, Taylor K. C, and Clark P. U. 1997. Holocene climatic instability - A prominent, widespread event 8200 yr ago. *Geology* 25, 483-486.

Alley R. B, Meese D. A, Shuman C. A, Gow A. J, Taylor K. C, Grootes P. M, White J. W. C, Ram M, Waddington E. D, Mayewski P. A and Zielinski G. A. 1993. Abrupt increase in Greenland snow accumulation at the end of the Younger Dryas event. *Nature* 362, 527-529.

Armit I. 2003. *Towers in the North; the brochs of Scotland*. Tempus, Gloucestershire.

Armit I and Ralston I. B. M. 2003. The Iron Age. In Edwards, K J and Ralston, I. B. M (eds.), *Scotland after the Ice Age: environment, archaeology and history 8000BC - AD 1000*. Edinburgh, Edinburgh University Press.

Arneborg J, Heinemeier J, Lynnerup N, Nielsen H. L, Rud N, and Sveinbjornsdottir A. E. 1999. Change of Diet of the Greenland Vikings determined from stable carbon isotope analysis and ^{14}C dating of their bones. *Radiocarbon* 41 (2), 157-168.

Ascough P, Cook G and Dugmore A. (in press). Methodological approaches to determining the marine radiocarbon reservoir effect. *Progress in Physical Geography*

Austin W. E. N, Bard E, Hunt J. B, Kroon D, and Peacock J. D. 1995. The ^{14}C age of the Icelandic Vedde ash; Implications for younger Dryas marine reservoir age corrections. *Radiocarbon* 37 (1), 53-62.

Austin W. E. N and Inall M. E. 2002. Deep water renewal in a Scottish fjord: temperature, salinity and oxygen isotopes. *Polar Research* 21(2), 251-258.

Barber D. C, Dyke A, Hillaire-Marcel C, Jennings A. E, Andrews J. T, Kerwin M. W, Bilodeau G, McNeely R, Southon J, Morehead M. D, and Gagnon J –M. 1999. Forcing of the cold event of 8,200 years ago by catastrophic drainage of Laurentide lakes. *Nature* 400, 344-348.

Barber J. 2003. Bronze Age farms and Iron Age farm mounds of the Outer Hebrides.]. *Scottish Archaeological Internet Reports*, [online] 3. Available from: http://www.sair.org.uk/sair3/index.html/ [Accessed 6 Oct 2003].

Bard E, Arnold M, Fairbanks R. G, and Hamelin B. 1993. ^{230}Th-^{234}U and ^{14}C ages obtained by mass spectrometry on corals. *Radiocarbon* 35 (1), 191-199.

Bard E, Arnold M, Hamelin B, Tisnerat-Laborde N, and Cabioch G. 1998. Radiocarbon calibration by means of mass spectrometric ^{230}Th/^{234}U and ^{14}C ages of corals. An updated database including samples from Barbados, Mururoa and Tahiti. *Radiocarbon* 40, 1085-1092.

Bard E, Arnold M, Mangerud J, Paterne M, Labeyrie L, Duprat J, Melieres M. A, Sonstegaard E, and Duplessy J. C. 1994. The North Atlantic atmosphere-sea surface C-14 gradient during the Younger Dryas climatic event. *Earth and Planetary Science Letters* 126 (4), 275-287.

Bard E, Hamelin B, Fairbanks R. G, and Zindler A. 1990. Calibration of the ^{14}C timescale over the past 30,000 years using mass spectrometric U-Th ages from Barbados corals. *Nature* 345, 405-410.

Barrett J. H. 1992. Robert's Haven (Canisbay parish): Norse/medieval middens, structures. *Discovery and Excavation, Scotland* 1992, 40.

Barrett J. H. 1993. Robert's Haven (Canisbay parish): medieval/Norse middens, undated structure. *Discovery and Excavation, Scotland* 1993, 42-43.

Barrett J and Gerrard J. 2002. *Excavations at Quoygrew, Westray, Orkney: Interim report, 2002.* [Online]. Available from: http://www.york.ac.uk/depts/arch/quoygrew/2002/index.html. [Accessed 2003 Nov 13].

Barrett J and Moore R. 2001. *Excavations at Quoygrew, Westray, Orkney: Interim report, 2001.* York, Department of Archaeology, University of York.

Bemis B. E, Spero H. J, Bijma J and Lee D. 1998. Re-evaluation of the oxygen isotopic composition of planktonic foraminifera: Experimental results and revised paleotemperature equations. *Paleoceanography* 13, 150-160.

Berger W H and Heath G.R. 1968. Vertical mixing in pelagic sediments. *Journal of Marine Research* 26, 134–143.

Berglund B. E, Björck S, Lemdahl G, Bergsten H, Nordberg K, and Kolstrup E. 1994. Late Weichselian environmental change in Southern Sweden and Denmark. *Journal of Quaternary Science* 9, 127-132.

Berkman P. A and Forman S. L. 1996. Pre-bomb radiocarbon and the reservoir correction for calcareous marine species in the Southern Ocean. *Geophysical Research Letters* 23, 363-366.

Bezerra F. H. R, Vita-Finza C, and Filho F. P. L. 2000. The use of marine shells for radiocarbon dating of marine deposits. *Revista Brazileira de Geociẽncias* 30 (1), 211-213.

Bianchi G. G and McCave I. N. 1999. Holocene Periodicity in North Atlantic Climate and Deep-Ocean Flow South of Iceland. *Nature* 397, 515-517.

Birks H. H, Gulliksen S, Haflidason H, Mangerud J, Possnert G. 1996. New radiocarbon dates from the Vedde Ash and the Saksunarvatn Ash from western Norway. *Quaternary Research* 45 (2), 119-127.

Birks C. J. A and Koç N. 2002. A high resolution diatom record of late Quaternary sea surface temperatures and oceanographic conditions from the Eastern Norwegian Sea. *Boreas* 31, 323-341.

Björck S, Koç N, and Goran S. 2003. Consistently large reservoir ages in the Norwegian Sea during the last deglaciation. *Quaternary Science Reviews* 22, 429-435.

Blytt A. 1876. *Essay on immigration of the Norwegian flora during alternating rainy and dry periods*. Christiania.

Boaretto E, Bryant C, Carmi I, Cook G, Gulliksen S, Harkness D, Heinemeier J, McClure J, McGee E, Naysmith P, Possnert G, Scott M, van der Plicht H, van Strydonck M. 2002. Summary findings of the fourth international radiocarbon intercomparison (FIRI) (1998-2001). *Journal of Quaternary Science* 17 (7), 633 – 637.

Bond G. H, Broecker W, Johnsen S, McManus J, Labeyrie L, Jouzel J, and Bonani G. 1993. Correlations between climate records from North Atlantic sediments and Greenland ice. *Nature* 365, 143-147.

Bond G, Kromer B, Beer J, Muscheler R, Evans M. N, Showers W, Hoffman S, Lotti-Bond R, Hadjas I, Bonani G. 2001. Persistent solar influence on North Atlantic climate during the Holocene. *Science* 294, 2130-2136.

Bond G, Showers W, Cheseby M, Lotti R, Almasi P, deMenocal P, Priore P, Cullen H, Hajdas I, and Bonani G. 1997. A pervasive millennial-scale cycle in North Atlantic Holocene and glacial climates. *Science* 278, 1257-1266.

Bondevik S, Birks H. H, Gulliksen S and Mangerud J. 1999. Late Weichselian Marine ^{14}C Reservoir Ages at the Western Coast of Norway. *Quaternary Research* 52, 104-114.

Bondevik S, Mangerud J, and Gulliksen S. 2001. The marine ^{14}C age of the Vedde Ash Bed along the west coast of Norway. *Journal of Quaternary Science* 16 (1), 3-7.

Boyle E. A and Keigwin L. D. 1987. North Atlantic thermohaline circulation during the past 20,000 years linked to high-latitude surface temperatures. *Nature* 330, 35-40.

Bowen G. J and Wilkinson B. 2002. Spatial distribution of $\delta^{18}O$ in meteoric precipitation. *Geology* 30 (4), 315–318.

Broecker W. S. 2000. Was a change in thermohaline circulation responsible for the Little Ice Age? *Proceedings of the National Academy of Sciences of the United States of America* 97 (4), 1339-1342.

Broecker W. S. 2001. Paleoclimate: Was the Medieval Warm Period Global? *Science* 291, 1497-1499.

Broecker W.S, Andree M, Wolfli W, Oeschger H, Bonani G, Kennett J, and Peteet D. 1988. The chronology of the last deglaciation: Implications to the cause of the Younger Dryas event. *Paleoceanography* 3, 1-19.

Broecker W. S, Bond G, Klas M, Bonani G, and Wolfli, W. 1990. A salt oscillator in the glacial Atlantic? .The concept. *Paleoceanography* 5, 469-77.

Broecker W. S, Klas M, Clark E, Bonani G, Ivy S, and Wolfli W. 1991. The influence of $CaCO_3$ dissolution on core top radiocarbon ages for deep sea sediments. *Paleoceanography* 6 (5), 593-608.

Broecker W. S and Olson E A. 1961. Lamont radiocarbon measurements VIII. *Radiocarbon* 3, 176-204.

Broecker W. S, Peteet D, Rind D. 1985. Does the ocean-atmosphere system have more than one stable mode of operation? *Nature* 315, 21-25.

Broecker W. S, Sutherland S, Smethie W, Peng T.-H, and Ostlund, G. 1995. Oceanic radiocarbon: Separation of the natural and bomb components. *Global Biogeochemical Cycles* 9, 263-288.

Bronk Ramsey C. 1994. Analysis of Chronological Information and Radiocarbon Calibration: The Program OxCal. *Archaeological Computing Newsletter* 41, 11-16.

Bronk Ramsey C. 1995. Radiocarbon Calibration and Analysis of Stratigraphy: The OxCal Program. *Radiocarbon* 37 (2), 425-430.

Bronk Ramsey C. 2001. Development of the Radiocarbon Program OxCal, *Radiocarbon*, 43 (2A) 355-363.

Bronk Ramsey C. 2005. OxCal v.3.01. [Online]. Available from http://www.rlaha.ox.ac.uk/orau/oxcal.html [Accessed 12/07/2005].

Brown T. A, Nelson D. E, Mathews R.W, Vogel J. S, and Southon J. R. 1989. Radiocarbon Dating of Pollen by Accelerator Mass spectrometry. *Quaternary Research* 32, 205-212.

Bruns M, Levin I, Munnich K. O, Hubberten H, and Fillipakis S. 1980. Regional sources of volcanic carbon dioxide and their influence on ^{14}C content of present-day plant material. *Radiocarbon* 22 (2), 532-536.

Buchanan D. L and Corcoran B. J. 1959. Sealed-tube combustions for the determination of carbon-13 and total carbon. *Analytical Chemistry* 31, 1635-1637.

Buck C.E and Blackwell P. G. 2004. Formal Statistical Models for Estimating Radiocarbon Calibration Curves. *Radiocarbon* 46 (3), 1093-1102.

Burman J and Schmitz B. (2005). Periwinkle (*Littorina littorea*) intrashell $\delta^{18}O$ and $\delta^{13}C$ records from the mid-Holocene Limfjord region, Denmark: a new high-resolution palaeoenvironmental proxy approach. *The Holocene* 15 (4), 567-575.

Burr G. S, Beck J. W, Taylor F. W, Recy J, Edwards R. L, Caioch G, Correge T, Donahue D. J, and O'Malley J. M. 1998. A high-resolution radiocarbon calibration between 11,700 and 12,400 calendar years BP derived from ^{230}Th ages of corals from Espiritu Santo Island, Vanuatu. *Radiocarbon* 40 (3), 1127-1151.

Burrows M, and Thorpe S. A. 1999. Drifter observations of the Hebrides slope current and nearby circulation patterns. *Annales Geophysicae* 17, 280-302.

Calvo E, Grimalt J, Jansen E. 2002. High resolution U^{K}_{37} sea surface temperature reconstruction in the Norwegian Sea during the Holocene. *Quaternary Science Reviews* 21, 1385-1394.

Campin J-M, Fichefet T, Duplessy J-C. 1999. Problems with using radiocarbon to infer ocean ventilation rates for past and present climates. *Earth and Planetary Science Letters* 165, 17-24.

Castagnoli G and Lal D. 1980. Solar modulation effects in terrestrial production of carbon-14. *Radiocarbon* 22 (2), 133-158.

Cerling T. E and Craig H. 1994. Geomorphology and in-situ cosmogenic isotopes. *Annual Review of Earth and Planetary Science* 22, 273-217.

Chappell J and Polach H.A. 1972. Some effects of partial recrystallisation on C dating of late Pleistocene corals and molluscs. *Quaternary Research* 2, 244-252.

Church M. J. 2002. *Plants and people in the later prehistoric and Norse periods of the Western Isles of Scotland.* Unpublished PhD thesis, Department of Archaeology, University of Edinburgh

Church M. J, Arge S. V, Brewington S, McGovern T. H, Woollett J, Perdikaris S, Lawson I. T, Cook G. T, Amundsen C, Harrison R, Krivogorskaya K and Dunbar E. *In press* .Puffins, Pigs, Cod, and Barley: Palaeoeconomy at Undir Junkarinsfløtti, Sandoy, Faroe Islands. *Environmental Archaeology*, 10.

Clarke D. V. 1976. Excavations at Skara Brae a summary account. In Burgess C and Miket, R (eds.) *Settlement and economy in the 3rd and 2nd millennium BC.* British Archaeological Reports, BAR British series, 33, Oxford, 233-50.

Clark P.U, Pisias N.G, Stocker T. F, and Weaver A. J. 2002. The role of the thermohaline circulation in abrupt climate change. *Nature* 415, 863-869.

Connock K. D. 1988. Carding Mill Bay (Kilmore & Kilbride parish) shell midden and later inhumation. *Discovery and Excavation, Scotland* 1988, 23.

Connock K. D. 1990. A shell midden at Carding Mill Bay, Oban. *Scottish Archaeological Review* 7, 74-76.

Connock K. D, Finlayson B, and Mills C. M. 1992. Excavation of a shell midden site at Carding Mill Bay near Oban, Scotland. *Glasgow Archaeological Journal* 17, 25-38.

Coplen T.B. 1994. Reporting of stable hydrogen, carbon and oxygen isotope abundances. *Pure and Applied Chemistry* 66, 273-76.

Craig H. 1957. Isotopic Standards for Carbon and Oxygen and Correction Factors for Mass-Spectrometric Analysis of Carbon Dioxide. *Geochimica et Cosmochimica Acta* 12,133-149.

Damon P. E, Lerman J. C and Long A.1978. Temporal fluctuations of atmospheric ^{14}C: Causal factors and implications. *Annual Review of Earth and Planetary Science* 6, 457-494.

Damon P. E and Linick T. 1986. Geomagnetic-heliomagnetic modulation of atmospheric radiocarbon production. Radiocarbon 28 (2A), 266-278.

Dansgaard W, Johnsen S. J, Clausen H. B, Dahl-Jensen D, Gundestrup N. S, Hammer C. U, Hvidberg C. S, Steffensen J. P, Sveinbjornsdottir A. E, Jouzel J and Bond G. 1993. Evidence for general instability of past climate from a 250-kyr ice-core record. *Nature* 364, 218-220.

Davis A.M, McAndrews J.H and Wallace B. 1988. Paleoenvironment and the archaeological record at the L'Anse aux Meadows site. *Geoarchaeology* 3, 53-64.

Deser C, Walsh J.E and Timlin M.S. 2000. Arctic sea ice variability in the context of recent wintertime atmospheric circulation trends. *Journal of Climate* 13, 617-633.

Desilets D and Zreda M. 2001. On scaling cosmogenic nuclide production rates for altitude and latitude using cosmic-ray measurements. *Earth and Planetary Science Letters* 193, 213-225.

Dettman D.L, Kendall C, Lohmann K.C, and Flessa K.W, 1999. A new method for isotope paleohydrology: Molluscan carbonate, North American rivers, and the seasonal oxygen isotope cycle of the pre-dam Colorado River. *EOS (Supplement), Transactions of the American Geophysical Union* 80 (46), F480.

Dickson R.R, Meincke J, Malmberg S.A and Lee A.J. 1984. The great salinity anomaly in the northern North Atlantic, 1968-82. *Progress in Oceanography* 20, 103-151.

Dockrill S. J, Turner V. E and Bond J. M. 1995. Scatness Broch Excavation (Dunrossness parish), multi-period settlement mound with broch. *Discovery and Excavation, Scotland* 1995, 104-105.

Dockrill S. J, Turner V. E, and Bond J. M. 1997. Old Scatness/Jarlshof Environs Project (Dunrossness parish), multi-period settlement mound. *Discovery and Excavation, Scotland* 1997, 69-70.

Dockrill S. J, Turner V. E and Bond J. M. 1998. Old Scatness/Jarlshof Environs Project (Dunrossness parish), broch; multi-period settlement mound. *Discovery and Excavation, Scotland* 1998, 83-84.

Dockrill S. J, Turner V. E and Bond J. M. 1999. Old Scatness/Jarlshof Environs Project (Dunrossness parish), broch; multi-period settlement mound. *Discovery and Excavation, Scotland* 1999, 80-81.

Dockrill S. J, Turner V. E, and Bond J. M. 2000. Old Scatness/Jarlshof Environs project, Shetland (Dunrossness parish), broch; multi-period settlement mound. *Discovery and Excavation, Scotland* 1 2000, 79-81.

Dockrill S. J, Turner V. E, and Bond J. M. 2001. Old Scatness/Jarlshof Environs Project (Dunrossness parish), broch; multi-period settlement mound. *Discovery and Excavation, Scotland* 2 2001, 86.

Dockrill S. J, Turner V. E, and Bond J. M. 2002. Old Scatness/Jarlshof Environs Project, Shetland (Dunrossness parish), Broch; multi-period settlement mound. *Discovery and Excavation, Scotland* 3 2002, 105-7.

Dockrill S. J, Turner V. E, and Bond J. M. 2003. Old Scatness/ Jarlshof Environs project (Dunrossness parish), broch; multi-period settlement mound. *Discovery and Excavation, Scotland* 4 2003, 118-9.

Donahue D. J, Linick T. W and Jull A. J. T. 1990. Isotope ratio and background corrections for accelerator mass spectrometry radio carbon measurements. *Radiocarbon* 32 (2), 135-142.

Donohoe G, Hensey M and O'Connor, B. 2000. An assessment of water quality data from Kilkieran Bay, Co. Galway. *Marine and environmental health series* 1.

Dooley H. D, Martin J, H, A and Payne R. 1976. Flow across the continental slope off northern Scotland. *Deep-Sea Research* 23, 875-880.

Dutta K, Bhushan R and Somayajula B. L. K. 2001. ΔR Correction values for the Northern Indian Ocean. *Radiocarbon* 43 (2A), 483-488.

Duplessy J. C, Bard E, Labeyrie L, Duprat J, and Moyes J. 1993. Oxygen isotope records and salinity changes in the northeastern Atlantic during the last 18,000 years. *Paleoceanography* 8, 341-350.

Dye T. 1994. Apparent Ages of Marine Shells: Implications for Archaeological Dating in Hawaii. *Radiocarbon* 36(1), 51-57.

Dyke A.S, Andrews J.T, Clark P.U, England J.H, Miller G.H, Shaw J and Veillette J.J. 2002. The Laurentide and Innuitian ice sheets during the Last Glacial Maximum. *Quaternary Science Reviews* 21, 9–31.

Dyke A. S, Dale J. E and McNeely R. N. 1996. Marine molluscs as indicators of environmental change in glaciated North America and Greenland during the last 18,000 years. *Géographie physique et Quaternaire* 36, 5-14.

Dyke A.S, McNeely R, Southon J, Andrews, J.T, Peltier W.R, Clague J.J, England J.H, Gagnon J-M and Baldinger, A. 2003. Preliminary assessment of Canadian marine reservoir ages. *Joint Annual Meeting of the Canadian Quaternary Association and the Canadian Geomorphology Research Group*. Halifax, Nova Scotia, June 8-12, 2003.

Edwards R. L, Beck J.W, Burr G.S, Donahue D.J, Chappell J.M.A, Bloom A.L, Druffel E.R.M and Taylor F.W. 1993. A large drop in atmospheric $^{14}C/^{12}C$ and reduced melting in the Younger Dryas, Documented with ^{230Th} ages of corals. *Science* 260, 962-968.

Edwards K. J and Ralston I. B. 1997. *Scotland: environment and archaeology, 8000 BC-AD 1000.* Chichester. Wiley.

Ehmann W. D, and Vance D. E. 1991. *Radiochemistry and Nuclear Methods of Analysis*. J. Wiley and Sons.

Eiríksson J, Knudsen K. L, Haflidason H and Heinemeier J. 2000a. Chronology of late Holocene climatic events in the Northern North Atlantic based on AMS ^{14}C dates and tephra markers from the volcano Hekla, Iceland. *Journal of Quaternary Science* 15 (6), 573-580.

Eiríksson J, Knudsen K. L, Haflidason H and Henriksen P. 2000b. Late-Glacial and Holocene Paleoceanography of the North Icelandic Shelf. *Journal of Quaternary Science* 15 (1), 23-42.

Eiríksson J, Larsen G, Knudsen K. L, Heinemeier J and Símonarson L. A. 2004. Marine reservoir age variability and water mass distribution in the Iceland Sea. *Quaternary Science Reviews* 23, 2247-2268.

Elliott M, deMenocal P. B, Linsley B. K and Howe S. S. 2003. Environmental controls on the seasonal isotopic records of Mercenaria mercenaria and potential application to paleoenvironmental studies. *Geochemistry Geophysics Geosystems* 4, 1056.

Elmore D, 1982. In Henning W, Kutschera W, Smither R. K and Yntema J. L. (eds.), *Proceedings of the symposium on Accelerator Mass Spectrometry*, Argonne, IL, 11 to 13 May 1981 (Argonne National Laboratory, Argonne, IL, 1982), 346-358.

Elmore D and Phillips F. M. 1987. Accelerator Mass Spectrometry for Measurement of Long-Lived Radioisotopes. *Science* 236, 543-550.

Epstein S, Buchsbaum R, Lowenstam H and Urey H. C. 1953. Revised carbonate water isotopic temperature scale. *Geological Society of America Bulletin,* 64, 1315-1326.

Evans J and O'Connor T. 1999. *Environmental Archaeology: Principles and Methods.* Sutton Publishing Ltd.

Facorellis Y and Maniatis Y. 1998. Apparent ages of marine mollusk shells from a Greek island: calculation of the Marine Reservoir Effect in the Aegean Sea. *Radiocarbon* 40 (2), 963-973.

Fairbanks R. G. 1989. A 17,000 years glacio-eustatic sea level record: Influence of glacial melting rates on the Younger Dryas event and deep ocean circulation. *Nature* 342, 637-642.

Fifield L. K. 1999. Accelerator mass spectrometry and its applications. *Reports on Progress in Physics* 62, 1223-1274.

Finkel R. C and Suter M. 1993. AMS in the Earth sciences: Techniques and applications In Hyman M and Rowe M. W. (eds.). *Advances in analytic geochemistry.* Greenwich, Connecticut, JAI Press, vol. 1, 1-114.

Finlayson B, Hardy K and Wickham-Jones C. 1999. Inner Sound (Applecross; Kilmuir; Portree; Snizort; Strath parishes), Survey and trial excavation. *Discovery and Excavation, Scotland* 1999, 49-50.

Fojut, N. 1981. Is Mousa a broch? *Proceedings of the Societies of Antiquities of Scotland* 111. 220-228.

Forman S. L and Polyack L. 1997. Radiocarbon content of pre-bomb marine molluscs and

variations in the 14C reservoir age for coastal areas of the Barents and Kara seas, Russia. *Geophysical Research Letters* 24 (8), 885-888.

Frank M. 2000. Comparison of cosmogenic radionuclide production and geomagnetic field intensity over the last 200000 yr. *Royal Society of London Philosophical Transactions A* 358, 1089-1107.

Geyh M. A and Schleicher. 1990. *Absolute Age Determination: Physical and Chemical Dating Methods and their Application*. Springer-Verlag

Gilbertson D, Kent M and Grattan J. (eds.). 1996. *The Outer Hebrides: The Last 14,000 Years*. Sheffield Environmental and Archaeological Research Campaign in the Hebrides, Vol. 2. Sheffield Academic Press.

Gillen C. 2003. *Geology and landscapes of Scotland*. Harpenden, Terra.

Gillibrand P. A, Sammes P. J, Slesser G, and Adams R. D. 2003. *Seasonal water column characteristics in the little and North Minches and the Sea of the Hebrides. I. Physical and chemical parameters*. Fisheries Research Services internal report No. 08/03. March 2003.

Giraudeau J, Cremer M, Manthe S, Labeyrie L and Bond G. 2000. Coccolith evidence for instabilities in surface circulation south of Iceland during Holocene times. *Earth and Planetary Science Letters* 179, 257-268.

Glasgow University Archaeological Research Division (GUARD). 2004. *Stenchme, Lopness cist burial*. Unpublished draft report of excavation by GUARD archaeological services, University of Glasgow.

Godwin H. 1962. Half-life of radiocarbon. *Nature* 195, 984.

Goodfriend G. A and Flessa K. W. 1997. Radiocarbon reservoir ages of the Gulf of California: Roles of upwelling and flow from the Colorado River. *Radiocarbon* 39, 139-148.

Gonfiantini R. 1984. Stable Isotope Reference Samples for Geochemical and Hydrological Investigations. In Advisory group meeting on stable isotope reference samples for geochemical and hydrological investigations, Sept. 19-21, 1983. *Report to the Director General, International Atomic Energy Agency, Vienna, 1984*. IAEA, 77.

Goslar T, Arnold M, Bard E, Kuc T, Mieczys A. W, Pazdur F, Ralska-Jasiewiczowa M, Róanski K, Tisnerat N, Walanus A, Wicik B and Wigkowski K. 1995. High concentration of atmospheric ^{14}C during the Younger Dryas cold episode. *Nature* 377, 414-417.

Gosse J. C and Phillips F. M. 2001. Terrestrial in situ cosmogenic nuclides: theory and application. *Quaternary Science Reviews* 20, 1475-1560.

Gregory R. A, Murphy E. M, Church M. J, Edwards K, Guttmann E. B and Simpson D. D. *In press*. Archaeological Evidence for the First Mesolithic Occupation of the Western Isles of Scotland. *The Holocene*, 15.

Grootes P. M, Mook W. G, Vogel J. C, de Vries A. E, Haring A, Kistemaker J. 1975. Enrichment of radiocarbon for dating samples up to 75,000 years. *Zeitschrift für Naturforschung* 30a, 1-14.

Grossman E. L and Ku T. L. 1986. Oxygen and carbon isotope fractionation in biogenic aragonite: Temperature effects. *Chemical Geology* 59, 59-74.

Grove J. M and Switsur V. R. 1994. Glacial geological evidence for the Medieval Warm Period. *Climate Change* 26, 143-169.

Gulliksen S. and Scott M. 1994: Report of TIRI Workshop, Saturday 13 August 1994. *Radiocarbon* 37, 820–821.

Guyodo Y and Valet J. P. 1999. Global changes in intensity of the Earth's magnetic field during the past 800 kyr. *Nature* 399, 249-252.

Haflidason H, Eiríksson J and Van Kreveld, S. 2000. The tephrochronology of Iceland and the North Atlantic region during the middle and Late Quaternary: a review. *Journal of Quaternary Science* 15 (1), 3-22.

Haflidason H, Sejrup H. P, Kristensen D. K and Johnsen S. 1995. Coupled response of the late glacial climatic shifts of northwest Europe reflected in Greenland ice cores: Evidence from the Northern North Sea. *Geology* 23 (12), 1059-1062.

Hajdas I, Ivy S. D, Beer J and Bonani G. 1993. AMS radiocarbon dating and varve chronology of Lake Soppensee. *Climate Dynamics* 9, 107-116.

Hannon G. E and Bradshaw R. H. W. 2000. Impacts and timing of the first human settlement on vegetation of the Faroe Islands. *Quaternary Research* 54, 404-13.

Hannon G. E, Wastegård S, Bradshaw E and Bradshaw R. H. W. 2001. Human impact and landscape degradation in the Faroe Islands. *Biology and Environment: Proceedings of the Royal Irish Academy* 101B (1-2), 129-139.

Hansen B and Meincke J. 1979. Eddies and meanders in the Iceland-Faroe Ridge area. *Deep-Sea Research* 26, 1067-1082.

Hansen B and Østerhus S. 2000. North Atlantic-Nordic Seas exchanges. *Progress in Oceanography* 45, 109-208.

Harding D. W and Gilmour S. M. D. 2000. *The Iron Age settlement at Beirgh, Riof, Isle of Lewis: excavations 1985-95: volume 1: the structures and stratigraphy*. Calanais Research Series number 1, Edinburgh.

Hardy K and Wickham-Jones C. R. 2003. Scotland's First Settlers: An Investigation into Settlement, territoriality and mobility during the Mesolithic in the Inner Sound, Scotland. In Larsson L, Kindgren H, Åkerlund A, Knutsson K and Loeffler D. (eds.). *Mesolithic on the move: Proceedings of the Mesolithic 2000 Conference, Oxford*. Oxbow books, 369-384.

Hardy K and Wickham-Jones C. R. 2004. Scotland's First Settlers. The study of an archaeological seascape. In Carver E and Lelong O. (eds.). Modern views-Ancient lands: New work and thought on cultural landscapes. *British Archaeological Reports British Series* 377, 51-64.

Hardy K and Wickham-Jones C. R. *in press*. Mesolithic and later sites around the Inner Sound, Scotland: The work of Scotland's First Settlers Project 1998-2004. [Online] *Scottish Archaeological Internet Reports*, forthcoming. Available at http://www.SAIR.org.uk.

Harkness D. D. 1983. The extent of natural ^{14}C deficiency in the coastal environment of the United Kingdom. *PACT, Journal of the European Study Group on Physical, Chemical and Mathematical Techniques Applied to Archaeology* 8 (IV.9), 351-364.

Håkansson S. 1983. University of Lund Radiocarbon Dates XVI. *Radiocarbon* 25, 875-891.

Hedges R.E.M and van Klinken G.J. 1992. A review of current approaches in the pretreatment of bone for radiocarbon dating by AMS. *Radiocarbon* 34 (3), 279-291.

Heier-Neilsen S, Heinemeier J, Nielsen H. L and Rud N. 1995. Recent reservoir ages for Danish Fjords and marine waters. *Radiocarbon* 37 (3), 875-882.

Hesshaimer V, Heimann M and Levin I. 1994. Radiocarbon evidence for a smaller oceanic carbon dioxide sink than previously believed. *Nature* 370, 201-203.

Hill, J.M., 2000. *Patella vulgata*. Common limpet. *Marine Life Information Network: Biology and Sensitivity Key Information Sub-programme* [on-line]. Plymouth: Marine Biological Association of the United Kingdom. [cited 21/07/2005]. Available from: http://www.marlin.ac.uk/species/Patellavulgata.htm

Hjort C. 1973. A sea correction for East Greenland. *Geolgiska Foreningens i Stockhom Forhandlingar* 95, 132-134.

Hogg A. G, Higham T. F. G and Dahm J.1998. ^{14}C Dating of Modern Marine and Estuarine Shellfish. *Radiocarbon* 40, 975-984.

Hughen K.A, Overpeck J.T, Lehman S.J, Kashgarian M and Southon. J. R. 1988. A New C-14 Calibration Data Set for the Last Deglaciations Based on Marine Varves. *Radiocarbon* 40, 483-494

Hughen K.A, Overpeck J.T, Lehman S.J, Kashgarian M and Southon. J. R. Peterson L. C, Alley R and Sigman D. M. 1988b. Deglacial changes in ocean circulation from an extended calibration. *Nature* Vol.391, 65-68.

Hughen K. A, Baillie M. G. L, Bard E, Beck J. W, Bertrand C. J. H, Blackwell P. G, Buck C. E, Burr G. S, Cutler K. B, Damon P. E, Edwards R. L, Fairbanks R. G, Friedrich M, Guilderson T. P, Kromer, B, McCormac G, Manning S, Bronk Ramsey C, Reimer P. J, Reimer R. W, Remmele S, Southon J. R, Stuiver M, Talamo S, Taylor F. W, van der Plicht J and Weyenmeyer, C. E. 2004. MARINE04 Marine radiocarbon age calibration, 0-26 cal kyr BP. *Radiocarbon* 46 (3), 1059-1086.

Humlum O. 1998. Rock glaciers on the Faeroe Islands, the North Atlantic, *Journal of Quaternary Science* 13, 293-308.

Hut G. 1987. Consultants' group meeting on stable isotope reference samples for geochemical and hydrological investigations, report to the Director General, 42 pp., International Atomic Energy Agency, Vienna.

Indermühle A, Stocker T.F, Joss F, Fischer H, Smith H. J, Wahlen M, Deck B, Mastroianni D, Tschumi J, Blunier T, Meyer R and Stauffer B. 1999. Holocene carbon-cycle dynamics based on CO_2 trapped in ice at Taylor Dome, Antarctica. *Nature* 398, 121-126.

Ingólfsson Ó, Bjorck S, Haflidason H and Rundgren, M. 1998. Glacial and climatic events in Iceland reflecting regional North Atlantic climatic shifts during the Pleistocene-Holocene transition. *Quaternary Science Reviews* 16, 1135-1144.

Ingram BL. 1996. Reservoir ages in Eastern Pacific coastal and estuarine waters. *Radiocarbon* 38(3): 573-582.

Ingram B. L and Southon J. R. 1996. Reservoir ages in Eastern Pacific coastal and estuarine waters. *Radiocarbon* 38, 573-582.

Jenkins S. R and Hartnoll R.G. 2001. Food supply, grazing activity and growth rate in the limpet Patella vulgata L.: a comparison between exposed and sheltered shores. *Journal of Experimental Marine Biology and Ecology* 258 (17), 123-139.

Jóhansen J. 1985. *Studies in the vegetational history of the Faroe and Shetland Islands.* Torshaven, Faroe Islands, Føroya Fróðskaparfelag.

Jones G. 1986. *The Norse Atlantic Saga: Being the Norse Voyages of Discovery and Settlement to Iceland, Greenland and North America.* Oxford, Oxford University Press.

Jones G. A, Jull A. J. T, Linick T.W and Donahue D.J. 1989. Radiocarbon dating of deep-sea sediments: A comparison of accelerator mass spectrometry and beta-decay methods. *Radiocarbon* 31 (2), 105-116.

Karpuz N and Jansen E. 1992. A high-resolution diatom record of the last deglaciation from the SE Norwegian Sea: Documentation of rapid climatic change. *Paleoceanography* 7, 499-520.

Keith M. L, Anderson G. M and Eichler R. 1964. Carbon and oxygen isotope composition of mollusk shells from marine and fresh-water environments. *Geochimica et Cosmochimica Acta* 28, 1757-86.

Klitgaard-Kristensen D, Sejrup H.P, Haflidason H, Johnsen S and Spurk M. 1998. The short cold period 8,200 years ago documented in oxygen isotope records of precipitation in Europe and Greenland. *Journal of Quaternary Sciences* 13, 165-169.

Knight P. J and Howarth M. J. 1999. The flow through the north channel of the Irish Sea. *Continental Shelf Research* 19 (5), 693-716.

Knudsen K.L and Eiríksson J. 2002. Application of tephrochronology to the timing and correlation of palaeoceanographic events in Holocene and Lateglacial shelf sediments off North Iceland. *Marine Geology* 191, 165-188.

Knudsen K. L, Eiríksson J, Jansen E, Jiang H, Rytter F and Gudmundsdóttir E. R. 2004. Paleoceanographic changes off North Iceland through the last 1200 years: foraminifera, stable isotopes, diatoms and ice rafted debris. *Quaternary Science* Reviews 23, 2231-2246.

Koç N, Jansen E and Haflidason H. 1993. Palaeoceanographic reconstructions of surface ocean conditions in the Greenland, Iceland and Norwegian Seas through the last 14ka based on diatoms. *Quaternary Science Reviews* 12, 115-140.

Korff S. A. and Mendell R. B. 1980. Variations on radiocarbon production in the Earth's atmosphere. *Radiocarbon* 22 (2), 159-165.

Kovanen D. J and Easterbrook D. J. 2002. Paleodeviations of radiocarbon marine reservoir values for the northeast Pacific. *Geology* 30 (3), 243-246.

Kratz G, Kohlmaier C. H, Siré E. O, Fischbach U and Bröhl, H. 1983. Carbon exchange between atmosphere and oceans in a latitude-dependant advection-diffusion model. *Radiocarbon* 25 (2), 459-471.

Krog H and Tauber H. 1974. C-14 chronology of late- and post-glacial marine deposits in north Jutland. *Danmarks geologiske Undersøgelse, Årbog*, 93-105.

Kroon D, Austin W. E. N, Chapman M. R, and Ganssen, G. M. 1997. Deglacial surface circulation changes in the northeastern Atlantic: Temperature and salinity records off NW Scotland on a century scale. *Paleoceanography* 12 (6), 755-763.

Kuijpers A, Hansen B, Hühnerbach V, Larsen B, Nielsen T and Werner F. 2002. Norwegian Sea overflow through the Faroe-Shetland gateway as documented by its bedforms. *Marine Geology* 188, 147-164.

Kuijpers A, Troelstra S. R, Wisse M, Heier Nielsen S and van Weering T. C. E. 1998: Norwegian Sea overflow variability and NE Atlantic surface hydrography during the past 150, 000 years. *Marine Geology* 152, 101-127.

Lal D. 1988. In-situ produced cosmogenic isotopes in terrestrial rocks. *Annual Reviews of Earth and Planetary Sciences* 16, 355-388.

Lal D. 1991. Cosmic ray labelling of erosion surfaces: in-situ production rates and erosion models. *Earth and Planetary Science Letters* 104, 424.

Lal D. 2000. Cosmogenic nuclide production rate systems in terrestrial materials: Present knowledge, needs and future actions for improvement. *Nuclear Instruments and Methods in Physics Research* B172, 772-781.

Lal D and Peters B. 1967. Cosmic ray produced radioactivity on the Earth. In Flugge S. (ed.). *Handbuch der Physik.* Springer Verlag, Berlin, 46, 551-612.

Lamb H. H. 1977. *Climate - Present, Past and Future. Volume 2. Climatic history and future.* Methuen, London.

Lamb H. H. 1985. *Climatic History and the Future.* Princeton University Press, Princeton, NJ.

Lambeck K. 1995. Late Devensian and Holocene shorelines of the British Isles from models of glacio-hydro-isostatic rebound. *Journal of the Geological Society* 152, 437-48.

Larsen G, Eiríksson J, Knudsen K.L and Heinemeier J. 2002. Correlation of late Holocene terrestrial and marine tephra markers, north Iceland: Implications for reservoir changes. *Polar Research* 21, 283–290.

Lehman S. J and Keigwin L. D. 1992. Sudden changes in North Atlantic circulation during the last deglaciation. *Nature* 356, 757-762.

Levin I, Münnich K.O and Weiss W. 1980. The effect of anthropogenic CO2 and 14C sources on the distribution of 14C in the atmosphere. *Radiocarbon* 22 (2), 379-91.

Levin I and Hesshaimer V. 2000. Radiocarbon – a unique tracer of global carbon cycle dynamics. *Radiocarbon* 42 (1), 69-80.

Levin I and Kromer B. 1997. Twenty years of atmospheric $^{14}CO_2$ observations at Schauinsland station, Germany. *Radiocarbon* 39 (2), 205-218.

Levitus S. 1982. *Climatological Atlas of the World Ocean.* NOAA Prof. Papers, 13, U.S. Government Printing Office, Washington, D. C.

Levitus S and Boyer T.P. 1994, World ocean atlas 1994, Volume 4: Temperature: Washington, D.C., NOAA Atlas NESDIS.

Libby W.F, Anderson E.C and Arnold J.R. 1949. Age determination by Radiocarbon content: world-wide assay of natural radiocarbon. *Science* 109, 227-28.

Libby W. F, Berger R, Mead J. F, Alexander G. V and Ross J. F. 1964. Replacement rates of human tissue from atmospheric radiocarbon. *Science*, 146, 1170-1172.

Liss P.S and Merlivat L. 1986, *Air-Sea Gas Exchange Rates: Introduction and Synthesis,* In Menard, P.B. (ed.). *The Role of Air-Sea Exchange in Geochemical Cycling.* Dordrecht, Holland, 113-127

Long A and Kalin R. M. 1992. High-Sensitivity Radiocarbon Dating in the 50,000 to 70,000 BP Range without Isotopic Enrichment. *Radiocarbon* Vol. 34 No. 3, 351-359.

Longin R. 1971. New method of collagen extraction for radiocarbon dating. *Nature* 230. 241-242.

Lowe C. 1998. *St Boniface Church, Orkney; Coastal erosion and archaeological assessment.* Sutton Publishing Ltd., Stroud.

Lowe D. C and Judd W. J. 1987. Graphite target preparation for radiocarbon dating by accelerator mass spectrometry. *Nuclear Instruments and Methods* Vol. B28, 113-116.

Lowe J.J and Walker M.J.C. 1984. *Reconstructing Quaternary Environments.* Longman, Harlow.

Mangerud J. 1972. Radiocarbon dating of marine shells, including a discussion of apparent age of recent shells from Norway. *Boreas* 1, 143-172.

Mangerud J and Gulliksen S. 1975. Apparent Radiocarbon ages of recent marine shells from Norway, Spitsbergen and Arctic Canada. *Quaternary Review* 5, 263-273.

Marchal O, Cacho I, Stocker T. F, Grimalt J. O, Calvo E, Martrat B, Shackleton N, Vautravers M, Cortijo E, van Kreveld S, Andersson C, Koç N, Chapman M, Sbaffi L, Duplessy J-C, Sarnthein M, Turon J-L, Duprat J and Jansen E. 2002. Apparent long-term cooling of the sea surface during the Holocene. *Quaternary Science Reviews* 21, 455-483.

Masarik J and Beer J. 1999. Simulation of particle fluxes and cosmogenic nuclide production in the Earth's atmosphere. *Journal of Geophysical Research* 104, 12,009-12,111.

Mayewski P. A and White F. 2002. *The Ice Chronicles.* University Press of New England.

McCormac F. G, Hogg A. G, Blackwell P. G, Buck C, Higham T. F. G, and Reimer P. J. 2004. SHCAL04 Southern hemisphere calibration, 0-11.0 cal kyr BP. *Radiocarbon* 46 (3), 1087-1092.

McCormac F. G, Hogg A. G, Higham T. F. G, Lynch-Stieglitz J, Broecker W, Ballie M. G. L, Palmer J, Xiong L, Pilcher J. R, Brown D, and Hoper S. T. 1998. Interhemispheric difference in ^{14}C: An anthropogenic effect. *Geophysical Research Letters* 25 (9), 1321-1324.

McCormac F. G, Reimer P. J, Hogg A. G, Higham T. F. G, Baillie M. G. L, Palmer J and Stuiver M. 2002. Calibration of the radiocarbon timescale for the Southern Hemisphere AD 1850-950. *Radiocarbon* 44 (3), 641-651.

McGovern T.H. 1991. Climate, correlation and causation in Norse Greenland. *Arctic Anthropology* 28. 77-100.

McGovern T. H, Vésteinsson O, Fridriksson A, Church M, Lawson I, Simpson I. A, Einarsson A, Dugmore A, Cook G, Perdikaris S, Edwards K, Thomson A M, Adderly P, Newton A, Lucas G, Aldred O. 2005. Landscapes of Settlement in Northern Iceland: Historical Ecology of Human Impact and Climate Fluctuation on the Millennial Scale. Submitted to *American Anthropologist.*

McKay W. A, Baxter J. M, Ellett D. J and Meldrum D. T. 1996. Radiocaesium and circulation patterns west of Scotland. *Journal of Environmental Radioactivity* 4, 205-232.

McNichol A. P, Jull A. J. T and Burr G. S. 2001. Converting AMS data to radiocarbon values: Considerations and conventions. *Radiocarbon* 43 (2A), 313-320.

Meese D.A, Alley R.B, Fiacco R.J, Germani M.S, Gow A.J, Grootes P.M, Illing M, Mayewski P.A, Morrison M.C, Ram M, Taylor K.C, Yang Q and Zielinski G.A. 1994. Preliminary depth-age scale of the GISP2 ice core. *Special CRREL Report* 94-1, US.

Merlivat L and Memery L. 1983. Gas exchange across an air-water interface: Experimental results and modelling of bubble contribution to transfer. *Journal of Geophysical Research* 88 (C1), 707-724.

Middleton R. 1983. A versatile high intensity negative ion source: Nuclear Instruments and Methods in Physics Research 214, 139–150.

Monge Soares A. M. 1993. The ^{14}C content of marine shells: evidence for variability in coast upwelling off Portugal during the Holocene. In *Isotope techniques in the Study of Past and Current Environmental Changes in the Hydrosphere and Atmosphere (Proceedings) Vienna.* IAEA-SM-329/49, 471-485.

Mook, W. G and Van der Plicht J. 1999. Reporting ^{14}C activities and concentrations. *Radiocarbon* 41 (3), 227-239.

Mook W.G and Waterbolk H.T. 1985. *Radiocarbon Dating. Handbook for Archaeologists No.3.* European Science Foundation Strasbourg.

Moros M, Endler R, Lackschewitz K. S, Wallrabe-Adams H.-J, Mienert J and Lemke W. 1997: Physical properties of Reykjanes Ridge sediments and their linkage to high-resolution Greenland Ice Sheet project 2 ice core data. *Paleoceanography* 12, 687-695.

Morris C, D. 1979. Birsay, Orkney: 'small sites' excavation and survey. *University of Durham Newcastle upon Tyne archaeological Report* 2, 11-19.

Morris C, D. 1989. The Birsay Bay project: coastal sites beside the Brough Road, Birsay, Orkney: excavations 1976-1982. *University of Durham, Dept of Archaeology, Monograph series* 1. Durham, passim.

Morris C. D, Batey C. E and Rackham D. J. 1995. Freswick Links, Caithness: Excavation and survey of a Norse settlement. *North Atlantic Biocultural Organisation, Monograph 1,* Highland Libraries.

Mueller K and Muzikar P. 2002. Quantitative study of contamination effects in AMS ^{14}C sample processing. *Nuclear Instruments and Methods in Physics research B* 197, 128-133.

Murray E. V. 1999. *Early evidence for coastal exploitation in Ireland.* Unpublished PhD thesis, Queens University, Belfast.

Muzikar P, Elmore D and Granger D. E. 2003. Accelerator mass spectrometry in geologic research. *Geological Society of America Bulletin*, June 2003, 115 (6), 643-654.

Myers J.S. 1971. The Late-Laxfordian granitic-migmatite complex of western Harris, Outer Hebrides. *Scottish Journal of Geology*, 7, 254-84.

Neftel A, Moor E, Oeschger H and Stauffer B. 1985. Evidence from polar ice cores for the increase in atmospheric CO_2 in the past two centuries. *Nature* 315, 45-47.

Neftel A, Oeschger H and Suess H. 1981. Secular non-random variations of cosmogenic Carbon-14 in the terrestrial atmosphere. *Earth and Planetary Science Letters* 56, 127-147.

Neighbour T. 2001. Excavation at Bostadh Beach, Great Bernera, Isle of Lewis. CFA Archaeology Ltd. Report No. 636.

Neighbour T and Burgess C. 1996. Traigh Bostadh (Uig parish), 1st millennium AD settlement. *Discovery and Excavation, Scotland* 1996, 113-114,

Neighbour T and Church M. 2001. The eroding settlement and Iron Age cemetery at Galson, Isle of Lewis. CFA Report No. 635.

Oeschger H, Siegenthaler U, Schotterer U and Gugelmann A. 1975. A box diffusion model to study the carbon dioxide exchange in nature. *Tellus* 27, 168-192.

Ogilvie A. E. J. 1996. Sea-ice conditions off the coast of Iceland AD 1601-1850 with special reference to part of the Maunder Minimum period (1675-1715). AmS-Varia 25, 9-12.

O'Keeffe T. 1994. Omey and the Sands of Time. *Archaeology Ireland* 8 (2), 22-4.

Olsson I. U. 1980. Content of ^{14}C in marine mammals from Northern Europe. *Radiocarbon* 22 (3), 662-675.

Olsson I. U. 1983. Radiocarbon dating in the Arctic region. *Radiocarbon* 25 (2), 393-394.

O'Neil J. R, Clayton R.N and Mayeda, T. 1969. Oxygen isotope fractionation in divalent metal carbonates. *Journal of Chemical Physics* 51, 5547-5558.

OSPAR Commission 2000. *Quality Status Report 2000.* OSPAR Commission London. 108 + vii pp.

Östlund H, Craig H, Broecker W. S and Spenser D. 1987. *GEOSECS Atlantic, Pacific and Indian ocean expeditions*, Vol. 7, IDOE NSF, Washington, DC.

Parker Pearson M and Sharples N. M. 1999. *Between Land and Sea: Excavations at Dun Vulan, South Uist.* Sheffield, Sheffield Academic Press.

Paull C. K, Hills S. J, Thierstein H.R, Bonani G and Wolfli W. 1991. ^{14}C offsets and apparently non-synchronous d ^{18}O stratigraphies between nanno-fossil and foraminiferal carbonates. *Quaternary Research* 35, 274-290.

Pearson G. W. 1987. How to cope with calibration. *Antiquity* 61, 98-103.

Pearson G. W, Becker B and Qua F. 1993 High-precision 14C measurement of German and Irish oaks to show the natural 14C variations from 7890 to 5000 BC. *Radiocarbon* 35, 93-104.

Pearson G. W and Stuiver M. 1993. High-precision bidecadal calibration of the radiocarbon time scale 500-2500 BC. *Radiocarbon* 35, 25-33.

Perdikaris, S and McGovern T. King Alfred, King Knut and the Codfish: new evidence for the beginning of North Atlantic Commercial Fisheries. Paper presented at the 2005 Society for American Archaeology Meetings, Salt Lake City, Utah.

Pilcher J. R. 1991. Radiocarbon dating. In Smart P. L and Frances P. O, (eds.). *Quaternary dating methods- a users guide.* Quaternary Research Association technical guide 4, 16-36.

Pilcher J. R, Baillie M. G. L, Schmidt B and Becker B. 1984. A 7,272 year tree ring chronology from W. Europe. *Nature* 312, 150-152.

Pistek P and Johnson D.R. 1992. A study of the Iceland-Faeroe Front using Geosat altimetry and current-following drifters. *Deep-Sea Research Part A* 39, 2029-2051.

Pomerantz M. A and Duggel S. P. 1974. The sun and cosmic rays. *Reviews of Geophysics and Space Physics* 12, 343-361.

Purser K. H, Schneider R. J, Dobbs, J. M and Post R. 1981. A preliminary description of a dedicated commercial ultra-sensitive mass spectrometer for direct atom counting of ^{14}C. *Proceedings of the Symposium on accelerator Mass Spectrometry*, ANL/PHY-81-1, Argonne National Laboratory, Chicago, IL, 431.

Reedy R. C. 1987. Predicting the production rates of cosmogenic nuclides in extra-terrestrial matter. *Nuclear Instruments and Methods in Physics Research* B29, 251-261.

Reimer P. J, Baillie M. G. L, Bard E, Bayliss A, Beck J. W, Bertrand C. J. H, Blackwell P. G, Buck C. E, Burr G. S, Cutler K. B, Damon P. E, Edwards R. L, Fairbanks R. G, Friedrich M, Guilderson T. P, Hogg A. G, Hughen K. A, Kromer B, McCormac G, Manning S, Bronk Ramsey C, Reimer R. W, Remmele S, Southon J. R, Stuiver M, Talamo S, Taylor F. W, van der Plicht J and Weyhenmeyer C. E. 2004. INTCAL04 Terrestrial radiocarbon age calibration, 0-26 cal kyr BP. *Radiocarbon* 46, (3), 1029-1058.

Reimer P. J, McCormac F. G, Moore J, McCormick F and Murray E. V. 2002. Marine radiocarbon reservoir corrections for the mid- to late Holocene in the eastern subpolar North Atlantic. *The Holocene* 12 (2), 129-135.

Reimer P. J and Reimer R. W. 2001. A marine reservoir correction database and on-line interface. *Radiocarbon* 43 (2A), 461-463.

Reimer P and Reimer R. (2005). Marine Reservoir Correction database. [Online]. Available from: http://www.qub.ac.uk/arcpal/marine/ [Accessed 23/5/05].

Renssen H, Goosse H and Fichefet T. 2002 Modelling the effect of freshwater pulses on the early Holocene climate: the influence of high-frequency climate variability. *Paleoceanography* 17 (2), 1020.

Renssen H, Goosse H, Fichefet T and Campin J.-M. (2001). The 8.2 kyr BP event simulated by a global atmosphere-sea-ice-ocean model. *Geophysical Research Letters* 28, 1567-1570.

Rhode J. 1998. The Baltic and North Seas; a process-orientated review of the physical oceanography. In Robinson A. R and Brink K. H. (eds.). *The Sea*. (Vol. 11). John Wiley and sons, ltd. 699-732.

Ritchie W. 1979. Machair development and chronology in the Uists and adjacent islands. *Proceedings of the Royal Society of Edinburgh B* 77, 107-22.

Ritchie W. 1985. Inter-tidal peats and sub-tidal organic deposits and sea-level change in the Uists, Outer Hebrides. *Scottish Journal of Geology* 21, 161-176.

Rohling E. J and Pälike H. 2005. Centennial-scale climate cooling with a sudden cold event around 8,200 years ago. *Nature* 434, 975-979.

Rose D. C, Fenton K. B, Katzman J and Simpson J. A. 1956. Latitude effect of the cosmic ray nucleon and meson components at sea level from the Arctic to the Antarctic. *Canadian Journal of Physics* 434, 968-984.

Rossby T, Prater M, Zhang H-M, Lazarevich P and Pérez-Bunius P. 1998. *Isopycnal Float Studies of the Subpolar Front: Preliminary Results.* Presented at the WOCE Conference in Halifax, Nova Scotia, Canada, May 25-29.

Ruddiman W. F and McIntyre A. 1981. The North Atlantic Ocean during the last deglaciation. *Palaeoceanography, Palaeoclimatology, Palaeoecology* 35, 145-214.

Ruddiman W.F, Sancetta C.D and McIntyre, A. 1977. Glacial/Interglacial response rate of subpolar North Atlantic waters to climate change: the record in oceanic sediments. Philosophical *Transactions of the Royal Society of London B* 280, 119-142

Santos G.M, Bird M.I, Pillans B, Fifield L.K, Alloway B.V, Chappell J, Hausladen P.A and Arneth A. 2001. Radiocarbon dating of wood using different pre-treatment procedures: Application of the chronology of Rotoehu Ash, New Zealand. *Radiocarbon* 43 (2), 239-248.

Sarnthein M, Jansen E, Weinelt M, Arnold M, Duplessy J. C, Erlenkeuser H, Flatøy A, Johannessen G, Johannessen T, Jung S, Koç N, Labeyrie L, Maslin M, Pflaumann U and Schultz H. 1995. Variations in Atlantic surface ocean paleoceanography, $50^0 - 80^0$N: A time-slice record of the last 30, 000 years. *Paleoceanography* 10 (6), 1063-1094.

Schell D. M, Saupe S. M and Habenstock N. 1988. Natural isotope abundances in bowhead whale (*Balaena mysticetus*) baleen; Markers of ageing and habitat use. In Rundel P. W, Ehringer J. H and Naggy N. A. (eds.). *Stable Isotopes in Ecological Research*. New York. Springer-Verlag, 260-269.

Schimel D, Enting I. G, Heimann M, Wigley T. M. L, Raynaud D, Alves D and Siegenthaler U. 1995. CO2 and the carbon cycle. In Houghton J.T, Meira Filho L.G, Bruce J, Lee H, Callander B.A, Haites E, Harris N and Maskell K. (eds.). *Climate Change 1994: Radiative Forcing of Climate Change, and An Evaluation of the IPCC IS92 Emission Scenarios, Intergovernmental Panel on Climate Change (IPCC).* Cambridge University Press, Cambridge, 35-71.

Scott E. M. 2003. The Third International Radiocarbon Intercomparison (TIRI) and The Fourth International Radiocarbon Intercomparison (FIRI), 1990-2002. Results, Analyses and Conclusions. *Radiocarbon* 45 (2), 135-408.

Seguin F. H, Schneider R. J, Jones G. A and von Reden K. F. 1994. Optimized data analysis for AMS radiocarbon dating. *Nuclear Instruments and methods in Physics Research B* 92, 176.

Sernander R. 1908. On the evidence of Postglacial changes of climate furnished by the peat-mosses of northern Europe. *Geologiska Föreningens i Stockholm Förhandlingar* 30, 465-473.

Siani G, Paterne M, Michel E, Sulpizio R, Sbrana A, Arnold M and Haddad G. 2001 Mediterranean Sea Surface Radiocarbon Reservoir Age Changes Since the Last Glacial Maximum. *Science* 294, 1917-1920.

Siani G, Paterne M, Arnold M, Bard E, Métivier B, Tisnerat N and Bassinot F. Radiocarbon reservoir ages in the Mediterranean Sea and Black Sea. *Radiocarbon* 42 (2), 271-280.

Sigman D. M and Boyle E. A. 2000. Glacial/interglacial variations in atmospheric carbon dioxide. *Nature* 407, 859-869.

Sikes E. L, Samso C R, Guilderson T P and Howard W R. 2000. Old radiocarbon ages in the southwest Pacific Ocean during the last glacial period and deglaciation. *Nature* 405, 555-559.

Slota P.J.J, Jull A.J.T, Linick T.W and Toolin L.J. 1987. Preparation of small samples for ^{14}C accelerator targets by catalytic reduction of CO. *Radiocarbon* 29, 303-306.

Spiker E. C. 1980. The behaviour of ^{14}C and ^{13}C in estuarine water: Effects of *in situ* CO_2 production and atmospheric exchange. *Radiocarbon* 22, (3), 647-654.

Spurk M, Friedrich M, Hofmann J, Remmele S, Frenzel B, Leuschner H.H and Kromer B. 1998. Revisions and extension of the Hohenheim oak and pine chronologies: New evidence about the timing of the Younger Dryas/Preboreal transition. *Radiocarbon* 40, 1107-1116.

Steig E.J, Grootes, P.M and Stuiver, M. 1994. Seasonal precipitation: timing and ice core records. *Science* 266, 1885-1886.

Stenhouse M. J and Baxter M. S. 1979. The uptake of bomb 14C in humans. In Berger R and Suess H. E. (eds.). *Radiocarbon dating.* University of California Press, Berkely, 324-341.

Stocker T. F and Wright D. G. 1996. Rapid changes in ocean circulation and atmospheric radiocarbon. *Paleoceanography* 11, 773–796.

Stocker, T. F. and Wright D. G. 1998. The effect of a succession of ocean ventilation changes on radiocarbon. *Radiocarbon* 40, 359-366

Stötter J, Wastl M, Caseldine C and Häbenle T. 1999. Holocene paleo-climate reconstruction in North Iceland: Approaches and results. *Quaternary Science Reviews* 18, 457-474.

Stuiver M. 1978. Atmospheric carbon dioxide and carbon reservoir changes. *Science* 199, 253-258.

Stuiver M and Braziunas T. F. 1993. Modelling atmospheric ^{14}C influences and ^{14}C ages of marine samples to 10,000 BC. *Radiocarbon* 35 (1), 137-189.

Stuiver M, Braziunas T.F, Grootes P.M and Zielinski, G.A. 1997. Is there evidence for solar forcing of climate in the GISP2 oxygen isotope record? *Quaternary Research* 48, 259-266.

Stuiver M, Grootes P.M and Braziunas, T.F. 1995. The GISP2 18O climate record of the past 16,500 years and the role of the sun, ocean and volcanoes. *Quaternary Research* 44, 341-354.

Stuiver M and Pearson G.W. 1993. High-precision bidecadal calibration of the radiocarbon time scale, AD 1950-500 BC and 2500-6000 BC. *Radiocarbon* 35(1), 1-25.

Stuiver M, Pearson G. W and Braziunas T. 1986. Radiocarbon age calibration of marine samples back to 9000 cal yr BP. *Radiocarbon* 28 (2), 980-1021.

Stuiver M and Polach H. 1977. Discussion: Reporting of ^{14}C data. *Radiocarbon* 19 (3), 355-363.

Stuiver M and Quay P. D. 1980. Changes in Atmospheric Carbon-14 Attributed to a Variable Sun. *Science* 207, 11-19.

Stuiver M and Reimer P. J. 1993, Extended 14C database and revised CALIB radiocarbon calibration program. *Radiocarbon* 35, 215-230.

Stuiver M, Reimer P. J, Bard E, Beck W, Burr G. S, Hughen K. A, Kromer B, McCormac G, Van der Plicht J and Spurk M. 1998a. INTCAL98 Radiocarbon age calibration, 24,000-0 cal BP. *Radiocarbon* 40 (3), 1041-1083.

Stuiver M, Reimer P. J and Braziunas T. F. 1998b. High-precision radiocarbon age calibration for terrestrial and marine samples. *Radiocarbon* 40 (3), 1127-1151.

Stuiver M, Reimer P. J and Reimer R. W. 2005. CALIB 5.0. [WWW program and documentation] [Online]. Available from: http://radiocarbon.pa.qub.ac.uk/calib/ [Accessed 23/5/05].

Suess H.E. 1955. Radiocarbon Concentration in Modern Wood. *Science* 120, 415-417.

Suess H.E. 1979. A calibration table for conventional radiocarbon dates. In Berger R, and Suess H. E. (eds.). *Radiocarbon Dating. Proceedings of the 9th International Radiocarbon Conference.* University of California Press, Berkeley, 777-785.

Suess H. 1986. Secular variations of cosmogenic ^{14}C on Earth: their discovery and interpretation. *Radiocarbon* 28 (2A), 259-65.

Tanaka N, Monaghan M.C and Rye D.M. 1986.Contribution of metabolic carbon to mollusc and barnacle shell carbonate. *Nature* 320, 520-523.

Tauber H and Funder S. 1975. C14 content of recent molluscs from Scoresby Sund, central East Greenland. *The Geological Survey of Greenland Report no. 75*, 95-99.

Taylor R.E. 1987. *Radiocarbon dating: An archaeological perspective.* Academic Press, Inc., Orlando, Florida.

Taylor K. C, Mayewski P. A, Alley R. B, Brook E. J, Gow A. J, Grootes P. M, Meese D. A, Saltzman E. S, Severinghaus J. P, Twickler M. S, White J. W. C, Whitlow S and Zielinski G. A. 1997. The Holocene-Younger Dryas Transition Recorded at Summit, Greenland. *Science* 278, 825-827.

Thurman H. V.1990. *Essentials of Oceanography.* Prentice Hall, London.

Trumbore S. E. 2000. *Radiocarbon Geochronology.* Quaternary Geochronology: Methods and Applications, AGU Reference Shelf 4, American Geophysical Union.

Tuniz C, Bird, J. R, Fink D and Herzog G. F. 1998. *Accelerator mass spectrometry: ultrasensitive analysis for global science.* CRC Press LLC.

Turner V. E, Dockrill S. J and Bond J. M. Old Scatness/Jarlshof Environs Project (Dunrossness parish), Broch, multi-period settlement mound. *Discovery and Excavation, Scotland* 1996, 94-95.

Uerpmann H.-P. 1990. Radiocarbon Dating of Shell Middens in the Sultanate of Oman. *PACT* 29, 335-347

Vandeputte K, Moens L and Dams R. 1996. Improved sealed-tube combustion of organic samples to CO_2 for stable isotopic analysis, radiocarbon dating and percent carbon determinations. *Analytical Letters* 29 (15), 2761-73.

Vita-Finzi C and Roberts N. 1984. Selective leaching of shells for 14C dating. *Radiocarbon* 26, 54-58.

Voelker A. H. L, Sarnthein M, Grootes P. M, Erlenkeuser H, Laj C, Mazaud A, Nadeau M-J and Schleicher M. 1998. Correlation of marine ^{14}C ages from the Nordic seas with the GISP2

isotope record: Implications for ^{14}C calibration beyond 25ka BP. *Radiocarbon* 40 (1), 517-534.

Voelker A. H. L, Grootes P. M, Nadeau M and Sarnthein M. 2000. Radiocarbon levels in the Iceland Sea from 25-53 Kyr and their link to the Earth's magnetic field intensity. *Radiocarbon* 42 (3), 437-452.

Vogel J. S, Southon J. R and Nelson D. E. 1987. Catalyst and binder effects in the use of filamentous graphite for AMS. *Nuclear Instruments and Methods* B29, 50-56.

Vogt S, Herzog G. F and Reedy R.C. 1990. Cosmogenic nuclides in extraterrestrial materials. *Reviews of geophysics* 28, 253-275.

Waelbroeck C, Duplessy J-C, Michel E, Labeyrie L, Paillard D and Dupratt J. 2001. The timing of the last deglaciation in North Atlantic climate records. *Nature* 412, 724 -727.

Wagner G. A. 1998. *Age determination of young rocks and artefacts*. Berlin, Springer.

Ward G. K and Wilson S. R. 1978. Procedures for comparing and combining radiocarbon age determinations: A critique. *Archaeometry* 20, 19-31.

Wefer G and Berger W.H. 1991. Isotope paleontology: growth and composition of extant calcareous species. *Marine Geology* 100, 207-248.

Whittow J. 1992. *Geology and scenery in Britain*. Chapman and Hall, London.

Wunsch C. 2003. Determining palaeoceanographic circulations, with emphasis on the Last Glacial Maximum. *Quaternary Science Reviews* 22, 371-385.

Yoneda M, Hirota M, Uchida M, Uzawa K, Tanaka A, Shibata Y and Morita M. 2001. Marine radiocarbon reservoir effect in the western North Pacific observed in archaeological fauna. *Radiocarbon* 43 (2A), 465-471.

Yoneda M, Hirota M, Uchida M, Tanaka A, Shibata Y, Morita M and Akazawa T. 2002. Radiocarbon and Stable Isotope Analyses on the Earliest Jomon Skeletons from the Tochibara Rockshelter, Nagano, Japan. *Radiocarbon* 44 (2), 549-557.